

# Physical Layer Loading Algorithms for Indoor Wireless Multicarrier Systems

*Alexander Wyglinski*



Department of Electrical & Computer Engineering  
McGill University  
Montreal, Canada

November 2004

---

A thesis submitted to McGill University in partial fulfillment of the requirements for  
the degree of Doctor of Philosophy.

© 2004 Alexander Wyglinski

## Abstract

The demand for wireless networks has been growing rapidly over the recent past due to improved reliability, higher supported data rates, seamless connectivity between users and the access point, and low deployment costs relative to wireline infrastructure. This increase in demand started with the popular IEEE 802.11b wireless local area network standard. Many recent wireless network standards are now employing multicarrier modulation in their design. Multicarrier modulation reduces the system's susceptibility to the frequency-selective fading channel, due to multipath propagation, by transforming it into a collection of approximately flat subchannels. As a result, this makes it easier to compensate for the distortion introduced by the channel. However, standardized wireless modems, such as the ETSI HiperLAN/2 and the IEEE 802.11a standards, employ the same operating parameters across all subcarriers, and thus do not exploit all the advantages offered by the multicarrier framework.

This dissertation investigates techniques to further enhance system throughput performance by tailoring several operating parameters on a per-subcarrier basis. These parameters are subcarrier modulation schemes, power levels, and equalizer lengths. The idea of tailoring modulation schemes and power levels, known as *bit allocation* and *power allocation*, has been studied for many years and for many applications. This work proposes two novel discrete bit allocation algorithms that strive to reach the optimal solution in a low computational complexity fashion, while constrained to a specified error performance. A novel power allocation algorithm is proposed that satisfies regulatory requirements by obeying a frequency interval power constraint.

Investigation of the third parameter, subcarrier equalizer lengths, has not been conducted before in the literature. Two algorithms are proposed that vary the lengths of the subcarrier equalizers such that the overall distortion is reduced to some specified amount, while the number of equalizer taps used by the system are kept small. Finally, the use of bit allocation is extended to the case when multiple antennas are employed by the wireless modems. Four algorithms are proposed that perform generalized antenna selection diversity at both the transmitter and receiver, in tandem with discrete bit allocation. Results show that employing two transmit and two receive antennas with discrete bit allocation can achieve an average increase in throughput of up to 33% when compared to a system without bit allocation.

## Sommaire

Au cours des dernières années, la demande de services sur des réseaux sans-fil s'est accrue rapidement, du fait entre autres de leur fiabilité améliorée, des débits de plus en plus élevés supportés, de la facilité de connexion entre les utilisateurs et les points d'accès, et de leur faible coût de déploiement en comparaison avec les technologies filaires. Cette tendance s'est marquée principalement depuis le succès de la norme de réseau local sans-fil IEEE 802.11b. De nombreuses normes de réseaux sans-fil récentes reposent sur la modulation à porteuses multiples. La modulation à porteuses multiples réduit la sensibilité du système aux canaux à évanouissement sélectif en fréquence, en les transformant en une collection de sous-canaux à évanouissement constant. Ceci simplifie la compensation de la distorsion due au canal. Cependant, les normes actuelles de modems sans-fil (comme HiperLAN/2 et IEEE 802.11a) utilisent les mêmes paramètres de fonctionnement sur toutes leurs sous-porteuses, et n'exploitent donc pas tous les avantages offerts par les systèmes.

La présente thèse étudie différentes techniques pour améliorer le débit de ce type de système en choisissant différents paramètres de fonctionnement individuellement pour chaque sous-porteuse. Les paramètres considérés sont le type de modulation, la puissance de transmission et la longueur des égaliseurs. L'idée d'adapter les modulations et les niveaux de puissance (appelée allocation binaire et de puissance) a déjà été étudiée pour différentes applications. Le présent travail propose deux algorithmes novateurs allocation binaire discrète, qui tentent d'atteindre l'allocation optimale avec une faible complexité de calcul, tout en respectant une contrainte sur le taux d'erreur binaire moyen. Un algorithme novateur d'allocation de puissance est proposé, qui satisfait les exigences des organismes de régulation, en obéissant à une contrainte de puissance sur des intervalles de fréquence.

L'étude du troisième paramètre considéré, la longueur des égaliseurs, n'a pas été envisagée auparavant dans la littérature. Nous proposons deux algorithmes qui font varier les longueurs des égaliseurs dans chaque sous-porteuse, de manière à réduire la distorsion jusqu'à un niveau prédéterminé, tout en minimisant la longueur des égaliseurs. Finalement, l'utilisation de l'allocation binaire est étendue au cas où plusieurs antennes sont utilisées dans le modem sans-fil. Nous proposons quatre algorithmes de diversité généralisée par sélection d'antennes, en conjonction avec une allocation binaire adaptative. Les résultats obtenus démontrent que l'utilisation de deux antennes au récepteur et à l'émetteur permettent jusqu'à 33% d'accroissement du débit une fois comparé à un système sans l'allocation.

## Acknowledgments

First and foremost, I would like to express my deepest gratitude to my supervisors, Professor Peter Kabal and Professor Fabrice Labeau, for their excellent guidance and continual support during the course of my degree. Working with them was a wonderful experience and they contributed significantly to both my thesis research and my professional development. I would also like to thank Professor Labeau for his French translation of the abstract for this dissertation.

The financial support provided by the Natural Science and Engineering Research Council of Canada (NSERC), le Fonds “Nature et Technologies” du Québec, and by Professors Kabal and Labeau are duly acknowledged.

I would like to thank Professor Benoît Boulet and Professor Benoît Champagne, members of my Ph.D. committee, for their feedback and suggestions during the development phase of my Ph.D. research topic.

I would also like to thank my external examiner, Professor Tim Davidson of McMaster University, and the members of my Ph.D. defence committee, namely, Professor Shauna Van Praagh, Professor Benoît Boulet, Professor Benoît Champagne, Professor Peter Kabal, Professor Fabrice Labeau, Professor Ioannis Psaromiligkos, and Professor Sofène Affes of INRS-EMT, for their useful comments and suggestions.

During my stay at McGill, I have met numerous students, faculty, and staff in the Telecommunications and Signal Processing (TSP) Lab, the ECE Department, and McGill University in general, who have made my Ph.D. experience all the more rewarding and to them I owe my thanks. In particular, I would like to thank three former Ph.D. students of the TSP Lab: Dr. Hossein Najafzadeh-Azghandi, Dr. Khaled Helmi El-Maleh, and Dr. Nader Sheikholeslami-Alagha. Their words of advice, support, and friendship did much to enhanced the quality of my research as well as my graduate experience at McGill.

As always, I am deeply indebted to my parents, my sisters Joanne and Laura, and the rest of my family, for their love and support throughout this degree and my life. Thank you for everything.

Finally, I would like to thank Linda Wang for her love, understanding, and unwavering belief in me.

---

# Contents

<b>1</b>	<b>Introduction</b>	<b>1</b>
1.1	Multicarrier Modulation: A “Divide-and-Conquer” Approach for Data Transmission . . . . .	1
1.2	Research Objectives . . . . .	3
1.3	Related Work . . . . .	5
1.4	Thesis Contributions . . . . .	6
1.5	Thesis Organization . . . . .	8
<b>2</b>	<b>Multicarrier Data Transmission</b>	<b>9</b>
2.1	Multicarrier Modulation . . . . .	11
2.1.1	Basic Theory . . . . .	11
2.1.2	Orthogonal Frequency Division Multiplexing . . . . .	15
2.1.3	Filterbank Multicarrier Systems . . . . .	21
2.2	Indoor Wireless Channel Models . . . . .	32
2.2.1	SISO Channel Models . . . . .	33
2.2.2	MIMO Channel Models . . . . .	36
2.3	Channel Estimation and Synchronization Techniques . . . . .	41
2.3.1	Data-Assisted Channel Estimation . . . . .	41
2.3.2	Synchronization . . . . .	43
2.4	Adaptive Allocation Algorithms . . . . .	43
2.4.1	Bit Allocation . . . . .	44
2.4.2	Bit Loading with Imperfect Channel Information . . . . .	51
2.4.3	Power Allocation . . . . .	51
2.5	Multicarrier Equalization Techniques . . . . .	54

---

2.5.1	Interference in Multicarrier Systems . . . . .	54
2.5.2	Distortion Reduction . . . . .	55
2.5.3	Optimal Single-Tap Per-Tone Equalization for OFDM Systems . . . . .	58
2.5.4	Frequency-Domain Equalizers for Multicarrier Systems . . . . .	59
2.6	Multiple-Antenna Multicarrier Systems . . . . .	60
2.6.1	Spatial Multiplexing . . . . .	61
2.6.2	Space-Time Coding . . . . .	63
2.7	Chapter Summary . . . . .	68
<b>3</b>	<b>BER-Constrained Multicarrier Loading Algorithms</b>	<b>70</b>
3.1	Discrete Bit Loading Algorithms . . . . .	71
3.1.1	Proposed Incremental Bit Loading Algorithm . . . . .	72
3.1.2	Proposed Peak BER-Constrained Bit Allocation Algorithm . . . . .	75
3.1.3	Effects of Imperfect Subcarrier SNR Information . . . . .	78
3.2	Power Loading Algorithm . . . . .	81
3.2.1	Proposed Frequency Interval Power Allocation Algorithm . . . . .	82
3.3	Equalizer Tap Loading Algorithms . . . . .	83
3.3.1	Proposed Subcarrier-Level Equalizer Tap Loading Algorithm . . . . .	84
3.3.2	Proposed Greedy Subcarrier Equalizer Tap Loading Algorithm . . . . .	85
3.4	Simulation Results . . . . .	87
3.4.1	Bit Allocation Results . . . . .	87
3.4.2	Subcarrier Equalizer Tap Allocation Results . . . . .	95
3.5	Chapter Summary . . . . .	98
<b>4</b>	<b>Multicarrier Systems with Multiple Antennas and Bit Loading</b>	<b>101</b>
4.1	Antenna Subset Selection Algorithms . . . . .	102
4.1.1	Signal-Based Selection . . . . .	105
4.1.2	Subcarrier-Based Selection . . . . .	106
4.2	Antenna Subset Selection Algorithm with Bit Loading . . . . .	108
4.2.1	Signal-Based Selection . . . . .	109
4.2.2	Subcarrier-Based Selection . . . . .	112
4.3	Results . . . . .	113
4.3.1	An Example . . . . .	121

---

4.4 Chapter Summary . . . . .	123
<b>5 Conclusion</b>	<b>124</b>
5.1 Research Achievements . . . . .	124
5.2 Future Work . . . . .	125
<b>A Data-Aided Channel Estimation Error</b>	<b>127</b>
<b>B Optimal Fractionally-Spaced MMSE Subcarrier Equalizers</b>	<b>130</b>
B.1 System Transfer Function . . . . .	130
B.2 Optimal MMSE Equalizer Derivation . . . . .	131
<b>C Subcarrier SNR Calculation for Multiple Antenna Systems</b>	<b>135</b>
C.1 SISO Scenario . . . . .	135
C.2 MISO Scenario . . . . .	136
C.3 SIMO Scenario . . . . .	137
C.4 MIMO Scenario . . . . .	138
<b>D Normalization of MIMO Channel Model Correlation Matrix</b>	<b>139</b>
<b>E Bit Error Rate Simulation Parameters</b>	<b>142</b>
E.1 Calculation of the Simulation Runtime Parameters . . . . .	142
<b>References</b>	<b>144</b>

---

## List of Figures

2.1	A generic multiple input/multiple output MCM system. . . . .	10
2.2	Schematic of a generic single input/single output MCM system. . . . .	11
2.3	The effects of an 8-subcarrier MCM transmitter and frequency-selective fading channel on the individual subcarrier spectra. . . . .	14
2.4	Schematic of an OFDM system employing a cyclic prefix. . . . .	17
2.5	The process of adding, capturing the intersymbol interference, and removal of a cyclic prefix. . . . .	21
2.6	Subcarrier spectra of $N = 8$ OFDM and FB-MC systems. . . . .	23
2.7	Implementation of MDFT pre- and post-processing components. . . . .	28
2.8	Impulse responses of square-root raised cosine and raised cosine filters. . .	31
2.9	Example of a channel response due to multipath propagation. . . . .	34
2.10	An example of an indoor environment response operating in the 5.15–5.25 GHz UNII band with a 50 m transmitter/receiver separation distance. . . . .	35
2.11	An example of multipath propagation when two transmit antennas are employed in a small office/home office environment. . . . .	37
2.12	Example of bit allocation performed on an 8 subcarrier system. . . . .	45
2.13	Channel capacity $C$ and the points for M-QAM given a $P_T$ of $10^{-6}$ corresponding to an SNR Gap $\Gamma$ of 8.8 dB. . . . .	49
2.14	An example of waterfilling for the transmitted spectrum (from [189]). . . .	52
2.15	Different types of distortion present in multicarrier systems (from [79]). . .	54
2.16	The effect of equalization on the noise spectrum. . . . .	56
2.17	Schematic of a spatial multiplexing system (adapted from [208]). . . . .	62
2.18	Schematic of a multiple antenna system employing transmit and receive antenna subset selection (from [33]). . . . .	67

2.19	Grouping of tones for complexity reduction in STF coding (from [28]). . . .	68
3.1	Proposed incremental bit loading algorithm based on a greedy approach [254–256]. . . . .	74
3.2	Proposed bit loading algorithm based on a peak BER constraint [256, 258].	76
3.3	Algorithm for determining the initial peak bit error rate [256, 258]. . . . .	77
3.4	Regions of uniform quantization of the $P_i$ waterfall curves for $P_T = 10^{-5}$ and $B = 4$ . . . . .	80
3.5	Proposed power allocation algorithm with frequency interval power constraint [254, 255]. . . . .	83
3.6	Proposed subcarrier equalizer tap loading algorithm applied to subcarrier $k$ [254, 255]. . . . .	84
3.7	Proposed subcarrier equalizer tap loading algorithm employing a “greedy” approach [260]. . . . .	86
3.8	Overall throughput of an $N = 8$ subcarrier system satisfying a $P_T$ of $10^{-3}$ . Except for the curve corresponding to Leke & Cioffi, all the curves are superimposed. . . . .	89
3.9	Mean BER of an $N = 8$ subcarrier system satisfying a $P_T$ of $10^{-3}$ . . . . .	90
3.10	Overall throughput of an $N = 52$ subcarrier system satisfying a $P_T$ of $10^{-5}$ using subcarrier SNR values with Gaussian noise of variance $\sigma^2$ added. Note that the algorithm of Leke & Cioffi and the proposed peak BER-constrained algorithm use the non-ideal subcarrier SNR values. . . . .	91
3.11	Mean BER of an $N = 52$ subcarrier system satisfying a $P_T$ of $10^{-5}$ with and without Gaussian noise of variance $\sigma^2$ added to $\gamma_i$ , $i = 0, \dots, N - 1$ . . . . .	92
3.12	Cumulative density function of computational time of an $N = 52$ subcarrier system satisfying a $P_T$ of $10^{-5}$ at SNR values of 10 dB (without circles) and 40 dB (with circles). . . . .	94
3.13	Outage probability (fraction of realizations for which $\bar{P} > P_T$ ) of a multi-carrier system employing the proposed peak BER algorithm at $P_T = 10^{-5}$ . . . . .	95

3.14 Overall throughput of a multicarrier system employing adaptive bit loading algorithms of the proposed peak BER algorithm (no circles) and Leke & Cioffi [12] (with circles) at $P_T = 10^{-5}$ when the subcarrier SNR values are quantized with $2^b$ levels. . . . .	96
3.15 Mean BER of a multicarrier system employing the proposed peak BER algorithm at $P_T = 10^{-5}$ when the subcarrier SNR values are quantized with $2^b$ levels. . . . .	97
3.16 BER performance for 8 subcarriers with BPSK (solid) and 16-QAM (dashed) modulation when adaptive subcarrier equalizer tap allocation is employed, along with fixed length equalizers with the same overall number of taps, using the ETSI HiperLAN/2 Channel A. . . . .	98
3.17 BER performance for 8 subcarriers with QPSK (solid) and 64-QAM (dashed) modulation when adaptive subcarrier equalizer tap allocation is employed, along with fixed length equalizers with the same overall number of taps, using the ETSI HiperLAN/2 Channel A. . . . .	100
3.18 Relationship between the subcarrier equalizer tap allocation and the channel frequency (magnitude) response using an 8 subcarrier portion of the ETSI HiperLAN/2 Channel A. . . . .	100
4.1 Proposed antenna subset selection algorithm (antenna configuration chosen on a signal basis). . . . .	105
4.2 Proposed antenna subset selection algorithm (antenna configuration chosen on a subcarrier basis). . . . .	107
4.3 Proposed antenna subset selection algorithm with bit allocation (antenna configuration chosen on a signal basis). . . . .	110
4.4 Proposed antenna subset selection algorithm with bit allocation (antenna configuration chosen on a subcarrier basis). . . . .	111
4.5 Throughput of a multicarrier system with several array configurations employing the proposed signal-based antenna subset selection algorithm. . . .	116
4.6 Mean BER of a multicarrier system with several array configurations employing the proposed signal-based antenna subset selection algorithm. . . .	116

---

4.7	Throughput results of the proposed subcarrier-based antenna subset selection algorithm. . . . .	117
4.8	Mean BER results of the proposed subcarrier-based antenna subset selection algorithm. . . . .	117
4.9	Throughput results of the proposed signal-based antenna subset selection algorithm with bit loading. . . . .	119
4.10	Mean BER results of the proposed signal-based antenna subset selection algorithm with bit loading. . . . .	119
4.11	Throughput results of the proposed subcarrier-based antenna subset selection algorithm with bit loading. . . . .	120
4.12	Mean BER results of the proposed subcarrier-based antenna subset selection algorithm with bit loading. . . . .	120
4.13	Throughput difference results between arrays with antenna spacings of $d = 5\lambda$ and $d = \lambda$ for the proposed subcarrier-based antenna subset selection algorithm employing bit loading. . . . .	122
4.14	Throughput difference results between arrays with antenna spacings of $d = 5\lambda$ and $d = \lambda$ for the proposed signal-based antenna subset selection algorithm employing bit loading. . . . .	122
C.1	Schematic of a SISO communication system ( $N_T = 1, N_R = 1$ ). . . . .	136
C.2	Schematic of a MISO communication system ( $N_T = 3, N_R = 1$ ). . . . .	136
C.3	Schematic of a SIMO communication system ( $N_T = 1, N_R = 3$ ). . . . .	137
C.4	Schematic of a MIMO communication system ( $N_T = 2, N_R = 2$ ). . . . .	138

---

## List of Tables

2.1	Relative advantages of single carrier and multitone modulation (for type of MCM) for ADSL, where $\checkmark$ denotes the system with better performance or lower cost (from [42]) . . . . .	15
2.2	Several implementations of multicarrier systems . . . . .	16
2.3	Mode-dependent parameters for IEEE 802.11a and HiperLAN/2 (from [94])	19
2.4	Channel models for line-of-sight (LOS) and non-LOS (NLOS) indoor environments at 5 GHz (from [136]) . . . . .	36
2.5	Layer 1 and 2 technologies for advanced non-line-of-sight fixed-wireless-access (from [204]) . . . . .	61
3.1	Number of $P_T$ Violations by the bit allocation algorithm of Leke & Cioffi. .	90
3.2	Mean (worst case) computation times in milliseconds at different SNR values, 52 subcarriers, $P_T = 10^{-5}$ . . . . .	93
4.1	Normalized transformation matrices for creating correlated MIMO channels, with correlation matrix $\Sigma$ , from uncorrelated MIMO channels, given $(N_T, N_R)$ .	114
4.2	Average (transmit antenna, receive antenna) usage for the four proposed algorithms at several SNR values with $(N_T = 2, N_R = 2)$ antennas available for selection. . . . .	118

# List of Terms

16-QAM	16-point Quadrature Amplitude Modulation
3GPP	Third Generation Partnership Project
3GPP2	Third Generation Partnership Project 2
64-QAM	64-point Quadrature Amplitude Modulation
ADSL	Asymmetric Digital Subscriber Line
ARQ	Automatic Repeat Request
ATM	Asynchronous Transfer Mode
AWGN	Additive White Gaussian Noise
BER	Bit Error Rate
BLAST	Bell Labs Layered Space-Time
BPSK	Binary Phase Shift Keying
BRAN	Broadband Radio Access Network
BSS	Basic Service Set
BST-OFDM	Band-Segmented Transmission Orthogonal Frequency Division Multiplexing
CBR	Constant Bit Rate
CCK	Complementary Code Keying
CDMA	Code Division Multiple Access
CIR	Channel Impulse Response
CMFB	Cosine-Modulated Filter Banks
CP	Cyclic Prefix
CRC	Cyclic Redundancy Check
CS	Cyclic Suffix
CSI	Channel State Information

---

CSMA/CA	Carrier-Sense Multiple Access with Collision Avoidance
DAB	Digital Audio Broadcasting
DECT	Digital European Cordless Telecommunications
DFE	Decision Feedback Equalizer
DFT	Discrete Fourier Transform
DMT	Discrete Multitone
DSL	Digital Subscriber Line
DSSS	Direct Sequence Spread Spectrum
DVB	Digital Video Broadcasting
EDGE	Enhanced Data GSM Environment
EGC	Equal Gain Combining
ETSI	European Telecommunication Standard Institute
FB-MC	Filterbank-Multicarrier
FCC	Federal Communications Commission
FDD	Frequency Division Duplexing
FDM	Frequency Division Multiplexing
FDMA	Frequency Division Multiple Access
FEC	Forward Error Correction
FEQ	Frequency-domain Equalizer
FEXT	Far-end Crosstalk
FFT	Fast Fourier Transform
FHSS	Frequency Hopped Spread Spectrum
FIR	Finite Impulse Response
FMT	Filtered Multitone
GSM	Global System for Mobile Communications
HiperLAN	High Performance Radio Local Area Network
HiSWAN	High Speed Wireless Access Network
HSDPA	High-Speed Downlink Packet Access
ICI	Interchannel Interference
IDFT	Inverse Discrete Fourier Transform
IEEE	Institute of Electrical and Electronic Engineers
IF	Intermediate Frequency
IFFT	Inverse Fast Fourier Transform

---

IID	Identically and independently distributed
IIR	Infinite Impulse Response
IMEC	Interuniversity Micro Electronics Center
ISDB-T	Integrated Service Digital Broadcasting-Terrestrial
ISI	Intersymbol Interference
ISM	Industrial, Scientific, Medical
ITU	International Telecommunications Union
LA	Link Adaptation
LMS	Least Mean-Squared
LOS	Line-of-Sight
MAC	Medium Access Control
Mb/s	Megabits per second
MC-CDMA	Multicarrier Code Division Multiple Access
MCM	Multicarrier Modulation
MDFT	Modified Discrete Fourier Transform
MIMO	Multiple-Input Multiple-Output
MISO	Multiple-Input Single-Output
ML	Maximum Likelihood
MMAC	Multimedia Mobile Access Communication System Promotion Council
MMSE	Minimum Mean-Squared Error
Modem	Modulator/Demodulator
MRC	Maximum Ratio Combining
MRT	Maximum Ratio Transmission
MSE	Mean-Squared Error
NEXT	Near-end Crosstalk
NLOS	Non-Line-of-Sight
OFDM	Orthogonal Frequency Division Multiplexing
OFDMA	Orthogonal Frequency Division Multiple Access
O-QAM	Offset Quadrature Amplitude Modulation
PAR	Peak-to-Average Ratio
PBCC	Packet-Based Binary Convolutional Codes
PDU	Protocol Data Unit

---

PER	Packet Error Rate
PHY	Physical Layer
PR	Perfect Reconstruction
PSNR	Peak Signal-to-Noise Ratio
QAM	Quadrature Amplitude Modulation
QoS	Quality-of-Service
QPSK	Quadrature Phase Shift Keying
RF	Radio Frequency
SC	Selection Combining
SC-FDE	Single Carrier-Frequency Domain Equalization
SIC	Successive Interference Cancellation
SINR	Signal-to-Interference-plus-Noise Ratio
SIMO	Single-Input Multiple-Output
SISO	Single-Input Single-Output
SNR	Signal-to-Noise Ratio
SOHO	Small Office/Home Office
STBC	Space-Time Block Codes
STC	Space-Time Codes
STTC	Space-Time Trellis Codes
SVD	Singular Value Decomposition
TDD	Time Division Duplexing
TDMA	Time Division Multiple Access
TEQ	Time-domain Equalizer
UHF	Ultra-High Frequency
UNII	Unlicensed National Information Infrastructure
VBR	Variable Bit Rate
VSB	Vestigial Sideband
WCDMA	Wideband CDMA
WER	Word Error Rate
WiFi	Wireless Fidelity
WMAN	Wireless Metropolitan Area Network
WLAN	Wireless Local Area Network
WPAN	Wireless Personal Area Network

# List of Symbols

$P_i$	Probability of bit error for subcarrier $i$
$P_T$	Probability of bit error threshold for the multicarrier system
$\hat{P}$	Peak probability of bit error threshold
$\bar{P}$	Mean probability of bit error of the multicarrier system
$\gamma_i$	Signal-to-noise ratio of subcarrier $i$
$\alpha_i$	Smallest possible bit error rate, given a set of modulation schemes, which is above $P_T$
$\beta_i$	Largest possible bit error rate, given a set of modulation schemes, which is below $P_T$
$\pi_i$	Power level of subcarrier $i$
$\sigma_v^2$	Noise variance
$\pi_{\max}$	Frequency interval power constraint across a specified bandwidth
$b_i$	Number of bits per symbol epoch of subcarrier $i$
$M_i$	Number of constellation points for a modulation scheme applied to subcarrier $i$
$P_{M_i,i}$	Probability of symbol error for a modulation scheme employing $M_i$ constellation points on subcarrier $i$
$\delta$	Step size value when modifying the peak bit error rate limit $\hat{P}$
$N_T$	Number of transmit antennas
$N_R$	Number of receive antennas
$N$	Number of subcarriers
$f^{(i)}(n)$	Impulse response for the analysis filter of subcarrier $i$
$g^{(i)}(n)$	Impulse response for the synthesis filter of subcarrier $i$
$w^{(i)}(n)$	Impulse response for the frequency-domain equalizer of subcarrier $i$

---

$J^{(i)}$	Distortion cost function of subcarrier $i$
$J_T$	Distortion cost function threshold
$\bar{J}$	Mean of the distortion cost functions across all subcarriers
$q^{(i)}$	Number of taps employed by the equalizer of subcarrier $i$
*	Linear convolution
$\textcircled{N}$	Circular convolution of periodicity $N$
$Re$	Real component operator
$Im$	Imaginary component operator
$\mathbf{x}_{n,n-L+1}^{(k)}$	A block of data from subcarrier $k$ with length $L$
$\mathbf{T}_{u,R,D}$	Upsampling matrix with sampling rate $R$ and delay $D$
$\mathbf{T}_{d,R,D}$	Downsampling matrix with sampling rate $R$ and delay $D$
$\text{mod}(A, B)$	Remainder operator with quotient $A$ and divisor $B$
$(\cdot)^*$	Complex conjugation operator
$(\cdot)^T$	Transpose operator
$(\cdot)^H$	Complex conjugate transpose operator
$\tau$	Overall system group delay operating in an ideal channel
$\tau_{\text{ch}}$	Channel group delay
$\otimes$	Kronecker matrix product
$\text{vec}$	Vector operator (stacks the columns of a matrix into a single column vector)
$\lambda$	Signal wavelength
$\rho_{ij}$	Fading correlation between antennas $i$ and $j$
$J_0$	Bessel function of the first kind with zero order
$E\{\}$	Expected value
$B$	Total number of modulation schemes available to the system
$\Gamma$	SNR Gap

# Chapter 1

## Introduction

### 1.1 Multicarrier Modulation: A “Divide-and-Conquer” Approach for Data Transmission

Data transmission has become an integral and ubiquitous component of today's world. Everyday actions, such as using a bank machine, making a phone call, watching television, and doing grocery shopping, all involve some sort of data transmission that makes these actions more convenient, cost effective, or feasible. This data transmission can be performed over a wireline infrastructure, a wireless network, or a combination of the two infrastructures. A consequence of this increased integration of data transmission in our day-to-day life is the demand for more throughput. As the level of integration increases and more people are connected, the amount of data generated grows. Therefore, the data rates of the data transmission systems must increase to keep up with the increase in information. Although the throughput supported by wireline networks are enormous, due to fiber optics and other technologies, the base station/mobile user interfaces of wireless networks are still trying to keep up with the demand for more throughput. Moreover, there are several significant restrictions when wireless modems transmit at high data rates. The first is bandwidth usage. Since the spectrum that wireless systems use to transmit data is regulated by government agencies, such as the Federal Communications Commission (FCC) in the United States and Spectrum Management and Telecommunications Canada, each operator of a wireless data transmission infrastructure must abide by the established guidelines. This is done in order to avoid interference between different wireless operators. Therefore, the rate

is constrained by the maximum bandwidth allotted to the operator. The second constraint is the channel environment that the data transmission system is operating through. At higher data rates, the amount of distortion introduced to the transmission becomes more pronounced, making it more difficult to compensate at the receiver.

Since the regulatory requirements of the spectrum cannot be modified or changed, researchers are investigating techniques for enhancing the performance of digital transmission systems operating in various channel conditions (e.g., additive white Gaussian noise, multipath fading, impulse noise). Several solutions have been proposed, including *multicarrier modulation* (MCM), which is currently employed mostly in digital subscriber lines (DSL) systems [1] and wireless local area networks (WLAN) [2–4]. MCM operates according to a “divide-and-conquer” approach: by transmitting the data across the channel at a lower data rate in several frequency subcarriers, the process of distortion compensation can be made simpler by treating each subcarrier separately. From a time-domain perspective, this translates the wideband transmission system in a collection of parallel narrowband transmission systems each operating at a lower data rate [5]. From the frequency-domain perspective, MCM transforms the frequency-selective channel, i.e., non-flat spectrum across the frequency band of interest, into a collection of approximately flat subchannels that the data gets transmitted over in parallel. Thus, MCM has become the technology of choice to combat the frequency-selective fading channel.

Despite the advantages of multicarrier modulation, many conventional WLAN systems do not fully exploit its potential, unlike DSL modems. Rather, conventional WLAN systems employing MCM use the same operating parameters across all subcarriers, including modulation scheme, coding rate, and transmit power level. However, the effects of the channel may vary on a subcarrier basis, and thus the overall error probability of the system is dominated by the error probabilities of the subcarriers with the worst performance [6]. For instance, systems that try to keep the error rate low usually transmit with the smallest subcarrier signal constellation possible. Equivalently, systems that require a high throughput have error probabilities dominated by the largest subcarrier error probability. Thus, to enhance system performance, the impact of these poorly-performing subcarriers should be mitigated. This is the rationale behind adaptive loading for MCM systems.

*Loading* refers to the process of distributing resources in a system employing MCM such that the performance is enhanced while satisfying some constraints. Resources that are commonly allocated to the different subcarriers are bits, i.e., through the choice of

modulation scheme, and power, i.e., transmit power levels. Since the channel that the data transmission system is operating in is usually frequency-selective, each subcarrier will have a different signal-to-noise ratio (SNR). Thus, tailoring the operating parameters could improve performance. The techniques for loading originated from other areas, including financial analysis [7] and quantizer design [8, 9]. However, a number of loading algorithms have been developed and implemented for several data transmission systems, including DSL modems [10–13].

Despite these efforts, a number of issues remain unresolved or require better solutions. For instance, several bit loading algorithms exist that use closed-form expressions to solve for the final solution. As a result, rounding errors and the errors introduced via the approximations applied to these expressions may result in solutions that are far from the optimal. However, many algorithms that do perform discrete bit loading use an incremental approach that may increase the computational complexity. With respect to power loading, almost all algorithms impose a total power constraint, which may result in a potential violation of regulatory requirements imposed on transmit power levels. To compensate for the distortion at the receiver, many multicarrier modulation systems employ subcarrier equalizers. If the channel is frequency-selective, the distortion of each subcarrier is different, with some subcarriers requiring more compensation than others. However, many systems employ equalizers of the same length across all the subcarriers, resulting in several equalizers using too many taps to combat the distortion while the other equalizers use too few taps. Finally, the use of multiple antennas and bit loading have not been fully exploited, especially in wireless local area network systems. Employing both multiple antennas and bit loading, each with its own performance gains, will result in a performance enhancement greater than each of the individual performance gains, although it will not be equal to the sum of individual performance enhancements.

## 1.2 Research Objectives

The main objective of this research is to develop a number of performance-enhancing techniques that are applicable to multicarrier-based wireless local area network modems. By exploiting the potential offered by adaptive loading algorithms and multiple antennas, which wireless local area networks normally do not employ, the throughput performance of these systems will increase at the cost of small increase in implementation complexity.

Moreover, the error robustness<sup>1</sup> of these systems will be constrained to be above some specified amount to ensure a minimum quality of service.

Therefore, to reach this main objective, several sub-objectives have been established in this dissertation, namely:

- The design of a discrete bit loading algorithm that can strive for the optimal solution in a low computational complexity fashion. Most discrete bit loading algorithms are iterative in nature. Thus it is important to find a final solution that is close to the optimal in as few iterations as possible<sup>2</sup>.
- The design of a power loading algorithm that allocates power to the subcarriers while satisfying a frequency interval power constraint. This constraint is imposed in order to avoid violations of regulatory requirements, which usually limits the transmit power levels according to some level across a specified bandwidth.
- The enhancements of the efficiency of the system to deal with ISI distortion by varying the subcarrier equalizer lengths according to the distortion present in each subcarrier. Instead of applying the same number of taps for each equalizer, the number of taps is varied for each subcarrier until the overall distortion is reduced to an acceptable level.
- The exploitation of the spatial diversity of a WLAN system by employing multiple antennas at both the transmitter and the receiver. To avoid excessive power consumption due to redundant antennas, an algorithm must be in place to employ only the necessary number of antennas to achieve an increase in throughput (the remaining antennas are “turned off”).
- The combination of the frequency and spatial diversity offered by both multiple antennas and MCM to enhance throughput while satisfying the error constraint. Combining these two techniques would yield a substantial performance improvement, although this improvement would not be equal to the sum of the individual performance gains of multiple antennas and MCM.

---

<sup>1</sup>In this dissertation, the error robustness is measured in terms of the *probability of bit error*, also known as the *bit error rate*.

<sup>2</sup>The same objective was defined by Krongold, Ramchandran, and Jones for their proposed bit and power loading algorithms [14]. See Section 2.4.1 for details.

Before outlining the contributions of this thesis, it is necessary to outline what others have done in this research area to reach some of these objectives.

### 1.3 Related Work

With respect to bit loading, one of the most prolific research teams in this area is that of Professor John Cioffi's group of Stanford University. Although their research focuses on applying data transmission techniques to DSL modems [11–13], their algorithms can also be applied to other MCM systems, such as WLAN systems. With respect to bit loading, Cioffi's algorithm and all its variants focus on an approximation of the channel capacity to define a non-integer number of bits per subcarrier. This expression is then used as a foundation for a number of different problems that perform bit loading. More information regarding this form of bit loading is found in Section 2.4.1. However, these bit loading algorithms suffer from two problems: error due to truncation/rounding, and error introduced by the expression. In the former, the expression yields a value for the number of bits that required some sort of rounding to make it an integer. The latter is due to the expression itself, which uses the Shannon capacity expression to compute the number of bits required to achieve a specific probability of error. However, this expression uses a number of approximations to achieve this and thus some errors are introduced. Overall, the combination of these two sources of error may lead to a solution that is far from the optimal. On the positive side, this type of algorithm is fast since it can quickly compute the solution using a closed-form expression.

Fasano, Zucchi, Baccarelli, and Biagi proposed a number of power loading algorithms that attempt to avoid violations of the power constraints imposed by regulatory agencies [15–19]. In particular, they impose a subcarrier power constraint on each subcarrier such that when power is allocated, it cannot exceed this constraint. As a result, violations will not occur. However, the power constraints imposed by the regulatory agencies are usually specified over a bandwidth. In many cases, including that of the wireless network standards IEEE 802.11a and ETSI HiperLAN/2, this bandwidth may contain several subcarriers. Therefore, their algorithm may be too strict due to the lack of flexibility of distributing power across a subband, as permitted by regulations. Thus the advantages of adaptive power loading are not fully realized.

For the design of equalizers in MCM systems, Van Acker proposed a number of design

methods for creating channel shortening time-domain equalizers (TEQ) used in tandem with single-tap frequency-domain equalizers (FEQ), as well as a transformation method to convert a TEQ into a collection of equal-length multi-tap FEQs [20, 21]. The former was also proposed by Benvenuto, Tomasin, and Tomba [22]. However, when multi-tap FEQs are designed, in all previous works they have been of the same lengths across all the subcarriers.

There has been some activity in the area of employing multiple antennas in hopes of improving the system's error robustness, both in single carrier and multicarrier systems. However, a number of researchers are investigating ways by which to reduce complexity of the system by performing antenna selection diversity at the transmitter and/or receiver. Blum [23–25], Gorokhov [26, 27], and Molisch [28–33] are actively pursuing designs of wireless data transmission systems that perform antenna subset selection, where only a subset of all the available antennas are chosen to be active. By choosing a subset of antennas, the computational complexity of the array processing algorithms is reduced and the power consumption for the system decreases. However, single carrier systems are mostly investigated, assuming flat fading channel paths and without loading of any sort. Moreover, the antenna subset selection schemes proposed only look at choosing a fixed antenna subset size rather than searching all possible antenna configurations.

## 1.4 Thesis Contributions

This dissertation presents the following novel contributions in the area of digital communications, data transmission, and signal processing for communication systems:

- A discrete bit loading scheme that performs the bit allocation in an incremental fashion. Starting with the largest modulation scheme employed on all subcarriers, the subcarrier signal constellation of the worst-performing is reduced in size at every iteration until the mean probability of bit error goes below a threshold. Unlike in the literature, this algorithm decreases rather than increases the size of the signal constellation, making it more advantageous at higher SNR values by initializing the allocation closer to the final allocation. Moreover, the subcarrier error probabilities are used as a metric of subcarrier performance.
- A low-complexity discrete bit loading algorithm that exploits the relationship between

the peak bit error rate (BER) allowed per subcarrier and the mean probability of error. By varying the peak BER limit, the mean probability of error will also change. Modifying the peak BER limit in an intelligent fashion will result in a final allocation faster than most incremental algorithms with a solution closer to the optimal relative to algorithms employing closed-form expressions for the bit allocation.

- A realistic power loading algorithm that obeys a frequency interval power constraint. The algorithm allocates power to the subcarriers according to a number of rules and then applies a sliding frequency window to check for violations of regulatory requirements. Whenever a violation occurs, the algorithm quickly modifies the power levels of the subcarriers located in that frequency window until there are no more violations. This is different relative to algorithms employing a total power constraint, which does not guarantee a compliant system, and to subcarrier-constrained systems, which are too strict in limiting the power.
- An algorithm that efficiently distributes equalizer taps across the subcarriers in a non-uniform fashion. Since the channel is usually frequency-selective, the distortion in each subcarrier is different, thus requiring equalizers of different lengths to reduce the overall distortion to below some prescribed level. By doing this instead of keeping the number of taps fixed per subcarrier, the overall number of equalizer taps employed by the system is kept small, putting the available taps to good use where they are needed most.
- A suboptimal output level placement technique for the quantization of subcarrier BER values. Since look-up tables can reduce the implementation complexity of a system when determining the BER values of a subcarrier, and considering that an infinite number of SNR values are possible, a scheme is proposed to quantize the SNR values so as to reduce the granular and overload errors present in the quantization process.
- Several antenna subset selection schemes that can either operate across all subcarriers simultaneously or on a per-subcarrier basis. By combining both multiple antennas and MCM, the resulting system performance will increase. Moreover, instead of using a fixed antenna subset size, the system can employ any number of antennas at the

transmitter and receiver, unlike conventional antenna selection. Furthermore, the trade-off between complexity and performance enhancement is studied.

- A combination of the proposed antenna subset selection algorithm with peak BER bit loading algorithm. By taking advantage of both the frequency and spatial domains, it is hoped to significantly improve the throughput performance of the system while satisfying the error constraint. Unlike other implementations, nobody in the literature has employed both antenna selection and bit loading together in this fashion.

## 1.5 Thesis Organization

An extensive literature survey and tutorial of several topics covered in this dissertation are presented in Chapter 2. Specifically, an introduction to MCM and its various implementations is presented. Also included is an overview of modelling indoor wireless channels for both single antenna systems and systems employing antenna arrays. Bit and power loading is covered, with a few illustrative examples. Equalization and MCM is briefly covered, with emphasis on the optimal single-tap equalizer and the multi-tap FEQ design. Finally, an overview of different spatial processing techniques is presented.

Chapter 3 introduces the reader to the two proposed bit loading algorithms, the proposed power loading algorithm, and two proposed variable-length equalizer tap algorithms. In this chapter, all systems are studied in the context of a single antenna applied at the transmitter and the receiver. Also studied are the effects of imperfect subcarrier SNR information and its impact on the loading algorithms. The results of these algorithms, in terms of throughput performance and error robustness are compared against several algorithms found in the literature.

Chapter 4 presents the proposed antenna subset selection algorithm. Two versions of the algorithm are discussed: a signal-based algorithm, and a subcarrier-based algorithm. Then, the algorithms are extended to the case when bit loading is performed in tandem with the algorithm. Throughput results are then presented and compared for a number of channel correlations.

In Chapter 5, the research achievements of this work are outlined and topics for future work are presented.

## Chapter 2

# Multicarrier Data Transmission

The objective of this work is to enhance the error robustness of a conventional wireless multicarrier transmission system operating in a frequency-selective fading channel by modifying several of its operating parameters. To this end, the modifications must be designed in such a way that the performance gains are justified by the penalty due to an increase in implementation complexity. To fully understand what operating parameters should be modified, one must understand several important components that make up a multicarrier system. Hence, this chapter will provide some insight into the multicarrier system, its building blocks, and its associated problems and solutions. Schematics of a generic multicarrier transmitter and receiver employing multiple antennas are shown Figs. 2.1(a) and 2.1(b).

This chapter is organized as follows: an introduction to the fundamentals of multicarrier modulation (MCM) is presented and two types of MCM are examined: orthogonal frequency division multiplexing (OFDM) and filter bank multicarrier (FB-MC). The single-input/single-output and multiple-input/multiple-output channel models are then described. Next, adaptive bit and power loading algorithms are motivated followed by a summary of other works found in the literature. Channel estimation techniques for MCM systems are covered, followed by a description of multicarrier equalization methods. Finally, several schemes for employing multiple antennas in MCM systems are presented.

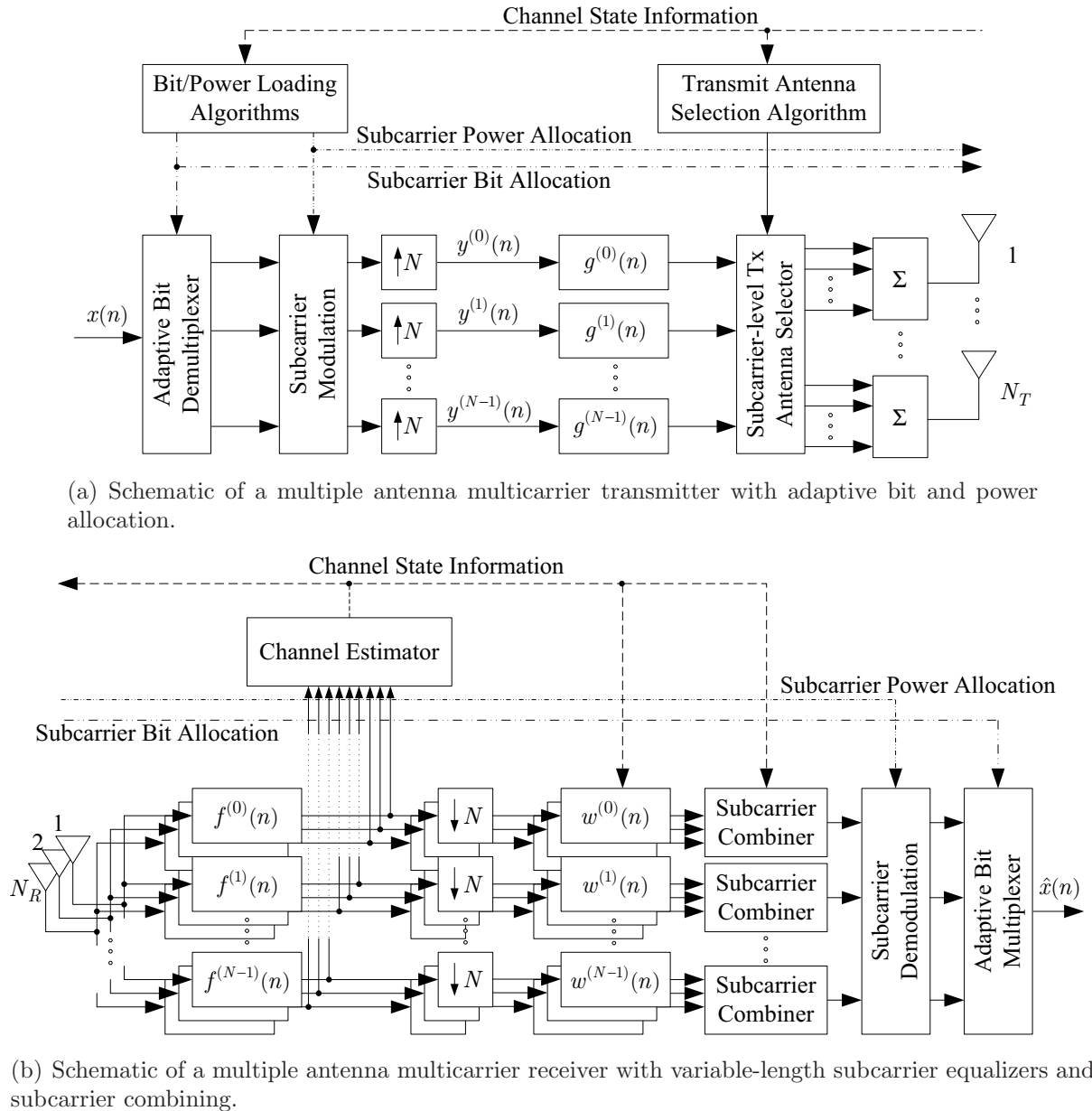
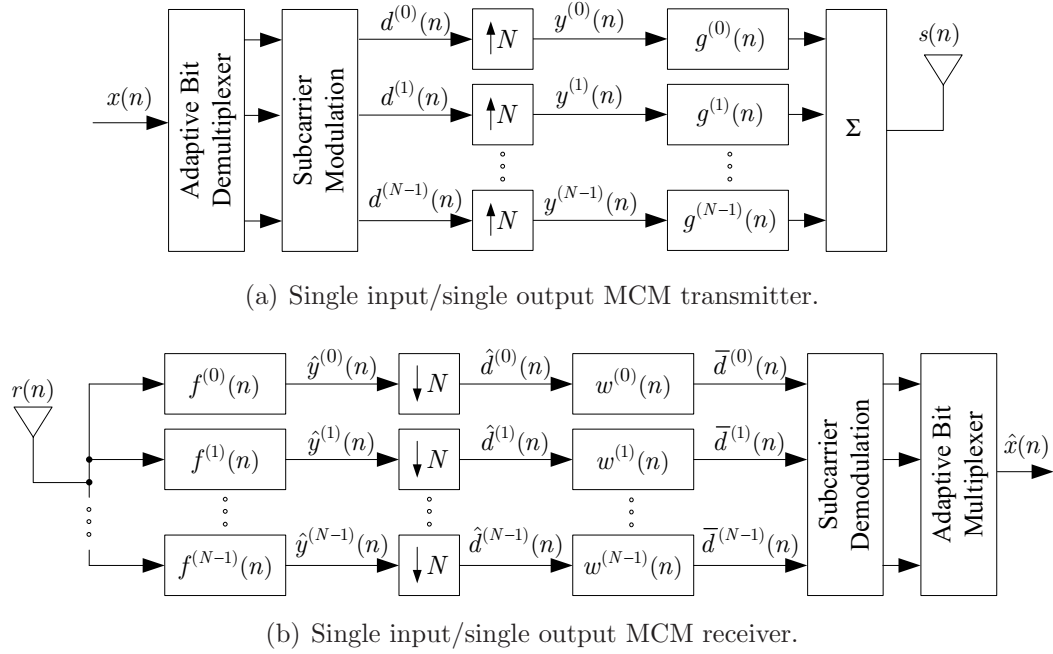


Fig. 2.1 A generic multiple input/multiple output MCM system.



**Fig. 2.2** Schematic of a generic single input/single output MCM system.

## 2.1 Multicarrier Modulation

### 2.1.1 Basic Theory

Multicarrier modulation (MCM) is a form of frequency division multiplexing (FDM), where data is transmitted in several narrowband streams at different carrier frequencies. However, unlike conventional FDM systems, where the narrowband subcarrier signals are separated by guard bands in the frequency domain [5], MCM systems allow for overlapping adjacent subcarriers when a certain set of conditions are satisfied [34–37] (see Section 2.1.3 for more information about these conditions). As a result, MCM systems are spectrally efficient.

A generic single input/single output MCM transceiver is shown in Fig. 2.2. A high-speed input data stream,  $x(n)$ , is parsed into  $N$  relatively slower streams and modulated using a prescribed signal constellation. The modulated streams,  $d^{(k)}(n)$ ,  $k = 0, \dots, N - 1$ , are then upsampled by a factor  $N$ , yielding the signals  $y^{(k)}(n)$ ,  $k = 0, \dots, N - 1$ . They are then filtered by a bank of synthesis filters,  $g^{(k)}(n)$ ,  $k = 0, \dots, N - 1$ , and the filtered

signals are summed together to form the composite transmit signal,  $s(n)$ , namely

$$s(n) = \sum_{k=0}^{N-1} \sum_{l=-\infty}^{\infty} g^{(k)}(l)y^{(k)}(n-l). \quad (2.1)$$

Equivalently, in the frequency domain, the manipulation of the subcarrier signals at the transmitter are outlined in Fig. 2.3 for an  $N = 8$  subcarrier MCM system<sup>1</sup>. For example, given  $d^{(1)}(n)$  in Fig. 2.3(a), its spectrum is compressed by a factor of 8 and repeated in frequency due to upsampling, to yield  $y^{(1)}(n)$ , as depicted in Fig. 2.3(b). Then a copy of the compressed spectrum from each subcarrier is bandpass-filtered and placed at the corresponding center frequencies, as shown in Fig. 2.3(c), forming the composite transmit signal  $s(n)$ . Thus the MCM transmitter is converting a parallel set of signals in the time domain into a parallel set of signals in the frequency domain using a combination of upsamplers and synthesis filters.

Between the transmitter and receiver lies a channel which introduces both noise (due to thermal excitation of the RF chain and antennas, atmospheric conditions, and interference from artificial and natural sources) and distortion (mainly due to multipath propagation) to the composite transmit signal. Although this topic will be discussed in greater detail in Section 2.2, it should be mentioned that the channel can be modelled as a finite impulse response (FIR) filter that possesses a frequency-selective fading characteristic (see Fig. 2.3(d)). As a result, when  $s(n)$  passes through the channel, assuming for now that no noise is present, the channel attenuates the spectrum of  $s(n)$  non-uniformly in frequency, as shown in Fig. 2.3(e).

At the receiver, a bank of analysis filters,  $f^{(k)}(n)$ ,  $k = 0, \dots, N - 1$ , are employed to separate the subcarriers out of the received composite signal,  $r(n)$ , into  $N$  individual signals,  $\hat{y}^{(k)}(n)$ ,  $k = 0, \dots, N - 1$ . These signals are then downsampled by a factor of  $N$ , yielding  $\hat{d}^{(k)}(n)$ ,  $k = 0, \dots, N - 1$ . To remove the distortion introduced by the channel, equalizers  $w^{(k)}(n)$ ,  $k = 0, \dots, N - 1$ , are employed on a per-subcarrier basis<sup>2</sup>. Several equalizer design approaches for MCM systems are discussed in Section 2.5. The outputs

<sup>1</sup>The diagram of Fig. 2.3, for simplicity, does not show any overlap between the adjacent subcarriers. However, MCM systems are capable of allowing overlap of the subcarriers. The spectral subcarrier shapes are intentionally exaggerated to identify the different subcarriers.

<sup>2</sup>Although linear per-subcarrier equalizers have been employed in Fig. 2.2(b), decision-feedback equalizers on each subcarrier [38] or per-subcarrier Tomlinson-Harashima precoding schemes [22, 39, 40] can also be used.

of the subcarrier equalizers,  $\bar{d}^{(k)}(n)$ ,  $k = 0, \dots, N - 1$ , are then demodulated and the resulting binary sequences combined using a multiplexer, yielding the reconstructed high-speed output  $\hat{x}(n)$  [5, 10, 41].

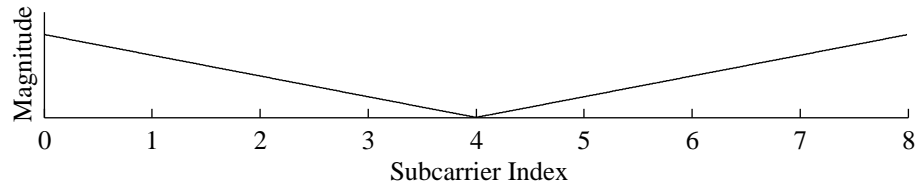
Although the modulation and demodulation stages of an MCM system are usually more complex relative to a single carrier system, MCM systems possess a number of advantages due to their “divide-and-conquer” nature in the frequency domain. Since the channel usually does not have a flat frequency response, it is easier to compensate for the channel distortion on a per-subcarrier basis rather than on the entire received signal, as will be shown in Section 2.5. Moreover, since the channel distortion may not be equivalent for all subcarriers, adapting the transmission parameters per subcarrier (i.e., signal constellation and transmit power levels) would allow for increased throughput while guaranteeing a prescribed error performance.

A thorough comparison between single carrier and multicarrier systems was performed by Saltzberg using a number of criteria, as summarized in Table 2.1 [42]<sup>3</sup>. There is little difference in performance between single carrier and multicarrier systems since the latter can be interpreted as a linear reversible transformation of the former. However, there are a number of practical differences. For instance, multicarrier systems can perform adaptive bit loading in a straightforward fashion, which can enhance system performance with respect to maximizing throughput or increasing error robustness. However, multicarrier systems are more sensitive to the effects of narrowband noise, amplitude clipping, timing jitter, and delay. With respect to the computational complexity, FFT-based multicarrier systems employing frequency-domain single-tap subcarrier equalizers usually use fewer multiplications and additions per unit time relative to single carrier systems, which require lengthy equalizers to eliminate the distortion introduced by the channel. As a result, multicarrier systems have fewer computations per unit time. On the other hand, when the multicarrier system performs adaptive bit loading, the complexity of the algorithm increases relative to a single carrier system due to the iterative search performed by the system for the appropriate subcarrier signal constellations.

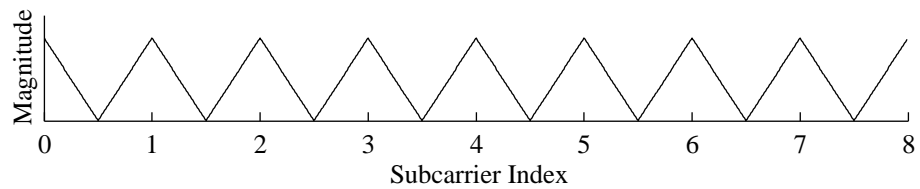
There exists a number of MCM implementations, as shown in Table 2.2. The implementations have been divided into two categories, depending on the choice of filters employed

---

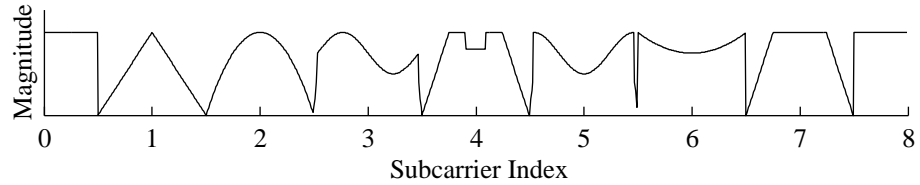
<sup>3</sup>The single and multicarrier implementations studied are based on ADSL systems, with the single carrier system employing decision feedback equalizers with Tomlinson filtering, while the multicarrier system used frequency-domain, single-tap subcarriers equalizers and adaptive bit loading.



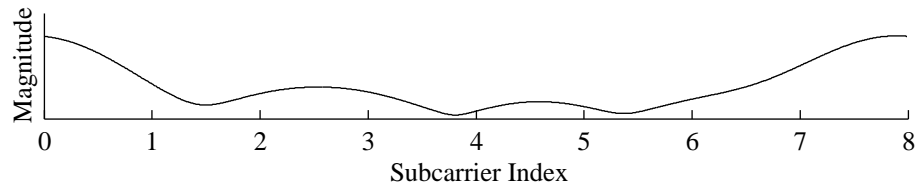
(a) Spectrum of the second subcarrier prior to upsampling.



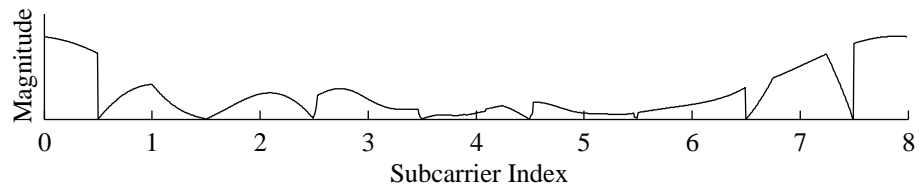
(b) Spectrum of the second subcarrier after upsampling by a factor of 8.



(c) Spectrum of the composite transmit signal.



(d) Example of a frequency-selective fading channel spectrum.



(e) Impact of frequency-selective fading channel on the composite transmit signal spectrum.

**Fig. 2.3** The effects of an 8-subcarrier MCM transmitter and frequency-selective fading channel on the individual subcarrier spectra.

**Table 2.1** Relative advantages of single carrier and multitone modulation (for type of MCM) for ADSL, where ✓ denotes the system with better performance or lower cost (from [42])

Issue	Single Carrier	Multitone	Equivalent
Performance in Gaussian noise			✓
Sensitivity to impulse noise (uncoded)		✓	
Sensitivity to narrowband noise (uncoded)	✓		
Sensitivity to clipping	✓		
Sensitivity to timing jitter	✓		
Latency (delay)	✓		
Need for echo cancellation	✓		
Computations per unit time		✓	
Complexity of algorithm	✓		
Cost and power consumption in analog sections	✓		
Adaptability of bit rate		✓	

by the analysis and synthesis filterbanks. The first category contains implementations that use the discrete Fourier transform in the filterbank implementation. This type of MCM implementation is widely employed in a number of wireless and wireline applications due to its efficient implementation involving the fast Fourier transform (FFT). The other category is based on employing bandpass filters at the synthesis and analysis filterbanks. The technique by which the filterbanks are created define each of the implementations in this category. For instance, most implementations modulate a single prototype lowpass filter to different center frequencies in order to keep the cost of designing the filters low.

Each implementation possesses a number of advantages and disadvantages. In the following sections, details for several of these implementations will be presented.

### 2.1.2 Orthogonal Frequency Division Multiplexing

The first implementation is an extremely popular one due to its efficient hardware implementation using the FFT and the inverse FFT (IFFT). Known in wireless applications as *orthogonal frequency division multiplexing* (OFDM) [22, 43–78], or in wireline applications as *discrete multitone* (DMT) [11–13, 15–17, 20, 21, 37, 79–89], these systems use discrete Fourier transform (DFT) basis functions to create the synthesis and analysis filterbanks.

**Table 2.2** Several implementations of multicarrier systems

Name	Description
<i>Discrete Fourier Transform-based Multicarrier</i>	<p>Employs the discrete Fourier transform basis functions to modulate subcarriers to different center frequencies. This can be efficiently implemented using FFTs.</p> <p>Several examples are:</p> <ul style="list-style-type: none"> <li>• <i>Orthogonal Frequency Division Multiplexing</i> (OFDM) is the name given to this technique when used in wireless applications.</li> <li>• In wireline applications, this technique is called <i>Discrete Multitone</i> (DMT).</li> </ul>
<i>Filterbank Multicarrier</i>	<p>Employs bandpass filters at both the transmitter and the receiver to filter the subcarriers prior to combining them and separating them, respectively.</p> <p>Several examples are:</p> <ul style="list-style-type: none"> <li>• <i>Complex Exponential-Modulated Filterbanks</i> modulates a prototype lowpass filter to different center frequencies using complex exponentials.</li> <li>• <i>Cosine-Modulated Filterbanks</i> modulates a prototype lowpass filter to different center frequencies using cosines.</li> <li>• <i>Transmultiplexers</i> are filterbanks used in multirate signal processing. They are the duals of subband coders.</li> <li>• <i>Perfect Reconstruction Filterbanks</i> are designed to eliminate cross-talk under ideal channel conditions.</li> <li>• <i>Oversampled Filterbanks</i> employ a sampling factor higher than the total number of subcarriers.</li> <li>• <i>Modified Discrete Fourier Transform Filterbanks</i> delay either the real or imaginary components of each subcarrier signal with respect to each other to minimize cross-talk.</li> </ul>

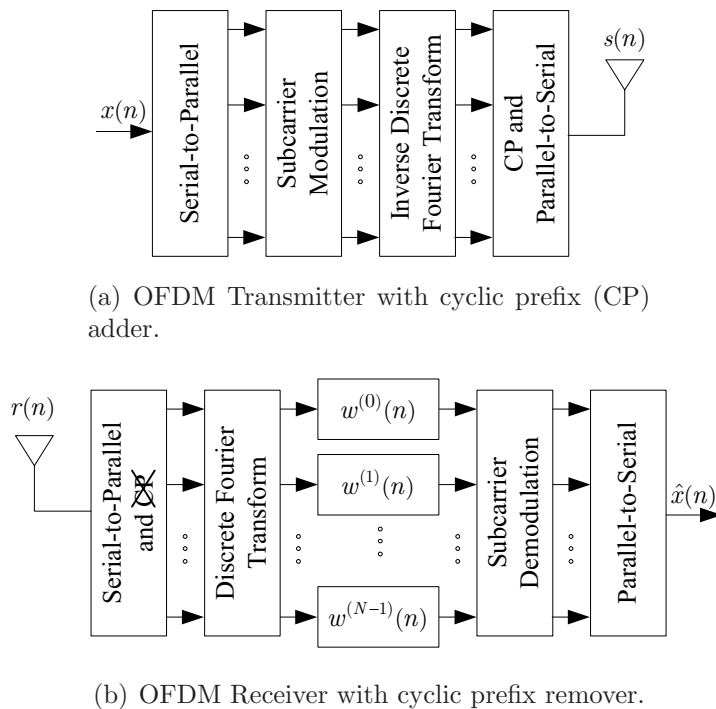


**Fig. 2.4** Schematic of an OFDM system employing a cyclic prefix.

The filters in the filterbanks are *odd-stacked*, which means they are uniformly distributed throughout the frequency domain, with one filter centered at  $\omega_0 = 0$  rad/s. Although OFDM systems could be implemented using a bank of sinusoid generators [90], practical implementations employ the FFT and IFFT, which results in a significant complexity reduction [43]. As a result, OFDM/DMT has become a popular choice in many multicarrier applications, including digital audio broadcast (DAB), digital subscriber line (DSL), digital video broadcast (DVB), and wireless local area networks (WLAN) such as the IEEE 802.11a/g, the ETSI HiperLAN/2, and the MMAC HiSWAN.

A schematic of an OFDM transceiver is shown in Fig. 2.4. A high-speed input stream  $x(n)$  is first demultiplexed into  $N$  data streams,  $x^{(k)}(n)$ ,  $k = 0, \dots, N-1$ , using a serial-to-parallel converter, where  $x^{(k)}(n)$  is the subcarrier data for subcarrier  $k$ . These streams are then individually modulated using  $M$ -QAM constellations, to yield  $y^{(k)}(n)$ ,  $k = 0, \dots, N-1$ , where  $y^{(k)}(n)$  is the  $M$ -QAM-modulated subcarrier data for subcarrier  $k$ . The inverse

DFT (IDFT) is then applied to the subcarriers, defined as [91]

$$s^{(l)}(n) = \frac{1}{N} \sum_{k=0}^{N-1} y^{(k)}(n) e^{j2\pi kl/N} \quad (2.2)$$

where  $l = 0, \dots, N - 1$ , resulting in the subcarriers being modulated to one of  $N$  evenly spaced center frequencies in the range  $[0, 2\pi)$ .

Before the subcarriers are converted to form the composite signal,  $s(n)$ , it is necessary to add some redundancy in order to compensate for one of the main disadvantages of OFDM: low spectral selectivity. Since OFDM employs the DFT and its inverse, the filters applied to the subcarriers have a low stopband attenuation since the frequency response of the filters are of the form  $\text{sinc}(x)$ . Therefore, the performance of the OFDM system would significantly decrease if it were operating in a time-dispersive environment. To counteract the time-dispersiveness of the channel, a cyclic extension is employed either before the symbol (i.e., cyclic prefix) or after it (i.e., cyclic suffix) to capture this effect (the details of how the cyclic extension works will be discussed in the following subsection). Without loss of generality, the system will add a cyclic prefix to the OFDM symbol.

At the receiver, the cyclic prefix is removed from the received composite signal,  $r(n)$ , and converted from a serial stream into a collection of parallel streams using a serial-to-parallel converter. The DFT is applied [91]

$$\hat{y}^{(k)}(n) = \sum_{l=0}^{N-1} r^{(l)}(n) e^{-j2\pi kl/N} \quad (2.3)$$

for  $k = 0, \dots, N - 1$ , where  $r^{(k)}(n)$ ,  $k = 0, \dots, N - 1$ , are the parallel input streams to the DFT. The subcarriers are then equalized with  $w^{(k)}(n)$ ,  $k = 0, \dots, N - 1$ , to compensate for the distortion introduced by the channel. The equalized subcarriers are then demodulated before being multiplexed together using the parallel-to-serial converter, forming the output  $\hat{x}(n)$ .

One of the first papers on the implementation of OFDM systems was by Weinstein and Ebert [43]. They were the first to use the DFT as a replacement to the banks of sinusoid generators traditionally employed in multicarrier systems up to that time. Hirosaki [45] extended the work of Saltzberg [90] by implementing his offset QAM system in an OFDM framework using DFT blocks. Siohan *et al.* [92] further enhanced the OFDM-offset QAM

**Table 2.3** Mode-dependent parameters for IEEE 802.11a and HiperLAN/2 (from [94])

Mode	Modulation	Code Rate $R$	Nominal Bit Rate [Mb/s]
1	BPSK	1/2	6
2	BPSK	3/4	9
3	QPSK	1/2	12
4	QPSK	3/4	18
5	16QAM	9/16	27
5	16QAM (H/2 only)	1/2	24
6	16QAM (IEEE only)	3/4	36
7	64QAM	3/4	54
8	64QAM	2/3	48

framework of Hirosaki [45] by employing filterbank theory to derive a condition for discrete orthogonality. Channel coding in OFDM systems was proposed by Zou and Wu [46] while vector coded OFDM was implemented by Diggavi [93].

Since the target application of this dissertation is WLAN systems, it is necessary to quickly survey current WLAN implementations. Of these, three WLAN standards that employ OFDM at the core of their design are the IEEE 802.11a, the IEEE 802.11g, and the ETSI HiperLAN/2 standards. In particular, the IEEE 802.11a and the ETSI HiperLAN/2 standards were both designed to possess a similar physical (PHY) layer implementation and set of operating modes, as shown in Table 2.3. As a result, the bit error rate performance was shown to be relatively similar [94]. However, the packet error rate performance of the two systems, for which the system's medium access control (MAC) layer plays a major role, was shown to be substantially different. In particular, HiperLAN/2 possessed the superior performance because of its centrally controlled MAC, unlike IEEE 802.11a, which employed carrier-sense multiple access with collision avoidance (CSMA/CA) [94]. A more detailed analysis of HiperLAN/2 was presented by Khun-Jush *et al.* [95]. As for the IEEE 802.11g standard, it is the multicarrier successor to the commercially successful IEEE 802.11b standard, which also operates in the 2.4 GHz Industrial, Scientific, Medical (ISM) band [96]. This standard is backwards compatible to the IEEE 802.11b standard and supports data rates of up to 54 Mb/s. Finally, the idea of implementing multicarrier extensions of current wireless standards has also been applied to the IEEE 802.16 wireless metropolitan area network (WMAN) standard, resulting in the IEEE 802.16a standard [97].

Finally, there exists a research community that is actively designing various hardware prototype OFDM-based WLAN systems with similar parameters to current standards and possessing enhanced system performance. For instance, the Interuniversity Micro Electronics Center (IMEC) of Belgium has been working on the design of several WLAN hardware implementations, including one capable of achieving 80 Mb/s [73, 74]. However, this increase in throughput was achieved by using 128 subcarriers instead of the 64 found in HiperLAN/2 or IEEE 802.11a. Moreover, several hardware prototypes have been implemented that employ multiple antennas, resulting in significant performance enhancements [98, 99].

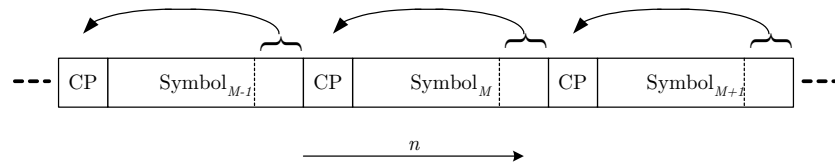
### OFDM with Cyclic Extension

As mentioned previously, the synthesis and analysis filters of OFDM have relatively poor spectral selectivity. Thus, a cyclic extension is appended to the OFDM symbol to compensate. Otherwise, the intersymbol interference of adjacent OFDM symbols due to the time dispersive channel will degrade the error performance of the system. Although a buffer of zeros would suffice in preventing the intersymbol interference [100, 101], the use of a cyclic extension has the added benefit of simplifying the design of an optimal subcarrier frequency-domain equalizer (see Section 2.5.3 for details).

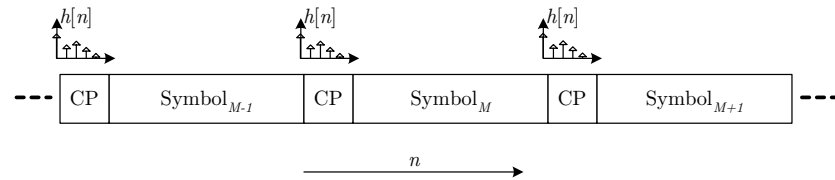
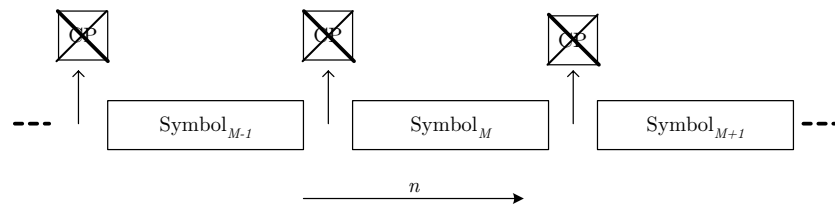
A graphical representation of how a cyclic extension functions is shown in Fig. 2.5. In this case, the cyclic prefix is created by copying the end of the OFDM symbol and placing that copy at the beginning of the symbol, for every symbol. This process is shown in Fig. 2.5(a).

With the channel impulse response (CIR) modelled as an FIR filter  $h(n)$ , the CIR is convolved with a sampled version of the transmitted signal with the included CP. As a result, the CIR spreads the samples of symbol  $M - 1$  onto the samples of symbol  $M$ , while the samples of symbol  $M$  will be spread onto the samples of symbol  $M + 1$ . However, observing Fig. 2.5(b), if the CP is of sufficient length to capture all the interference due to the CIR, the symbols only experience the spreading of samples from within their own symbol. At the receiver, the CP is removed, as shown in Fig. 2.5(c), and the OFDM symbols proceed with demodulation and equalization.

Despite the usefulness of the cyclic prefix, there are several disadvantages. First, the length of the cyclic prefix must be sufficient to capture the effects of the CIR. If not, the cyclic prefix fails to prevent distortion introduced from other symbols. The second



(a) Add cyclic prefix to an OFDM symbol.

(b) Spreading by channel impulse response  $h(n)$  from previous symbol into cyclic prefix.

(c) Removal of cyclic prefix.

**Fig. 2.5** The process of adding, capturing the intersymbol interference, and removal of a cyclic prefix.

disadvantage is the amount of overhead introduced by the cyclic prefix. By adding more samples to buffer the symbols, we must send more information across the channel to the receiver. This means to get the same throughput as a system without the cyclic prefix, we must transmit at a higher data rate.

### 2.1.3 Filterbank Multicarrier Systems

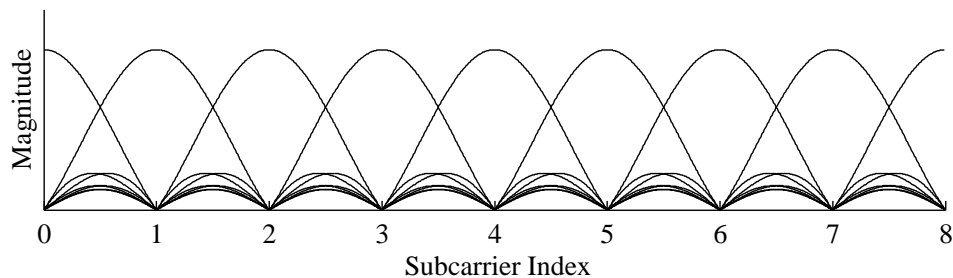
Although an OFDM system can possess a computationally-efficient implementation, it also has several drawbacks, of which poor spectral selectivity being the worst. The use of a cyclic extension to prevent the intersymbol interference, although effective, requires a significant amount of overhead in terms of the addition of redundant information to the transmitted signal. One solution to this problem is to employ an MCM system that uses synthesis and analysis filters with relatively high spectral selectivity. For instance, Rizos, Proakis, and Nguyen showed that the interference due to overlapping frequency responses

of the subcarrier filters in a DMT system was worst relative to a cosine-modulated filterbank system when no pre-receiver processing (e.g., cyclic extension with a time-domain equalizer) were employed [102]. Only when the DMT system employs pre-receiver processing while operating in a linearly distorted channel (additive white Gaussian noise and near-end crosstalk (NEXT)) does its performance exceed that of the cosine-modulated filterbank system at the cost of reduced throughput. This is the motivation of the second implementation called *filterbank multicarrier* (FB-MC) [34, 39, 103–120].

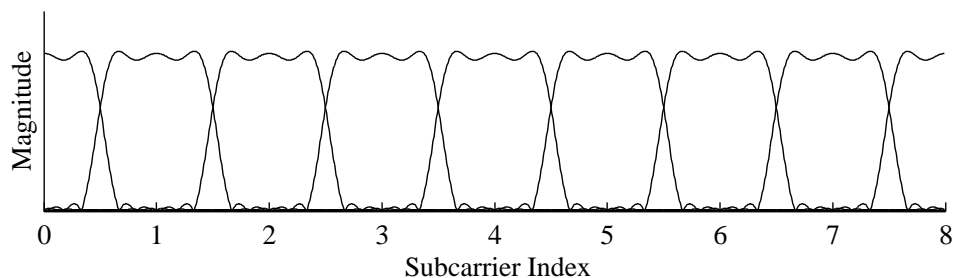
In FB-MC, a set of synthesis and analysis filters are designed such that they have both adequate spectral selectivity and bandwidth efficiency. Although each filter could be designed on an individual basis, a more efficient approach is to design a single prototype lowpass filter and then modulate it to several specified center frequencies in order to generate the synthesis and analysis filters  $g^{(k)}(n)$  and  $f^{(k)}(n)$ ,  $k = 0, \dots, N - 1$ . Usually the filters are uniformly spaced, designed to be highly spectrally selective to minimize crosstalk with adjacent subcarriers, and can either be odd-stacked or *even-stacked*, i.e., no center frequency at  $\omega_0 = 0$  rad/s. For example, in Fig. 2.6 the subcarrier frequency responses of the synthesis filters for an OFDM system and an FB-MC system employing square-root raised cosine filters is shown for  $N = 8$  subcarriers. Notice how in Fig. 2.6(a) the sidelobe levels are significantly higher to the sidelobe levels found in Fig. 2.6(b). With respect to cyclic extensions, FB-MC systems usually need to introduce equalization strategies in order to mitigate intersymbol and intercarrier interference, especially when they operate in a critically sampled mode, since a cyclic extension is not applicable.

Referring to the schematic of a generic single input/single output MCM system in Fig. 2.2, a high-speed input stream  $x(n)$  is first demultiplexed into  $N$  data streams and individually modulated using a specified signal constellation, resulting in the modulated data streams,  $d^{(k)}(n)$ ,  $k = 0, \dots, N - 1$ . The subcarriers are then upsampled by  $N$  before being filtered by the synthesis filters  $g^{(k)}(n)$ ,  $k = 0, \dots, N - 1$ , and summed together, forming  $s(n)$ . At the receiver, the received composite signal,  $r(n)$ , is separated into the  $N$  subcarriers using the analysis filterbank, then the subcarriers are downsampled by a factor  $N$  and equalized before being demodulated and multiplexed together, forming the reconstructed output signal,  $\hat{b}(n)$ .

Scaglione, Barbarossa, and Giannakis [111] developed a unifying framework for multicarrier systems. Similarly, Akansu *et al.* [114] also proposed a unifying transmultiplexer framework for various communications systems. Scaglione, Barbarossa, and Giannakis then



(a) OFDM subcarrier spectrum.



(b) FB-MC subcarrier spectrum (employing a square-root raised cosine prototype lowpass filter with a rolloff of 0.25).

**Fig. 2.6** Subcarrier spectra of  $N = 8$  OFDM and FB-MC systems.

extended their framework to include blind channel estimation, block synchronization, and equalization while not imposing restrictions on the location of channel zeros [112]. They also derived the optimal FIR transmit and receive filterbanks for their unifying framework [121].

Observing the subcarrier filter spectra in Fig. 2.6, all of the filters overlap with the adjacent filters, which may give rise to distortion. However, if these filters satisfy certain conditions, it is possible to have distortionless transmission between the transmitter and receiver even if the subcarriers overlap.

### Perfect Reconstruction Filterbanks

In an ideal case, when a collection of bandpass filters are employed and spectral efficiency is a concern, the filters can be designed to have a narrow transition bandwidth and a high stopband attenuation. When placed side-by-side in a non-overlapping fashion, the interference between adjacent filters, known as *cross-talk*, is minimized. However, this type of filter design is very complicated and difficult to realize in hardware.

An alternative approach is to design a single prototype lowpass filter and modulate

copies of it to different center frequencies. The prototype lowpass filter design parameters, such as the passband and transition bandwidth, as well as the center frequencies and relative phases between adjacent filters are chosen such that it is possible to realize a filterbank system whose output signal is exactly the same as the input signal. Such filterbanks are referred to as *Perfect Reconstruction* (PR) filterbanks.

Suppose that the transfer matrix between the input and output subcarriers of an MCM system operating in an ideal channel is defined as

$$\mathbf{S}(z) = \mathbf{E}(z)\mathbf{\Gamma}(z)\mathbf{R}(z) \quad (2.4)$$

where  $\mathbf{\Gamma}(z)$  is the parallel-to-serial-to-parallel conversion matrix between the synthesis and analysis filterbanks, while  $\mathbf{E}(z)$  and  $\mathbf{R}(z)$  are the polyphase matrix representations of the analysis and synthesis filterbanks  $f^{(k)}(n)$  and  $g^{(k)}(n)$ ,  $k = 0, \dots, N-1$ , respectively. In turn, the matrices  $\mathbf{E}(z)$  and  $\mathbf{R}(z)$  are defined as

$$\mathbf{E}(z) = \begin{pmatrix} E_{00}(z) & E_{01}(z) & \cdots & E_{0,N-1}(z) \\ E_{10}(z) & E_{11}(z) & \cdots & E_{1,N-1}(z) \\ \vdots & \vdots & \ddots & \vdots \\ E_{N-1,0}(z) & E_{N-1,1}(z) & \cdots & E_{N-1,N-1}(z) \end{pmatrix} \quad (2.5)$$

and

$$\mathbf{R}(z) = \begin{pmatrix} R_{00}(z) & R_{01}(z) & \cdots & R_{0,N-1}(z) \\ R_{10}(z) & R_{11}(z) & \cdots & R_{1,N-1}(z) \\ \vdots & \vdots & \ddots & \vdots \\ R_{N-1,0}(z) & R_{N-1,1}(z) & \cdots & R_{N-1,N-1}(z) \end{pmatrix}. \quad (2.6)$$

where the polyphase components of Eq. (2.5) are specified by

$$E_{kl}(z) = \sum_{n=-\infty}^{\infty} f^{(k)}(Nn+l)z^{-n}. \quad (2.7)$$

As for Eq. (2.6), assuming that  $\mathbf{E}(z)$  is *para-unitary*, i.e.,  $\tilde{\mathbf{E}}(z)\mathbf{E}(z) = d\mathbf{I}$  for some  $d >$

0 [35]<sup>4</sup>, and  $g^{(k)}(n) = f^{(k)}(-n)$ , the polyphase components of  $\mathbf{R}(z)$  can be specified as

$$R_{kl}(z) = E_{k,N-1-l}(z). \quad (2.8)$$

Given that  $\mathbf{\Gamma}(z)$  is defined as

$$\mathbf{\Gamma}(z) = \begin{bmatrix} \mathbf{0} & 1 \\ z^{-1}\mathbf{I}_{N-1} & \mathbf{0} \end{bmatrix}, \quad (2.9)$$

the sufficient condition for PR was specified by Vaidyanathan as [35]

$$\mathbf{S}(z) = cz^{-n_0}\mathbf{I}_N \quad (2.10)$$

or equivalently

$$\mathbf{R}(z)\mathbf{E}(z) = cz^{-n_0} \begin{bmatrix} \mathbf{0} & \mathbf{I}_{N-1} \\ z^{-1} & \mathbf{0} \end{bmatrix} \quad (2.11)$$

for an appropriate choice of integer  $n_0$ . Note that  $\mathbf{I}_N$  is the  $N \times N$  identity matrix.

Although it is possible to eliminate distortion due to the synthesis and analysis filterbanks under ideal circumstances, it is difficult to achieve this when all the filters are based on a single FIR prototype lowpass filter since there are few filters that satisfy Eq. (2.10). Furthermore, the elimination of distortion works well when the channel is ideal. However, when the channel also introduces distortion, PR will not be achievable with channel-independent filterbanks.

### Complex Exponential-Modulated Filterbanks

One efficient technique of creating the synthesis and analysis filterbanks is to modulate a prototype lowpass filter  $p(n)$  of length  $P$  from the center frequency of  $\omega_0 = 0$  rads to the center frequencies  $\omega_k$ ,  $k = 1, \dots, N - 1$ , by multiplying  $p(n)$  with a complex exponential [104, 107, 120]. The modulation to  $\omega_k$  occurs since multiplying a sequence by a complex exponential in the time domain is equivalent to shifting the frequency response of the sequence in the frequency domain.

---

<sup>4</sup>The *para-conjugate* of  $\mathbf{E}(z)$  is  $\tilde{\mathbf{E}}(z) = \mathbf{E}_*(z^{-1})^T$ , where the subscript  $(\cdot)_*$  denotes conjugation of the coefficients.

Therefore, the expressions for modulating the synthesis and analysis filterbanks using complex exponentials is given by [34, 35]

$$g^{(k)}(n) = p(n - \delta_k) \exp [j\omega_k (n - \delta_k) + \alpha_k], \quad k = 0, \dots, N - 1 \quad (2.12)$$

and

$$f^{(k)}(n) = p(n - \eta_k) \exp [j\omega_k (n - \eta_k) + \beta_k], \quad k = 0, \dots, N - 1 \quad (2.13)$$

where  $\alpha_k$  and  $\beta_k$  are the phase angles,  $\delta_k$  and  $\eta_k$  are the delays, and  $\omega_k$  is the center frequency.

According to the study of bandwidth-efficient filterbank transmultiplexers by Ramachandran and Kabal [34, 108, 109], five different implementations of transmultiplexers, where the system achieves PR under ideal channel conditions, were proposed. Three of those implementations were multicarrier QAM systems while the other two were vestigial sideband implementations. Referring to Eqs. (2.12) and (2.13), the parameters that defined each implementation were the center frequency spacing and the bandwidth of the prototype lowpass filter. Hence, the transfer function of the system was derived and the values for the relative phase relationship between adjacent subcarriers and the delays of the synthesis and analysis filters were set in order to eliminate cross-talk (i.e., cross-talk between the subcarrier filters).

Louveaux [103] investigated the use of filterbanks as a replacement for OFDM in xDSL modems and he developed a general multicarrier framework for this application. Wornell presented a multirate filterbank system employing fast lapped transforms that resulted in an efficient multitone modulation scheme [110]. Finally, modulated filterbanks were studied by Cherubini *et al.* [39, 40], as well as Borna and Davidson [122], for use in xDSL modems. In particular, they both used filtered multitone to implement the filterbanks, where a prototype lowpass filter is modulated using the discrete Fourier transform (i.e., a collection of complex exponential weights). However, unlike *critically sampled* filterbanks, i.e., the upsampling factor is equal to the number of subcarriers employed in the system, these proposed modulated filterbanks focus on *oversampled* implementations, i.e., the upsampling factor is greater than the number of subcarriers.

### Oversampled Filterbanks

Under ideal conditions, critically-sampled filterbanks are capable of eliminating cross-talk when the appropriate analysis and synthesis filters have been chosen. However, when a dispersive channel is present, the system does not have much leeway to compensate for the distortion introduced by the channel. Thus, to provide some additional redundancy to the system in order to combat the distortion introduced by the channel, many systems have been proposed that employ oversampled filterbanks. For instance, Scaglione, Barbarossa, and Giannakis introduced a provision for oversampling in their unifying framework for filterbanks [111]. Thus, the additional degrees of freedom introduced in the design process of the system could potentially lead to an increase in system performance. One example where oversampling is employed is in multicarrier code division multiple access systems.

Oversampled filterbanks can be translated into one of several implementations. For instance, an oversampled system may have its subcarriers spaced out more relative to a critically-sampled system since there are fewer subcarriers given the same sampling rate. As a result, there is more of a buffer between subcarriers at the cost of a less bandwidth-efficient system. Another example of oversampled filterbanks, which will be discussed further in Section 2.4, deals with “turning off” poorly performing subcarriers. Thus, the system can improve its error robustness at the cost of some bandwidth.

Lin and Akansu [115] presented a non-maximally decimated multirate filterbank structure that is employed in conjunction with blind channel identification and optimal MMSE equalization. The system possesses a precoder structure at the transmitter, which includes both the analysis and synthesis filters, while a subcarrier MMSE equalizer is employed at the receiver to reverse the effects of intersymbol interference. Lin and Phoong [123] determine the minimum amount of redundancy that needs to be added to an FIR transceiver operating in non-ideal channel conditions in order to achieve total intersymbol interference mitigation. Finally, Milanovic *et al.* looked at the design of robust oversampled precoding filterbank structures with zero-forcing equalizers when operating in frequency-selective fading channels that are not known to the system [124].

### Modified Discrete Fourier Transform Filterbanks

According to Fliege [36], complex modulated filterbanks alone do not sufficiently eliminate cross-talk between adjacent subcarriers. Rather, the complex information on each subcar-

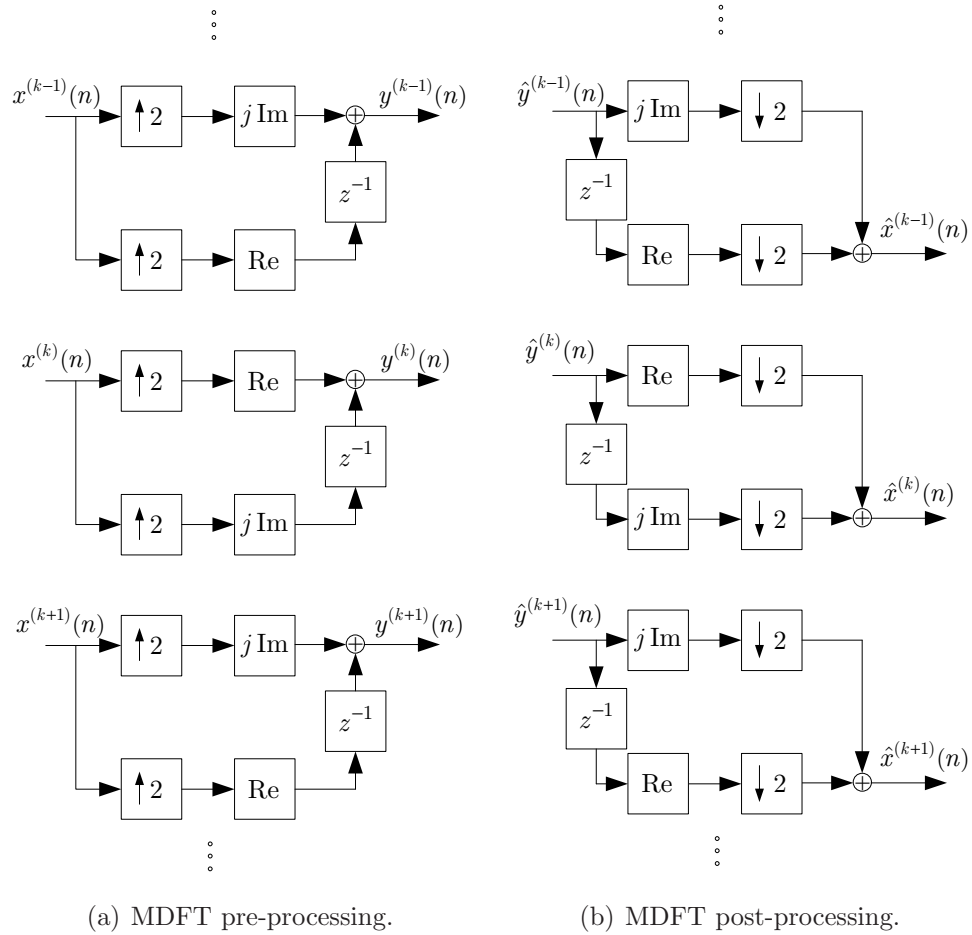


**Fig. 2.7** Implementation of MDFT pre- and post-processing components.

rier must be pre-processed at the transmitter and post-processed at the receiver to achieve the minimization of cross-talk. The complex information is modified such that the real and imaginary components of the complex information are offset after the upsampling at the transmitter by half the sampling period. This type of implementation is called a *modified discrete Fourier transform* (MDFT) filterbank [36, 116, 117, 125]. In digital communication circles, this is equivalently called offset QAM, when QAM modulation is used on the subcarriers [44, 45].

To convert the generic single input/single output MCM transmitter and receiver of Fig. 2.2 into an MDFT filterbank system, the upsampling stage of the transmitter in Fig. 2.2(a) would be replaced by the MDFT pre-processing stage shown in Fig. 2.7(a). Similarly, the downsampling stage of the receiver in Fig. 2.2(b) would be replaced by the

MDFT post-processing stage shown in Fig. 2.7(b). Thus, the transmitter would cause the  $N/2$  delay offset between the real and imaginary components of the subcarrier while the receiver would recombine the real and imaginary components.

Given an input block of length  $L$ ,  $\mathbf{x}_{n,n-L+1}^{(k)}$ , defined as

$$\mathbf{x}_{n,n-L+1}^{(k)} = \left[ x^{(k)}(n) \quad \cdots \quad x^{(k)}(n-L+1) \right]^T,$$

its real and imaginary components are separated and interleaved into a vector  $\mathbf{y}_{0,2L-1}^{(k)}$ . This is achieved by MDFT pre-processing:

$$\begin{aligned} \mathbf{y}_{0,2L-1}^{(k)} &= \mathbf{T}_{u,2,\text{mod}(k,2)} \text{Re}\{\mathbf{x}_{n-L+1,n}^{(k)}\} + j \cdot \mathbf{T}_{u,2,\text{mod}(k+1,2)} \text{Im}\{\mathbf{x}_{n-L+1,n}^{(k)}\} \\ &= \frac{1}{2} \mathbf{T}_{u,2,\text{mod}(k,2)} (\mathbf{x}_{n-L+1,n}^{(k)} + \mathbf{x}_{n-L+1,n}^{(k)*}) + \frac{1}{2} \mathbf{T}_{u,2,\text{mod}(k+1,2)} (\mathbf{x}_{n-L+1,n}^{(k)} - \mathbf{x}_{n-L+1,n}^{(k)*}) \\ &= \frac{1}{2} (\mathbf{T}_{u,2,\text{mod}(k,2)} + \mathbf{T}_{u,2,\text{mod}(k+1,2)}) \mathbf{x}_{n-L+1,n}^{(k)} \\ &\quad + \frac{1}{2} (\mathbf{T}_{u,2,\text{mod}(k,2)} - \mathbf{T}_{u,2,\text{mod}(k+1,2)}) \mathbf{x}_{n-L+1,n}^{(k)*} \end{aligned} \quad (2.14)$$

where  $\mathbf{T}_{u,R,\varepsilon}$  is an upsampling matrix, defined as

$$\mathbf{T}_{u,R,\varepsilon} = \begin{bmatrix} \mathbf{0}_{R+\varepsilon-1,L} \\ \cdots \\ 1 & 0 & 0 & \cdots & 0 \\ \cdots \\ \mathbf{0}_{R-1,L} \\ \cdots \\ 0 & 1 & 0 & \cdots & 0 \\ \cdots \\ \vdots \\ \cdots \\ 0 & 0 & 0 & \cdots & 1 \end{bmatrix} \quad (2.15)$$

where  $\mathbf{0}_{r,c}$  is a zero matrix of  $r$  rows and  $c$  columns,  $R$  is the sampling rate, and  $\varepsilon$  is the delay.

The output of the MDFT pre-processing stage is then upsampled by applying the up-sampling matrix  $\mathbf{T}_{u,N/2,D}$ , with the total group delay  $D$  equal to

$$D = 2\lceil \tau \rceil + \lceil \tau_{\text{ch}} \rceil, \quad (2.16)$$

where  $\tau$  is the group delay of the synthesis or analysis filters, and  $\tau_{\text{ch}}$  is the group delay of the channel [85]. The combined upsampling rate of the MDFT pre-processing stage, which performs an upsampling by a factor of 2, and the  $N/2$  upsampling matrix is  $N$  (i.e., critically-sampled filterbanks).

The resulting signal is then filtered by the  $k^{\text{th}}$  synthesis filter  $\mathbf{g}_{0,P-1}^{(k)}$ , defined as

$$\mathbf{g}_{0,P-1}^{(k)} = [g^{(k)}(0)g^{(k)}(1)\cdots g^{(k)}(P-1)]^T, \quad (2.17)$$

a channel impulse response  $\mathbf{h}_{0,S-1}$ , and the  $k^{\text{th}}$  analysis filter  $\mathbf{f}_{0,P-1}^{(k)}$ , before being down-sampled by the downsampling matrix  $\mathbf{T}_{d,N/2,0} = \mathbf{T}_{u,N/2,0}^T$ . In this derivation, filtering is performed using convolution matrices. Therefore,  $\mathbf{g}_{0,P-1}^{(k)}$  can be represented as an  $(NL + D - P + 1) \times (NL + D)$  convolution matrix

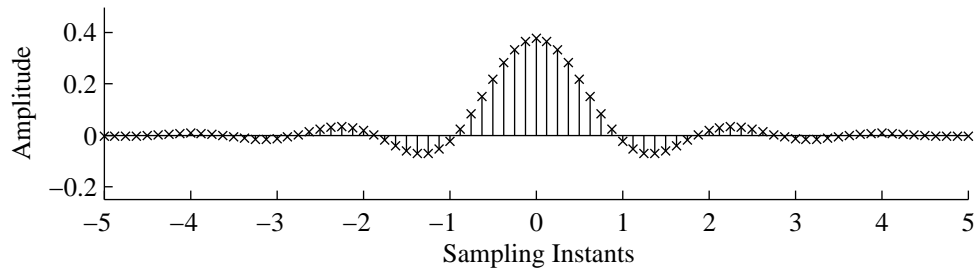
$$\mathbf{G}^{(k)} = \begin{bmatrix} \boxed{\mathbf{g}_{0,P-1}^{(k)T}} & & & \mathbf{0} \\ & \boxed{\mathbf{g}_{0,P-1}^{(k)T}} & & \\ & & \ddots & \\ \mathbf{0} & & & \boxed{\mathbf{g}_{0,P-1}^{(k)T}} \end{bmatrix}. \quad (2.18)$$

Furthermore, the channel  $\mathbf{h}_{0,S-1}$  and the  $k^{\text{th}}$  analysis filter  $\mathbf{f}_{0,P-1}^{(k)}$ , can be represented as  $(NL + D - P - S + 2) \times (NL + D - P + 1)$  and  $(NL + D - 2P - S + 3) \times (NL + D - P - S + 2)$  convolution matrices,  $\mathbf{H}$  and  $\mathbf{F}^{(k)}$ , respectively.

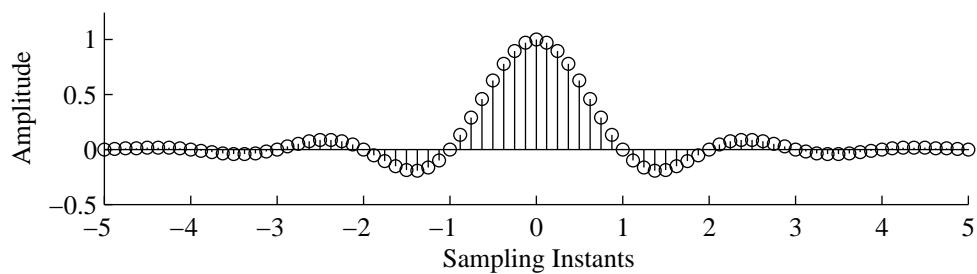
In order to extract the desired real and imaginary information from the output of the  $N/2$  downsampler,  $\hat{\mathbf{y}}_{0,2L-1}^{(k)}$ , and combine them together in order to form the recovered signal,  $\bar{\mathbf{x}}_{n,n-L+1}^{(k)}$ , MDFT postprocessing is employed:

$$\begin{aligned} \bar{\mathbf{x}}_{n,n-L+1}^{(k)} &= \mathbf{T}_{d,2,\text{mod}(k,2)} \text{Re}\{\hat{\mathbf{y}}_{0,2L-1}^{(k)}\} + j \cdot \mathbf{T}_{d,2,\text{mod}(k+1,2)} \text{Im}\{\hat{\mathbf{y}}_{0,2L-1}^{(k)}\} \\ &= \frac{1}{2} (\mathbf{T}_{d,2,\text{mod}(k,2)} + \mathbf{T}_{d,2,\text{mod}(k+1,2)}) \hat{\mathbf{y}}_{0,2L-1}^{(k)} \\ &\quad + \frac{1}{2} (\mathbf{T}_{d,2,\text{mod}(k,2)} - \mathbf{T}_{d,2,\text{mod}(k+1,2)}) \hat{\mathbf{y}}_{0,2L-1}^{(k)*}. \end{aligned} \quad (2.19)$$

One of the important design decisions involved in the implementation of an FB-MC system is the choice of prototype lowpass filter. Although a variety of choices exist, from prototype filter design routines [34, 108, 109] to wavelets [118, 126], in this thesis square-



(a) Square-root raised cosine impulse response.



(b) Raised cosine impulse response.

**Fig. 2.8** Impulse responses of square-root raised cosine and raised cosine filters.

root raised cosine filters are used. In the following subsection, details of this filter will be presented.

### Square Root-Raised Cosine Filter

In 1928, Nyquist specified the condition by which the overall response of the transmitter, channel, and receiver achieves zero intersymbol interference (ISI) [127]. In his honour, this condition is called the *Nyquist Criterion*. One filter that satisfies this criterion is the *raised cosine* filter. However, the raised cosine filter is the desired overall response of the system. Therefore, to obtain the responses of the transmitter and receiver that yield a raised cosine response (the channel is assumed to be ideal), one takes the square root of the Fourier transform of the raised cosine filter. The result yields a *square-root raised cosine* filter. The impulse responses of the raised cosine filter and the square-root raised cosine filter are shown in Fig. 2.8.

If a square-root raised cosine filter was chosen for the prototype lowpass filter  $p(n)$ , its

time domain representation would be [127]

$$p(n) = \frac{4\alpha}{\pi\sqrt{T}} \frac{\cos((1+\alpha)\pi n) + \sin((1-\alpha)\pi n)/4\alpha n}{1 - (4\alpha n)^2} \quad (2.20)$$

where  $\alpha$  is the *roll-off factor*, which represents the normalized excess bandwidth occupied by the filter beyond its minimum bandwidth, and  $T$  is the symbol period. The value of  $\alpha$  is limited to the range  $0 \leq \alpha \leq 1$ .

A useful property of square-root raised cosine filters is that the overall magnitude response of the transmitter and receiver filters will be a raised cosine filter, which satisfies the Nyquist Criterion [127]. Moreover, the overall phase response will be linear. Finally, according to [128], the power delivered to the channel, when square-root raised cosine filters are employed at the transmitter, will be independent of the roll-off factor.

It should be noted that since the prototype filter was implemented in this work as an FIR filter of length  $P$ , it will be approximately a square-root raised cosine filter due to truncation of the impulse response. Nevertheless, matched filtering would be performed by the  $k^{\text{th}}$  receiver and transmitter filters, thus maximizing the signal-to-noise ratio (SNR) of the received signal [127].

Although ISI is eliminated through the use of square-root raised cosine filters, the application of these filters in the analysis and synthesis filterbanks do not guarantee the perfect reconstruction of the input signal at the output of the receiver under ideal conditions.

## 2.2 Indoor Wireless Channel Models

In digital communications, the transmitted signal is subjected to distortion caused by its interaction with the physical operating environment. The reflections and diffractions caused by this interaction results in multiple copies of the same signal arriving at the receiver with different amplitudes, phases, and delays. As a result, this gives rise to constructive or destructive interference at the receiver known as *multipath fading* [129]. In the following two subsections, several multipath fading channel models are presented where either the system possesses a single antenna at the transmitter and receiver (known as a *single-input single-output* (SISO) system) or when multiple antennas are employed (known as *multiple-input multiple-output* (MIMO), *multiple-input single-output* (MISO), and *single-input multiple-output* (SIMO) systems).

### 2.2.1 SISO Channel Models

The behaviour of energy transmitted from one point in space to another point in space is modelled by the physics of radio wave propagation, including the effects of constructive and destructive interference, as well as the reflection of energy. These same physical properties can be used to model the channel environment of high speed data transmission systems.

In a wireless communication system, the transmitter emanates radiation in all directions. Thus, the energy would propagate until some of it reaches the receiver antenna, either via the line-of-sight path from the transmitter antenna to the receiver antenna (if it exists) or after the energy has been reflected by a number of objects located between the transmitter and receiver antennas. As for the rest of the energy, it would continue to propagate and eventually dissipate.

For an indoor environment, such as a typical small office/home office environment depicted in Figure 2.9(c), the line-of-sight component (if it exists),  $p_1$ , would arrive at the receiver antenna first. As for the energy reflected by the walls and other objects in the room, several of these reflections, such as  $p_2$  and  $p_3$ , would make their way to the receiver antenna, although not with the same phase, amplitude, or delay. All of these received components are functions of several parameters, including their overall distance between the transmitter and receiver antennas as well as the number of reflections. Therefore, one can model the channel as a finite impulse response that is being convolved with the transmitted signal. This models how an indoor environment would have a several copies of the transmitted signal intercepted at the receiver antenna, resulting in an impulse response of the type shown in Figure 2.9(a). The corresponding frequency response of the example channel impulse response is shown in Figure 2.9(b).

A simple statistical multipath model of the indoor radio channel was presented by Saleh and Valenzuela [130] and verified via several measurement campaigns. The indoor channel was modelled as clusters of rays, where the clusters behave as Poisson arrival processes. Furthermore, individual rays within a cluster were also modelled as a Poisson arrival process. Finally, the amplitudes of the clusters and the individual rays are exponentially dampened. The model also depends on the center frequency of operation and the separation distance between the transmitter and receiver. An example of a channel produced using this method is presented in Fig. 2.10.

An overview of various fundamental spatial channel models for communication systems

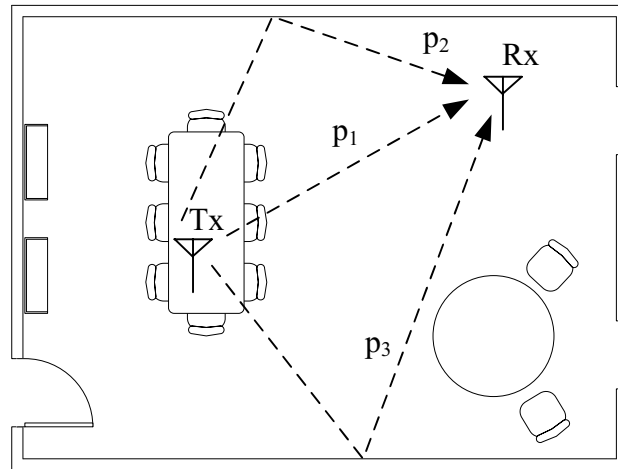
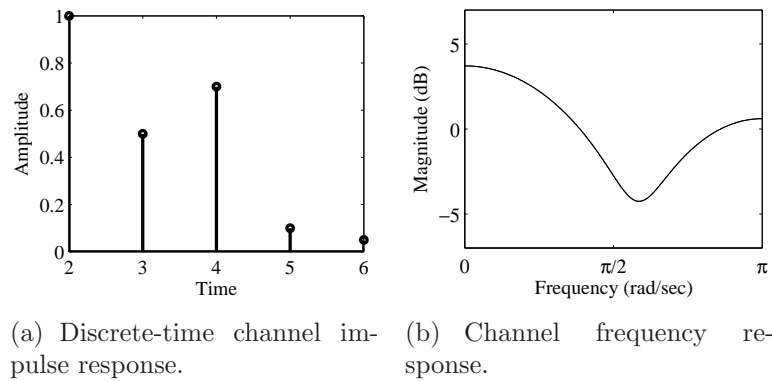


**Fig. 2.9** Example of a channel response due to multipath propagation.

employing antenna arrays was presented by Ertel *et al.* [131]. The characteristics of each model are dependent on the physical local environment in which the antennas are situated. Therefore, the channel model is dependent on the physical geometry of the scattering objects in the vicinity of the antennas. These spatial channel models can be divided into three groups, namely: general statistically based models, more site-specific models based on measurement data, and entirely site-specific models.

Since indoor environments may drastically vary in the way they affect the propagation of transmitted signals, there are techniques to determine the channel impulse response specific to that environment. One such technique is *ray tracing*. Instead of determining a statistical

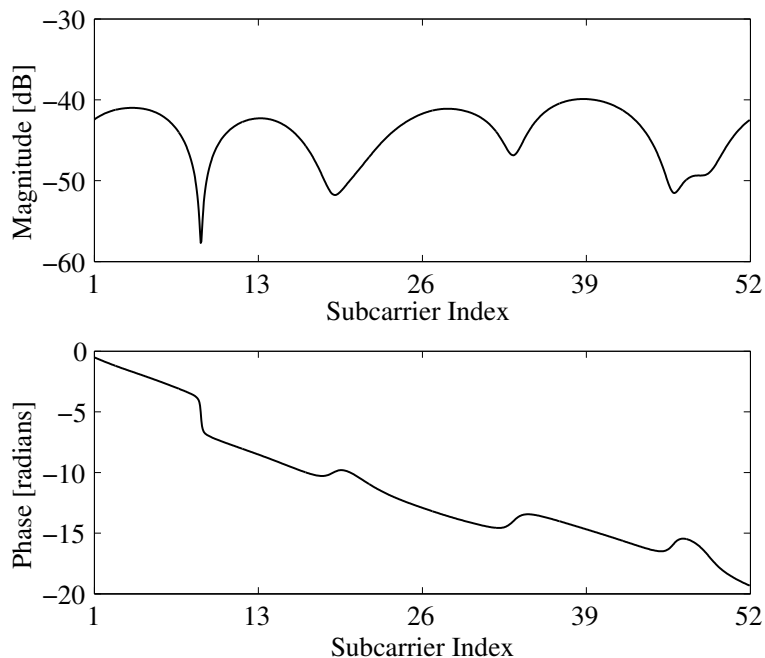


**Fig. 2.10** An example of an indoor environment response operating in the 5.15–5.25 GHz UNII band with a 50 m transmitter/receiver separation distance.

model that generalizes the properties of the environment, ray tracing uses computers to determine the paths, amplitudes, phases, and delays of rays emanating from the transmitter to the receiver by applying the laws of reflection, diffraction, and other laws of physics in the calculations. Thus, models created through ray tracing programs are tailored specifically to the parameters of the environment provided by the user. However, such programs are very complex and researchers are currently investigating ways of providing accurate results while maintaining a reasonable complexity. Ji *et al.* [132] presented the application of several ray-tracing algorithms, in combination with the Uniform Theory of Diffraction, for efficient prediction of propagation in the ultra-high frequency (UHF) band for an indoor environment. Computational efficiency is increased by rearranging objects in an indoor environment into irregular cells. Furthermore, three-dimensional propagation prediction models are formed from a collection of two-dimensional ray-tracing results, which have an observed speed-up of 99 percent over traditional three-dimensional ray-tracing models. This model also considers reflection and refraction of layered materials and diffraction from wall corners. A patched-wall model is used to improve the accuracy of prediction in this method

**Table 2.4** Channel models for line-of-sight (LOS) and non-LOS (NLOS) indoor environments at 5 GHz (from [136])

Name	RMS Delay Spread	Characteristic	Environment
A	50 ns	Rayleigh	Office NLOS
B	100 ns	Rayleigh	NLOS
C	150 ns	Rayleigh	NLOS
D	140 ns	Ricean	LOS
E	250 ns	Rayleigh	NLOS

and the simulated results agree very strongly with the measurements. Another ray tracing technique was presented by McKown and Hamilton [133], where an image-based, dual grid, scalar, coherent, ray tracing program that generates two-dimensional slices of three-dimensional standing wave patterns for continuous wave illumination is described. The program estimated the quality of system coverage as well as investigated design alternatives for antenna arrays, such as beamwidths, boresight orientations, and spatially-averaged signal strengths.

Although ray tracing works well when the channel is time-invariant, there are several environments where the time-varying behaviour of the channel needs to be considered. Thoen, Van der Perre, and Engels [134] developed an improved stochastic model for time-varying channels applied to fixed indoor wireless communications. The improved model was shown to be more accurate than the model proposed by Jakes [135], which assumes the transmitter and receiver are in motion. The results produced by the improved model were compared to measurement campaigns found in literature.

Communication standards organizations, such as the IEEE, the ITU, and ETSI, usually publish channel models that can be used to benchmark communication systems for the purpose of fair comparison. For wireless systems operating indoors at 5 GHz, the ETSI broadband radio access network (BRAN) project has published a technical report specifying five different channel models [136]. A summary of these channels and their associated parameters are shown in Table 2.4.

### 2.2.2 MIMO Channel Models

To enhance system performance, several communication systems employ multiple antennas at the transmitter and/or receiver with an array signal processing algorithm (this is discussed further in Section 2.6). However, the modelling of the channel environment given

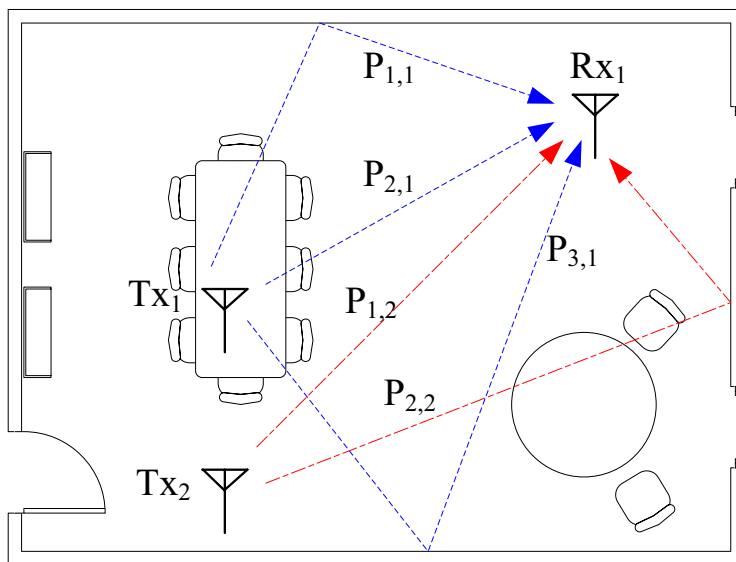


**Fig. 2.11** An example of multipath propagation when two transmit antennas are employed in a small office/home office environment.

multiple antennas is more complex than the single antenna case. An intuitive solution is to model the environment between each transmit and receive antenna as a SISO channel impulse response. Thus for a system possessing  $N_T$  transmit antennas and  $N_R$  receive antennas, the MIMO channel can be represented as a collection of  $N_T N_R$  SISO channel impulse responses. Referring to Fig. 2.11 where  $N_T = 2$  and  $N_R = 1$ , the paths of the signal emanating from the transmitter  $Tx_1$ , namely  $p_{1,1}$ ,  $p_{2,1}$ , and  $p_{3,1}$ , give rise to the SISO channel impulse response  $h_{11}(n)$ , while the paths  $p_{1,2}$  and  $p_{2,2}$  from the transmitter  $Tx_2$  will give rise to  $h_{21}(n)$ .

Although intuitive, this type of MIMO channel model relies on the assumption that the SISO channel responses are independent, which might not be the case given specific physical conditions (e.g., antenna spacing, amount of scattering, delay spread). Since operating environments can drastically vary from rural settings to an indoor office space, many researchers opt to develop models for a specific environment and then compare it against channel measurements. For example, a narrowband MIMO measurement campaign was conducted in Manhattan at 2.11 GHz with 16 transmitters and 16 receivers in an outdoor environment [137]. This was done in order to validate a four-parameter correlated MIMO channel model. It was shown that the proposed model was more accurate in computing the

system capacity than assuming the channel to be independently and identically distributed (i.i.d.) Rayleigh since it includes the effects of correlation at the transmitter and receiver. Similarly, a measurement campaign performed at 5.8 GHz in an office environment with no line-of-sight showed that for an adjacent antenna spacing of  $2\lambda$ , where  $\lambda$  is the signal wavelength in metres, the results closely matched those produced by a simulator using i.i.d. SISO channels [138]. Finally, a measurement campaign for an indoor wireless system operating at 5.2 GHz was performed in order to validate the use of smart antennas [139]. The results showed that the corridor behaved like a waveguide under line-of-sight conditions while positions adjacent to the corridor (i.e., non-line-of-sight) depended on leakage from the corridor, therefore different techniques must be employed when dealing with either condition.

Although several researchers have attempted to validate their models with measurement campaigns, the cost of the equipment may be quite high. An alternative solution is to develop mathematical models that approximately reflect the behaviour of the operating environment. For instance, a model for intercarrier interference in MIMO channels was developed by Stamoulis, Diggavi, and Al-Dhahir [140]. The channels of two distinct pairs of transmit/receive antennas were assumed to be uncorrelated and each channel was i.i.d. Moreover, each channel was modelled as a wide-sense stationary uncorrelated scattering channel. From the analysis, it was observed that the intercarrier interference was accentuated with the presence of multiple antennas and that the covariance matrix of the intercarrier interference was spatially white. Moreover, multiple antennas can mitigate the intercarrier interference using just spatial filtering alone, although that may be very complicated. A geometry-based generic model for a MIMO channel was derived by Molisch for either macrocell or microcell environments [32]. Using a set of the most important propagation mechanisms, a number of effects were included in this model, namely, rings of scatterers around the base station and mobile, “waveguiding”, scattering from distant objects, and diffraction from roof edges.

Although many models attempt to accurately model the scattering effects of the operating environment, very few try to account for the mutual coupling associated with closely spaced arrays. One study in which the effects of mutual coupling, scattering, and imperfect power control were simultaneously considered in a capacity analysis of a code division multiple access (CDMA) system employing “smart antennas” was by the present author in his previous research [141]. It turns out that when mutual coupling effects are included in

the analysis, the capacity is less than the ideal case.

### Modelling Correlation between Channel Paths

One of the main parameters of interest in a MIMO channel model is the fading correlation between a pair of receiving antennas. Since the degree of correlation between components of a MIMO channel model can impact the performance of the system, it is important to accurately model the correlation in an efficient manner. The fading correlation can be approximated using physical parameters such as the angular spread [142, 143], the delay spread [142], the antenna separation distance [135, 142–144].

One of the first approximations for the fading correlation between antennas  $i$  and  $j$  was by Clarke, who derived the relationship [144]

$$\rho_{ij} \approx J_0^2\left(\frac{2\pi d_{ij}}{\lambda}\right) \quad (2.21)$$

where  $J_0^2(\cdot)$  is the Bessel function of the first kind with zero order, and  $d_{ij}$  is the separation between antennas  $i$  and  $j$  in metres. In the formulation of Eq. (2.21), it was assumed that the arrival distribution in the azimuth was uniform and the antennas in the array were omnidirectional. This was later extended by Jakes to several other scenarios [135].

In the work by Shiu, Foschini, Gans, and Kahn, the fading correlation was considered in the capacity derivation of a communication system employing a multiple antenna array [143]. Using an approach based on Jakes' model [135], they were able to analytically determine the capacity of the system, which matched closely to their Monte Carlo simulations.

Another model for the fading correlation was recently developed by Durgin, who developed the following model [142]

$$\rho_{ij} = e^{-\frac{23\Lambda^2 d_{ij}^2}{\lambda^2}} \quad (2.22)$$

where  $\Lambda$  is the angular spread of the incoming signal intercepted by an array of omnidirectional antennas. Durgin also show that there exists a relationship between the angular spread and delay spread for both indoor and outdoor environments [142].

To transform the channel impulse responses of an uncorrelated MIMO channel model into a correlated MIMO channel model, the correlation matrix of the model must first be determined. One can use data obtained from measurement campaigns [145], or this

$(N_T \cdot N_R) \times (N_T \cdot N_R)$  matrix could be approximately determined by the expression [146, 147]

$$\begin{aligned}\boldsymbol{\Sigma} &= \boldsymbol{\Sigma}_{\text{Tx}} \otimes \boldsymbol{\Sigma}_{\text{Rx}} \\ &= E\{\text{vec}\{\mathbf{H}\}\text{vec}\{\mathbf{H}\}^H\}\end{aligned}\quad (2.23)$$

where  $\boldsymbol{\Sigma}_{\text{Tx}}$  and  $\boldsymbol{\Sigma}_{\text{Rx}}$  are the correlation matrices of the transmit and receive antenna arrays,  $\mathbf{H}$  is the  $N_T \times N_R$  correlated MIMO channel matrix,  $\text{vec}\{\}$  is the vector operation of stacking the columns of a matrix into a single column vector, and  $\otimes$  is the *Kronecker product*.

To determine  $\boldsymbol{\Sigma}_{\text{Tx}}$ , it was shown that the fading correlation parameters from either Eqs. (2.21) or (2.22) could be used in the  $N_T \times N_T$  matrix expression [147]

$$\boldsymbol{\Sigma}_{\text{Tx}} = \begin{bmatrix} 1 & \rho_{ij} & \rho_{ij}^4 & \cdots & \rho_{ij}^{(N_T-1)^2} \\ \rho_{ij} & 1 & \rho_{ij} & \cdots & \rho_{ij}^{(N_T-2)^2} \\ \rho_{ij}^4 & \rho_{ij} & 1 & \cdots & \rho_{ij}^{(N_T-3)^2} \\ \vdots & \vdots & \vdots & \ddots & \rho_{ij} \\ \rho_{ij}^{(N_T-1)^2} & \rho_{ij}^{(N_T-2)^2} & \rho_{ij}^{(N_T-3)^2} & \cdots & 1 \end{bmatrix}\quad (2.24)$$

assuming that all adjacent antennas in the array have the same distance, and  $\rho_{ij}$  is the correlation for antennas  $i$  and  $j$  with the minimum separation distance. The  $N_R \times N_R$  matrix  $\boldsymbol{\Sigma}_{\text{Rx}}$  could be expressed in a similar way.

Finally, to transform an uncorrelated MIMO channel model into a correlated model with correlation matrix  $\boldsymbol{\Sigma}$ , apply  $\boldsymbol{\Sigma}_{\text{Tx}}$  and  $\boldsymbol{\Sigma}_{\text{Rx}}$  to the expression [146–149]

$$\mathbf{H} = \boldsymbol{\Sigma}_{\text{Tx}}^{1/2} \mathbf{G} \boldsymbol{\Sigma}_{\text{Rx}}^{1/2}\quad (2.25)$$

where  $\mathbf{G}$  is the  $N_T \times N_R$  uncorrelated MIMO channel matrix, respectively. Equivalently, another technique is to apply the *Cholesky factorization* to  $\boldsymbol{\Sigma}$  and take that result and apply it to  $\mathbf{G}$  [146]. In either case, one needs to normalize the correlation matrix prior to any transform (see Appendix D for more information).

## 2.3 Channel Estimation and Synchronization Techniques

### 2.3.1 Data-Assisted Channel Estimation

Many communication systems rely on some sort of channel knowledge in order to operate with a decent level of error robustness. The process of attaining this knowledge is called *channel estimation*, of which two basic types exist: (1) data-assisted channel estimation, and (2) blind channel estimation. The former uses training symbols to capture the characteristics of the channel while the latter, as the name implies, extracts the channel information from the transmission without any training. Although there is no transmission overhead in blind channel estimation, it does require a more complex implementation and a substantial amount of time to converge to the final solution. Thus, to reduce implementation complexity, most WLAN standards such as the IEEE 802.11a make use of data-assisted channel estimation techniques [2, 47].

For data-assisted channel estimation in multicarrier systems, the training sequences are inserted in each subcarrier, or a subset thereof, prior to transmission. Furthermore, the extraction of the channel estimate can be performed in either the frequency domain (i.e., subcarrier-level at the receiver) or the time domain (i.e., prior to decomposition into subcarriers at the receiver). In the frequency domain version for the IEEE 802.11a standard [2, 47], two sufficiently long and identical training sequences are inserted in the preamble of subcarrier  $k$ . At the receiver, the frequency response of the received training symbols in subcarrier  $k$ ,  $R_{1,k}$  and  $R_{2,k}$ , are defined as

$$R_{l,k} = H_k \cdot X_k + V_{l,k} \quad (2.26)$$

where  $X_k$  is the transmitted signal from subcarrier  $k$ ,  $H_k$  is the channel frequency response over subcarrier  $k$ , and  $V_{l,k}$  is additive noise over training sequence  $l$ . Thus the channel

estimate over subcarrier  $k$  can be calculated as [47]

$$\begin{aligned}
 \hat{H}_k &= \frac{1}{2}(R_{1,k} + R_{2,k})X_k^* \\
 &= \frac{1}{2}(H_k X_k + V_{1,k} + H_k X_k + V_{2,k})X_k^* \\
 &= H_k |X_k|^2 + \frac{1}{2}(V_{1,k} + V_{2,k})X_k^* \\
 &= H_k + \frac{1}{2}(V_{1,k} + V_{2,k})X_k^*
 \end{aligned} \tag{2.27}$$

where the training data amplitudes are chosen to be unity and the noise samples  $V_{1,k}$  and  $V_{2,k}$  are statistically identical and independent.

One of the important issues of training sequence aided channel estimation is training sequence placement. Park and Kang [57] investigated the impact of various training sequence insertion and arrangement techniques. The optimal training sequence arrangement, given a set of channel conditions, was also derived. A pilot-aided channel estimation scheme was proposed by Vandenameele *et al.* [150] for OFDM spatial division multiple access (SDMA) systems. On the other hand, a blind channel estimation scheme for MIMO-OFDM was proposed by Bai, He, Jiang, and Zhu [151]. In a study of ICI in MIMO OFDM systems was presented by Stamoulis, Diggavi, and Al-Dhahir, a channel estimation technique and pilot tone placement method was implemented for time-varying MIMO channel parameters within a transmission block [140]. Li, Winters, and Sollenberger [152] presented an enhanced channel estimation technique based on decision-directed channel parameter estimation with optimum training sequences for OFDM employing multiple antennas. A robust pilot-aided channel estimation technique was designed by Chang and Su that was based on a two-dimensional regression model for Rayleigh fading channels [58]. An expectation-maximization (EM) algorithm for OFDM receivers was proposed by Al-Naffouri, Bahai, and Paulraj [72]. Finally, Catreux *et al.* [153] presented methods of obtaining accurate channel state information while the environment was rapidly changing. These methods included mean SNR values, multiple statistics of the SNR, packet and bit error rate information, and a hybrid error performance/SNR technique.

### 2.3.2 Synchronization

The accuracy of the symbol and frequency synchronization in multicarrier systems dramatically affects the overall system performance with respect to the probability of error [6]. To minimize the computational effort and redundancy in determining the symbol and frequency synchronization, the synchronization process is split into a coarse acquisition phase and a fine tracking phase. Moreover, there exist several synchronization techniques that could be employed, ranging from channel group delay estimation to blind methods using the received signal's autocorrelation [85]. For example, a symbol time offset estimator for coherent OFDM systems was proposed that exploited the redundancy in the cyclic prefix and the pilot signals used in channel estimation [60]. The former was used to perform a coarse estimate while the latter allowed for a fine tuning of the estimate. Two blind algorithms, one for symbol synchronization [59] and the other for carrier frequency recovery [61], were also proposed that used the received signal's autocorrelation.

In this dissertation, it is assumed that both the symbol sampling time and the carrier frequencies have been recovered by one of the above algorithms.

## 2.4 Adaptive Allocation Algorithms

As mentioned previously, multicarrier systems possess a “divide-and-conquer” quality which may be exploited under certain conditions in order to improve system performance. For instance, by subdividing a frequency-selective fading channel frequency response into a collection of relatively flat subchannels, each subchannel then has a different amount of distortion and a different instantaneous SNR value. Thus, by adapting the operating parameters of the subcarriers to each subchannel, such as the choice of modulation scheme and/or power level, the system can be optimized in one of two ways:

1. The system throughput can be maximized given an error constraint.
2. The aggregate error can be minimized given a throughput limit.

In the next two subsections, two popular types of allocation algorithms will be discussed.

### 2.4.1 Bit Allocation

The term *bit allocation*, also known as *bit loading* or *adaptive modulation*, defines a process for assigning a modulation scheme to each subcarrier, given a set of available modulation schemes, to achieve a performance objective while satisfying some prescribed constraint(s). For example, the objective could be throughput maximization while the constraint could be a prescribed upper bound on the mean BER.

To illustrate how bit loading works, suppose the channel is subdivided into  $N$  disjoint approximately flat subchannels with complex gains  $H_i$ ,  $i = 0, \dots, N - 1$ . Furthermore, let the transmit power levels for the subcarriers be specified as  $\pi_i$ ,  $i = 0, \dots, N - 1$ . Therefore, if the additive noise is white with variance  $\sigma_\nu^2$  and the equalizer at the receiver is a single complex gain per subcarrier, the signal-to-noise ratio (SNR) of subcarrier  $i$  can be defined by

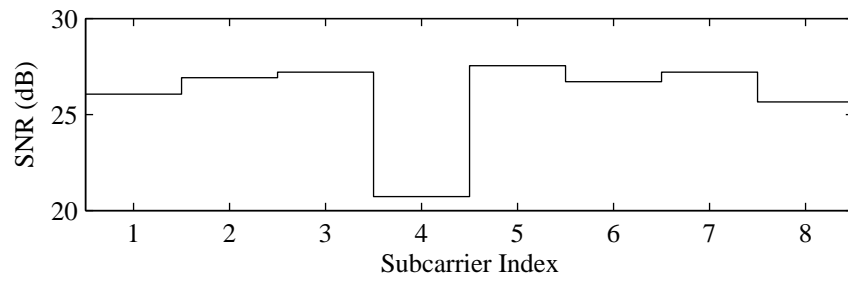
$$\gamma_i = \frac{\pi_i |H_i|^2}{\sigma_\nu^2} \quad (2.28)$$

where  $|H_i|^2 \leq 1$  is always true due to path loss<sup>5</sup>.

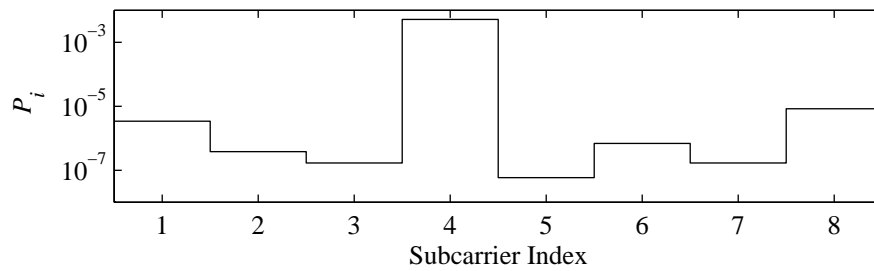
Given a set of different modulation schemes, suppose the objective is to determine which scheme possesses the largest throughput for subcarrier  $i$ , given the subcarrier SNR in Eq. (2.28), while operating below the pre-defined error probability threshold  $P_T$ . An exhaustive search is performed by evaluating the closed form expressions of the probability of bit error,  $P_i$ , for all available modulation schemes and subcarriers. Furthermore, since the case of  $|H_i|^2 \neq |H_k|^2$  for  $i \neq k$  is very likely, the best choice of modulation scheme for subcarrier  $i$  may not be for subcarrier  $k$  and thus this exhaustive search procedure must be applied for each subcarrier.

An example of bit allocation is shown in Fig. 2.12 for  $N = 8$  subcarriers. For  $\pi_i = 0.833$  mW,  $i = 0, \dots, N - 1$ , and  $\sigma_\nu^2 = 1 \times 10^{-13}$  W, the subcarrier SNR values are computed using Eq. (2.28) and shown in Fig. 2.12(a). Note that there exists a deep spectral depression in the vicinity of subcarrier 3, resulting in a relatively low subcarrier SNR value. If 64-QAM modulation is applied to all subcarriers, the resulting mean bit error rate (BER) is  $\bar{P} = 6.442 \times 10^{-4}$  and the overall throughput is 48 bits per symbol epoch. If the BER threshold is  $P_T = 10^{-5}$ , this configuration is unacceptable since  $\bar{P} > P_T$ . Since the BER

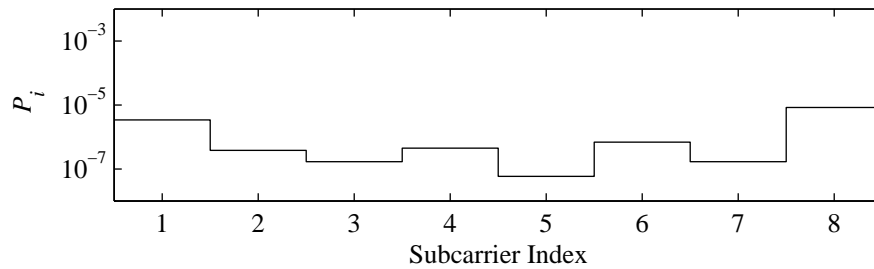
<sup>5</sup>For OFDM-type systems with a sufficiently long cyclic prefix, Eq. (2.28) becomes increasingly accurate as  $N$  increases. However, for other multicarrier schemes, this approximation may be less accurate if other sources of distortion, such as ISI and ICI, are not adequately suppressed.



(a) Subcarrier SNR values (in dB).



(b) 64-QAM modulation applied across all subcarriers.



(c) 64-QAM modulation for all subcarriers except subcarrier 4, which employs 16-QAM.

**Fig. 2.12** Example of bit allocation performed on an 8 subcarrier system.

of subcarrier 3 dominates the mean BER (refer to Fig. 2.12(b)), the modulation scheme of that particular subcarrier is changed to 16-QAM. Observing Fig. 2.12(c), all  $P_i$  are below  $P_T$  and  $\bar{P} = 1.767 \times 10^{-6}$ , which satisfies the BER constraint. However, the overall throughput is reduced by two bits per symbol epoch.

One of the classic works on bit loading strategies for multicarrier systems was presented by Kalet [80]. Using a multitone quadrature amplitude modulation (QAM) framework, the overall bit rate of the system was maximized when operating in an additive white Gaussian noise (AWGN) channel, first with a two-level transfer function and then extended to a multiple level transfer function. To assist in the derivation, a number of simplifying assumptions were made in this work. First, there was only a total power constraint on the system. Second, there was no limit on the size of QAM constellation that can be used. Third, the framework was designed for a continuous distribution of bits rather than a more realistic discrete distribution. Thus, the value for the number of bits per channel was non-integer for analytical convenience.

Focusing on the third simplifying assumption, several other researchers have also used closed-form expressions that yielded non-integer allocations [48, 81]. However, this may introduce rounding errors, resulting in a bit allocation that may further from the optimal solution in terms of throughput. Discrete bit allocation is one possible solution to this problem. Although discrete bit allocation algorithms for communication systems have been around since 1987 [154], they have been influenced by discrete allocation algorithms developed in other areas, such as financial analysis [7] and quantization theory [8]. However, for multicarrier communication systems, the formulation of the algorithm may be unique, and could vary depending on what quantity the system is allocating. For instance, a “unified” framework for an OFDM system, which performs both bit and power allocation, and can perform either transmission power minimization, error rate minimization, or throughput maximization is presented in [78]. Many discrete bit allocation algorithms are simply executed in an incremental fashion [55, 154]. However, incremental algorithms tend to be computationally expensive. As a result, there exists a need for practical and efficient loading algorithms. One such discrete loading algorithm was proposed by Krongold, Ramchandran, and Jones, which used lookup tables and a fast Lagrange bisection search to determine the final bit and power allocation [14].

Several researchers have considered a number of refinements for multicarrier systems employing bit allocation algorithms. For instance, instead of using a large number of

modulation schemes for bit allocation, which could increase the computational complexity of the algorithm, simply “turning off” or *nulling* subcarriers would be sufficient to improve the error robustness of the system [49]. Another refinement that has been investigated is with respect to the choice of a metric representing the quality of transmission across the subcarriers. Although the majority of algorithms use either the instantaneous BER or SNR of the subcarrier, there have been studies performed investigating the use of Euclidean distance metrics [155], which are mapped to the signal-to-interference-plus-noise ratio, and the peak SNR criterion [156]. When bit allocation for multicarrier systems is studied, the system is usually assumed to be uncoded in order to ascertain only the benefits of bit allocation. However, all WLAN standards employ channel coding in their specifications. As a result, channel coding has been included in several studies where bit allocation is performed [68, 157].

Due to the increase in implementation complexity when bit allocation algorithms are employed, there have been several attempts to reduce the complexity while still attaining some of the benefits offered by bit allocation. For instance, for terrestrial Integrated Service Digital Broadcasting (ISDB-T), instead of performing bit allocation across each subcarrier, the subcarriers are grouped together and share the same modulation scheme allocated to them by the algorithm [51, 52]. When the channel conditions are very poor, the system may temporarily stop transmission and wait for when the conditions improve. However, instead of completely terminating the transmission, the idea of buffering the transmitted data until the channel conditions improve has been studied [158]. Moreover, to keep the transmission overhead to a minimum, several researchers have looked at ways of reducing the overhead, such as performing the allocation algorithms offline [159], and study the impact of the transmission overhead on the actual data throughput [160]. Finally, studies have been performed where proposed bit allocation algorithms are employed in existing communication systems [50].

Most allocation algorithms assume that the channel conditions are time-invariant. In WLAN research, the channel is assumed to be *quasi-stationary*, where the channel conditions change very slowly over a very long period of time. However, these assumptions are not realistic, and the impact of outdated allocations can significantly impact the error performance of the system. While several researchers have investigated ways of modelling the behaviour of time-varying channels and the type of errors they introduce in the allocation process [161–166], others have sought techniques of predicting the time-varying behaviour

of channel and using that information in the allocation algorithm [54, 167].

Another simplification employed by most studies is that the system is evaluated in a single user scenario. However, most communication systems are equipped to operate under multiuser conditions, including WLAN systems. As a result, the interference introduced to the system from other users is not being considered<sup>6</sup>. Since users within the same system may have different requirements with respect to throughput and error robustness, a number of bit allocation algorithms have been proposed that satisfy these different requirements within the same system [53, 168, 169]. One way to assign different throughput values is to assign a different number of subcarriers to each user [170], while some multiuser bit allocation algorithms allow different total power constraints per user [71].

Finally, many multicarrier systems that employ bit allocation do not consider the performance benefits of using antenna arrays at the transmitter and receiver. While bit allocation exploits the frequency diversity offered by the system, antenna arrays can further improve performance by exploiting spatial diversity. For instance, a number of systems have been implemented that employ both beamforming and bit allocation to increase the user capacity of the system [169, 171–175]. However, all of these schemes use multiple antennas to support a greater number of users and mitigate the interference due to other users.

### Capacity Approximation-Based Bit Loading

The maximum data rate for error-free transmission, or *capacity*, of a communication system transmitting in an additive white Gaussian noise channel is given by

$$C = W \log_2(1 + \gamma) \quad (2.29)$$

where  $W$  is the signal bandwidth and  $\gamma$  is the SNR. Practical communication systems can be characterized by how close they are from achieving capacity. The distance between the SNR values for the maximum number of bits the system can sustain, given a target probability of error  $P_T$ , and the capacity normalized by the signal bandwidth is the *SNR gap*,  $\Gamma$ . The maximum number of bits that can be sustained is (with error  $P_T$ )

$$b = \log_2 \left( 1 + \frac{\gamma}{\Gamma} \right). \quad (2.30)$$

---

<sup>6</sup>If the interference due to other users was taken into account, this would translate into an increase in the error floor of the BER results.

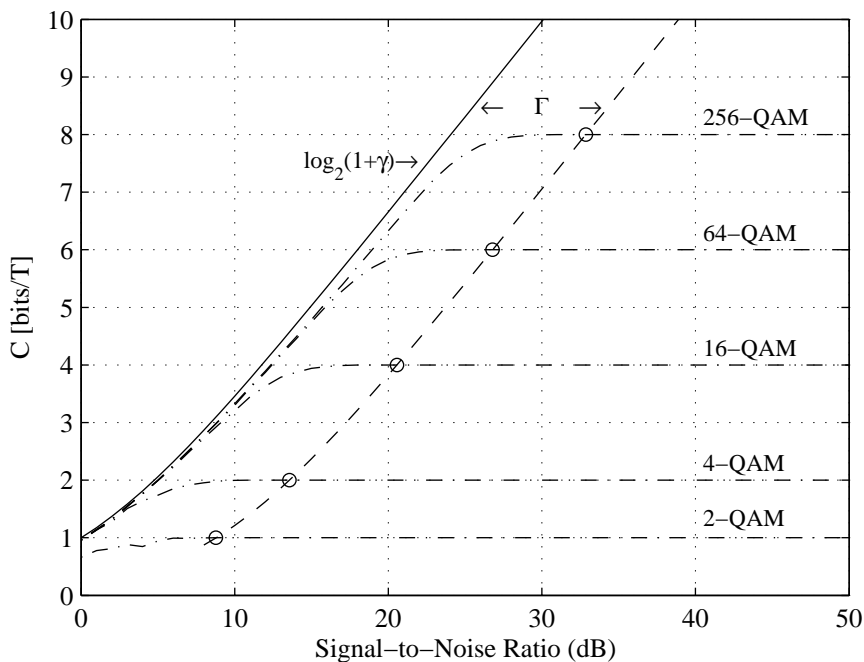


**Fig. 2.13** Channel capacity  $C$  and the points for M-QAM given a  $P_T$  of  $10^{-6}$  corresponding to an SNR Gap  $\Gamma$  of 8.8 dB.

The SNR gap can be expressed using the expression for the union bound on the error probability, yielding [64]

$$\Gamma \approx \frac{1}{3} \left[ Q^{-1} \left( \frac{P_T}{4} \right) \right]^2 \quad (2.31)$$

where  $Q^{-1}(\cdot)$  is the inverse of the Q-function, defined as

$$Q(x) = \frac{1}{\sqrt{2\pi}} \int_x^\infty e^{-t^2/2} dt. \quad (2.32)$$

An example of the SNR gap is shown in Fig. 2.13. The SNR gap between the normalized channel capacity and an uncoded M-QAM system operating at a  $P_T$  of  $10^{-6}$  for  $M \geq 2$ , represented by the circles connected by the dashed-dotted line, is approximately 8.8 dB. Also plotted are several normalized capacity curves as computed by Ungerboeck [176] for M-QAM systems operating in bandlimited additive white Gaussian noise channels, with discrete-valued inputs and continuous-valued outputs, and assuming equiprobable occurrences of signal constellation points.

The allocation algorithm of Chow, Cioffi, and Bingham [11] makes use of the SNR gap

to compute the number of bits for subcarrier  $i$ , namely

$$b_i = \log_2 \left( 1 + \frac{\gamma_i}{\Gamma} \right), \quad (2.33)$$

where  $\gamma_i$  is the SNR of subcarrier  $i$ . Assuming equal energy across all used subcarriers,  $\Gamma$  is adjusted until the target bit rate is exceeded. For a geometric interpretation, we refer to the dashed line in Fig. 2.13. The dashed line represents the system operating at  $P_T$ . For a subcarrier with SNR  $\gamma_i$ , this curve maps  $\gamma_i$  to a (non-integer) number of bits, which is rounded to the nearest integer value (the point on the curve is moved either vertically up or down). After the bit allocation, the transmission power levels are then adjusted in order to achieve the same subcarrier bit error rate,  $P_i$ , per non-nulled subcarrier.

The allocation algorithm presented by Leke and Cioffi [12, 82] assigns energy to different subcarriers in order to maximize the data rate for a given SNR margin. The subcarrier SNR values are sorted and a search is performed in order to find which subcarriers should be left on while others shut off. The bits are then allocated to each subcarrier are calculated using the SNR gap approximation. Campello introduced necessary and sufficient conditions for the optimality of a discrete bit allocation algorithms [84], and then extended these conditions to bit loading algorithms employing the capacity approximation [83]. Lee, Sonalkar, and Cioffi proposed a multiuser bit and power loading algorithm for DSL modems based on the capacity approximation [86, 87]. This work was followed up by Yu, Ginis, and Cioffi, who modelled the power control problem in a frequency selective multiuser network as a non-cooperative game [89]. Rhee and Cioffi studied the use of subcarrier allocation, based on Eq. (2.33), in order to increase capacity in multiuser OFDM systems [177]. Hoo, Telado, and Cioffi proposed a bit and power loading algorithm in which two services that each have a different quality-of-service (QoS) [13, 178]. In particular, one service is of constant bit rate while the other has a variable bit rate. Kim, Chen, and Cioffi investigated methods of speeding up the bit allocation process with an adaptive look-up table for the capacity approximation values [179]. Lim and Cioffi studied the performance of an adaptive rate MQAM system which employs a simple on/off power control scheme [180]. Finally, Ding, Davidson, and Wong proposed two algorithms for improving the BER performance of bit loading systems, based on Eq. (2.33), that involve DFT-based linear combining and power reallocation [181].

### 2.4.2 Bit Loading with Imperfect Channel Information

Although many of the bit and power allocation algorithms covered in the previous subsection may provide significant performance improvements, they are usually evaluated when the channel conditions are perfectly known to the algorithm and the channel is time-invariant. However, the performance results may be overly optimistic and thus a more accurate performance analysis of bit and power loading algorithms is required.

Most researchers have focused on developing a more realistic scenario that these systems will experience. In particular, the impact of the following three effects that usually occur in the system are studied:

1. The effects of a time-varying channel and outdated channel state information [65, 182–187].
2. Channel estimation error and the propagation of that error [65, 66, 182].
3. Imperfect feedback due to distortion and/or quantization [188].

Since the effectiveness of the loading algorithms are heavily dependent on the quality of the channel state information, any of these effects would have a serious impact on its performance.

### 2.4.3 Power Allocation

In the previous section, various bit loading algorithms were presented that provided performance enhancements over systems employing a fixed signal constellation across all subcarriers. However, another method for improving system performance is tailoring the subcarrier power levels, thus changing the subcarrier SNR and BER values. Usually, power allocation is performed in tandem with bit allocation, as observed in several of the references mentioned in the previous subsection. In this subsection, the focus is on how power allocation is performed and the constraints imposed on the algorithm.

To compute the optimal power allocation, one may approach this problem using the Shannon capacity expression. Suppose for a single carrier system that the power distribution across the channel bandwidth  $W$  is defined as  $\pi(f)$ . Therefore, from an information

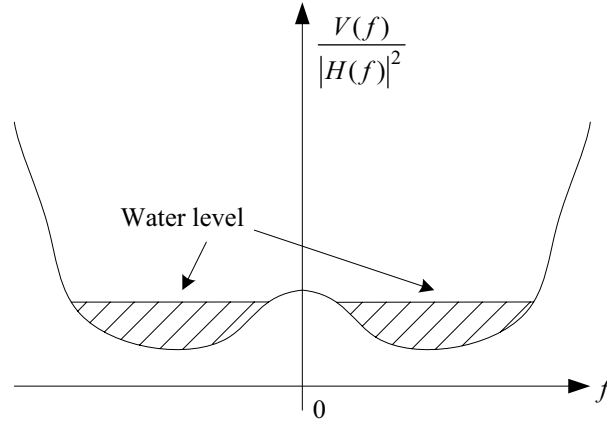


**Fig. 2.14** An example of waterfilling for the transmitted spectrum (from [189]).

theory perspective [47, 80, 189, 190], the total capacity of the system is defined as

$$C = \int_W \log_2 \left( 1 + \frac{\pi(f)|H(f)|^2}{V(f)} \right) df \quad (2.34)$$

where  $H(f)$  is the channel frequency response and  $V(f)$  is the noise power spectral density.

Suppose that the transmit power across the frequency domain is constrained according to

$$\int_W \pi(f)df \leq \pi_{\max}, \quad (2.35)$$

where  $\pi_{\max}$  is the maximum power allowed. Then, using Lagrange multipliers, the capacity  $C$  in Eq. (2.34) is maximized with respect to  $\pi(f)$ , yielding [47, 189]

$$\pi(f) = \left[ \mu - \frac{V(f)}{|H(f)|^2} \right]^+ \quad (2.36)$$

where  $f \in W$ ,  $\mu$  is chosen such that  $\pi(f)$  satisfies Eq. (2.35), and  $[\cdot]^+$  sets all negative values to zero. Notice how in Eq. (2.36) that more energy is allocated to regions in the spectrum where the noise, after being shaped by the channel frequency response, is the lowest. This approach is known as *waterfilling*, as illustrated by the shaded areas in Fig. 2.14

Substituting Eq. (2.36) into (2.34), the optimal capacity is given as [47, 189]

$$C_{\text{Optimal}} = \int_W \left[ \log_2 \left( \mu \frac{|H(f)|^2}{V(f)} \right) \right]^+ df. \quad (2.37)$$

It should be noted that this procedure could be applied to each subchannel, as is the case with multicarrier systems [47, 189]. In fact, Kalet derived the discrete version of waterfilling for multicarrier systems [80]. Yoshiki, Sampei, and Morinaga proposed a multi-level transmit power control for OFDM adaptive modulation systems to achieve high bit rate transmission without increasing the overall transmit power level [56]. The power levels per subcarrier were chosen so as to maximize the transmitted bits per OFDM symbol while keeping the transmit power level constant using a conventional transmit power control technique. Furthermore, no power was allocated to subcarriers experiencing deep fades, i.e., null subcarrier placement [49]. Goldfeld and Lyandres proposed a power allocation algorithm for multicarrier systems operating in frequency-selective Nakagami channels [191]. They then compared their results to equal power loading and noticed that the performance was enhanced, especially at low SNR values. Goldfeld, Lyandres, and Wulich proposed another power loading algorithm for OFDM systems operating in a fading environment where the objective is to minimize the overall BER [63]. Scaglione and Barbarossa proposed a power loading algorithm for underspread Rayleigh time-varying channels [67].

Thus far, most of the power loading algorithms studied in both the previous and current subsection only have a total power constraint to satisfy. However, this constraint is not sufficient if the spectrum used by the system has some regulatory requirements, such as the Unlicensed National Information Infrastructure (UNII) band at 5 GHz [192] (see Section 3.2 for more information)<sup>7</sup>. Thus power allocation schemes with stricter power constraints are required in order for them to be feasible in an actual implementation. Choi, Cheong, and Cioffi proposed a power allocation scheme for single carrier schemes that limits the peak power in order to avoid violations of regulatory requirements [193]. Fasano, Baccarelli, Zucchi, and Biagi proposed several power allocation algorithms for multicarrier systems that limit the peak power per subcarrier such that the requirements are satisfied [15–19].

---

<sup>7</sup>For the lower UNII band of 5.15–5.25 GHz, the power constraint is 2.5 mW/MHz, while for the 5.25–5.35 GHz middle UNII band it is 12.5 mW/MHz, and for the 5.725–5.825 GHz upper UNII band the power constraint is 50.0 mW/MHz.

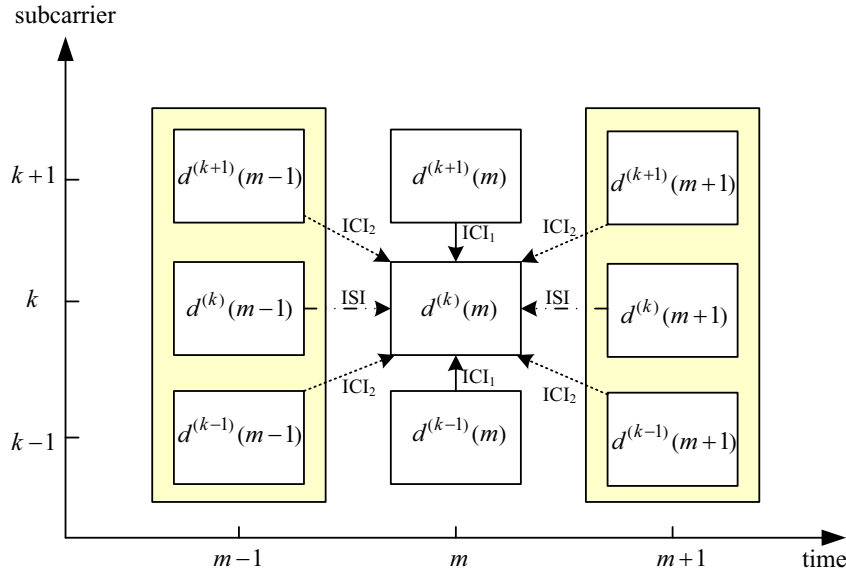


**Fig. 2.15** Different types of distortion present in multicarrier systems (from [79]).

## 2.5 Multicarrier Equalization Techniques

From the previous sections, it is obvious that there exists a number of performance advantages when employing adaptive allocation. To improve the quality of the received signal, equalizers are employed to remove most of the distortion introduced by the channel. The design decisions involved in the implementation of an equalizer depend on a number of factors, including the type of distortion present in the received signal and the implementation complexity. In this section, a description of the distortion normally found in multicarrier transmission systems and techniques to remove the distortion is presented. Moreover, two frequency domain equalization techniques will be covered.

### 2.5.1 Interference in Multicarrier Systems

There are several types of distortion which are found in multicarrier signals. Pollet *et al.* define the three types of interference prevalent in multicarrier systems based on the origin of the interference [79]. A graphical relationship of these types of distortion with respect to multicarrier transmission is shown in Fig. 2.15. Considering the interference on symbol  $m$  in subcarrier  $k$ , these three types are:

- ICI<sub>1</sub> This form of *intercarrier interference* (ICI) occurs when the interference contains the symbols transmitted over the other subcarriers of the  $m^{\text{th}}$  symbol period.
- ICI<sub>2</sub> This ICI occurs when the interference contains the symbols transmitted during periods other than the  $m^{\text{th}}$  symbol period from subcarriers other than subcarrier  $k$ .
- ISI This *intersymbol interference*, or ISI, occurs when the interference contains the symbols  $d^{(k)}(n)$ , where  $n \neq m$ .

As discussed in Section 2.1.2, the cyclic prefix in OFDM systems is used to capture the effects of ISI and ICI<sub>2</sub>. As for ICI<sub>1</sub>, the analysis filterbank of the OFDM system transforms it into a set of complex gains affecting the subcarriers.

With respect to a performance analysis of an OFDM system when these forms of interference are present, Li and Cimini derived a bound on the capacity of an OFDM system when intersymbol interference and time-varying impairments were considered [77].

### 2.5.2 Distortion Reduction

To mitigate the effects of the distortion introduced by the channel, there exists two techniques which may be employed by the system. One technique is *channel coding*, where the data is encoded with some redundancy so as to increase the probability of correctly recovering the original data from the intercepted transmission at the receiver. There exists several classes of channel codes that can be employed to correct for impulse errors in the transmission. Moreover, when an interleaver is employed by the encoder, channel coding can also compensate for predictable channel behaviour by randomizing the errors to make them appear as burst errors.

The other technique is *channel equalization*, where the effects of the channel are inverted at the receiver. This technique is specifically designed for channels with predictable distortion behaviour. In most cases, FIR filters are used at the receiver to equalize the incoming signal. One approach is to use multicarrier systems with FIR equalizers employed in each subcarrier. Due to the “divide-and-conquer” nature of MCM, where the data is transmitted in several subcarrier simultaneously, each subcarrier is only affected by a portion of the channel in terms of bandwidth, and thus requires fewer taps to compensate for the distortion. For instance, if the channel is frequency selective and a single carrier system is employed, the equalizer at the receiver will require a large number of taps to invert the

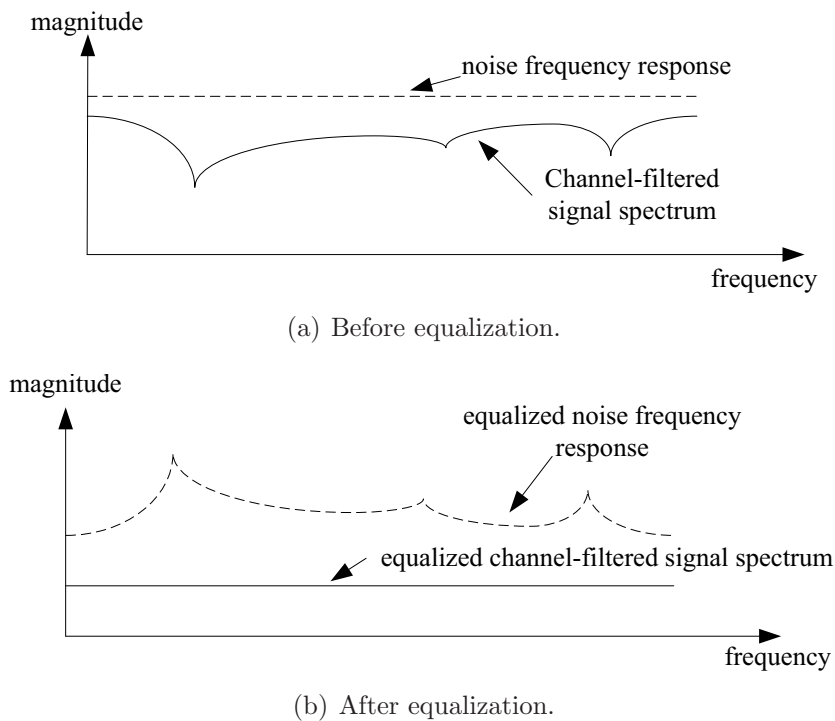


**Fig. 2.16** The effect of equalization on the noise spectrum.

channel. If a multicarrier system is employed, where  $N$  is sufficiently large, the frequency-selective fading channel is transformed into  $N$  approximately flat subchannels. Thus, the  $N$  subcarrier equalizers may consist of nothing more than a complex gain. This complex gain compensates for the gain and phase of the channel affecting the subcarrier. It is this procedure that is employed in ADSL modems [10, 41, 79, 103]. The details of this type of equalizer are discussed in Section 2.5.3. Even when  $N$  is not large enough to transform the channel into flat subchannels, equalizers with lengths greater than 1 could be employed per subcarrier.

Although equalization may compensate for the channel distortion, caution must be used when dealing with the noise that is added to the received signal. Suppose that the channel frequency response at the center of subcarrier  $i$  is defined by  $H_i$ . If a single-tap equalizer is used, it is equal to  $C_i = 1/H_i$ . However, since there is noise present in the received signal, it also gets multiplied by the equalizer. If the noise frequency response in subcarrier  $i$  is

given by  $V_i(\omega)$ , the post-equalized noise frequency response would be

$$V_i'(\omega) = \frac{V_i(\omega)}{H_i(\omega)}, \quad (2.38)$$

where  $H_i(\omega)$  is the channel frequency response over subcarrier  $i$ . Since  $|H_i(\omega)| < 1$  due to path loss, this means that  $|V_i'(\omega)| > |V_i(\omega)|$ . An illustrative example of the effect of equalization on the noise spectrum is shown in Fig. 2.16 for an input signal with an initially-flat spectrum. One solution is to pre-compensate the information for the distortion before transmission. This process is known as *pre-equalization* [55, 194]. However, pre-equalization only works if accurate channel knowledge is available at the transmitter, thus requiring a feedback path back from the receiver.

One of the advantages that multicarrier modulation has over single carrier modulation is that equalization can be performed on each subcarrier, as opposed to a long time-domain equalizer employed by single carrier systems. However, several researchers have devised a number of equalization schemes for single carrier systems that possess the same complexity as a multicarrier system implementing per-subcarrier equalization. Moreover, these single carrier systems do not suffer from a large peak-to-average ratio<sup>8</sup> problem experienced by multicarrier systems. Falconer *et al.* [195] conducted a comparison between single carrier systems employing a frequency-domain equalization technique and a multicarrier system. The results showed that the two systems have the same error rates but that the multicarrier system suffered from a large peak-to-average ratio. Two frequency-domain equalization techniques for MIMO systems were presented by Zhu and Murch [196], where the first technique was a conventional frequency-domain equalization with a time-domain decision feedback equalizer (DFE) while the second technique combined the first technique with parallel interference cancellation. Choi and Murch [197] designed a pre-frequency-domain equalization technique for use in a multiple input/single output system.

Although single carrier FEQ techniques may be superior to multicarrier systems with respect to PAR, single carrier systems with FEQ cannot perform adaptive bit allocation. Moreover, although adaptive power allocation can be performed in a single carrier system by changing the spectral pulse shape applied to the transmitted data stream, it is more difficult relative to a multicarrier system. As a result, they cannot fully exploit their advantages. For instance, Czylwik performed a comparison between an OFDM employing

---

<sup>8</sup> *Peak-to-average ratio* is the ratio between the peak transmitted power of a signal and its average power.

bit allocation and subcarrier FEQs and a single carrier system with a FEQ [198]. The results showed that the adaptive OFDM system outperformed the single carrier system.

### 2.5.3 Optimal Single-Tap Per-Tone Equalization for OFDM Systems

Once the cyclic prefix of appropriate length has been removed, the received signal is decomposed into separate subcarriers using the DFT. Then, to equalize the gain of the desired signal, the subcarriers are multiplied with the inverse of the channel frequency response across each of the subcarriers.

The importance of the cyclic prefix resides in the fact that it transforms the linear convolution between the transmitted signal  $s(n)$  and the channel impulse response  $h(n)$  into a symbol-by-symbol circular convolution. Suppose the OFDM symbol starts at time  $n = 0$ . Denoting  $s(0), \dots, s(N - 1)$  as the  $N$  output samples of the transmitter IDFT for the first OFDM symbol, the addition of the cyclic prefix of length  $K$  gives rise to a new signal, namely

$$\tilde{s}(n) = \begin{cases} s(n + N - K) & 0 \leq n \leq K - 1 \\ s(n - K) & K \leq n \leq N + K - 1 \end{cases}.$$

Defining  $\tilde{r}(n)$  as the result of the convolution of the signal  $\tilde{s}(n)$  with a channel impulse response  $h(n)$  of length  $S$ , assuming  $S \leq K + 1$ , this yields

$$\begin{aligned} \tilde{r}(n) &= \sum_{k=0}^{S-1} h(k)\tilde{s}(n - k) \\ &= \begin{cases} \sum_{k=0}^{n-K} h(k)s(n - K - k) + \sum_{k=n-K+1}^{S-1} h(k)s(n - k + N - K), & K \leq n \leq K + S - 1 \\ \sum_{k=0}^{S-1} h(k)s(n - K - k), & K + S \leq n \leq N + K - 1 \end{cases} \end{aligned}$$

From the above equation, it is observed that after the removal of the cyclic prefix, the received sequence  $r(n) = \tilde{r}(n + K)$  is

$$r(n) = \sum_{k=0}^{N-1} h(k)s(((n - k))_N) = h(n) \circledast_N s(n). \quad (2.39)$$

Thus, the received samples, after removal of the cyclic prefix, are just made up of the

circular convolution of the sent signal (i.e.,  $N$  samples per symbol) with the channel impulse response  $h(n)$ . If now one looks at Eq. (2.39) in the frequency domain, it looks like

$$R(k) = H(k) \cdot S(k),$$

where capital letters represent  $N$ -point DFTs of the corresponding sequences. With the multiplication of the corresponding frequency samples, each of the subcarriers experiences a different complex channel “gain”  $H(k)$ . Therefore, what must be done is to multiply each subcarrier with a gain that is an inverse to the channel frequency response acting on that subcarrier. This is the principle behind *per tone equalization*. Knowing what the channel frequency gains are at the different subcarriers, one can use them to reverse the distortion caused by the channel by dividing the subcarriers with them. For instance, if the system has 64 subcarriers centered at frequencies  $\omega_k = 2\pi k/64$ ,  $k = 0, \dots, 63$ , then one would take the CIR  $h(n)$  and take its 64-point FFT, resulting with the frequency response  $H(k)$ ,  $k = 0, \dots, 63$ . Then, to reverse the effect of the channel on each subcarrier, one would simply take the inverse of the channel frequency response point corresponding to that subcarrier,

$$W(k) = \frac{1}{H(k)} \quad (2.40)$$

and multiply the subcarrier with it.

#### 2.5.4 Frequency-Domain Equalizers for Multicarrier Systems

Although the single-tap per-tone equalizer for OFDM has the advantage of being simple and is optimal with respect to compensating for channel distortion, it has a few drawbacks, namely:

- The length of the cyclic prefix must be sufficiently long to capture the effects of ISI and ICI<sub>2</sub>. If the channel impulse response is long, the cyclic prefix will constitute a greater percentage of the OFDM symbol.
- This type of equalization works well only with OFDM.

Therefore, other implementations should be considered when conditions for the single-tap equalizer are unfavourable. One solution is to employ multi-tap equalizers on each subcarrier. Since each subcarriers operates across a smaller portion of the channel in the frequency

domain, the equalizer design may be less complex. For instance, Van Acker proposed a method for transforming a single time-domain equalizer, which is placed before the analysis filterbank for the purpose of *channel shortening*<sup>9</sup>, into a collection of multi-tap MMSE frequency-domain equalizers for each subcarrier [21]. This was done to allow for a larger bit rate, reduced complexity, and reduced sensitivity to synchronization delays [20]. Similarly, a multi-tap per-tone equalizer design for MIMO OFDM systems was proposed [200].

As for filterbank-based multicarrier systems, which do not employ a cyclic extension, the design of the per-subcarrier equalizers is a bit more complex and usually the final design has multiple taps. For instance, three different multi-tap FEQ designs for an MDFT filterbank system were proposed [201] where the difference in design was dependent on the location of the equalizers in the receiver chain. A tandem multi-tap TEQ phase equalizer with single-tap FEQs was also proposed so that the phase response of the received signal becomes linear, and thus easier to handle by the FEQs [105]. Finally, a multi-tap subcarrier equalizer design was proposed for critically-sampled CMFBs that used parallel cosine- and sine-modulated filterbanks [106].

## 2.6 Multiple-Antenna Multicarrier Systems

The idea of employing multiple antennas in wireless communication systems has been around for over a century. By exploiting the spatial dimension made available through multiple antennas, a communication system has the flexibility of either increasing throughput or error robustness depending of the choice of signal processing routines employed by the wireless transceiver. When the system employs signal processing algorithms that increase the overall throughput, this is called *spatial multiplexing* [202, 203]. On the other hand, when the algorithms enhance the error robustness of the system, this is known as *space-time coding* [202, 203].

Gesbert *et al.* discussed how to select design features at the physical layer, such as spatial diversity, frequency diversity, and MIMO-spatial multiplexing, and at the link layer, such as automatic repeat request fragmentation (ARQF) and adaptive modulation, in order to maximize bandwidth efficiency while maintaining a certain degree of link reliability for multiple transmitter/receiver antenna broadband wireless access systems in non-line-of-

---

<sup>9</sup>This involves a time-domain equalizer that partially equalizes the received signal such that the resulting channel impulse response after the time-domain equalizer is shorter than the cyclic prefix [199].

**Table 2.5** Layer 1 and 2 technologies for advanced non-line-of-sight fixed-wireless-access (from [204])

Technology	Impact (Qualitative)
ARQF	Set Point ↓
Adaptive Modulation	Data Rate ↑
Diversity (space)	Set Point ↓
Diversity (frequency)	Set Point ↓
MIMO-spatial multiplexing	Data Rate ↑

sight environment [204]. Also discussed were systems that employed MIMO-based spatial multiplexing and coded OFDM, which benefited from a channel environment with multipath delay spread. Finally, an overview of the effects of these techniques on the *set point*<sup>10</sup> of the system was presented and summarized in tabular form, as in Table 2.5.

An active area of research is the design and implementation of WLAN modems employing multiple antennas and the underlying signal processing routines. Currently, none of the ratified WLAN standards have included any details on the use of multiple antennas, although there have been a number of commercially-available MIMO WLAN systems, some of which are backward-compatible with a SISO WLAN standard [98, 99, 205]. However, a number of issues remain and thus work is continuing in the design of computationally-efficient, cost-effective MIMO WLAN systems. In this section, a brief overview of spatial multiplexing will be presented, followed by a more detailed discussion about space-time coding.

### 2.6.1 Spatial Multiplexing

Spatial multiplexing operates by transmitting independent data streams on each antenna, an example of which is the Bell Labs Layered Space-Time (BLAST) [206, 207]. At the receiver, each antenna intercepts the transmissions, performs some signal processing on all the received intercepts, and outputs the recovered data streams. A schematic of a simplified spatial multiplexing system is shown in Fig. 2.17. In the high-speed input data stream is demultiplexed and processed into a set of signals,  $s_i(n)$ ,  $i = 1, \dots, N_T$ , that are each transmitted by a dedicated antenna. After passing through the  $N_T \times N_R$  MIMO

<sup>10</sup>The level of SINR required at any one of the receive antennas in order to meet the link reliability target at a specified level of throughput.

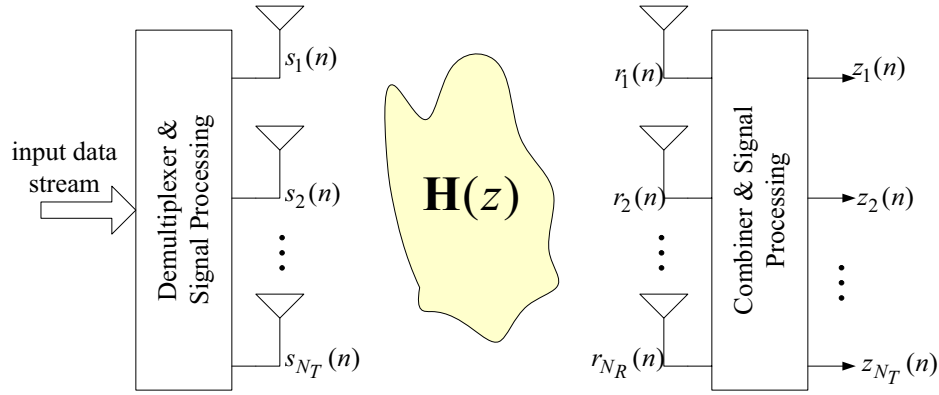


**Fig. 2.17** Schematic of a spatial multiplexing system (adapted from [208]).

channel  $\mathbf{H}(z)$ , defined as [208]

$$\mathbf{H}(z) = \begin{bmatrix} \mathbf{h}_{11}(z) & \mathbf{h}_{12}(z) & \cdots & \mathbf{h}_{1N_R}(z) \\ \mathbf{h}_{21}(z) & \mathbf{h}_{22}(z) & \cdots & \mathbf{h}_{2N_R}(z) \\ \vdots & \vdots & \ddots & \vdots \\ \mathbf{h}_{N_T1}(z) & \mathbf{h}_{N_T2}(z) & \cdots & \mathbf{h}_{N_TN_R}(z) \end{bmatrix}, \quad (2.41)$$

where  $\mathbf{h}_{ij}(z)$  is the channel response between transmit antenna  $i$  and receive antenna  $j$ , the signals received at each antenna,  $r_i(n)$ ,  $i = 1, \dots, N_R$ , are processed, yielding the recovered data streams,  $z_i(n)$ ,  $i = 1, \dots, N_T$ . The processing at the receiver can be performed using one of several techniques, including an ML approach or a zero-forcing or MMSE approach [208].

To ascertain the benefits of spatial multiplexing, a number of studies have been performed to evaluate the overall improvement of the system [88]. Several studies have focused on the signal processing techniques performed at the receiver [209, 210] while others have investigated the use of OFDM in a multiuser scenario with spatial multiplexing [150, 211, 212]. However, most of these studies do not consider the impact of imperfect feedback, which could negatively impact the performance of the system. Thus, several studies have been performed to assess its impact on system performance [188, 213]. Finally, several researchers have implemented hardware prototypes of spatial multiplexing OFDM systems for use in WLAN applications [203].

### Spatial Multiplexing with Beamforming

Another signal processing technique that can be employed at either end of the transceiver is *beamforming*, also known as *smart antennas* [214, 215]. Beamforming is an array processing technique that uses a set of phased antennas which are spaced close together, usually on the order of half a wavelength, in order to produce radiation beampatterns that are highly receptive at certain angles-of-arrivals while not receptive in others [141, 214–216]. This technique is extremely useful in environments where the presence of strong interferers exist at specific angle-of-arrivals, in which case beamforming can “null out” these interferers by directing the nulls at them. Furthermore, the main beam can be focused on the desired signals. As a result, strong interferers can be mitigated. Furthermore, multiple beampatterns can be employed to transmit different signals at the same frequencies. This frequency reuse can significantly increase system capacity, depending on the number of non-overlapping mainlobe beampatterns that can be supported by the antenna array. In the spatial multiplexing context, each of these petals would be directed at its own receive antenna [216].

Currently researchers are investigating techniques of combining adaptive beamforming with multicarrier systems [217–220]. One of the target applications of this research is WLAN systems, which do not currently employ adaptive beamforming at either the base station or the mobile, although in several studies the results show that its introduction could improve system performance [221]. However, a number of practical considerations need to be addressed, including an efficient implementation of beamformers in the multicarrier system [222], the use of partial channel state information [223], and various multiuser resource allocation algorithms [224].

#### 2.6.2 Space-Time Coding

Space-time coding (STC) is designed to increase the error robustness of the system by providing information redundancy in the spatial domain. Unlike spatial multiplexing, where each channel path between the transmitter and receiver carries an independent data stream, an STC system essentially sends one data stream that is spread across all the channel paths. There exists two categories of STC systems that are classified on the basis of how this spreading is achieved. The first is *spatial diversity*, where the same data stream is transmitted on each antenna. The second is the *space-time coder*, where each antenna transmits an

encoded version of the data stream that contains a certain amount of redundancy [225, 226]. Within this category, space-time coders can be classified as either space-time trellis codes (STTC) [164, 227–229] and space-time block codes (STBC) [227, 230, 231]. In the remaining part of this section, the details of the spatial diversity techniques will be presented.

### Spatial Diversity Techniques

Spatial diversity works by transmitting the same data stream on each antenna and performing some sort of combining at the receiver. If the antennas at the transmitter and receiver arrays are sufficiently spaced, then the channel paths between each transmit antenna and each receive antenna are uncorrelated, as discussed earlier. As a result, each copy of the transmitted data stream will experience distortion that is uncorrelated with the distortion of other channel paths. Thus, the probability that all copies of the data stream are severely affected by the channel is small when compared to a SISO system.

Spatial diversity can be performed at either the transmitter, which is known as *transmit diversity*, or at the receiver, which is called *receive diversity*, or both. Three types of transmit diversity commonly used in multiple antenna systems are *delay diversity* [227], *phase diversity* [232], and *cyclic delay diversity* [232], while three receive diversity techniques are *antenna selection* [33, 142, 233], *equal gain combining* [142, 233], and *maximum ratio combining* [142, 233].

In delay diversity, the signal at each of the transmit antennas is a delayed version of the other. As a result, this artificially spreads the signal in the time domain, resulting in the transformation of a flat fading channel into a frequency selective fading channel. A positive consequence of this is that it reduces the probability that all copies of the signal would be in a deep fade [232]. Unfortunately, a negative side effect of delay diversity is increased ISI. Thus, if the system uses OFDM, the cyclic prefix might have to be lengthened to cope with the ISI. An alternative is phase diversity, where the signal on each transmit antenna possesses a different phase with respect to the other signals. Mathematically, applying a phase delay  $\delta_l$  to the signal  $s(n)$  on transmit antenna  $l$  yields the signal [232, 234]

$$s_l(n) = \frac{1}{\sqrt{K}} \sum_{k=0}^{K-1} e^{j2\pi k\delta_l/K} \cdot S(k) \cdot e^{j2\pi kn/K} \quad (2.42)$$

where  $S(k)$  is the DFT of  $s(n)$ , and a  $K$ -point DFT is employed. However, in the case on an

OFDM system, the phase diversity must be performed prior to modulation by the IDFT. Thus, if there are  $N_T$  transmit antennas and  $N$  subcarriers, Eq. (2.42) must be performed  $N \cdot N_T$  times. An alternative is to use cyclic delay diversity. Cyclic delay diversity works by transmitting on each antenna a copy of the data stream, each of which with a different cyclic shift. Mathematically, this is represented as [232, 234]

$$s_l(n) = s(\text{mod}((n - \delta_l), K)) \quad (2.43)$$

where  $\delta_l$  is an integer shift of the cyclic extension. Comparing Eqs. (2.42) and (2.43), the expressions are mathematically equal. However, cyclic delay diversity has a lower implementation complexity relative to phase diversity since it only needs to be used  $N_T$  times.

Antenna selection diversity, also known as *switch diversity*, involves choosing the best signal from a set of received signals based on some prescribed metric [142, 233]. Usually this metric is signal strength, however BER or SNR can also be used as metrics. Although this scheme chooses a single receive antenna, it is possible to choose a subset of receive antennas and combine them using the other two receive diversity techniques (this is discussed in Section 2.6.2). Equal gain combining (EGC) takes advantage of all the receive antennas by co-phasing all the received signals and combining them together equally [142, 233]. Maximum ratio combining (MRC) is considered the optimal (SNR-maximizing) diversity combining technique [142]. Instead of weighting the signals from all the receive antennas equally, the weights are chosen to maximize the post-combining SNR. Suppose that receive antenna  $l$  intercepts a signal transmitted by a single antenna:

$$r_l(n) = h_l s(n) + \nu(n), \quad (2.44)$$

where  $h_l$  is the gain of the channel,  $s(n)$  is the original transmitted signal,  $\nu(n)$  is the additive white Gaussian noise, and  $l = 1, \dots, N_R$ . Therefore, using the combining weights

$c_l$ ,  $l = 1, \dots, N_R$ , the combined received signal is defined as

$$\begin{aligned} y(n) &= \sum_{l=1}^{N_R} c_l^* r_l(n) \\ &= \sum_{l=1}^{N_R} c_l^* h_l s(n) + \sum_{l=1}^{N_R} c_l^* \nu(n). \end{aligned} \quad (2.45)$$

Let the energy of  $s(n)$  be equal to  $\epsilon$  and the power spectral density of  $\nu(n)$  be  $N_0$ . Then, the post-combining SNR is defined as

$$\gamma = \frac{\epsilon \cdot \sum_{l=1}^{N_R} |c_l^* h_l|^2}{N_0 \cdot \sum_{l=1}^{N_R} |c_l|^2}, \quad (2.46)$$

where the maximum value can be found by applying the Cauchy-Schwartz inequality [47]

$$\begin{aligned} \gamma_{\text{opt}} &= \frac{\epsilon}{N_0} \cdot \sum_{l=1}^{N_R} |c_l|^2 \\ &= \frac{\epsilon}{N_0} \cdot \sum_{l=1}^{N_R} |h_l|^2 \end{aligned} \quad (2.47)$$

given that the optimal choice for  $c_l$  is  $c_l = h_l$ . Therefore, if one of the received signals passed through a deep fade, it would be weighed less relative to a signal that was attenuated less.

There have been a number of diversity schemes proposed by several researchers, either for the transmit antenna array [235–238] or the receive antenna array [239, 240]. In particular, several diversity techniques have been proposed for multicarrier systems that operate on each subcarrier [76, 241–243]. Several researchers have also investigated the use of channel coding with OFDM and antenna diversity [244], while others have derived closed-form expressions for the error probabilities of the OFDM system employing various receiver combining techniques [245].

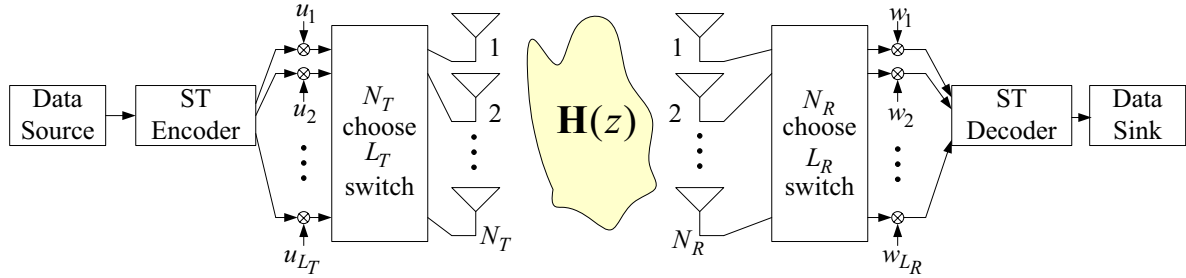


**Fig. 2.18** Schematic of a multiple antenna system employing transmit and receive antenna subset selection (from [33]).

### Antenna Subset Selection with Diversity

From the previous subsection, three receive diversity schemes were presented. Moreover, it was assumed that all the transmit antennas were active in the transmit diversity schemes. However, using a large number of antennas at the transmitter and receiver can be computationally expensive in terms of the signal processing involved. The cost of employing more radio frequency (RF) chains in the system also does not justify the improvement in performance, which follows the law of diminishing returns [33]. Therefore, researchers are looking at ways of reducing the complexity and cost of MIMO systems while accepting a small penalty in error performance. One solution is antenna subset selection, also known as *generalized selection combining*, where a subset of antennas at either the transmitter, the receiver, or both are chosen to be active in the transmission. The subset selection is preceded in the transmitter and succeeded in the receiver by some space-time processing. A schematic of antenna subset selection is shown in Fig. 2.18. The idea behind antenna subset selection is that contribution of the weak signals to the calculation of the SNR is too small. Thus, the system chooses the  $L_T$  ( $L_R$ ) antennas out of  $N_T$  ( $N_R$ ) antennas that yield the best performing signals.

In the area of antenna subset selection, the research activities are either focused on evaluating its performance gains relative to full diversity systems [23–25, 27, 29–31, 246, 247] or developing algorithms that efficiently search for the best  $L_T$  ( $L_R$ ) out of  $N_T$  ( $N_R$ ) antennas [26, 248–251].

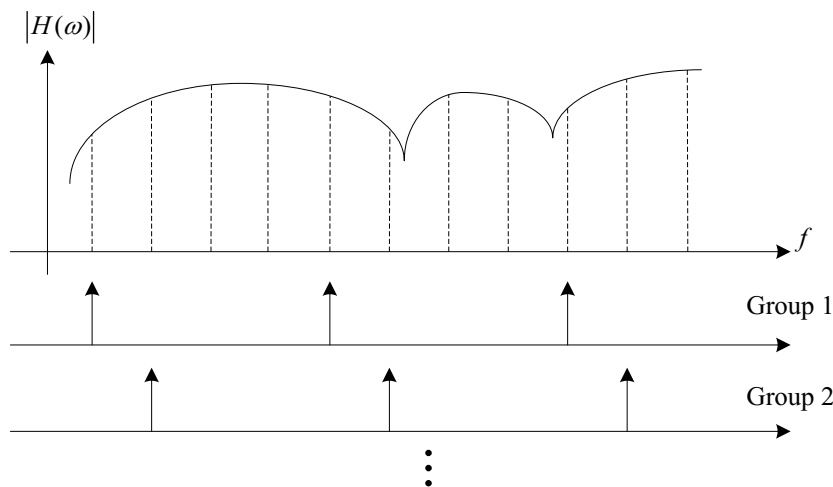


**Fig. 2.19** Grouping of tones for complexity reduction in STF coding (from [28]).

### Space-Time-Frequency Coding

Although much work has gone into the design of STC by numerous researchers [229, 230, 252], most make the assumption that the channel experiences flat fading. In the work by Molisch, Win, and Winters [28], an STC system was proposed that operated in frequency-selective fading conditions by including OFDM at each of the antennas. The frequency-selective fading channels were decomposed into a collection of approximately flat fading subchannels using OFDM. Following this, STC was then applied across groups of tones, where the tones in each group are separated by an amount equal to or greater than the coherence bandwidth (see Fig. 2.19). This new framework was dubbed space-time-frequency (STF) coding. Moreover, it was shown that existing STC schemes, which were originally designed for flat fading environments, can be employed in this setup.

A novel joint STF coding scheme for multiple antenna OFDM systems operating in frequency-selective channels was proposed by Liu, Xin, and Giannakis [253]. Space-time-frequency coding is space-time coding with redundancy added in the frequency domain, such as linear precoding, in order to exploit the maximum diversity gain possible in frequency selective channels.

## 2.7 Chapter Summary

In this chapter, details regarding the basic physical layer components of a wireless communication system employed in WLAN applications were presented.

Section 2.1 started with a tutorial on MCM. In particular, the fundamentals of MCM and how it works in both the time and frequency domains were presented. The principles behind OFDM, including the importance of the cyclic prefix, were covered. The details behind filterbank multicarrier modulation, including the PR condition, complex exponential-modulated filterbanks, and MDFT filterbanks, were presented.

Indoor wireless channel models were then covered for both SISO and MIMO systems in Section 2.2. The physics behind multipath fading were described, as well as several SISO and MIMO channel models. The modelling of a correlated MIMO channel was also derived. Data-assisted channel estimation and synchronization techniques were also covered in Section 2.3.

Adaptive bit and power allocation algorithms for MCM systems were then presented in Section 2.4. Besides an example illustrating the benefits of bit loading, several types of bit loading algorithms were covered, including the capacity approximation-based algorithms. The impact of imperfect channel state information on the performance of these algorithms was also covered. Power allocations algorithms, with emphasis on frequency interval power-constrained algorithms were presented.

Equalization techniques employed in MCM systems were covered in Section 2.5. The section provided an overview of the types of distortion present in a multicarrier symbol (e.g., an OFDM symbol). Equalization techniques were also presented, including the single-tap optimal per-tone equalizer for OFDM systems with a sufficiently long cyclic prefix and several multi-tap FEQ designs. The problem of insufficient cyclic extensions was also addressed.

In Section 2.6, array signal processing techniques were presented, some with an emphasis on MCM systems. The differences between spatial multiplexing and space-time coding were outlined. The details of each category were provided, although the latter category was emphasized. Various transmit and receive diversity schemes were covered and the antenna subset selection technique was presented. Finally, the importance of STF coding was briefly covered.

## Chapter 3

# BER-Constrained Multicarrier Loading Algorithms

One of the focuses of this dissertation is to tailor the operating parameters of multicarrier systems to the channel environment, which will yield an enhancement in system performance. In particular, several cost-efficient performance-enhancing techniques applicable to multicarrier WLAN systems are investigated. Two system parameters that are usually tailored to the subchannels on a per-subcarrier basis are the modulation scheme and the transmit power level. Since the subcarrier bit error rate (BER) is a function of the minimum distance between two symbols of a signal constellation, changing the number of symbols in the signal constellation (i.e., number of bits per symbol) and/or the transmit power level (i.e., the spacing between symbols) will directly impact the BER. In this work, throughput is maximized while the mean BER is constrained to be below some prescribed value.

Another system parameter that can be tailored to the channel conditions on a per-subcarrier basis is the length of the subcarrier equalizers. Since adding more equalizer taps usually reduces the MSE, equalizer taps can be non-uniformly allocated across the subcarriers, with more taps allocated to poorly-performing subcarriers and fewer taps to the other subcarriers. As a result, the mean MSE of the system is lowered while the total number of equalizer taps employed is kept to a minimum, resulting in a reduction of power consumption by the system.

All allocation algorithms require some feedback from the receiver on the prevailing chan-

nel conditions. As in other studies [6, 11, 12, 48, 49, 63, 64, 80, 81, 83, 84, 254], the transmitter and receiver usually have perfect knowledge of the channel conditions (obtained through data-assisted channel estimation techniques). However, it is possible that the feedback information can be outdated, contains channel estimation errors, or quantized due to a bandlimited feedback channel. Thus, the impact of imperfect feedback is an important issue that will be covered in this chapter.

Finally, this work seeks to improve the performance of conventional WLAN systems through the use of adaptive allocation algorithms. Thus, unless otherwise stated, the system parameters, such as the number of subcarriers, operating frequency, bandwidth, and available modulation schemes, correspond to the IEEE 802.11a standard [2]. However, this does not mean that these algorithms cannot be extended to other systems, such as wireless metropolitan area networks (WMAN) [62], digital subscriber line (DSL) modems [39], or other multicarrier communication systems.

### 3.1 Discrete Bit Loading Algorithms

Channel coding can be used to enhance system performance, as in the IEEE 802.11a and the ETSI HiperLAN/2 WLAN standards, which employ convolutional codes (refer to Table 2.3). In these standards, a single “outer” convolutional encoder, combined with an interleaver, is applied to the high-speed input stream prior to multicarrier modulation and a single “outer” decoder is applied to the reconstructed high-speed data stream<sup>1</sup>. In this work, the multicarrier modulation section (i.e., the “inner” portion of the system) is abstracted in order to study the improvements associated with tailoring the multicarrier transmission parameters to the channel conditions. For instance, the number of signal constellation points employed by a subcarrier modulation scheme can be assigned, i.e., bit allocation. To keep the implementation simple and straightforward, the proposed bit allocation algorithms assign an integer number of bits, i.e., implements *discrete bit allocation*. Moreover, for systems that perform decoding based on hard decisions from the channel information, or are uncoded altogether (e.g., only the multicarrier portion of the system), the average BER of a multicarrier system is an appropriate metric for the optimization of the inner portion of the system. This metric is employed in most of the proposed allocation algorithms in this dissertation.

---

<sup>1</sup>According to [2], it is recommended that decoding is performed using the Viterbi algorithm.

The two discrete bit allocation algorithms presented in this chapter configure the modulation schemes of each subcarrier so as to maximize the overall system throughput while achieving an error performance that is less than some prescribed threshold, even at the cost of some throughput. Mathematically, this is defined as

$$\max_{b_i} \sum_{i=0}^{N-1} b_i, \quad \text{subject to} \quad \bar{P} = \frac{\sum_{i=1}^N b_i P_i}{\sum_{i=1}^N b_i} \leq P_T \quad (3.1)$$

where  $b_i$  is the number of bits for subcarrier  $i$ ,  $\bar{P}$  is the mean bit error rate (BER),  $P_T$  is the specified BER threshold, and  $P_i$  is the BER for subcarrier  $i$ , which is determined from the subcarrier SNR value,  $\gamma_i$ . In [14], the optimization problem is different relative to Eq. (3.1), where the throughput is maximized given simultaneous constraints on the total power allocated and the maximum-allowed BER per subcarrier.

In this dissertation, square  $M_i$ -QAM modulation schemes are employed on a per subcarrier basis, where  $M_i = 2, 4, 16, 64$ . The choice of the subcarrier modulation scheme is dependent on the subcarrier SNR, which varies for each subcarrier due to the frequency selectivity of the channel. Although the objective functions and constraints of the two algorithms are the same, the way each performs the bit allocation is different, yielding different computational complexities and throughput results. One of the main goals of this research is to develop a set of algorithms that can achieve a balance between computational complexity and closeness to the optimal throughput.

### 3.1.1 Proposed Incremental Bit Loading Algorithm<sup>2</sup>

An incremental allocation algorithm distributes the bits in an iterative fashion across the subcarriers, one bit per iteration. Most incremental allocation algorithms can be classified as *greedy* algorithms, where the algorithm allocates one bit at a time to the subcarrier that will do the most good for the allocation at that instant. The algorithm is called greedy since it only maximizes the quantity of interest for the current allocation without regard to the global effects of its choice [9]. Both Campello [84] and Fox [7] defined conditions which

---

<sup>2</sup>The work was presented in parts at the *56th IEEE Vehicular Technology Conference* [254], the *15th International Conference on Wireless Communications* [255], and the *IEEE Transactions on Wireless Communications* [256].

yield an optimal allocation<sup>3</sup>.

The proposed incremental bit allocation algorithm is presented in Fig. 3.1. At the transmitter, the system first employs the modulation scheme with the largest signal constellation across all the subcarriers. In this case,  $b_i = 6$ , for  $i = 0, \dots, N - 1$ . This is unlike most of the other incremental allocation algorithms in the literature, which usually initialize the allocation with the smallest modulation schemes. However, the proposed algorithm has the advantage of fewer iterations in reaching the final allocation for medium to high SNR values. The subcarrier BER values,  $P_i$ ,  $i = 0, \dots, N - 1$ , are then computed using *a priori* knowledge of the channel and the initial values of transmit power levels.

Averaging the subcarrier BER values using

$$\bar{P} = \frac{\sum_{i=1}^N b_i P_i}{\sum_{i=1}^N b_i}, \quad (3.2)$$

the mean BER  $\bar{P}$  is compared against a BER threshold  $P_T$ . If the mean BER is below the threshold, the system configuration is kept. Otherwise, the signal constellation of the subcarrier with the worst BER is reduced in size. The rationale behind choosing the worst-performing subcarrier is that its BER would dominate the overall average, masking the performance of those subcarriers with smaller BER values. Then,  $\bar{P}$  is recomputed using Eq. (3.2) and compared against the threshold. This process is repeated until either the threshold is met or until all the subcarriers are nulled.

To compute the probability of bit error for all subcarriers, closed-form expressions are employed. For instance, the probability of bit error for BPSK is given by [257]

$$P_{2,i}(\gamma_i) = Q(\sqrt{2\gamma_i}) \quad (3.3)$$

while the probability of symbol error for QPSK ( $M_i = 4$ ), square 16-QAM ( $M_i = 16$ ), and

---

<sup>3</sup>Campello showed for a bit rate maximization problem that the optimal bit allocation exists if the rate-distortion surface across all the subcarriers is *efficient* and *E-tight* [84]. As for Fox, he showed that the optimal allocation can be determined if the objective function is concave and strictly increasing [7].

1. Initialization: set the modulation scheme of all the subcarriers to 64-QAM.
2. Determine  $P_i$ ,  $i = 1, \dots, N$ , given the subcarrier SNR values, using Eqs. (3.3) or (3.4).
3. Compare  $\bar{P}$ , with  $P_T$ . If  $\bar{P}$  is less than  $P_T$ , the current configuration is kept and the algorithm ends.
4. Search for the subcarrier with the worst  $P_i$  and reduce the constellation size. If  $b_i = 1$ , null the subcarrier (i.e., set  $b_i = 0$ ).
5. Recompute  $P_i$  of all subcarriers with changed allocations and return to Step 3.

**Fig. 3.1** Proposed incremental bit loading algorithm based on a greedy approach [254–256].

square 64-QAM ( $M_i = 64$ ) is given by [257]

$$P_{M_i,i}(\gamma_i) = 4 \left( 1 - \frac{1}{\sqrt{M_i}} \right) Q \left( \frac{3\gamma_i}{M_i - 1} \right) \cdot \left( 1 - \left( 1 - \frac{1}{\sqrt{M_i}} \right) Q \left( \frac{3\gamma_i}{M_i - 1} \right) \right) \quad (3.4)$$

where  $\log_2(M_i)$  gives the number of bits to represent a signal constellation point<sup>4</sup>. To obtain the probability of bit error from the symbol error of Eq. (3.4), use the approximation  $P_i \approx P_{M_i,i} / \log_2(M_i)$ . Note that the proposed bit loading algorithm does not explicitly perform power allocation, although it can be easily modified to include it [254, 255].

The objective function of the proposed algorithm is to maximize the overall throughput of the system. However, it is possible for the proposed algorithm to yield a bit allocation that is not equal to the optimal allocation, i.e., the largest throughput satisfying the mean BER constraint. The following scenario illustrates how the algorithm could yield a sub-optimal bit allocation: For the final iteration of the algorithm, there exists two subcarriers with the worst BER,  $i$  and  $j$ . Reducing the number of bits in either subcarrier will result in  $\bar{P} \leq P_T$ . If subcarrier  $i$  is chosen, two bits are removed. On the other hand, if subcarrier

<sup>4</sup>Although Eqs. (3.3) and (3.4) depend on the interference being Gaussian, this is likely to be true in the case of OFDM-type systems with a sufficiently long cyclic extension. In the case of filterbank modulation, the distribution of the interference from ISI and both forms of ICI can either be assumed to be Gaussian in order to make the expressions more tractable, or the contributions of the ISI and ICI are too small to be significant due to the spectral selectivity of the synthesis and analysis filters.

$j$  is chosen, only one bit is removed. This is possible since  $\log_2(64) - \log_2(16) = \log_2(16) - \log_2(4) = 2$  bits per symbol epoch, while  $\log_2(4) - \log_2(2) = \log_2(2) - 0 = 1$  bits per symbol epoch. Therefore, if  $P_i < P_j$ , then the algorithm will choose subcarrier  $j$  to be decremented, resulting with an overall allocation that is optimal.

### 3.1.2 Proposed Peak BER-Constrained Bit Allocation Algorithm<sup>5</sup>

Although the proposed incremental bit allocation algorithm might attain near-optimal solutions (see Section 3.4), its computational complexity is still rather high at low SNR values. What is needed is an algorithm which accurately maps the subcarrier SNR values to some final bit allocation in an iterative, low computational complexity fashion. This is the rationale behind the proposed peak BER-constrained bit allocation algorithm.

Instead of iteratively adding a bit to a subcarrier and checking if the mean BER constraint is not violated, which is computationally expensive, the proposed peak BER-constrained algorithm allocates bits to each subcarrier so that all subcarrier BERs  $P_i$  is below some peak BER constraint  $\hat{P}$ . The proposed algorithm is shown in Fig. 3.2. First, the probability of bit error for a constellation of  $M_i$  points for subcarrier  $i$ ,  $P_{M_i,i}$ , is evaluated for  $i = 0, \dots, N-1$  and  $b_i = \{0, 1, 2, 4, 6\}$ . Then the constellation size  $M_i = 2^{b_i}$  that is maximum while still having  $P_{M_i,i} \leq \hat{P}$  is chosen, i.e.,  $P_i = P_{M_i,i}$ , for  $i = 0, \dots, N-1$ . The initial value of the peak BER constraint  $\hat{P}$  is chosen as a proxy to satisfying an average BER constraint  $\bar{P}$ . A first guess on  $\hat{P}$  is taken, the bits  $b_i$  are allocated accordingly, and the resulting  $\bar{P}$  is computed using Eq. (3.2). If  $\bar{P}$  is below (above)  $P_T$ ,  $\hat{P}$  is increased (decreased) by an amount  $\delta$  in the logarithmic domain at every iteration. The value of  $\hat{P}$  is adjusted in this way until  $\bar{P}$  exceeds (goes below)  $P_T$ , in which case  $\delta$  is reduced.

The terminating criterion in Step 10 is explained as follows: In the case that the previous and current  $\bar{P}$  values straddle  $P_T$ , the allocations are compared in order to see if they differ by one signal constellation. If they do, it is obvious that the additional bit(s) is/are the cause of the violation of the mean BER constraint. Otherwise,  $\delta$  is reduced until the case of one differing signal constellation is achieved. Note that Steps 3 and 4 provide a quick exit from the algorithm when the subcarrier SNR values are either large enough to have the system operate at maximum throughput or lower than the minimum SNR required to yield a non-zero throughput, respectively. Also note that the rationale behind Step 10 is that if

<sup>5</sup>The work was presented in parts at the *IEEE Wireless Communications and Networking Conference* [258] and the *IEEE Transactions on Wireless Communications* [256].

1. Given  $\gamma_i$ ,  $i = 0, \dots, N - 1$ , calculate  $P_i$  for all  $i$  and modulation schemes.
2. Compute  $\bar{P}$ , the average BER, using Eq. (3.2) for the largest  $M_i$ ,  $i = 0, \dots, N - 1$ , where  $b_i = \log_2(M_i)$  is the number of bits.
3. If  $\bar{P} \leq P_T$ , choose largest  $M_i$ ,  $i = 0, \dots, N - 1$ , and end algorithm, else go to Step 4.
4. If  $\min_i P_i > P_T$ , then  $M_i = 0$ ,  $i = 0, \dots, N - 1$ , and end algorithm, else go to Step 5.
5. Find  $M_i$  for which  $P_i < \hat{P}$  for all  $i$ .
6. Compute  $\bar{P}$ .
7. If first iteration of algorithm, reduce  $\hat{P}$  by  $\delta$  and go to Step 5, else go to Step 8.
8. If both current and previous  $\bar{P}$  values are above or below  $P_T$ , go to Step 9, else go to Step 10.
9. If both current and previous  $\bar{P}$  values are above  $P_T$ , reduce  $\hat{P}$  by  $\delta$  and go to Step 5, else increase  $\hat{P}$  by  $\delta$  and go to Step 5.
10. If previous and current allocations differ by one signal constellation level, make the allocation with  $\bar{P} \leq P_T$  the final allocation and end the algorithm, else go to Step 11.
11. Reduce  $\delta$ .
12. If the current allocation gives a  $\bar{P} > P_T$ , reduce  $\hat{P}$  by  $\delta$  and go to Step 5, else increase  $\hat{P}$  by  $\delta$  and go to Step 5.

**Fig. 3.2** Proposed bit loading algorithm based on a peak BER constraint [256, 258].

the previous and current  $\bar{P}$  values straddle  $P_T$  as well as differ by one signal constellation, it can be safely assumed that the additional bit(s) is/are the cause of the violation of the mean BER constraint.

### Initial Peak Bit Error Rate Threshold Calculation

The speed at which the proposed peak BER-constrained algorithm reaches its final allocation depends on the choice of the initial  $\hat{P}$  and the  $\delta$  it uses. One approach to this problem is to determine how much any given subcarrier can individually exceed  $P_T$  while  $\bar{P}$  remains below it. Given that a subcarrier can support  $B$  possible modulation schemes (in this

1. Given the subcarrier SNR values,  $\gamma_i$ , calculate  $P_i$  for all the different modulation schemes which could potentially be employed in the system.
2. Find  $\beta_i$ , the largest  $P_i$  that does not exceed  $P_T$ .
3. Find  $\alpha_i$ , the smallest  $P_i$  that exceeds  $P_T$ .
4. Find all values of  $\beta_i$  that are within an order of magnitude of  $\max_i \beta_i$  and assign their indices to a set  $\mathcal{S}$  ( $\beta_i$  not within an order of magnitude can be neglected).
5. Given  $\beta_i, i \in \mathcal{S}$ , we need to solve for  $\Delta P$ , given

$$\Delta P = \sum_{i \in \mathcal{S}} b_i (P_T - \beta_i).$$

in order to determine by how much several subcarriers can violate the condition  $P_i \leq P_T$  while the system still satisfies  $\bar{P} \leq P_T$ .

6. Sort the values of  $\alpha_i$  in an increasing order. Find the largest value of  $I$  for which

$$\Delta P \geq \sum_{i=0}^I b_i (\alpha_i - P_T)$$

is true, where  $0 \leq I < N$ , and set  $\alpha_I$  as the initial  $\hat{P}$  for the algorithm described in Section 3.1.2.

**Fig. 3.3** Algorithm for determining the initial peak bit error rate [256, 258].

dissertation,  $B=5$  is considered), resulting in  $B$  possible values for  $P_i$ , the largest  $P_i$  value that is below  $P_T$  is defined as  $\beta_i$  while the smallest value of  $P_i$  above  $P_T$  is defined as  $\alpha_i$ . Therefore, knowing that the mean of  $\beta_i, i = 0, \dots, N-1$ , is below  $P_T$ , we incrementally replace the smallest  $\beta_i$  with the corresponding  $\alpha_i$  until  $\bar{P} > P_T$ . The algorithm for finding the initial peak BER  $\hat{P}$  estimate is shown in Fig. 3.3.

The initial value of  $\delta$  is proportional to the average SNR of the system,  $\bar{\gamma}$ . It has been observed in several simulations that for low  $\bar{\gamma}$  values, small values for  $\delta$  resulted in the algorithm converging quickly to a final solution, while for high  $\bar{\gamma}$  values, large values of  $\delta$  resulted in quickly obtaining the solution. Thus, choosing the values for  $\delta$  between the two extremities,  $\delta$  decreases linearly as a function of  $\bar{\gamma}$ .

Using these values of  $\delta$  in conjunction with the initial  $\hat{P}$  algorithm, the number of

iterations required to find the final  $\hat{P}$  can be reduced by as much as half when compared to a scheme using a random initialization.

### 3.1.3 Effects of Imperfect Subcarrier SNR Information<sup>6</sup>

Although many studies on adaptive bit loading algorithms make the assumption that the subcarrier SNR values are perfectly known, this is not the case in reality. As a result, the performance of the allocation algorithms can be significantly affected by this imperfect channel information. There are a number of sources that can create imperfections in the channel information: channel estimation, time-varying channels, band-limited feedback channel, inadequate training symbol design. Therefore, it is necessary to investigate the impact of imperfect subcarrier SNR information, which is derived from the channel information, on the throughput performance of systems using the proposed bit allocation algorithms. In particular, channel estimation errors and quantization errors will be examined.

#### Gaussian Subcarrier SNR Error Model

A derivation of the expression of the channel estimation error for a multicarrier system employing data-assisted channel estimation is presented in Appendix A. Referring to Eq. (A.4), it is observed that the channel estimation error consists of the term  $\Delta^{(i)}(m)$ , which refers to the estimation error on subcarrier  $i$ . Therefore, the derivation for the SNR of subcarrier  $i$  based on the channel estimates is presented in Eq. (A.6), with the final expression given as

$$\hat{\gamma}^{(i)} = \gamma^{(i)} + \epsilon^{(i)}(\gamma^{(i)}) \quad (3.5)$$

where the estimation error  $\epsilon^{(i)}(\gamma^{(i)})$  is a function of the subcarrier SNR.

In this work, the subcarrier channel estimation error  $\epsilon^{(i)}(\gamma^{(i)})$  is approximated by a Normal distribution with zero mean and variance  $\sigma^2$  [182]<sup>7</sup>. However, the negative values of  $\epsilon^{(i)}(\gamma^{(i)})$  are constrained such that Eq. (3.5), being the ratio of powers, is never negative.

<sup>6</sup>The work will be presented at the *IEEE Global Telecommunications Conference* [259] and has been partially presented in the *IEEE Transactions on Wireless Communications* [256].

<sup>7</sup>The variance  $\sigma^2$  should be a function of the subcarrier SNR, i.e.,  $\sigma^2(\gamma^{(i)})$ . However, a range of constant variance values across all SNR values is used instead to allow for a straightforward comparison of the algorithms.

### SNR Quantization Error Model

Adaptive bit loading algorithms use the channel state information to determine the bit allocation. However, the information is usually transformed into a metric that indicates the quality of the transmission across the different subcarriers. In this work, the channel state information is used to compute the subcarrier SNR values, which are then used to compute the subcarrier BER values via closed form expressions for a given modulation scheme, e.g., Eqs. (3.3) and (3.4). To reduce the implementation complexity, a look-up table can be used instead to translate subcarrier SNR values into subcarrier BER values,  $P_i$ , for each subcarrier  $i$ . However, this implies that the subcarrier SNR values must first be quantized before using the look-up table. Due to the quantization, additional errors are introduced to the subcarrier SNR values that may cause the bit allocation to deviate further from the ideal. These errors can be classified as either *granular errors*, when the input signal is within the range of the quantizer but does not fall exactly on an output level, or *overload errors*, when the input signal falls outside of the range of the quantizer [91].

In this work, a mid-rise uniform quantizer is employed to quantize the subcarrier SNR values (in decibels). The SNR estimation is performed at the receiver while bit allocation is normally performed at the transmitter, as shown in Fig. 2.1. A feedback channel is employed to transmit quantized SNR values. However, in order to ensure that the impact of the quantization error is minimized when considering all the modulation schemes, the locations of the quantizer reproduction (i.e., output) levels,  $d_k$ , must be determined. Since an adequate resolution of the bit error rate waterfall curves is desired around the target probability of bit error,  $P_T$ , the output levels should be concentrated about that point. A novel sub-optimal  $d_k$  placement technique that tries to minimize the overall error while providing adequate resolution will now be presented.

### Quantization Reproduction Level Placement Technique

To obtain adequate resolution of the BER waterfall curves for the modulation schemes employed by the system, where the rate of decrease for each curve may vary drastically, the following technique is proposed that tries to perform a sub-optimal placement of  $d_k$ :

1. Given  $q$  bits to represent a quantizer reproduction level, the number of levels is defined as  $2^q$ , which corresponds to a  $2^q$ -entry look-up table.

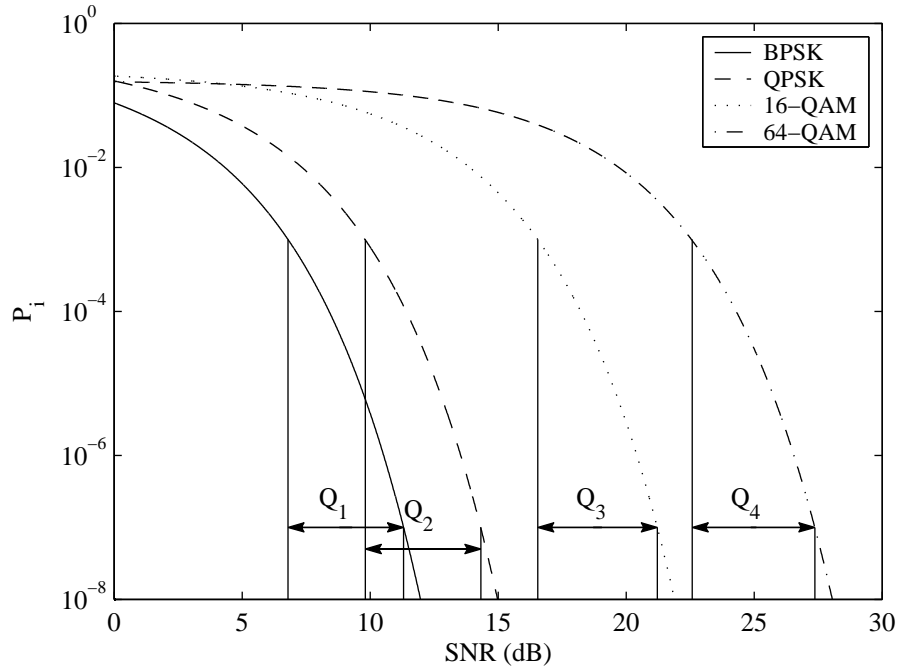


**Fig. 3.4** Regions of uniform quantization of the  $P_i$  waterfall curves for  $P_T = 10^{-5}$  and  $B = 4$ .

2. Determine the pair of SNR values to obtain the probability of bit error values,  $P_i$ , that are two orders of magnitude above and below  $P_T$  for each modulation scheme, thus forming regions  $Q_k$ , for  $k = 1, \dots, B$ , where  $B$  is the number of modulation schemes.
3. For the  $B$  modulation schemes, put  $2^q/B$  output levels uniformly in  $Q_k$  for all  $k$ . In the case of overlapping regions, combine them and their allocation of output levels, distributing the levels uniformly across the combined region.

An example of this procedure is shown in Fig. 3.4 for  $P_T = 10^{-5}$  and  $B = 4$ . In this case, the  $P_i$  curves correspond to BPSK, QPSK, 16-QAM, and 64-QAM. If  $P_i > 10^{-3}$ , quantizing that part of the BER curve is not worthwhile since the  $P_i$  is so high that the subcarrier would be nulled. On the other hand, if  $P_i < 10^{-7}$ , then  $P_i$  is so far below  $P_T$  that any quantization would not significantly affect the mean BER of the system,  $\bar{P}$ . Where  $Q_1$  and  $Q_2$  overlap, the output levels allocated to the two regions would be combined and distributed uniformly across the aggregate region.

By distributing  $d_k$ ,  $k = 0, \dots, 2^a - 1$ , in this way, the BER waterfall curves can be quantized with sufficient resolution.

### 3.2 Power Loading Algorithm

Power allocation is a powerful technique for enhancing system performance when the multicarrier system operates in a frequency selective fading channel. From the optimal power allocation solution presented in Section 2.4.3, it was observed that a frequency selective channel combined with additive white noise will yield varying SNR values across frequency (see Fig. 2.14). In this situation, the allocation of a non-uniform amount of power across the transmission spectrum could yield an increase in performance. In the context of multicarrier systems, the modification of the transmit power levels can be performed on a subcarrier basis rather than in a continuous fashion across frequency.

There exist a substantial number of power allocation algorithms for multicarrier systems, most of which employ a total power constraint, i.e.,

$$\pi_{\text{total}} = \sum_{i=0}^{N-1} \pi_i \quad (3.6)$$

where  $\pi_{\text{total}}$  is the total power allowed for the system. This implies that for any subcarrier that is “switched off” or nulled, the power that was allocated to it can be transferred to the remaining active subcarriers. However, such a strategy can result in a possible violation of regulatory requirements for the frequency band of operation.

A practical constraint is to limit the total power across a frequency window of a specified width. For instance, the FCC has imposed requirements based on the amount of transmit power across a specified bandwidth in the UNII band [192]. These requirements are imposed since these bands are usually unlicensed and the users are non-cooperative. As a result, it is necessary to impose a stricter power constraint relative to Eq. (3.6) when performing power allocation. Other researchers have devised power allocation schemes based on a peak subcarrier power constraint [15–19] to avoid violations of regulatory requirements. Unlike this algorithm, our proposed power allocation algorithm in this dissertation is more flexible since it redistributes the unallocated power to other subcarriers while still satisfying the regulatory requirements. For example, suppose the power level of a subcarrier is just short

of achieving the next largest signal constellation for a specified BER threshold due to the subcarrier power constraint. Under the same circumstances, a power loading algorithm, with a frequency window power constraint, would decrease the power levels of the adjacent subcarriers to allow the specified subcarrier to reach the desired power level while still satisfying the constraint. From another point of view, the peak subcarrier power-constrained algorithm is a subcase of the proposed power allocation algorithm, where the frequency window is the width of one subcarrier.

### 3.2.1 Proposed Frequency Interval Power Allocation Algorithm<sup>8</sup>

Since the FCC and other spectrum regulators have imposed power constraints based on a total power across a frequency window, the proposed power allocation algorithm, which is shown in Fig. 3.5, follows the same rationale. The proposed algorithm commences by searching for groupings of  $M$  or more non-nulled subcarriers and allocates them  $\pi_{\max}/M$ , where  $M$  is the number of subcarriers that can fit the frequency window specified by the regulatory agency, and  $\pi_{\max}$  is the total power allowed across the  $M$  subcarriers. The remaining non-nulled subcarriers are assigned  $\pi_{\max}$ .

Then sliding the frequency window across the signal spectrum, the power for every grouping of  $M$  subcarriers is computed. If the largest frequency interval power exceeds  $\pi_{\max}$ , the subcarrier power levels are reduced in that frequency interval using

$$\pi_i = \pi_{\max} - \sum_{\substack{k=l \\ k \neq i}}^{l+M} \pi_k \quad (3.7)$$

with  $l$  chosen to satisfy

$$l = \arg \max_{(i-M) \leq l \leq i} \left\{ \sum_{k=l}^{l+M} \pi_k \right\}. \quad (3.8)$$

From this algorithm with the frequency window power constraint, it is obvious that power will not be reallocated when the SNR of the system is high, since no subcarriers will be nulled. However, at low SNR values, where most of the subcarriers are nulled, there is enough freedom to perform power allocation while satisfying the frequency window power

---

<sup>8</sup>The work was presented in parts at the *56th IEEE Vehicular Technology Conference* [254] and the *15th International Conference on Wireless Communications* [255].

1. Let  $\pi_i = 0, \forall i \in \mathcal{S}_{\text{nulled}}$ , where  $\mathcal{S}_{\text{nulled}}$  is the set of nulled subcarriers.
2. Search consecutive groups of  $M$  or more non-nulled subcarriers, allocate each subcarrier in those groups  $\pi_{\text{max}}/M$ .
3. Assign the remaining subcarriers  $\pi_{\text{max}}$ .
4. Starting from one end of the signal bandwidth, compute the total power for every possible consecutive group of  $M$  subcarriers.
5. If the total power of any group exceeds  $\pi_{\text{max}}$ , proceed to Step 6, else finalize the power allocation and exit algorithm.
6. Select the trio of subcarriers with the largest total power, reduce the power of those subcarriers initially allocated with  $\pi_{\text{max}}$  until the total power equals  $\pi_{\text{max}}$ , then proceed to Step 4.

**Fig. 3.5** Proposed power allocation algorithm with frequency interval power constraint [254, 255].

constraint.

An example where the proposed algorithm could be applied is the IEEE Std. 802.11a, which operates in the UNII band at 5 GHz. In the 5.15–5.25 GHz UNII lower band [192],  $\pi_{\text{max}}$  is equal to 2.5 mW for a frequency window of 1 MHz. The OFDM symbol occupies a bandwidth of 16.6 MHz and employs 52 subcarriers. This translates into each frequency window having about 3 subcarriers.

### 3.3 Equalizer Tap Loading Algorithms

From Section 2.5, using subcarrier equalizers in the frequency-domain (i.e., after passing through the analysis filterbank), instead of a single time-domain equalizer at the beginning of the receiver (i.e., before the analysis filterbank), efficiently reverses the effects of the channel without using too many equalizer taps. In several applications, the subcarrier equalizer usually consists of a single complex weight to invert the channel gain over a particular subcarrier. However, this might not work due to gain fluctuations in the frequency band (i.e., the channel is not totally flat within the subcarrier band), and thus multi-tap per tone equalizers are required per subcarrier.

1. Initialization: commence with  $q^{(k)} := 1$  and compute  $J^{(k)}$ .
2. If  $J^{(k)} < J_T$ , end the algorithm, otherwise proceed to Step 3.
3. Let  $q^{(k)} := q^{(k)} + 1$  and recompute  $J^{(k)}$ .
4. If the change between the previous and current  $J^{(k)}$  is below some percentage or  $J^{(k)} < J_T$ , end the algorithm, otherwise proceed to Step 3.

**Fig. 3.6** Proposed subcarrier equalizer tap loading algorithm applied to subcarrier  $k$  [254, 255].

In this work, the number of taps allocated to each subcarrier equalizer is a function of the channel conditions affecting that subcarrier. For subcarriers experiencing a flat portion of the channel frequency response, a single tap can correct for the distortion. On the other hand, subcarriers located in deep channel nulls or steep portions of the channel response require several taps to compensate for the distortion. Therefore the number of taps for each subcarrier will be different if the channel is frequency selective.

The rationale behind allocating equalizer taps is that the system only uses enough taps to achieve an overall distortion that is below some specified threshold, subject to a constraint on the maximum number of taps per subcarrier. A side benefit of this algorithm is power savings due to a reduction in the average number of computation cycles. Suppose a fixed number of taps are allocated across all subcarriers, it might be too few for some subcarriers to overcome the distortion while too many for others. Moreover, the power efficiency of the system is lower since the excess equalizer taps are being employed. By allocating the taps based on channel conditions, the following proposed algorithms attempt to reduce the complexity of the system and the power consumption associated with the multi-tap per-tone equalizers.

### 3.3.1 Proposed Subcarrier-Level Equalizer Tap Loading Algorithm<sup>9</sup>

In this proposed algorithm, the length of each equalizer is computed on the basis of reducing the distortion cost function for each subcarrier below some prescribed threshold. Thus, if a subcarrier experiences more distortion than the other subcarriers, a longer equalizer is

<sup>9</sup>The work was presented in parts at the *56th IEEE Vehicular Technology Conference* [254] and the *15th International Conference on Wireless Communications* [255].

employed in order to further reduce the distortion. The algorithm, which operates on a per-subcarrier basis, is shown in Fig. 3.6. By performing this allocation, the subcarrier equalizers can reduce the distortion introduced by the channel while keeping the overall number of equalizer taps to a minimum. Reducing the number of taps translates into a decrease in power consumption.

In the initialization phase, the equalizer weights and minimum cost function for subcarrier  $k$  are computed with  $q^{(k)} := 1$  taps<sup>10</sup>. The equalizer weights  $w^{(k)}(n)$  and corresponding theoretical distortion values  $J^{(k)}$  for all the data-bearing subcarriers are computed given the lengths  $q^{(k)}$ . If  $\min(J^{(k)})$  exceeds a pre-established threshold,  $J_T$ , the number of taps is increased as  $q^{(k)} := q^{(k)} + 1$  and the minimum cost function is recomputed. The process of adding equalizer taps is repeated until the distortion constraint  $\min(J^{(k)}) \leq J_T$  is satisfied or until the difference between two successive cost functions is less than a specified percentage. This algorithm is then applied to all subcarriers  $k = 0, \dots, N - 1$ .

However, without information from the other subcarriers regarding the length of their equalizers, the resulting equalizer tap allocation could potentially contain more taps than necessary in order to attain the target mean distortion. In the next section, an algorithm is presented which allocates taps in a “greedy” fashion across all the subcarriers, thus accounting for all subcarrier information in the allocation process.

### 3.3.2 Proposed Greedy Subcarrier Equalizer Tap Loading Algorithm<sup>11</sup>

The proposed algorithm for obtaining the lengths of the subcarrier equalizers is shown in Fig. 3.7. Given a multicarrier system with  $N$  subcarriers, there exists a subset of those subcarriers  $\mathcal{S}_{\text{data}}$  that are data-bearing and have subcarrier equalizer lengths below some prescribed value. The algorithm begins by setting the lengths of the equalizers for the data-bearing subcarriers,  $q^{(k)}$ ,  $k \in \mathcal{S}_{\text{data}}$ , to a length of 1. The mean of the  $J^{(k)}$ ,  $\bar{J}$ , is compared with the prescribed overall distortion threshold for the system,  $J_T$ . To choose the optimal equalizer coefficients, we minimize the distortion. Assuming the BER is monotonically related to the distortion, this would also minimize the BER. As a result, the distortion is used as a metric of performance in this algorithm for convenience. If  $\bar{J} \leq J_T$ , then none of the equalizer lengths need to be increased in order to reduce  $\bar{J}$  and the algorithm ends.

<sup>10</sup>Note that all equalizer weights employed in this dissertation are computed using a closed-form MSE expression (refer to Appendix B for details).

<sup>11</sup>The work was presented at the *60th IEEE Vehicular Technology Conference* [260].

1. Initialization:  $q^{(k)} = 1, \forall k \in \mathcal{S}_{\text{data}}$ , where  $\mathcal{S}_{\text{data}}$  is the set of data-bearing subcarriers with  $q^{(k)} \leq q_{\text{max}}$  ( $q_{\text{max}}$  is the maximum-allowable number of equalizer taps per subcarrier).
2. Compute  $J^{(k)}, \forall k \in \mathcal{S}_{\text{data}}$ .
3. If  $\bar{J} \leq J_T$ , end the algorithm, else proceed to Step 4.
4. Set  $q^{(k)'} = q^{(k)} + 1$  and compute  $J^{(k)'}, \forall k \in \mathcal{S}_{\text{data}}$ .
5. Calculate the difference  $\Delta^{(k)} = J^{(k)} - J^{(k)'}, \forall k \in \mathcal{S}_{\text{data}}$ .
6. If  $\mathcal{S}_{\text{data}} = \{\}$ , end the algorithm, else proceed to Step 7.
7. If  $\max \Delta^{(k)} \leq \Delta_T, k \in \mathcal{S}_{\text{data}}$ , end the algorithm, else go to Step 8.
8. For subcarrier  $l = \arg \min_{l \in \mathcal{S}_{\text{data}}} \Delta^{(l)}$ , set  $q^{(l)} = q^{(l)} + 1$ , recompute  $J^{(l)}$ , and go to Step 3.

**Fig. 3.7** Proposed subcarrier equalizer tap loading algorithm employing a “greedy” approach [260].

However, if  $\bar{J} > J_T$ , then the algorithm needs to increase some of the lengths  $q^{(k)}$  in order to satisfy  $\bar{J} \leq J_T$ .

This algorithm operates in a “greedy” fashion [9]. It incrementally increases the length of the subcarrier equalizer that maximizes the decrease in  $\bar{J}$ . Therefore, the algorithm computes the equalizer weights  $w^{(k)'}(n)$  and corresponding theoretical distortion values  $J^{(k)'}$  when the lengths are  $q^{(k)'} = q^{(k)} + 1$  for all subcarriers belonging to  $\mathcal{S}_{\text{data}}$ . The differences  $\Delta^{(k)} = J^{(k)} - J^{(k)'}$  are computed and the maximum difference is chosen. If the set  $\mathcal{S}_{\text{data}}$  is empty, which means that all data-bearing subcarriers have reached the maximum allocation of equalizer taps,  $q_{\text{max}}$ , the algorithm finalizes the allocation and exits. Otherwise  $\Delta^{(k)}, k \in \mathcal{S}_{\text{data}}$ , is compared with the prescribed difference threshold  $\Delta_T$ . If  $\max(\Delta^{(k)}) \leq \Delta_T$ , then the algorithm breaks out and ends since the largest difference in distortion is considered negligible. If  $\max(\Delta^{(k)}) > \Delta_T$ , then the algorithm chooses subcarrier  $l, l \in \mathcal{S}_{\text{data}}$ , which has the largest  $\Delta^{(k)}$ . The algorithm updates  $q^{(l)} = q^{(l)} + 1$  then computes  $J^{(l)}$ . Finally,  $\bar{J} \leq J_T$  is compared and the process repeats.

## 3.4 Simulation Results

### 3.4.1 Bit Allocation Results

The multicarrier system, employing both the proposed loading algorithms and several others found in the literature, used the operating parameters specified in the IEEE Std. 802.11a [2], including the number of non-guard subcarriers (52 subcarriers), the frequency band of operation (5.15–5.25 GHz), and the available modulation schemes (BPSK, QPSK, square 16-QAM, and square 64-QAM). However, unlike the standard, where the same modulation scheme is employed across all the subcarriers, the proposed bit loading algorithms can use a different modulation scheme for each subcarrier. In addition, subcarriers can be turned off. Results from the adaptive bit loading algorithms were obtained for  $P_T$  values of  $10^{-3}$  and  $10^{-5}$ . Furthermore, an exhaustive search algorithm was also employed for a case with a reduced number of subcarriers over a portion of the band, to keep the complexity manageable, in order to make it possible to determine the optimal solution to the bit allocation problem. Finally, instead of an OFDM-type multicarrier transmission scheme, a complex exponential-modulated filterbank system was employed.

Several WLAN standards, such as IEEE Std. 802.11a [2] or HiperLAN/2 [3], operate at approximately 5 GHz, such as the lower portion of the unlicensed national information infrastructure (UNII) band at 5.15–5.25 GHz for IEEE Std. 802.11a [192]. In these simulations, the system is transmitting in the lower portion of the UNII band. Moreover, the transmitter/receiver separation was varied between 1 m and 60 m. As for the channel, there was no line-of-sight component and it was time-invariant<sup>12</sup>. The signal, which is composed of 52 subcarriers, is transmitted across a 16.6 MHz bandwidth<sup>13</sup>. Finally, only a single pair of antennas was employed. For each channel realization, the algorithms were operating at 70 different averaged SNR values ranging from  $-11$  dB to 59 dB. The trials were repeated for 10000 different channel realizations and the results averaged. Furthermore, the change in SNR corresponds to the change in transmitter/receiver separation distance.

For comparison purposes, two algorithms from the literature are also simulated and their

<sup>12</sup>The channel impulse responses were generated using the method presented in [130]. The channel model used a cluster arrival rate of  $1.66 \times 10^{-7} \text{ s}^{-1}$ , a ray arrival rate of  $1.66 \times 10^{-8} \text{ s}^{-1}$ , a cluster power-decay time constant of  $40 \times 10^{-8} \text{ s}$ , a ray power-decay time constant of  $8 \times 10^{-8} \text{ s}$ , and five clusters, each of which contained 100 rays.

<sup>13</sup>The complex baseband representation of the channel frequency response, obtained from the channel impulse response, was employed across the available bandwidth.

results compared to that of the proposed algorithms. These algorithms are the incremental bit allocation algorithm of Fox [7], and the capacity approximation-based bit allocation algorithm of Leke and Cioffi [12]. However, for a straightforward comparison, all the subcarriers have a uniform power allocation. Therefore, several modifications of these algorithms are required. In the case of the algorithm by Fox, no modifications are necessary since it performs only adaptive bit loading (the power allocation is set to be uniform across all subcarriers). Starting with zero bits across all subcarriers as an initial allocation, the algorithm allocates to subcarrier  $i$  for which  $\Delta b_i/\Delta P_i$  is a maximum. The incremental allocation continues until  $\bar{P} > P_T$ .

As for the algorithm by Leke & Cioffi, the expression for the noise to signal ratio (NSR), used by this algorithm to determine which subcarriers to turn off, is modified such that constant uniform power allocation is employed. To achieve this, the NSR expression is modified to

$$\text{NSR} = \frac{\pi_{\text{sc}}}{\Gamma} + \frac{1}{N_{\text{on}}} \sum_{n=1}^{N_{\text{on}}} \frac{1}{\gamma^{(n)}} \quad (3.9)$$

where  $\pi_{\text{sc}}$  is the subcarrier power (a constant value across all subcarriers),  $N_{\text{on}}$  is the number of subcarriers that are “on”,  $\Gamma$  is the aforementioned SNR gap<sup>14</sup>, and  $\gamma^{(n)}$  is the SNR of subchannel  $n$  (i.e.,  $\gamma^{(n)} = |H_n|^2/\sigma_v^2$ , where  $\sigma_v^2$  is the noise variance,  $H_n$  is the channel frequency response across subcarrier  $n$ ). By defining the NSR this way, the subcarrier power levels are fixed, instead of keeping the total power allocation fixed, as was done by Leke & Cioffi. Other than this modification, the algorithm is essentially the same as the original.

### Perfect Subcarrier SNR Information

In Fig. 3.8, the overall throughputs of the five bit allocation algorithms are presented for the case of 8 subcarriers. This reduced number of degrees of freedom allows for an exhaustive search of the optimal allocation. The constant power allocation variant of the algorithm by Leke and Cioffi [12] does not reach the same throughput as the other systems until high SNR values of 49 dB<sup>15</sup>. As for the other methods, the difference in

<sup>14</sup>In this work,  $\Gamma = 6.06$  dB for  $P_T = 1 \times 10^{-3}$ ,  $\Gamma = 7.37$  dB for  $P_T = 1 \times 10^{-4}$ , and  $\Gamma = 8.42$  dB for  $P_T = 1 \times 10^{-5}$ .

<sup>15</sup>The comparatively poor performance of Leke and Cioffi’s algorithm in this chapter is due to the fact that the approximations in that algorithm are not very accurate, and is not an artifact of the modifications

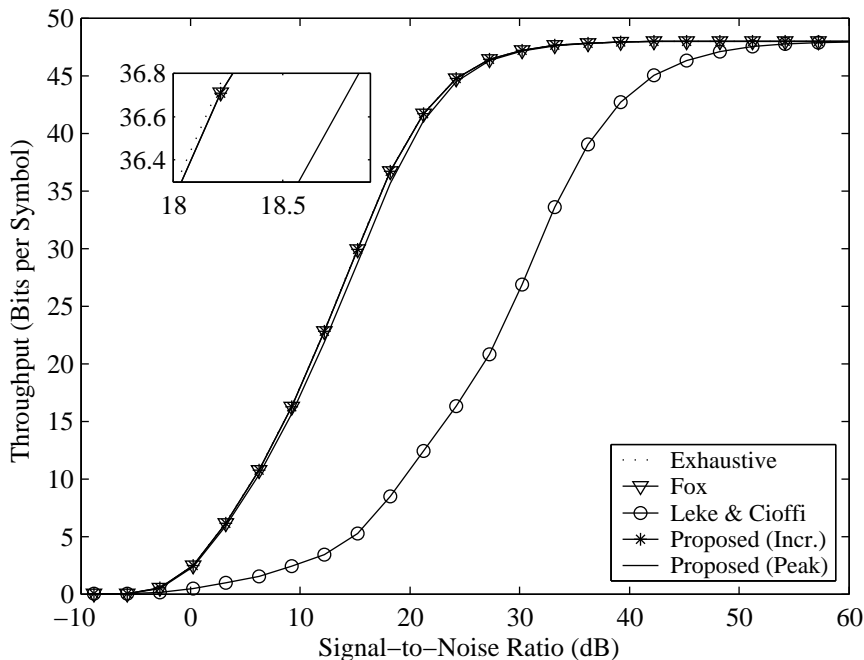


**Fig. 3.8** Overall throughput of an  $N = 8$  subcarrier system satisfying a  $P_T$  of  $10^{-3}$ . Except for the curve corresponding to Leke & Cioffi, all the curves are superimposed.

throughput between them is very small since they all perform discrete allocations rather than non-integer allocations followed by rounding. The largest throughput is produced by the exhaustive search algorithm, followed by both Fox’s and the proposed incremental allocation algorithms, and finally by the proposed peak BER algorithm. Since the objective function is not concave<sup>16</sup> and the constraint function is not strictly convex, there is no guarantee that Fox’s algorithm would reach the optimal allocation [7].

The  $\bar{P}$  values corresponding to the throughputs in Fig. 3.8 are shown in Fig. 3.9. It can be observed that all the algorithms, except for Leke and Cioffi, have approximately the same values as the exhaustive search. The error rates are low at low SNR values due to the nulling of poorly performing subcarriers. This leaves the best-performing subcarriers, combined with small signal constellations (e.g., BPSK), which results in low error rates. In the mid-range SNR region, all the subcarriers are on, including the poorly performing ones.

made to the algorithm to utilize uniform power allocation.

<sup>16</sup>“A function defined only on the integers is called concave if its first differences are decreasing.” [7]

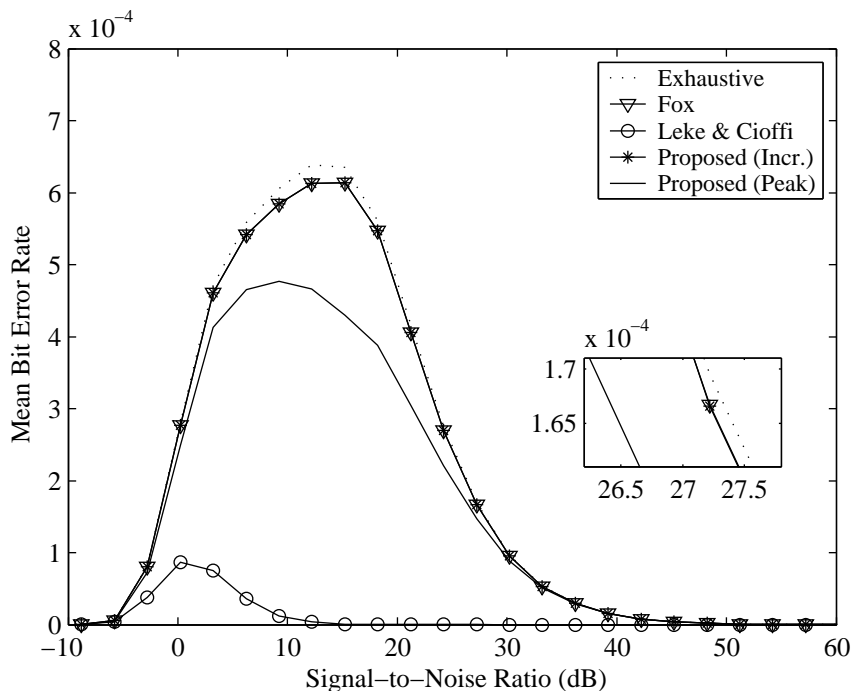


**Fig. 3.9** Mean BER of an  $N = 8$  subcarrier system satisfying a  $P_T$  of  $10^{-3}$ .

**Table 3.1** Number of  $P_T$  Violations by the bit allocation algorithm of Leke & Cioffi.

SNR	0 dB	5 dB	10 dB	25 dB	35 dB
$N = 8, P_T = 10^{-3}$	8.23%	3.53%	0.66%	0.00%	0.00%
$N = 52, P_T = 10^{-5}$	54.95%	96.84%	99.94%	19.62%	1.99%

Thus, their BER values will dominate the mean BER of the system. At high SNR values, all subcarriers are modulated with the largest constellation sizes and all have  $P_i \leq P_T$ . As for the algorithm by Leke & Cioffi, its values for  $\bar{P}$  are significantly lower at the expense of lower throughput. Since the algorithm of Leke & Cioffi does not check if the bit allocation exceeds  $P_T$ , there is a possibility that  $P_T$  may be violated. For the cases where these violations occur, these cases were omitted from the graphs. Table 3.1 shows the number of violations as a percentage of the total number of channel realizations per SNR value.

When 52 subcarriers are employed, as shown in Fig. 3.10, the algorithms, except for Leke & Cioffi, achieve nearly the same throughput with some small differences. The throughput

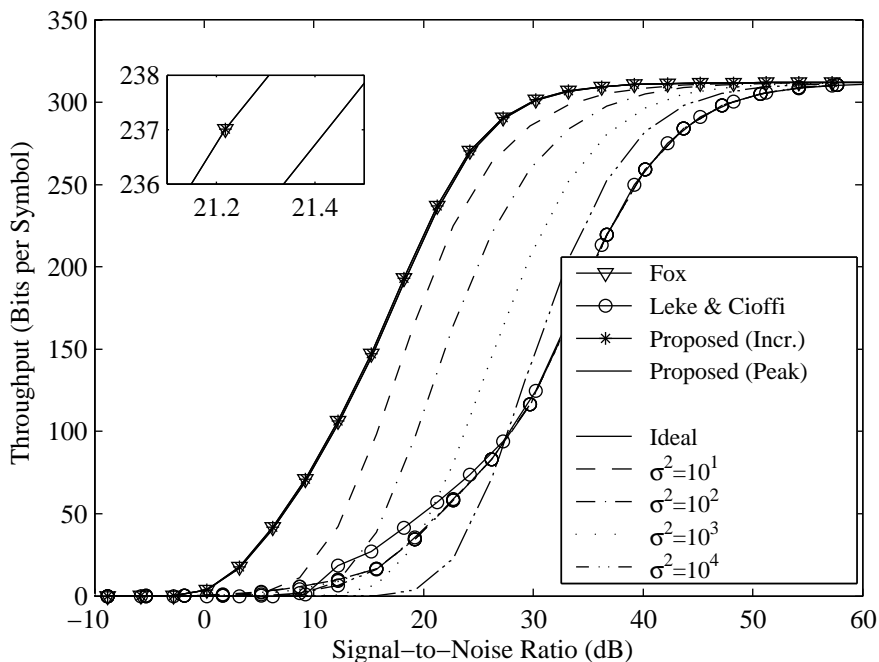


**Fig. 3.10** Overall throughput of an  $N = 52$  subcarrier system satisfying a  $P_T$  of  $10^{-5}$  using subcarrier SNR values with Gaussian noise of variance  $\sigma^2$  added. Note that the algorithm of Leke & Cioffi and the proposed peak BER-constrained algorithm use the non-ideal subcarrier SNR values.

of the algorithm of Leke & Cioffi is substantially less than that of the other methods, only reaching the performance of other algorithms at high SNR values. Note how at low SNR values, the throughput of the algorithm of Leke & Cioffi goes to zero. This is due to either the algorithm producing an allocation that exceeds  $P_T$  or the algorithm nulling all the subcarriers. Table 3.1 shows the number of violations. The corresponding  $\bar{P}$  values are shown in Fig. 3.11. As in the 8 subcarrier case, except for Leke & Cioffi, all the algorithms have approximately the same values.

As seen in Fig. 3.8, the throughput of the proposed algorithms is very close to that of the optimal allocation produced by the exhaustive search algorithm. Furthermore, the proposed peak BER algorithm executes more quickly than the algorithm by Fox. As for the two proposed algorithms, both perform similarly in terms of throughput and complexity at high SNR values. However, at low SNR values, the proposed peak BER algorithm executes faster than the proposed incremental (both mean and worst cases). This is due to the

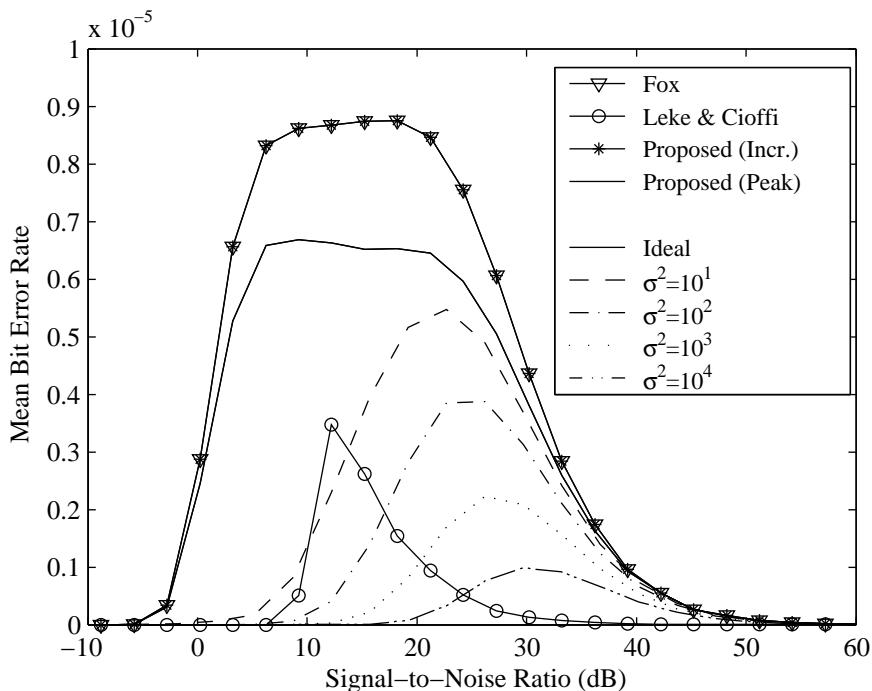


**Fig. 3.11** Mean BER of an  $N = 52$  subcarrier system satisfying a  $P_T$  of  $10^{-5}$  with and without Gaussian noise of variance  $\sigma^2$  added to  $\gamma_i$ ,  $i = 0, \dots, N - 1$ .

fact that the proposed incremental algorithm is a bit removing algorithm, which means at low SNR values, it takes numerous iterations to reach the final allocation. Although Leke & Cioffi may execute at the same speed as the proposed peak BER algorithm, the latter achieves far greater throughput. A summary of mean and worst-case computation times for a 52 subcarrier system with a  $P_T$  of  $10^{-5}$  is shown in Table 3.2 for several SNR values. Furthermore, the cumulative density functions of the computation times at SNR values of 10 dB and 40 dB are shown in Fig. 3.12. For a fair comparison, all algorithms were programmed in C and executed on the same workstation (Intel Pentium IV 2 GHz processor). It should be noted that although the algorithms may vary in execution time, all the worst case execution times are of the same order of magnitude. This is due to the fact that the worst case computational complexity of all the algorithms under study are of  $\mathcal{O}(N^2)$ <sup>17</sup>.

<sup>17</sup>Since the number of candidate modulation schemes employed by most bit allocation algorithms is relatively small (e.g., in this work  $B = 5$ ), its impact on the computational complexity of the algorithm is a multiplicative factor  $B$  at most.

**Table 3.2** Mean (worst case) computation times in milliseconds at different SNR values, 52 subcarriers,  $P_T = 10^{-5}$ 

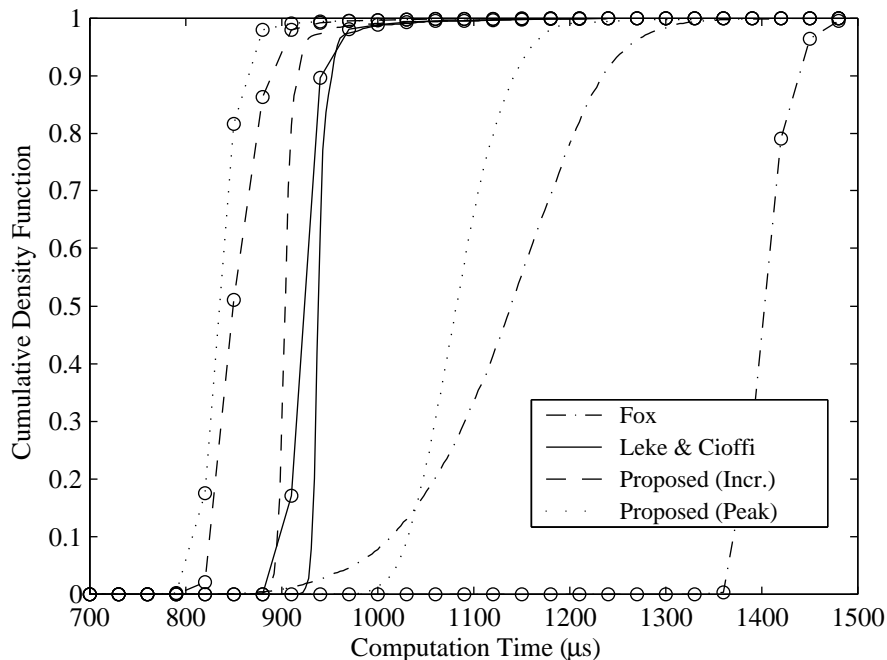
Algorithm	10 dB	25 dB	40 dB	55 dB
Fox	1.13 (3.23)	1.48 (5.01)	1.41 (5.00)	1.37 (4.40)
Leke & Cioffi	0.94 (2.78)	0.96 (4.98)	0.93 (4.24)	0.90 (4.66)
Proposed (Incr.)	1.09 (2.86)	<b>0.91</b> (4.10)	<b>0.84</b> (2.09)	<b>0.80</b> (2.62)
Proposed (Peak)	<b>0.91</b> (2.96)	<b>0.91</b> (2.71)	0.86 (3.98)	0.82 (4.54)

### Imperfect Subcarrier SNR Information

The effect on throughput performance of adding Gaussian noise to the subcarrier SNR values is studied first. Although results for the algorithms of Fox [7], the proposed algorithms, and Leke & Cioffi [12] were obtained, the first three algorithms all had similar results. Therefore, only the throughput results for the proposed peak BER algorithm as well as for the algorithm of Leke & Cioffi [12] are presented in Fig. 3.10, while Figs. 3.11 and 3.13 show the  $\bar{P}$  and outage probability results for the proposed peak BER algorithm. The value of  $P_T$  was set to  $10^{-5}$ . The results are obtained when the variance of the Gaussian noise is either  $\sigma^2 = 10, 10^2, 10^3$ , or  $10^4$  across all SNR values<sup>18</sup>. Compared to the case where no Gaussian noise is added to the subcarrier SNR values, the throughput of the system decreases as the variance increases. In particular, the throughput curves shift to the right as the noise variance  $\sigma^2$  increases. Moreover, except at low SNR values for  $\sigma^2 = 10^4$ , the algorithm of Leke & Cioffi [12] performs relatively poorly.

Since most of the adaptive bit loading algorithms are close to the maximum achievable throughput given the maximum error constraint, the addition of Gaussian noise to the subcarrier SNR values can either cause the system to violate the constraint (when  $\hat{\gamma}_i > \gamma_i$ ) or decrease in throughput (when  $\hat{\gamma}_i \leq \gamma_i$ ). Since  $\bar{P} > P_T$  is not acceptable, when the former occurs, the throughput of the system is set to zero and a record of the number of times this occurs is kept. The fraction of realization violations is shown in Fig. 3.13. When the latter occurs, the throughput and  $\bar{P}$  are lower, as in Figs. 3.10 and 3.11. Note that at low SNR

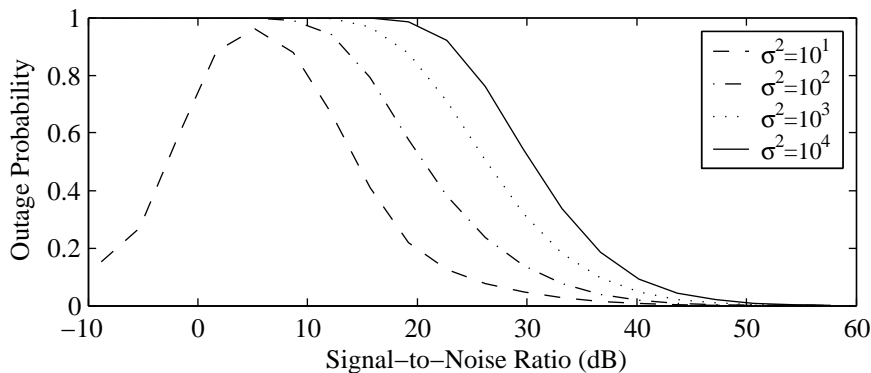
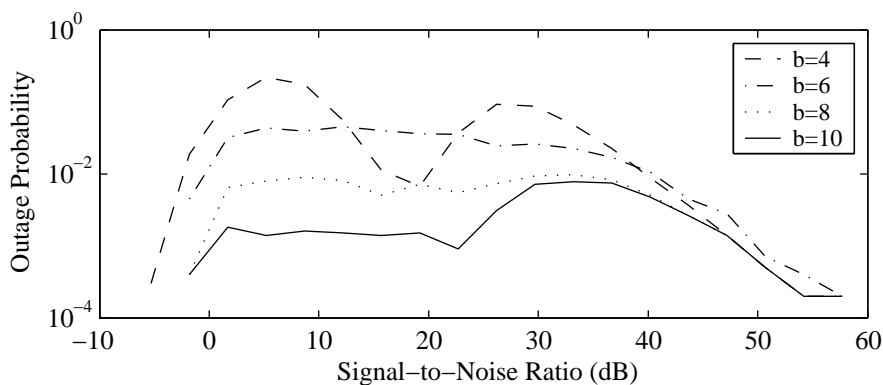
<sup>18</sup>Although the error variance would be dependent on the nominal SNR, in this work the error variance was chosen to be constant for all SNR values in order to evaluate the robustness of these algorithms at different SNR values. Moreover, instead of employing a single error variance value across all SNR values, a range of error variance values were examined, with the smaller error variances realistically occurring at low nominal SNR values while the larger values occurring at higher SNR values.



**Fig. 3.12** Cumulative density function of computational time of an  $N = 52$  subcarrier system satisfying a  $P_T$  of  $10^{-5}$  at SNR values of 10 dB (without circles) and 40 dB (with circles).

values,  $\sigma^2$  is large enough that the algorithm experiences violations every time. As the SNR increases, the frequency of violations decrease. Other than the case of  $\sigma^2 = 10$  violations occurred 100% of the time due to the SNR values being the same order of magnitude as the Gaussian noise.

The outage probability, throughput, and  $\bar{P}$  results of the proposed peak BER algorithm using quantized subcarrier SNR values are presented in Figs. 3.13, 3.14, and 3.15, respectively. From Fig. 3.14 it can be observed that there is some degradation. However, the algorithm of Leke & Cioffi [12] still has significantly lower throughput. For instance, at an SNR of 11 dB, the difference in throughput between the ideal case and the case where the subcarrier SNR values are quantized to  $2^3$  output levels is 40 bits/s. However, as the number of output levels increases, the throughput approaches that of the ideal case. At an SNR of 19 dB, the difference in throughput between the ideal and a quantized subcarrier SNR employing  $2^{10}$  output levels is 0.2 bits/s. Equivalently, the  $\bar{P}$  curves in Fig. 3.15 also approach the ideal case when the number of output levels increases. The difference in

(a) Gaussian noise of variance  $\sigma^2$  added to the subcarrier SNR values.(b) Subcarrier SNR values quantized with  $2^b$  levels.

**Fig. 3.13** Outage probability (fraction of realizations for which  $\bar{P} > P_T$ ) of a multicarrier system employing the proposed peak BER algorithm at  $P_T = 10^{-5}$ .

performance is dependent on granular error. More output levels results in a smaller granular error and correspondingly a result closer to the ideal case. The fraction of realization violations (when  $\bar{P} > P_T$ ) are shown in Fig. 3.13.

### 3.4.2 Subcarrier Equalizer Tap Allocation Results

Using the ETSI HiperLAN/2 indoor channel models [136], the proposed greedy algorithm is employed in an MDFT filterbank multicarrier system [201]. The synthesis and analysis filters are modulated versions of a root raised cosine lowpass filter. In the experimental results using the algorithm, we used  $J_T = 1 \times 10^{-3}$  as a performance threshold and

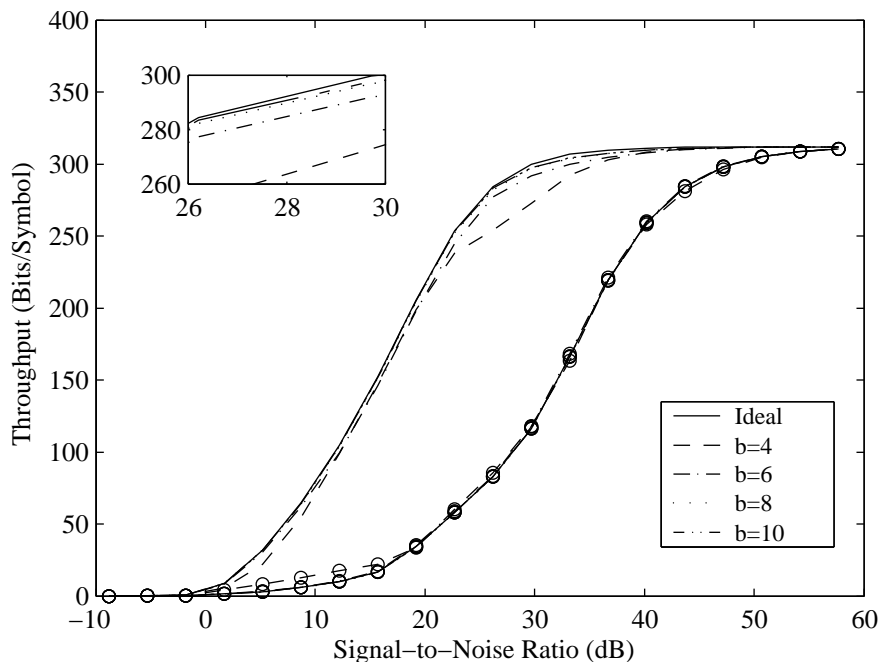


**Fig. 3.14** Overall throughput of a multicarrier system employing adaptive bit loading algorithms of the proposed peak BER algorithm (no circles) and Leke & Cioffi [12] (with circles) at  $P_T = 10^{-5}$  when the subcarrier SNR values are quantized with  $2^b$  levels. Note the latter uses another set of quantization reproduction levels.

$\Delta_T = 0.1\%$  as a stopping criterion. Many of the operating parameters of the system correspond to the IEEE Std. 802.11a [2], including the modulation schemes (BPSK, QPSK, square 16-QAM, and square 64-QAM modulation), number of subcarriers (52 data-bearing subcarriers), bandwidth (16.6 MHz), and operating frequency (5 GHz). Since the system is operating in an indoor environment, the channel is quasi-stationary. Therefore, the channel is time-invariant over a sufficiently long period of time and that the equalizer weights and lengths need to be determined once for a specific channel. Moreover, it is assumed that the channel is perfectly known at the receiver, although in practice data-aided channel estimation techniques would be employed. Finally, the simulations for each point on the BER curves lasted until 100 bit errors were obtained (see Appendix E for details).

Figs. 3.16 and 3.17 show the bit error rate (BER) performance of an 8 subcarrier section of the MDFT filterbank multicarrier system, operating in an ETSI HiperLAN/2 Channel A, employing the proposed algorithm. The average length of the equalizers range from

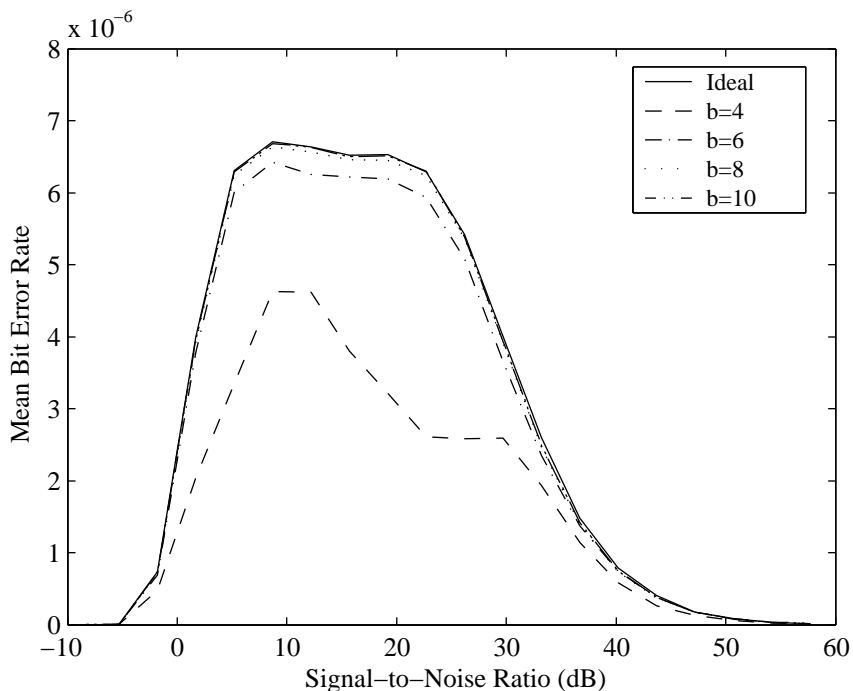


**Fig. 3.15** Mean BER of a multicarrier system employing the proposed peak BER algorithm at  $P_T = 10^{-5}$  when the subcarrier SNR values are quantized with  $2^b$  levels.

$\bar{q} = 1.25$  taps per subcarrier (BPSK at 7 dB) to  $\bar{q} = 2.875$  taps per subcarrier (64-QAM at 52 dB). However, the majority of taps in this case were used by the equalizer of the 5<sup>th</sup> subcarrier since it was located in a spectral null. For instance, in the BPSK case, all the equalizers used 1 tap, except for the 5<sup>th</sup> subcarrier, which used 3 taps. To determine the benefits of variable-length subcarrier equalizers and the proposed algorithm, the impact on BER performance with systems employing constant-length subcarrier equalizers having lengths equal to  $\lfloor \bar{q} \rfloor$  and  $\lceil \bar{q} \rceil$  is compared. This is to ensure a fair comparison by making the overall number of taps used by the three systems equivalent.

The results show that compared to the systems employing subcarrier equalizers of constant lengths, the system employing our proposed algorithm outperforms them in BER. For instance, in Fig. 3.16, the difference at a signal-to-noise ratio (SNR) of 23 dB for BPSK modulation is two orders of magnitude. The same is true for the other modulation schemes (QPSK at an SNR of 29 dB, 16-QAM at an SNR of 46 dB, and 64-QAM at an SNR of 58 dB). This is due to the fact that several poorly performing subcarriers do not employ

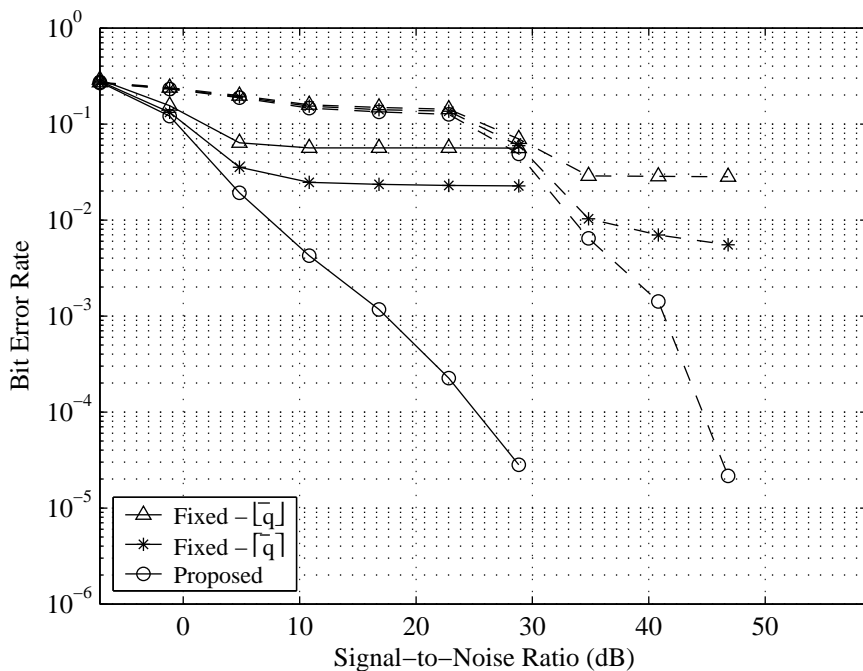


**Fig. 3.16** BER performance for 8 subcarriers with BPSK (solid) and 16-QAM (dashed) modulation when adaptive subcarrier equalizer tap allocation is employed, along with fixed length equalizers with the same overall number of taps, using the ETSI HiperLAN/2 Channel A.

an equalizer of a sufficient length. As a result, the error due to this subcarrier dominates the overall error performance of the system. However, with the proposed algorithm, each subcarrier uses an equalizer which has a sufficient length, as can be seen from Fig. 3.18.

The formulation of the optimal MMSE equalizers derived in Appendix B accounts for the cross-talk contributions from the rest of the subcarriers. Due to the spectral selectivity of the synthesis and analysis filters, only the immediately adjacent subcarriers would contribute any non-negligible amount of interference. Moreover, due to the MDFT filter-bank framework, the adjacent subcarriers are  $90^\circ$  out-of-phase with the desired subcarrier. Therefore, the overall cross-talk contribution in this system would be relatively small.

### 3.5 Chapter Summary

In this chapter, two bit allocation algorithms, one power allocation algorithm, and two subcarrier equalizer tap allocation algorithms have been presented. The proposed bit allo-

cation algorithms, one of which was based on a greedy approach while the other employed a subcarrier peak BER constraint, were designed in order to come close to the optimal allocation in a low computational complexity fashion. According to the results, the proposed algorithms were the fastest of the algorithms evaluated and their final allocations came close to the optimal allocation.

The proposed power allocation algorithm is based on the need of current WLAN systems to obey the regulatory requirements while attempting to enhance system performance. However, the difference between a multicarrier system employing the proposed power allocation algorithm and a system that does not perform power allocation is small [254, 255]. There is only a difference in throughput at low SNR values.

The two proposed subcarrier equalizer tap allocation algorithms attempt to reduce the overall number of equalizer taps employed in a system. The first algorithm allocates taps independent of the allocations performed in other subcarriers. As a result, the mean BER of the system might be unnecessarily lower than the required amount. The second algorithm allocates taps, in an incremental fashion, across all subcarriers, limiting to total number of taps to some prescribed amount. The results show that for the same total number of equalizer taps, the proposed algorithm yields the best BER performance.

Finally, the effects of imperfect channel information and its impact on the performance of bit allocation algorithms was presented. In particular, using a model for the uncertainty associated with channel estimation, the performance of the bit allocation algorithms with respect to the throughput and the mean BER was studied.

A scheme to distribute the quantizer output levels in order to minimize granular error and avoid overload error was proposed. By performing the quantization, the values for the BER can be stored in a look-up table, thus saving time and implementation complexity.

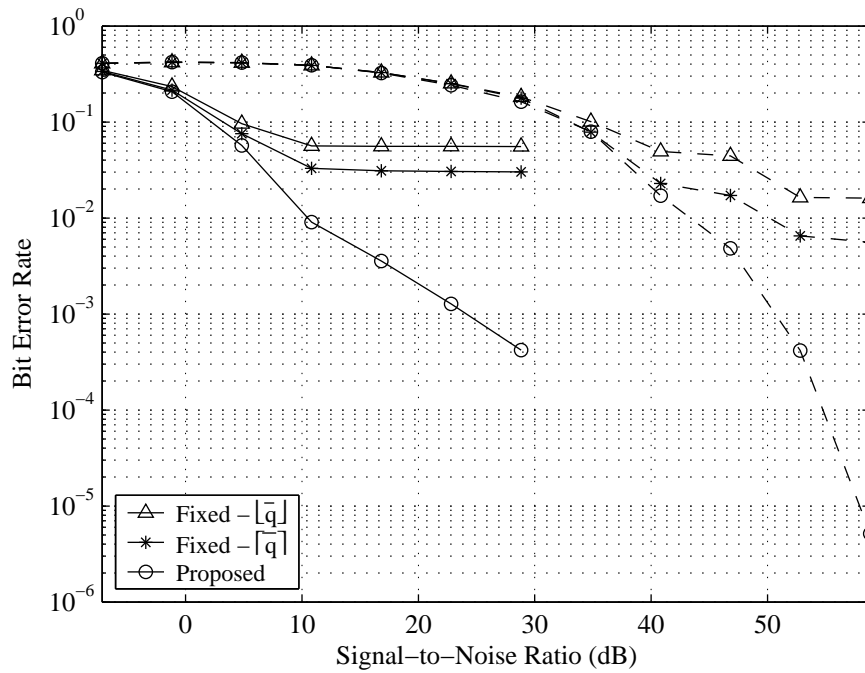


**Fig. 3.17** BER performance for 8 subcarriers with QPSK (solid) and 64-QAM (dashed) modulation when adaptive subcarrier equalizer tap allocation is employed, along with fixed length equalizers with the same overall number of taps, using the ETSI HiperLAN/2 Channel A.

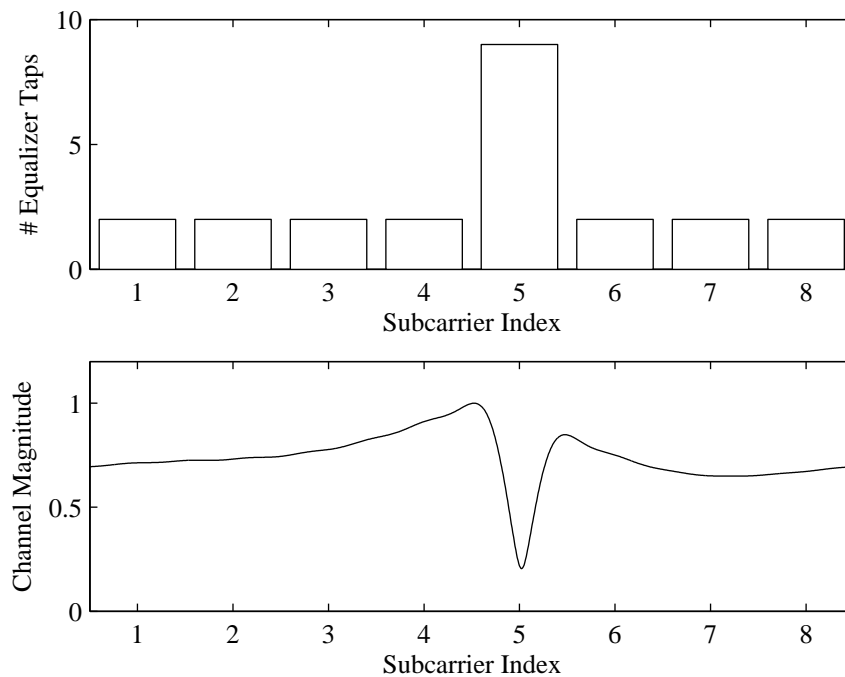


**Fig. 3.18** Relationship between the subcarrier equalizer tap allocation and the channel frequency (magnitude) response using an 8 subcarrier portion of the ETSI HiperLAN/2 Channel A.

## Chapter 4

# Multicarrier Systems with Multiple Antennas and Bit Loading

In Chapter 3, several algorithms were proposed that tailored the operating parameters of a multicarrier system to the prevailing channel conditions, yielding a performance gain with respect to throughput while maintaining the same error robustness. However, the systems employing these algorithms used only a single antenna at the transmitter and at the receiver. Therefore, continuing with the main focus of this dissertation, namely, to develop and apply performance-enhancing techniques that are applicable to multicarrier WLAN systems, the next step is to exploit the spatial dimension by extending the bit loading algorithms to systems with multiple antennas performing only diversity transmission and combining.

Four bit loading algorithms are proposed in this chapter that allocate bits in both the frequency and spatial dimensions. Multiple antennas are employed at both the transmitter and the receiver to exploit the spatial diversity that exists in a MIMO channel to enhance the error robustness of the system. Specifically, both the transmit and receive antenna arrays perform an adapted form of antenna subset selection, as discussed in Section 2.6.2, while the proposed peak BER-limited bit loading algorithm of Section 3.1.2 is employed in tandem. Two of the algorithms perform antenna subset selection on a per-subcarrier level, which would have a greater cost because they would require more RF chains to be active. As we will see, an increase in the complexity of the algorithm only gives a modest increase in the overall throughput.

The complexity associated with each of the four proposed algorithms is different. For

instance, when bit loading is performed in tandem with antenna subset selection, the complexity of the algorithm and its hardware implementation increases substantially. Furthermore, assigning different antenna configurations for each subcarrier requires a more complex implementation relative to assigning the same antenna configuration across all subcarriers. However, algorithms with the higher complexity also have better performance results relative to the low complexity solutions. In this chapters, the results for all four proposed algorithms are presented in order to compare the tradeoffs between complexity and performance enhancement. Although some of the proposed algorithms may be difficult to implement in hardware, it is important to understand the potential these algorithms can obtain.

The combined process of bit allocation and antenna subset selection will follow a similar objective function and constraints relative to the SISO case: the algorithms will attempt to maximize the overall throughput of the system while ensuring that the mean BER does not exceed the prescribed threshold.

## 4.1 Antenna Subset Selection Algorithms

Before investigating the tandem implementation of antenna subset selection and bit allocation, it is necessary to establish a benchmark for the performance gains obtained by only employing antenna subset selection. In this section, two algorithms are proposed that perform antenna subset selection at both the transmitter and receiver for OFDM systems and without bit loading.

Most antenna subset selection schemes proposed in the literature are designed to choose  $L_T$  ( $L_R$ ) antennas out of  $N_T$  ( $N_R$ ) antennas. The value of  $L_T$  and  $L_R$  is always defined as a fixed quantity. However, in this work the antenna subset selection is generalized in an attempt to provide the system with just the necessary number of antennas to maximize the overall throughput while ensuring the mean BER does not exceed a specific limit. Instead of only using a set of antenna configurations that consist of  $L_T$  ( $L_R$ ) antennas, the proposed antenna subset selection forms a set of antenna configurations consisting of all possible non-zero groupings of antennas. For example, for a transmitter with  $N_T = 3$  antennas using conventional antenna subset selection and  $L_T = 2$  would result in a set of transmit antenna configurations

$$\mathcal{S}_{\text{Tx}} = \{\{1, 2\}, \{1, 3\}, \{2, 3\}\}$$

while with the proposed antenna subset selection, the set of configurations would be

$$\mathcal{S}'_{\text{Tx}} = \{\{1\}, \{2\}, \{3\}, \{1, 2\}, \{2, 3\}, \{1, 3\}, \{1, 2, 3\}\},$$

where the numbers represent the transmit antenna index<sup>1</sup>. Although the number of configurations for  $\mathcal{S}'_{\text{Tx}}$  is greater than for  $\mathcal{S}_{\text{Tx}}$ , thus requiring a longer search for the final configuration, the larger number of configurations also provides some additional flexibility when trying to maximize the throughput.

Referring to Eq. (3.1), the objective function is similar with the antenna subset selection except that the optimization is also performed across different antenna array configurations. Moreover, there is a second optimization involving the minimization of the sum of the number of transmit and receive antennas when several configurations have the same maximum throughput. In the case where bit loading is not performed, all subcarrier modulation schemes are constrained to be identical. In other words, given the set of all possible transmit and receive antenna configurations,  $\mathcal{S}_{\text{config}}$ , the algorithms first solve

$$\begin{aligned} & \max_{s_i, b_i} \sum_{i=0}^{N-1} b_i \\ \text{subject to } & \bar{P} = \frac{\sum_{i=1}^N b_i P_i}{\sum_{i=1}^N b_i} \leq P_T \\ & b_0 = b_1 = \dots = b_{N-1} \end{aligned} \quad (4.1)$$

where  $P_i$  is the BER for subcarrier  $i$  determined from  $\gamma_i$  and  $b_i$ . Now let  $\mathcal{S}_{\text{max}}$  denote the set of maximizing antenna configurations from Eq. (4.1), where  $\mathcal{S}_{\text{max}} \subseteq \mathcal{S}_{\text{config}}$ . Then the algorithm solves

$$\min_{s_i \in \mathcal{S}_{\text{max}}} (\mu_{T,i} \cdot n_{T,i}(s_i) + \mu_{R,i} \cdot n_{R,i}(s_i)) \quad (4.2)$$

where  $n_{T,i}(s_i)$  and  $n_{R,i}(s_i)$  are the number of transmit and receive antennas for antenna configuration  $s_i$ , and  $\mu_{T,i}$  &  $\mu_{R,i}$  are weights such that  $\mu_{T,i} + \mu_{R,i} = 1$ . In this work, since minimizing the number of transmit and receive antennas is equally important, these weights

---

<sup>1</sup>In the worst case, all transmit antennas would be employed by the system in order to achieve the specified performance goal at the cost of increased complexity.

are set to  $\mu_{T,i} = \mu_{R,i} = 0.5$ .

It should be noted that the SNR value for subcarrier  $i$ ,  $\gamma_i$ , is the composite SNR value due to the recombining of the different signal paths from the transmitter to the receiver. As a result,  $\gamma_i$  is also a function of the antenna configuration. The value of  $\gamma_i$  when the transceiver is operating in SISO, MISO, SIMO, and MIMO configurations are

$$\gamma_i = \frac{\pi_i \cdot |H_i|^2}{\sigma_\nu^2}, \quad (4.3)$$

$$\gamma_i = \frac{\frac{\pi_i}{N_T} \cdot |H_{i,11}(\omega) + H_{i,21}(\omega) + \cdots + H_{i,N_T1}(\omega)|^2}{\sigma_\nu^2}, \quad (4.4)$$

$$\gamma_i = \frac{\pi_i \cdot |a_{i,1} \cdot H_{i,11}(\omega) + a_{i,2} \cdot H_{i,12}(\omega) + \cdots + a_{i,N_R} \cdot H_{i,1N_R}(\omega)|^2}{(a_{i,1}^2 + a_{i,2}^2 + \cdots + a_{i,N_R}^2) \cdot \sigma_\nu^2}, \quad (4.5)$$

and

$$\gamma_i = \frac{\frac{\pi_i}{N_T} \cdot |a_{i,1} \cdot (H_{i,11}(\omega) + \cdots + H_{i,N_T1}(\omega)) + \cdots + a_{i,N_R} \cdot (H_{i,1N_R}(\omega) + \cdots + H_{i,N_TN_R}(\omega))|^2}{(a_{i,1}^2 + \cdots + a_{i,N_R}^2) \cdot \sigma_\nu^2}, \quad (4.6)$$

where  $\pi_i$  is the transmit signal power of  $x_i(n)$ ,  $\sigma_\nu^2$  is the power of the noise  $\nu(n)$ ,  $H_{i,n_t1}(\omega)$ ,  $n_t = 1, \dots, N_T$ , are the channel frequency responses across subcarrier  $i$  due to multipath propagation between the receive antenna and transmit antennas  $1, \dots, N_T$ ,  $H_i$  is the frequency response of  $h(n)$  across subcarrier  $i$ , and  $\{a_{i,r}\}$ ,  $r = 1, \dots, N_R$  are a set of combining weights<sup>2</sup>. For information on how to derive the composite SNR for subcarrier  $i$ , please refer to Appendix C.

The proposed antenna subset selection method can be implemented either on a subcarrier basis (i.e., each subcarrier may possess a different antenna configuration in order to satisfy Eqs. (4.1) and (4.2)) or on a signal basis (i.e., all subcarriers must have the same antenna configuration). The proposed signal-based algorithm will be presented first, followed by the proposed subcarrier-based algorithm.

1. Initialization: Compute  $P_i$ ,  $i = 0, \dots, N - 1$ , for all available modulation schemes and antenna configurations.
2. If the largest  $P_i$  for square 64-QAM modulation is less than  $P_T$ , set all subcarriers to 64-QAM, 1 transmit antenna, 1 receive antenna, and exit algorithm, else go to Step 3.
3. If smallest  $P_i$  for BPSK is greater than  $P_T$ , null all subcarriers and exit algorithm, else proceed to Step 4.
4. Set  $b_0 = b_1 = \dots = b_{N-1} = 6$ .
5. Choose the same antenna configuration across all subcarriers for which  $\bar{P} \leq P_T$  (in case of tie, choose antenna configuration with smallest total sum of antennas). If none of the configurations satisfy  $\bar{P} \leq P_T$ , proceed to Step 6, else exit the algorithm.
6. Reduce  $b_0, \dots, b_{N-1}$  to the number of bits used to represent the next available signal constellation and go to Step 5. In the case of  $b_0 = b_1 = \dots = b_{N-1} = 0$ , exit the algorithm.

**Fig. 4.1** Proposed antenna subset selection algorithm (antenna configuration chosen on a signal basis).

#### 4.1.1 Signal-Based Selection

The proposed signal-based antenna subset selection algorithm is presented in Fig. 4.1. The algorithm, like all the other proposed algorithms in this chapter, commences by computing the theoretical values for  $P_i$ , using Eqs. (3.3) and (3.4), for all possible antenna configurations and modulation schemes. These values are then stored in a look-up table for easy access by the algorithm in the subsequent steps.

Steps 2 and 3 allow for a quick exit from the algorithm in the event that the channel conditions are either too good, allowing for all subcarriers to be active with the largest modulation scheme available, or too poor, with turning off all the subcarriers as the only option. Otherwise, the algorithm evaluates the mean BER across all the subcarriers, each using the same antenna configuration, for all possible antenna configurations. Starting with square 64-QAM (i.e.,  $b_i = 6$ ,  $i = 0, \dots, N - 1$ ), the algorithm checks if any of the configurations satisfy  $\bar{P} \leq P_T$ . If several configurations satisfy this constraint, the

---

<sup>2</sup>After the antenna configuration has been chosen by the algorithm, the system only performs diversity combining (either EGC or MRC) using the active antennas.

configuration employing the fewest antennas is chosen and the algorithm ends. If none of the configurations satisfy  $\bar{P} \leq P_T$ , the procedure repeats for incrementally smaller signal constellation sizes until either the mean BER constraint is satisfied or all the subcarriers have been nulled.

Although the proposed algorithm exploits the spatial dimension to some extent with the selection of various antenna configurations followed by diversity combining, it does not take full advantage of the subchannels created using MCM. The next algorithm will take advantage of the subchannels.

#### 4.1.2 Subcarrier-Based Selection

Since MCM is employed by the system, the frequency selective fading channels that constitute the MIMO channel will all be transformed into multiple approximately flat subchannels. At the receiver, the gains of the subchannels with the same center frequency will be added together to form a composite subchannel, depending on the transmit and receive antenna array configuration. However, the composite subchannel for each antenna configuration and each subcarrier will be different. Therefore, the proposed algorithm, presented in Fig. 4.2, exploits both the frequency and spatial diversity in order to maximize throughput while minimizing the average number of antennas employed by the system.

Referring to Fig. 4.2, the algorithm commences by computing the theoretical values for  $P_i$  for all possible antenna configurations and modulation schemes. Steps 2 and 3 allow for a quick exit from the algorithm if antenna selection is not worthwhile. In Step 4, the idea of limiting the peak BER of a subcarrier in order to satisfy the mean BER constraint is introduced. Specifically, the peak BER limit  $\hat{P}$  is applied across all the subcarriers and antenna configurations. The largest constellation size supported by all subcarriers is then chosen for each subcarrier. If several configurations exist that yield the same signal constellation for a given subcarrier, the configuration employing the fewest antennas is chosen. Note that this algorithm is different with respect to the previous algorithm since all the subcarriers are not constrained to use the same antenna configuration.

Following the calculation of  $\bar{P}$ ,  $\hat{P}$  is modified by a stepsize  $\delta$  and Step 4 is repeated in Step 7. The resulting configuration is then used to compute the mean BER  $\bar{P}'$ . Given  $\bar{P}$  and  $\bar{P}'$ , the algorithm can perform one of several tasks depending if they are below of above  $P_T$ . The objective of the algorithm is to get the two mean BER values to straddle  $P_T$ . If

1. Initialization: Compute  $P_i$ ,  $i = 0, \dots, N - 1$ , for all available modulation schemes and antenna configurations.
2. If the largest  $P_i$  for 64-QAM modulation is less than  $P_T$ , set all subcarriers to 64-QAM, 1 transmit antenna, 1 receive antenna, and exit algorithm, else go to Step 3.
3. If smallest  $P_i$  for BPSK is greater than  $P_T$ , null all subcarriers and exit algorithm, else proceed to Step 4.
4. For each subcarrier, find the antenna configuration yielding the largest  $b_i$  for which  $P_i \leq \hat{P}$ ,  $i = 0, \dots, N - 1$ , and  $b_0 = b_1 = \dots = b_{N-1}$  (in case of a tie for the maximum  $b_i$  in any given subcarrier, choose the configuration with the smallest total number of antennas).
5. Compute  $\bar{P}$ .
6. If  $\bar{P} < P_T$ , let  $\hat{P} = \hat{P} + \delta$ , else  $\hat{P} = \hat{P} - \delta$ .
7. For each subcarrier, find the antenna configuration yielding the largest  $b_i$  for which  $P_i \leq \hat{P}$ ,  $i = 0, \dots, N - 1$ , and  $b_0 = b_1 = \dots = b_{N-1}$  (in case of a tie for the maximum  $b_i$  in any given subcarrier, choose the configuration with the smallest total number of antennas).
8. Compute  $\bar{P}'$ .
9. If both  $\bar{P} > P_T$  and  $\bar{P}' > P_T$  (resp.  $\bar{P} \leq P_T$  and  $\bar{P}' \leq P_T$ ), and no previous straddling of  $P_T$ , let  $\bar{P} = \bar{P}'$ ,  $\hat{P} = \hat{P} - \delta$  (resp.  $\hat{P} = \hat{P} + \delta$ ), and go to Step 7, else go to Step 10.
10. If both  $\bar{P} \leq P_T$  and  $\bar{P}' \leq P_T$ , and  $P_T$  was straddled before, let  $\bar{P} = \bar{P}'$ ,  $\hat{P} = \hat{P} + \delta$ , and go to Step 7, else go to Step 11.
11. If both  $\bar{P}$  and  $\bar{P}'$  are straddling  $P_T$  and the number of times this occurred is less than a specified amount, reduce  $\delta$ , let  $\bar{P} = \min(\bar{P}, \bar{P}')$ , set  $\hat{P} = \hat{P} \pm \delta$  (the future  $\bar{P}'$  should be on the same side of  $P_T$  as  $\bar{P}$ ), and go to Step 7. Otherwise, finalize the allocation and end the algorithm.

**Fig. 4.2** Proposed antenna subset selection algorithm (antenna configuration chosen on a subcarrier basis).

both  $\bar{P}$  and  $\bar{P}'$  are above or below  $P_T$ , then  $\hat{P}$  is modified such that after several iterations the two mean BER values straddle  $P_T$ . Once  $\bar{P}$  and  $\bar{P}'$  straddle  $P_T$ , the objective of the algorithm is to search for the configurations that maximize the throughput while coming as close as possible to  $P_T$  while not exceeding it.

Despite how complicated this algorithm may sound, it is less computationally intensive relative to an algorithm performing the same task in an incremental fashion. Moreover, unlike the previous algorithm, the proposed algorithm in this section also exploits the frequency domain in order to achieve a larger throughput at the cost of some complexity. Finally, with all the RF chains implemented in the hardware, most of the time only a subset of the chains are actually employed. Although the proposed algorithm makes use of the frequency diversity, it does not completely capitalize on its potential. In the next part of this chapter, two more algorithms are proposed that further exploit the frequency domain by employing bit loading in tandem with the proposed antenna subset selection algorithm.

## 4.2 Antenna Subset Selection Algorithm with Bit Loading

In the previous section, the proposed algorithms performed antenna subset selection in order to maximize the throughput while constrained by a mean BER limit and a fixed bit rate per subcarrier. In this section, two algorithms are proposed which first solve

$$\begin{aligned} & \max_{s_i, b_i} \sum_{i=0}^{N-1} b_i \\ & \text{subject to } \bar{P} = \frac{\sum_{i=1}^N b_i P_i}{\sum_{i=1}^N b_i} \leq P_T \end{aligned} \quad (4.7)$$

where the constraint of the same modulation scheme across all subcarriers has been dropped, followed by

$$\min_{s_i \in \mathcal{S}_{\max}} (\mu_{T,i} \cdot n_{T,i}(s_i) + \mu_{R,i} \cdot n_{R,i}(s_i)). \quad (4.8)$$

This means that bit allocation can be employed to further maximize the throughput of the system. Therefore, the next two proposed algorithms are designed such that they attempt to maximize the overall throughput of the system while constrained to operate below a

mean BER limit using the fewest antennas possible.

As was done with the previously proposed antenna subset selection algorithms, the two following proposed algorithms differ on how the antenna subset selection is performed. The first algorithm performs the selection on a signal basis (i.e., each subcarrier in the final allocation has the same antenna configuration) while the second algorithm has this constraint relaxed.

#### 4.2.1 Signal-Based Selection

The proposed antenna subset selection algorithm employing bit allocation is presented in Fig. 4.3. The proposed algorithm initializes by computing the theoretical values for  $P_i$  for all possible antenna configurations and modulation schemes. Steps 2 and 3 are in place to allow for a quick exit from the algorithm if the bit loading and antenna selection are not worthwhile. Then the algorithm searches for the largest signal constellation that satisfies  $P_i \leq \hat{P}$  per subcarrier per antenna configuration. Since the algorithm is constrained to choose a single antenna configuration for the final allocation, a search is performed to find the antenna configuration that yields the largest throughput. If a tie occurs, the configuration employing the fewest antennas is chosen.

Once a configuration has been chosen,  $\bar{P}$  is computed and the value of  $\hat{P}$  is changed by an amount  $\delta$ . Then repeat Steps 4 and 5 with the new  $\hat{P}$  and compute the mean BER  $\bar{P}'$ . The values of  $\bar{P}$  and  $\bar{P}'$  are then compared against the BER threshold  $P_T$ . If both  $\bar{P}$  and  $\bar{P}'$  are above or below  $P_T$ , the algorithm will steadily change the value of  $\hat{P}$  by an amount  $\delta$  until the two values straddle  $P_T$ . Once this occurs, the algorithm will zoom in on  $P_T$  until a configuration is found that maximizes throughput while  $\bar{P} \leq \bar{P}'$  is satisfied.

Although this proposed algorithm performs both antenna subset selection and bit allocation, it is still not taking advantage of the frequency diversity that can be easily achieved using MCM. By restricting the antenna configuration to be the same across all subcarriers, several configurations that could have yielded greater throughput were ignored while lowering the complexity. The next proposed algorithm relaxes the constraint on choosing the same antenna configuration for all subcarriers.

1. Initialization: Compute  $P_i$ ,  $i = 0, \dots, N - 1$ , for all available modulation schemes and antenna configurations.
2. If the largest  $P_i$  for 64-QAM modulation is less than  $P_T$ , set all subcarriers to 64-QAM, 1 transmit antenna, 1 receive antenna, and exit algorithm, else go to Step 3.
3. If smallest  $P_i$  for BPSK is greater than  $P_T$ , null all subcarriers and exit algorithm, else proceed to Step 4.
4. Find largest signal constellation for all subcarriers and antenna configurations such that  $P_i < \hat{P}$ .
5. Select the antenna configuration which yields the largest overall throughput (in case of a tie in the total number of bits, choose configuration with fewest overall antennas).
6. Compute  $\bar{P}$ .
7. If  $\bar{P} < P_T$ , let  $\hat{P} = \hat{P} + \delta$ , else  $\hat{P} = \hat{P} - \delta$ .
8. Find largest signal constellation for all subcarriers and antenna configurations such that  $P_i < \hat{P}$ .
9. Select the antenna configuration which yields the largest overall throughput (in case of a tie in the total number of bits, choose configuration with fewest overall antennas).
10. Compute  $\bar{P}'$ .
11. If both  $\bar{P} > P_T$  and  $\bar{P}' > P_T$  (resp.  $\bar{P} \leq P_T$  and  $\bar{P}' \leq P_T$ ), and no previous straddling of  $P_T$ , let  $\bar{P} = \bar{P}'$ ,  $\hat{P} = \hat{P} - \delta$  (resp.  $\hat{P} = \hat{P} + \delta$ ), and go to Step 8, else go to Step 12.
12. If both  $\bar{P} \leq P_T$  and  $\bar{P}' \leq P_T$ , and  $P_T$  was straddled before, let  $\bar{P} = \bar{P}'$ ,  $\hat{P} = \hat{P} + \delta$ , and go to Step 8, else go to Step 13.
13. If both  $\bar{P}$  and  $\bar{P}'$  are straddling  $P_T$  and the number of times this occurred is less than a specified amount, reduce  $\delta$ , let  $\bar{P} = \min(\bar{P}, \bar{P}')$ , set  $\hat{P} = \hat{P} \pm \delta$  (the future  $\bar{P}'$  should be on the same side of  $P_T$  as  $\bar{P}$ ), and go to Step 8. Otherwise, finalize the allocation and end the algorithm.

**Fig. 4.3** Proposed antenna subset selection algorithm with bit allocation (antenna configuration chosen on a signal basis).

1. Initialization: Compute  $P_i$ ,  $i = 0, \dots, N - 1$ , for all available modulation schemes and antenna configurations.
2. If the largest  $P_i$  for 64-QAM modulation is less than  $P_T$ , set all subcarriers to 64-QAM, 1 transmit antenna, 1 receive antenna, and exit algorithm, else go to Step 3.
3. If smallest  $P_i$  for BPSK is greater than  $P_T$ , null all subcarriers and exit algorithm, else proceed to Step 4.
4. Find largest signal constellation for all subcarriers and antenna configurations such that  $P_i < \hat{P}$ .
5. Select antenna configuration with largest  $b_i$ ,  $i = 0, \dots, N - 1$  (in case of a tie in the number of bits, choose configuration with fewest overall antennas).
6. Compute  $\bar{P}$ , the average BER, using Eq. (3.2).
7. If  $\bar{P} < P_T$ , let  $\hat{P} = \hat{P} + \delta$ , else  $\hat{P} = \hat{P} - \delta$ .
8. Find largest signal constellation for all subcarriers and antenna configurations such that  $P_i < \hat{P}$ .
9. Select antenna configuration with largest  $b_i$ ,  $i = 0, \dots, N - 1$  (in case of a tie in the number of bits, choose configuration with fewest overall antennas).
10. Compute  $\bar{P}'$ .
11. If both  $\bar{P} > P_T$  and  $\bar{P}' > P_T$  (resp.  $\bar{P} \leq P_T$  and  $\bar{P}' \leq P_T$ ), and no previous straddling of  $P_T$ , let  $\bar{P} = \bar{P}'$ ,  $\hat{P} = \hat{P} - \delta$  (resp.  $\hat{P} = \hat{P} + \delta$ ), and go to Step 8, else go to Step 12.
12. If both  $\bar{P} \leq P_T$  and  $\bar{P}' \leq P_T$ , and  $P_T$  was straddled before, let  $\bar{P} = \bar{P}'$ ,  $\hat{P} = \hat{P} + \delta$ , and go to Step 8, else go to Step 13.
13. If both  $\bar{P}$  and  $\bar{P}'$  are straddling  $P_T$  and the number of times this occurred is less than a specified amount, reduce  $\delta$ , let  $\bar{P} = \min(\bar{P}, \bar{P}')$ , set  $\hat{P} = \hat{P} \pm \delta$  (the future  $\bar{P}'$  should be on the same side of  $P_T$  as  $\bar{P}$ ), and go to Step 8. Otherwise, finalize the allocation and end the algorithm.

**Fig. 4.4** Proposed antenna subset selection algorithm with bit allocation (antenna configuration chosen on a subcarrier basis).

### 4.2.2 Subcarrier-Based Selection<sup>3</sup>

The proposed antenna subset selection algorithm performing bit allocation is presented in Fig. 4.4. Unlike the previous proposed algorithm, there is no constraint on the subcarriers to use the same antenna configuration. Although the flexibility of the proposed algorithms may allow them to come closer to the optimal allocation, its complexity may be too high for an actual hardware implementation. However, the proposed algorithms indicates the performance gains a system can achieve when the flexibility (and the associated complexity) increases.

As with the other algorithms, the proposed algorithm in this section starts off by computing the theoretical values for  $P_i$  for all possible antenna configurations and modulation schemes and storing them in a look-up table for easy access. The Steps 2 and 3 are performed to allow a quick exit in case it is not worth performing antenna subset selection and bit allocation. The algorithm then performs a search of each subcarrier and antenna configuration for the largest signal constellation such that  $P_i \leq \hat{P}$  is satisfied. The antenna configuration that yields the largest subcarrier throughput is then chosen for each subcarrier. In the case of a tie, the configuration employing the fewest antennas is chosen. Then  $\bar{P}$  is computed and the value of  $\hat{P}$  is modified by an amount  $\delta$ .

Steps 4 and 5 are then repeated with the new value of  $\hat{P}$  to yield a new configuration, from which the mean BER  $\bar{P}'$  is computed. The values of  $\bar{P}$  and  $\bar{P}'$  are compared with  $P_T$  and their relation with the mean BER threshold will determine the next steps the algorithm will perform. If both are above or below  $P_T$ , the value of  $\hat{P}$  is steadily modified until  $\bar{P}$  and  $\bar{P}'$  straddle  $P_T$ , in which case the algorithm zooms in on  $P_T$ . The algorithm stops when it has found a configuration and allocation that has maximized the throughput while satisfying  $\bar{P} \leq P_T$ .

From the four proposed algorithms, each of them vary in terms of complexity and ability to maximize throughput. The more complex an algorithm is relative to another, the better its chances are at achieving a larger throughput. The opposite also holds true. In the next section, the throughput results of the four proposed algorithms are presented for both uncorrelated and correlated MIMO channels.

---

<sup>3</sup>The work has been submitted to the *IEEE International Conference on Communications* [261].

### 4.3 Results

To evaluate the performance of the proposed algorithms found in this chapter, a multicarrier system based on some of the operating parameters used in the IEEE 802.11a standard are employed. In particular, the system possesses  $N = 64$  subcarriers, with 6 subcarriers at each end of the 16.6 MHz bandwidth set as “guard subcarriers”, i.e., nulled in order to avoid interference with adjacent bands [2]. The available modulation schemes for each subcarrier are BPSK, QPSK, square 16-QAM, and square 64-QAM. The option to null subcarriers also exists in circumstances where the prevailing channel conditions are too poor. However, unlike the standard, where the same modulation scheme is employed across all the subcarriers, the proposed algorithms that employ bit loading can use a different modulation scheme for each subcarrier. Results from all the proposed algorithms were obtained for a  $P_T$  value of  $10^{-5}$ .

The operating frequency of the system is 5 GHz, resulting in a wavelength of  $\lambda = 0.06$  m. The antenna elements employed by the antenna arrays are  $\lambda/2$  omnidirectional dipole antennas placed in a uniformly-spaced linear array with adjacent antenna separation of  $d$  and oriented such that they are all perpendicular to the  $xy$ -plane, i.e., vertically polarized. In the literature, there have been many studies on the performance of systems employing large multiple antenna arrays. Both for reasons of complexity and physical size constraints, we examine only a system employing a maximum of 2 antennas. Moreover, when multiple antennas are used at the transmitter, they all transmit the same signal on a per-subcarrier basis. At the receiver, MRC is performed to recombine the received signals (results for when EGC is employed showed a small decrease in throughput performance).

The physical separation between the basestation (transmitter) and mobile (receiver) was varied between 1 m and 60 m. The change in transmitter/receiver separation distance corresponds to an SNR change ranging from 59 dB to -11 dB. The MIMO channel consists of a collection of SISO channel responses generated using the method proposed by Saleh and Valenzuela [130]. The channel was assumed to be time-invariant and no line-of-sight existed between the transmitter and receiver. The SISO components of the MIMO channel were assumed to be uncorrelated. However, the effect of antenna separation on system performance was also examined for  $d = \lambda$  and  $d = 0.25\lambda$ . To model the correlation in the MIMO channel model for these antenna separation values, the procedure outlined in Section 2.2.2 and Appendix D were employed using Clarke’s correlation expression [144].

**Table 4.1** Normalized transformation matrices for creating correlated MIMO channels, with correlation matrix  $\Sigma$ , from uncorrelated MIMO channels, given  $(N_T, N_R)$ .

$d = 0.25\lambda$	
(1,2) or (2,1):	$\mathbf{P} = \begin{bmatrix} 0.9043 & 0.0000 \\ 0.2015 & 0.8816 \end{bmatrix}$
(2,2):	$\mathbf{P} = \begin{bmatrix} 0.8178 & 0.0000 & 0.0000 & 0.0000 \\ 0.1822 & 0.7973 & 0.0000 & 0.0000 \\ 0.1822 & 0.0000 & 0.7973 & 0.0000 \\ 0.0406 & 0.1776 & 0.1776 & 0.7772 \end{bmatrix}$
$d = \lambda$	
(1,2) or (2,1):	$\mathbf{P} = \begin{bmatrix} 0.9766 & 0.0000 \\ 0.0474 & 0.9754 \end{bmatrix}$
(2,2):	$\mathbf{P} = \begin{bmatrix} 0.9537 & 0.0000 & 0.0000 & 0.0000 \\ 0.0463 & 0.9526 & 0.0000 & 0.0000 \\ 0.0463 & 0.0000 & 0.9526 & 0.0000 \\ 0.0022 & 0.0462 & 0.0462 & 0.9515 \end{bmatrix}$
$d = 5\lambda$	
(1,2) or (2,1):	$\mathbf{P} = \begin{bmatrix} 0.9950 & 0.0000 \\ 0.0100 & 0.9949 \end{bmatrix}$
(2,2):	$\mathbf{P} = \begin{bmatrix} 0.9900 & 0.0000 & 0.0000 & 0.0000 \\ 0.0099 & 0.9899 & 0.0000 & 0.0000 \\ 0.0099 & 0.0000 & 0.9899 & 0.0000 \\ 0.0001 & 0.0099 & 0.0099 & 0.9899 \end{bmatrix}$

The resulting transformation matrices to convert an uncorrelated MIMO channel into a correlated MIMO channel model with correlation matrix  $\Sigma$  are shown in Table 4.1. Finally, for each MIMO channel realization, the algorithms were operating at 70 different averaged SNR values equally spaced in the logarithmic domain. The trials were repeated for 10000 different MIMO channel realizations and the results averaged.

The throughput and mean BER results of a system employing the proposed signal-based antenna subset selection algorithm for array configurations  $(N_T = 1, N_R = 1)$ ,  $(N_T = 1, N_R = 2)$ ,  $(N_T = 2, N_R = 1)$ , and  $(N_T = 2, N_R = 2)$  are shown in Figs. 4.5 and 4.6. It is observed that as the total number of antennas increase, so does the overall throughput and mean BER results. This is due to the spatial diversity offered by the antenna arrays, where several copies of the same signal are filtered by different CIRs and combined at the receiver. The combination process smoothes out the composite CIR, keeping the impact of the frequency selectivity to a minimum. It should also be noted that if the total number of antennas used by the system is equal, the configuration with more receive antennas will possess better performance. For instance, observing the throughput results for  $(N_T = 1, N_R = 2)$  and  $(N_T = 2, N_R = 1)$ , the former has better performance since it uses MRC, which weights each of the received signals according to its received quality. As for the  $(N_T = 2, N_R = 1)$  configuration, the received signal is essentially combined equally<sup>4</sup>.

The throughput and mean BER results for the same array configurations employing the proposed subcarrier-based antenna subset selection algorithm are shown in Figs. 4.7 and 4.8. It is observed that relative to the signal-based algorithm, the throughput and mean BER results are larger. For instance, the largest mean BER value in Fig. 4.6 is  $1.8 \times 10^{-6}$  while in Fig. 4.8 it is  $7.5 \times 10^{-6}$ . Moreover, the throughput for all array configurations, except for the  $(N_T = 1, N_R = 1)$  case, have increased by up to 100 bits per symbol. Finally, the gap in throughput between the  $(N_T = 1, N_R = 2)$  and  $(N_T = 2, N_R = 1)$  cases is smaller relative to the system employing the signal-based algorithm. This is all due to the additional flexibility introduced to the system by performing the antenna subset selection per-subcarrier. As a result, the algorithm now has the opportunity to choose configurations that may yield solutions that are closer to the optimal allocation while obeying the mean BER constraint.

---

<sup>4</sup>The antenna subset selection algorithm and the communication system that employs it are based on the principles of diversity combining. Thus, it has a diversity gain (depending on adjacent antenna spacing) but no multiplexing gain [262].

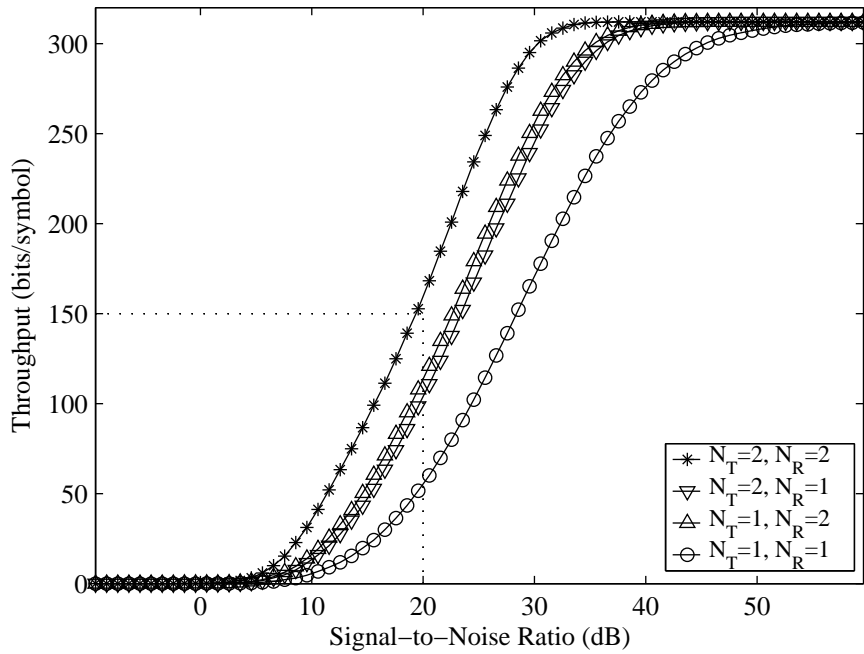


**Fig. 4.5** Throughput of a multicarrier system with several array configurations employing the proposed signal-based antenna subset selection algorithm.

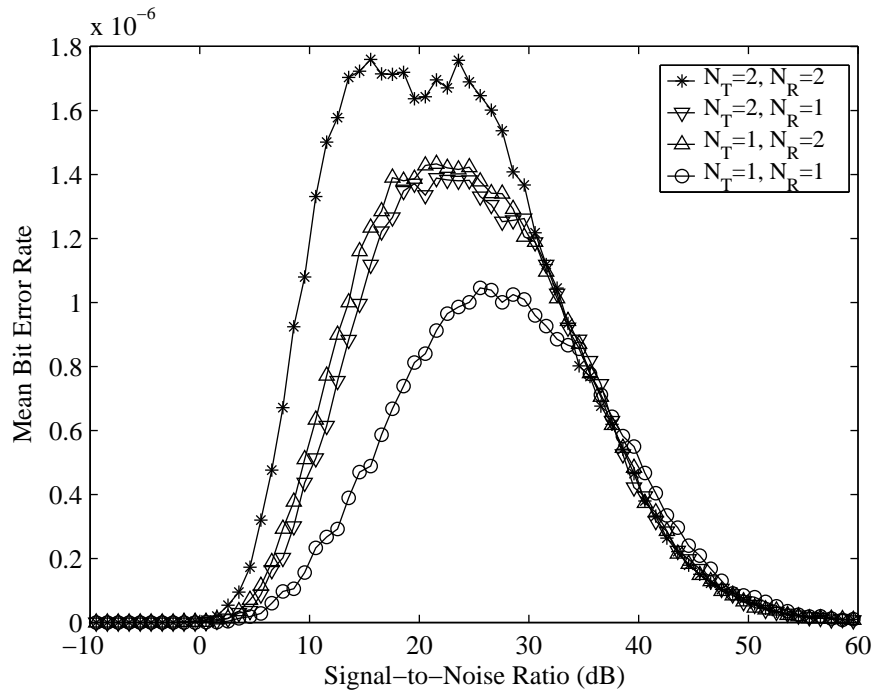


**Fig. 4.6** Mean BER of a multicarrier system with several array configurations employing the proposed signal-based antenna subset selection algorithm.

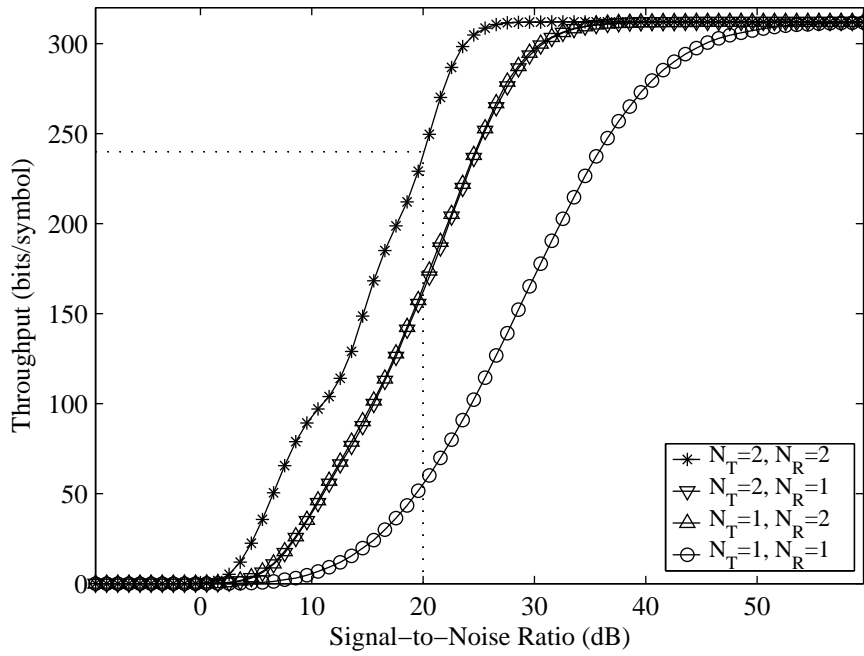


**Fig. 4.7** Throughput results of the proposed subcarrier-based antenna subset selection algorithm.

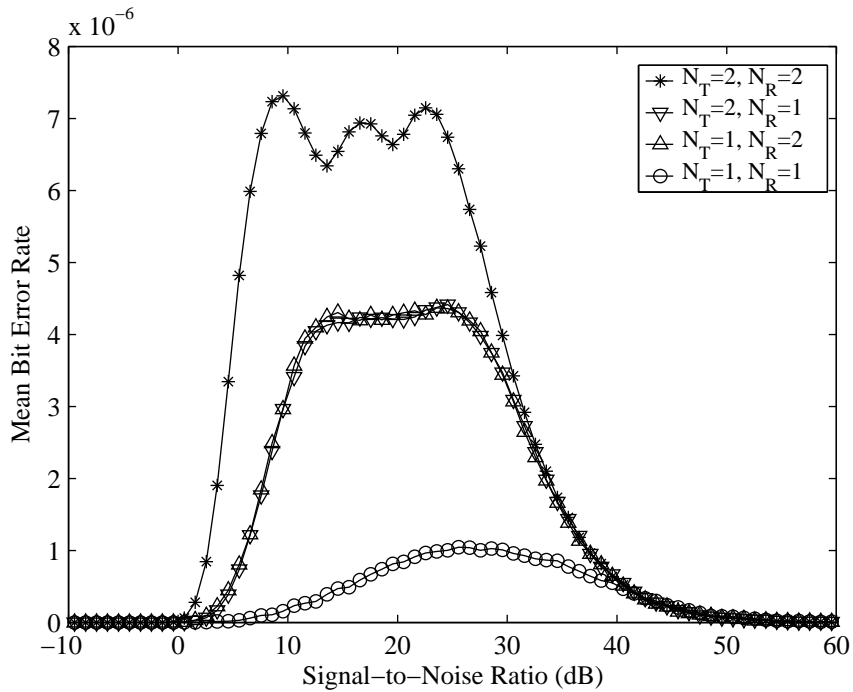


**Fig. 4.8** Mean BER results of the proposed subcarrier-based antenna subset selection algorithm.

**Table 4.2** Average (transmit antenna, receive antenna) usage for the four proposed algorithms at several SNR values with ( $N_T = 2, N_R = 2$ ) antennas available for selection.

SNR (dB)	Signal-level (no bit loading)	Subcarrier-level (no bit loading)	Signal-level (with bit loading)	Subcarrier-level (with bit loading)
14.6	(1.1713,1.2447)	(1.0024,1.0017)	(1.2370,1.5684)	(1.0583,1.0615)
24.6	(1.1611,1.2154)	(1.0006,1.0003)	(1.2337,1.4343)	(1.0010,1.0007)
34.6	(1.0470,1.0339)	(1.0000,1.0000)	(1.0490,1.0320)	(1.0000,1.0000)

Substantial increases in both the overall throughput and mean BER results are observed when bit allocation is employed in tandem with the antenna subset selection algorithms. The throughput and mean BER results for a system employing the proposed signal-based antenna subset selection algorithm with bit loading are shown in Figs. 4.9 and 4.10. When compared to Figs. 4.5 and 4.5, the difference in throughput is as large as 135 bits per symbol while the mean BER is close to  $0.9 \times 10^{-5}$ . As explained previously, the introduction of bit loading allows for a greater number of configurations that the algorithm can choose. As for the difference in throughput and mean BER with Figs. 4.7 and 4.8, there is still an increase when bit loading is employed. For example, the maximum increase in throughput is about 45 bits per symbol. This is due to the greater flexibility available in bit loading, which has  $N$  subcarriers to modify, relative to the antenna subset selection, which has at most two antennas at either the transmitter or receiver.

Finally, the throughput and mean BER results for the proposed subcarrier-based antenna subset selection algorithm employing bit loading is shown in Figs. 4.11 and 4.12. Compared to all the other proposed algorithms, this algorithm achieves the largest throughput results and possess mean BER values that are the closest to  $P_T = 1 \times 10^{-5}$ . This is due to the numerous configurations, which is a combination of all the possible bit allocations and array configurations, that the algorithm can choose. In fact, the configurations available to the previous algorithms are all subsets of the configurations available to this algorithm. As a result, the algorithm can choose a configuration whose throughput is the closest to the throughput of the optimal configuration.

To reduce the power consumption of multiple antenna system, antennas that yield no increase in the overall throughput of the system are identified by the proposed algorithms in this chapter and are turned off. The remaining antennas are then used in a diversity

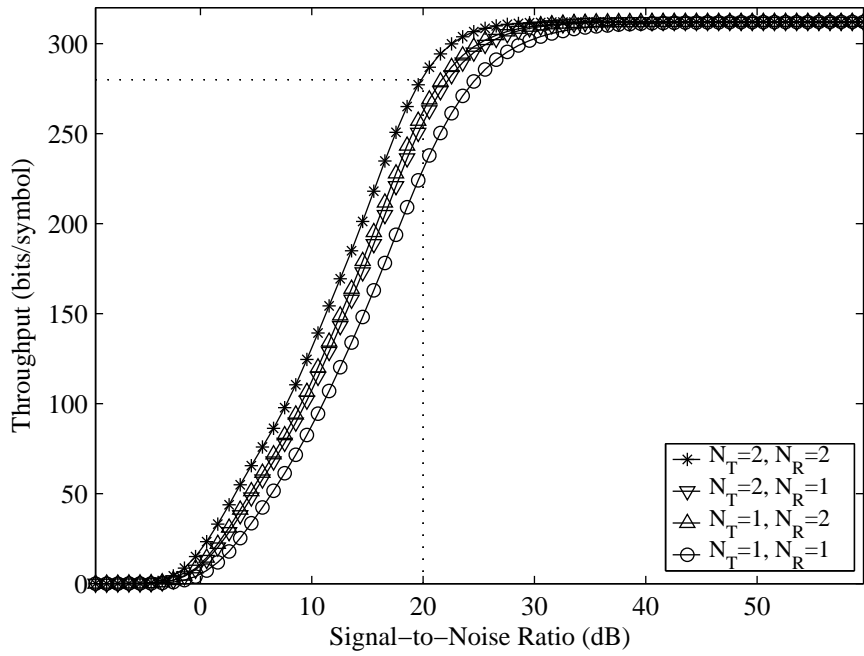


**Fig. 4.9** Throughput results of the proposed signal-based antenna subset selection algorithm with bit loading.

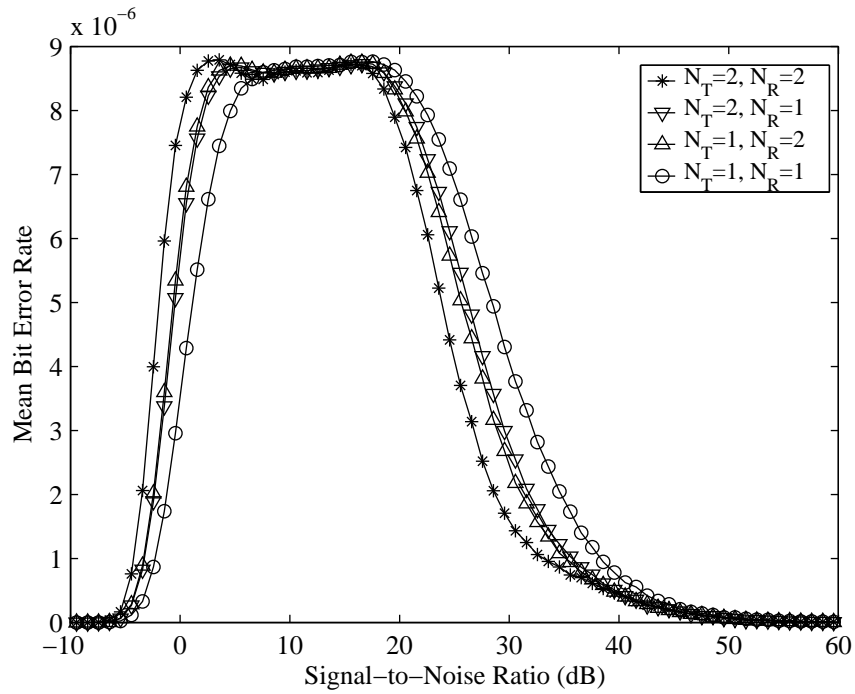


**Fig. 4.10** Mean BER results of the proposed signal-based antenna subset selection algorithm with bit loading.

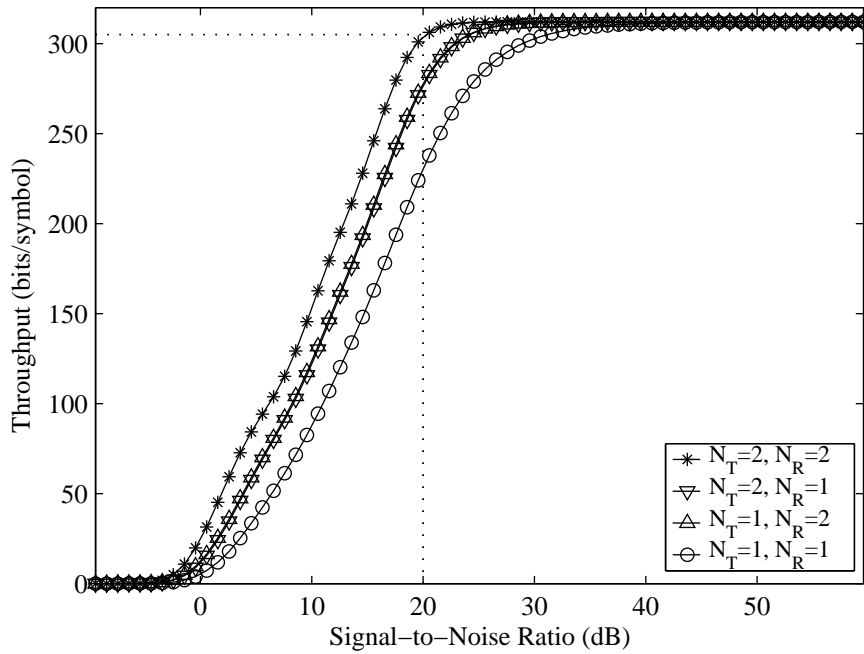


**Fig. 4.11** Throughput results of the proposed subcarrier-based antenna subset selection algorithm with bit loading.

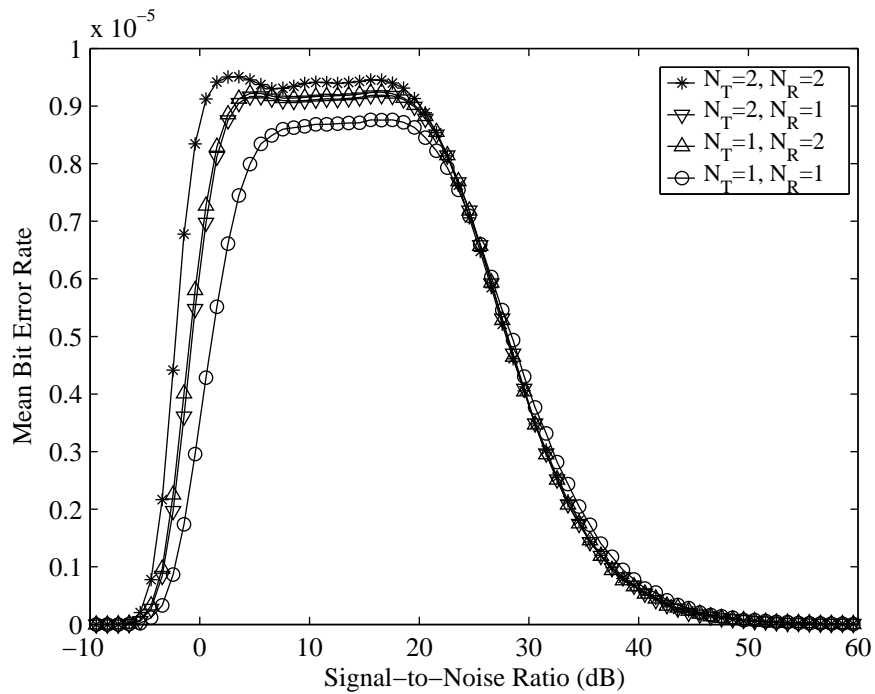


**Fig. 4.12** Mean BER results of the proposed subcarrier-based antenna subset selection algorithm with bit loading.

transmission/combining scheme by the system. However, different channel conditions may require a different number of transmit and receive antennas. The results for the average transmit and receive antenna usage by the four proposed algorithms are presented in Table 4.2. The algorithm has a choice of  $N_T = 2$  transmit antennas and  $N_R = 2$  receive antennas, although none of the results reach the maximum number of transmit and receive antennas. It is observed that the algorithms using the same antenna configuration for all subcarriers have a higher usage of antennas relative to the algorithms with different antenna configurations across the subcarriers. This is due to the increased flexibility of the subcarrier-level algorithms (i.e., different antenna configurations for each subcarrier) to tailor the antenna configurations to the prevailing channel conditions. As a result, these algorithms need fewer antennas to achieve the same performance relative to the signal-level algorithms (i.e., same antenna configurations across all subcarriers).

The results presented thus far are only use an uncorrelated MIMO channel model. However, when correlation is introduced into the MIMO channel model, it negatively impacts the throughput performance of the system. The difference in throughput between the uncorrelated and correlated cases, with an adjacent antenna spacing of  $d = \lambda$ , is shown in Figs. 4.13 and 4.14 for the subcarrier- and signal-based algorithms, respectively. It is observed that the largest decrease in throughput is between 6 and 8 bits per symbols. As for an antenna separation of  $d = 0.25\lambda$ , the decrease in throughput is more significant, i.e., on the order of 20 to 30 bits per symbols. It is observed that the array configuration ( $N_T = 2, N_R = 2$ ) experiences the largest loss in throughput relative to the other configurations. Since the other array configurations have smaller gains relative to the ( $N_T = 2, N_R = 2$ ) case, they have less to lose when the spatial diversity decreases. However, even with some correlation, the performance of the proposed subcarrier-based antenna subset selection algorithm employing bit loading possesses the best throughput performance of all the proposed algorithms, at the expense of increased complexity.

### 4.3.1 An Example

To evaluate the relative performance of the four proposed algorithms, the throughput values for a ( $N_T = 2, N_R = 2$ ) system operating at an SNR of 20 dB and employing these algorithms are compared. For the proposed subcarrier-based antenna subset selection algorithm with bit loading, the throughput is 305 bits per symbol (indicated by the cross-hairs

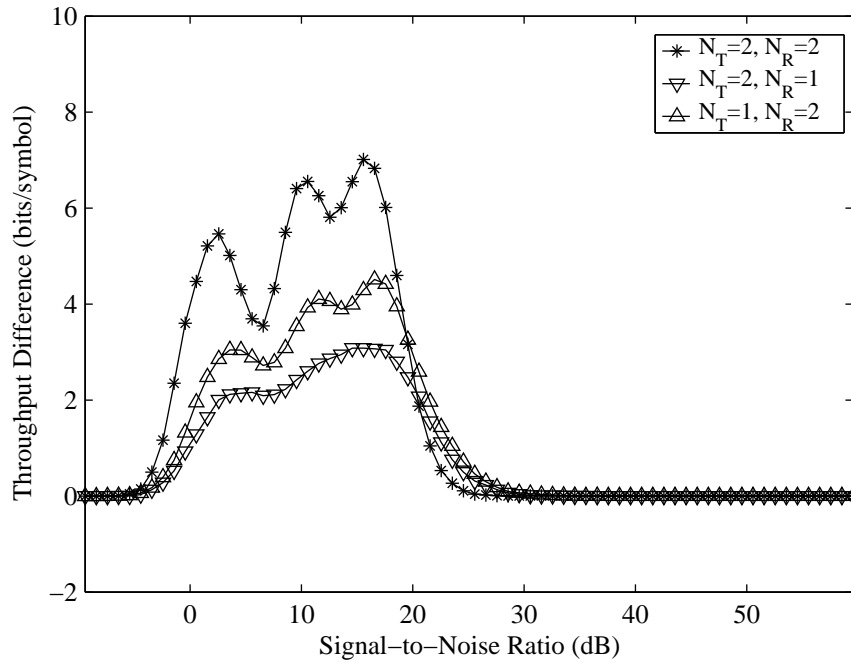


**Fig. 4.13** Throughput difference results between arrays with antenna spacings of  $d = 5\lambda$  and  $d = \lambda$  for the proposed subcarrier-based antenna subset selection algorithm employing bit loading.

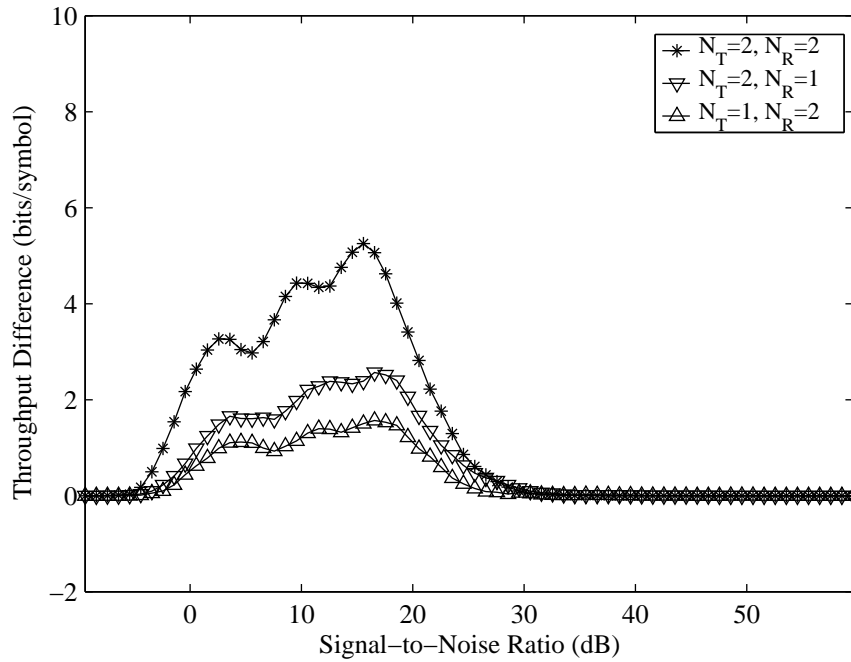


**Fig. 4.14** Throughput difference results between arrays with antenna spacings of  $d = 5\lambda$  and  $d = \lambda$  for the proposed signal-based antenna subset selection algorithm employing bit loading.

on Fig. 4.11). The throughput for the proposed signal-based antenna subset selection algorithm with bit loading is 280 bits per symbol (indicated by the cross-hairs on Fig. 4.9). The throughput values for the proposed signal- and subcarrier-based antenna subset selection algorithms are 150 and 240 bits per symbol, respectively (indicated by the cross-hairs on Figs. 4.5 and 4.7). It is observed that as the flexibility of the algorithm to choose a configuration increases, the system experiences a modest increase in the overall throughput.

#### 4.4 Chapter Summary

Four novel antenna subset selection algorithms were proposed in this chapter. Each of the algorithms possessed a different amount of computational and implementation complexity, yielding different throughput performances. Two of the proposed algorithms performed bit allocation while the other two did not. For each pair of algorithms, one would perform the antenna subset selection on a per-subcarrier basis while the other would do so on a signal basis. Moreover, the antenna subset selection algorithm made use of all possible configurations, unlike what is found in the literature where algorithms must choose a fixed number of antennas.

The results show that as the complexity of the algorithm increases, it gains flexibility in its choices of possible allocations. Therefore, the granularity for the set of possible allocations becomes finer, resulting in solutions that are closer to the mean BER limit  $P_T$  and yielding greater throughputs. However, there is a tradeoff between enhanced performance and complexity. In particular, the subcarrier-level antenna subset selection with bit loading yields the best results while having the largest implementation complexity. On the other hand, the simple signal-level antenna subset selection algorithm has the lowest implementation complexity but the lowest throughput results.

The effects of correlation due to adjacent antenna spacing was also studied for the system employing the proposed algorithms that performs diversity transmission/combining. However, as the antenna spacing decreases, so does the throughput due to the decrease in spatial diversity. The results show that the effects of correlation are more pronounced when more array elements are present.

It can be concluded that for systems employing multiple antennas that are spaced far enough, and bit allocation is performed in tandem, the resulting throughput performance of the system is significantly enhanced.

# Chapter 5

## Conclusion

### 5.1 Research Achievements

In this dissertation, a number of contributions have been made in the area of adaptive loading for multicarrier data transmission for indoor wireless networks. The research achievements of this thesis are the following:

- Two low-complexity discrete bit loading algorithms that achieve a final allocation close to the optimal solution. Moreover, the speed at which these algorithms reach their final solution is significantly faster relative to several other algorithms found in the literature. These proposed algorithms have achieved a balance between computational complexity and closeness to the optimal solution.
- A realistic power loading algorithm that obeys a frequency interval power constraint. Other published power loading algorithms employ a total power constraint. The proposed algorithm uses a stricter constraint in order to avoid any violation of the regulatory requirements. Moreover, this algorithm has more flexibility to allocate power relative to algorithms that employ a subcarrier power constraint, which is considered too strict.
- Two algorithms that allocate equalizer taps non-uniformly across all the subcarriers. The first algorithm allocates taps per subcarrier in order to reduce the subcarrier distortion to be below some subcarrier distortion threshold. The rationale behind the second algorithm is to allocate taps to subcarriers that achieve the greatest reduction

in overall distortion. The number of taps that can be allocated to each subcarrier is limited, and the algorithm stops allocating taps once the change in overall distortion is negligible. Results for an MCM system employing the proposed algorithms show that the error performance is significantly better relative to a uniform allocation of equalizer taps with the same overall number of equalizer taps employed.

- A suboptimal output level placement technique for the quantization of subcarrier SNR values. By quantizing the SNR values in a non-uniform fashion, where the output levels are placed based on the characteristics of the BER curves, the amount of error due to quantization is reduced.
- An antenna subset selection scheme that can either operate across all subcarriers simultaneously or on a per-subcarrier basis. The algorithm allows the system to employ any number of antennas at the transmitter and receiver, unlike conventional antenna selection where the number of antennas to choose from is always of a fixed size. Thus, the granularity of the possible allocations and configurations is significantly reduced. Thus, systems can reach a solution that can maximize the throughput while come very close to, but not exceed, the mean BER threshold.
- A combination of the proposed antenna subset selection algorithm with peak BER bit loading algorithm. Using the two algorithms in tandem, the results show that the throughput performance significantly increased relative to when only either is employed.

## 5.2 Future Work

There exists a number of topics that have resulted from this research that could be continued.

- In the literature and in this dissertation, research was performed on multi-tap FEQs. However, the idea of channel shortening was not addressed, as well as variable-length cyclic prefixes. One research topic is to create an algorithm that designs a channel shortening TEQ and subcarrier FEQs while attempting to minimize the length of the cyclic prefix in OFDM systems.

- 
- Although spatial diversity techniques presented in Chapter 4 allowed the system to increase throughput while maintaining the same robustness to errors, it would be interesting to extend the bit loading algorithms of Chapter 3 to a spatial multiplexing framework.
  - All the algorithms in this dissertation assumed there was no latency in the feedback between the transmitter and the receiver. Since the channel conditions of indoor environments do change over time, the impact of outdated channel state information on the performance of the proposed bit loading and power loading algorithms, as well as the equalizer tap allocation algorithms and antenna subset selection algorithms, would be significant. Two aspects of this problem should be studied: (1) evaluating the impact of outdated channel state information on system performance through mathematical analysis and computer simulations, and (2) devising techniques to make these algorithms more robust to outdated channel state information (e.g., predicting the long-term behaviour of the channel).
  - The case of a single user receiving information from an access point was studied. However, this is not realistic since the system should be able to support multiple users. Thus the impact of multi-user interference on the performance of the system should be studied in the context of adaptive loading. In particular, the proposed power loading algorithm in conjunction with the proposed bit loading algorithm could be modified to reduce interference to other users. This could further be improved with beamforming.

# Appendix A

## Data-Aided Channel Estimation Error

The deviation between the actual bit allocation and the optimal allocation is dependent on the adaptive bit loading algorithm employed and the quality of the CSI. This quality is partially dependent on the channel estimation technique. In this work, data-aided channel estimation is employed, where the transmission of data is interrupted as needed in order for training symbols to be sent across the channel. At the receiver, the training symbols are extracted and a channel estimate is communicated back to the transmitter using the reverse channel. Thus, the data throughput decreases due to increase in transmission overhead.

Referring to Fig. 2.1, let  $x^{(i)}(n)$ ,  $i = 0, \dots, N - 1$ , be a collection of BPSK-modulated training signals which are known at the receiver. Given that the  $K$ -point DFT is defined as

$$X(m) \triangleq \sum_{n=0}^{K-1} x(n)e^{-j2\pi nm/K}, \quad 0 \leq m \leq K - 1, \quad (\text{A.1})$$

where  $K$  is sufficiently long, the  $K$ -point DFT of  $y^{(i)}(n)$ ,  $g^{(i)}(n)$ ,  $h(n)$ ,  $v(n)$ , and  $f^{(i)}(n)$  is  $Y^{(i)}(m)$ ,  $G^{(i)}(m)$ ,  $H(m)$ ,  $V(m)$ , and  $F^{(i)}(m)$ , respectively.

Under ideal channel conditions (i.e., no noise is present, no multipath propagation), the output of the  $i^{\text{th}}$  analysis filter in terms of  $Y^{(i)}(m)$  is given by

$$\hat{Y}_{\text{Ideal}}^{(i)}(m) = F^{(i)}(m) \sum_{k=0}^{N-1} G^{(k)}(m)Y^{(k)}(m). \quad (\text{A.2})$$

However, when a dispersive channel  $h(n)$  and noise  $v(n)$  are present in the system, Eq. (A.2) becomes

$$\begin{aligned}\hat{Y}^{(i)}(m) &= F^{(i)}(m)H(m) \sum_{k=0}^{N-1} G^{(k)}(m)Y^{(k)}(m) \\ &\quad + F^{(i)}(m)V(m) \\ &= H(m)\hat{Y}_{\text{Ideal}}^{(i)}(m) + F^{(i)}(m)V(m).\end{aligned}\tag{A.3}$$

Given that  $y^{(i)}(n)$ ,  $g^{(i)}(n)$ , and  $f^{(i)}(n)$  are known at the receiver, the channel estimate in the passband of subcarrier  $i$ , with the frequency range corresponding to the bins  $m_L^{(i)} \leq m < m_U^{(i)}$ , is computed using [198]:

$$\begin{aligned}\hat{H}^{(i)}(m) &= \frac{\hat{Y}^{(i)}(m)}{\hat{Y}_{\text{Ideal}}^{(i)}(m)} = \frac{\hat{Y}^{(i)}(m)\hat{Y}_{\text{Ideal}}^{(i)*}(m)}{\left|\hat{Y}_{\text{Ideal}}^{(i)}(m)\right|^2} \\ &= H(m) + \frac{F^{(i)}(m)V(m)\hat{Y}_{\text{Ideal}}^{(i)*}(m)}{\left|\hat{Y}_{\text{Ideal}}^{(i)}(m)\right|^2} \\ &= H(m) + \Delta^{(i)}(m),\end{aligned}\tag{A.4}$$

where  $\hat{H}^{(i)}(m)$  is the  $K$ -point DFT of the channel estimate  $\hat{h}^{(i)}(n)$ ,  $\Delta^{(i)}(m)$  is the channel estimation error associated with subcarrier  $i$ , and  $m_L^{(i)}$  (resp.  $m_U^{(i)}$ ) is the frequency bin corresponding to the lowest (resp. highest) frequency portion of the passband for subcarrier  $i$ . The estimate of the entire channel response is simply the sum of Eq. (A.4) across all the subcarriers, which yields

$$\hat{H}(m) = H(m) + \sum_{i=0}^{N-1} \Delta^{(i)}(m).\tag{A.5}$$

From Eq. (A.5), it is observed that the  $\Delta^{(i)}(m)$  term represents the uncertainty of the channel estimation procedure. Therefore, the accuracy of the channel estimation is dependent on the amount of noise present in the channel as well as on the choice of synthesis and analysis filters used by the system.

Referring to Eq. (A.4), the SNR for subcarrier  $i$  based on channel estimates is given by

$$\begin{aligned}
\hat{\gamma}^{(i)} &= \frac{1}{M_{\text{bins}}^{(i)}} \sum_{m=m_L^{(i)}}^{m_U^{(i)}} \frac{\pi^{(i)} |\hat{H}^{(i)}(m)|^2}{\sigma_v^2} \\
&= \frac{1}{M_{\text{bins}}^{(i)}} \sum_{m=m_L^{(i)}}^{m_U^{(i)}} \frac{\pi^{(i)} |H(m) + \Delta^{(i)}(m)|^2}{\sigma_v^2} \\
&= \frac{1}{M_{\text{bins}}^{(i)}} \sum_{m=m_L^{(i)}}^{m_U^{(i)}} \left( \frac{\pi^{(i)} |H(m)|^2}{\sigma_v^2} + \frac{\pi^{(i)} (2\text{Re}\{H(m)\Delta^{(i)*}(m)\} + |\Delta^{(i)}(m)|^2)}{\sigma_v^2} \right) \\
&= \gamma^{(i)} + \epsilon^{(i)}(\gamma^{(i)})
\end{aligned} \tag{A.6}$$

where  $M_{\text{bins}}^{(i)} = m_U^{(i)} - m_L^{(i)} + 1$  is the number of frequency bins corresponding to the passband of subcarrier  $i$ ,  $\pi^{(i)}$  is the transmit power for subcarrier  $i$ ,  $\sigma_v^2$  is the noise variance,  $\gamma^{(i)}$  is the actual SNR of subcarrier  $i$ , and  $\epsilon^{(i)}(\gamma^{(i)})$  is the contribution of the channel estimation error to the subcarrier SNR. Note that  $\epsilon^{(i)}(\gamma^{(i)})$  is a function of the subcarrier SNR,  $\gamma^{(i)}$ .

The system performance is also affected by the time variation of the channel and the rate at which the channel estimate is updated [65, 66]. When the channel varies rapidly over time, the rate at which the channel estimate needs to be updated must also be high, resulting in increased transmission overhead. If the update rate is too low, the system will use outdated channel estimates which may lead to significant performance degradation. On the other hand, if the rate is too high, the data throughput significantly decreases (with no additional performance gain). Thus, the dynamics of the channel must be known in order to determine the appropriate channel estimate update rate. Since indoor wireless networks are studied in this work, where the channel is assumed to be quasi-stationary due to the low velocities of the mobiles in this environment [198], it can be assumed that the channel is time invariant over a reasonably long period of time.

## Appendix B

# Optimal Fractionally-Spaced MMSE Subcarrier Equalizers

### B.1 System Transfer Function

The system transfer function of a MDFT filterbank multicarrier system is derived using the framework developed in Section 2.1.3. Referring to Figs. 2.2 and 2.7, the modulated data streams  $x^{(i)}(n)$ ,  $i = 0, \dots, N - 1$ , are each defined in this derivation as a vector of length  $L$

$$\mathbf{x}_{n,n-L+1}^{(k)} = \begin{bmatrix} x^{(k)}(n) & \dots & x^{(k)}(n - L + 1) \end{bmatrix}^T,$$

for  $k = 0, \dots, N - 1$ . These vectors are then used as inputs to the MDFT pre-processing stage of the system, the outputs of which are the vectors  $\mathbf{y}_{n,n-2L+1}^{(k)}$ ,  $k = 0, \dots, N - 1$ , with length  $2L$ . These outputs are then upsampled using a  $(2LR + D) \times (2L)$  upsampling matrix  $\mathbf{T}_{u,R,D}$ , defined by Eq. (2.15), where  $R$  is the sampling rate, and  $D$  is the delay. In this case, the sampling rate is  $R = \frac{N}{2}$  since combined with the MDFT pre-processing stage, which performs an upsampling by a factor of 2, the overall sampling rate is  $N$  (i.e., critically-sampled filterbanks). The delay is  $D = 2\lceil\tau\rceil + \lceil\tau_{\text{ch}}\rceil$ , where  $\tau$  is the group delay of the synthesis or analysis filter, and  $\tau_{\text{ch}}$  is the group delay of the channel. By sufficiently zero-padding the transmitted signal, the total group delay introduced by the system would be adequately compensated for prior to downsampling [85].

The upsampled signals are then filtered by the synthesis filters  $\mathbf{g}_{0,P-1}^{(k)}$ ,  $k = 0, \dots, N - 1$ , of length  $P$ . The filtered signals are then summed together and transmitted across the

channel, with an impulse response  $\mathbf{h}_{0,S-1}$  of length  $S$ . The received signal is decomposed into  $N$  subcarriers using the analysis filters  $\mathbf{f}_{0,P-1}^{(k)}$ ,  $k = 0, \dots, N-1$ , of length  $P$  before being downsampled by the  $(2Q) \times (2LR+D-2P-S+3)$  downsampling matrix  $\mathbf{T}_{d,N/2,0} = \mathbf{T}_{u,N/2,0}^T$ , where  $2Q$  is the length of the fractionally-spaced MMSE equalizer.

Filtering is performed in this derivation using convolution matrices [254, 255]. Therefore,  $\mathbf{g}_{0,P-1}^{(k)}$  can be represented as an  $(2LR+D-P+1) \times (2LR+D)$  convolution matrix defined by Eq. (2.18). Furthermore, the channel  $\mathbf{h}_{0,S-1}$  and the  $k^{\text{th}}$  analysis filter  $\mathbf{f}_{0,P-1}^{(k)}$ , can be represented as  $(2LR+D-P-S+2) \times (2LR+D-P+1)$  and  $(2LR+D-2P-S+3) \times (2LR+D-P-S+2)$  convolution matrices,  $\mathbf{H}$  and  $\mathbf{F}^{(k)}$ , respectively.

The transfer function for the  $k^{\text{th}}$  subcarrier prior to the equalization and MDFT post-processing is given by

$$\begin{aligned} \bar{\mathbf{y}}_{n,n-2Q+1}^{(k)} &= \mathbf{T}_{d,R,0} \mathbf{F}^{(k)} \mathbf{H} \sum_{l=0}^{N-1} \mathbf{G}^{(l)} \mathbf{T}_{u,R,D} \mathbf{y}_{n,n-2L+1}^{(l)} \\ &+ \mathbf{T}_{d,R,0} \mathbf{F}^{(k)} \mathbf{v}_{0,2LR+D-P-S+2} \end{aligned} \quad (\text{B.1})$$

where  $\mathbf{v}_{0,NL+D-P-S+1}$  is the additive white Gaussian noise (AWGN) contribution of the channel.

To compensate for the distortion added to  $\bar{\mathbf{y}}_{n,n-2Q+1}^{(k)}$  by the channel, as well as the synthesis and analysis filters, optimal  $2Q$ -tap fractionally-spaced MMSE equalizers  $\mathbf{w}_{0,2Q-1}^{(k)}$ ,  $k = 0, \dots, N-1$ , are employed before performing MDFT post-processing. Thus, the output of the equalizer is given by

$$\hat{y}^{(k)}(n) = \mathbf{w}_{0,2Q-1}^{(k)H} \bar{\mathbf{y}}_{n,n-2Q+1}^{(k)}. \quad (\text{B.2})$$

In the next subsection, the derivation for the MMSE cost function at the output of the MDFT post-processing stage and optimal equalizer are presented.

## B.2 Optimal MMSE Equalizer Derivation

Since the desired real and imaginary information of  $\bar{\mathbf{y}}_{n,n-2Q+1}^{(k)}$  are  $90^\circ$  out-of-phase with each other and that they occur only at every second sample, the distortion of the real and imaginary components must be reduced separately at specific sampling instants.

Therefore, the mean squared error (MSE) cost function of the desired real and imaginary

components can be defined as

$$\begin{aligned}
 J^{(k)} &= \frac{1}{2}E\{|Re(y^{(k)}(2m) - \hat{y}^{(k)}(2m))|^2\} \\
 &\quad + \frac{1}{2}E\{|Im(y^{(k)}(2m+1) - \hat{y}^{(k)}(2m+1))|^2\} \\
 &= \frac{1}{8}E\{|y^{(k)}(2m) - \hat{y}^{(k)}(2m) \\
 &\quad + y^{(k)*}(2m) - \hat{y}^{(k)*}(2m)|^2\} \\
 &\quad + \frac{1}{8}E\{|y^{(k)}(2m+1) - \hat{y}^{(k)}(2m+1) \\
 &\quad - y^{(k)*}(2m+1) + \hat{y}^{(k)*}(2m+1)|^2\}
 \end{aligned} \tag{B.3}$$

where, without loss of generality,  $n = 2m$  corresponds to the desired sampling instants for the real information in subcarrier  $k$  while  $n = 2m + 1$  defines the desired sampling instants for the imaginary data.

Expanding Eq. (B.3) and employing Eq. (B.2) yields

$$\begin{aligned}
 J^{(k)} &= \sigma_y^2 - Re\{\mathbf{p}_{y,r}^{(k)H} \mathbf{w}^{(k)}\} - Re\{\mathbf{p}_{y,i}^{(k)H} \mathbf{w}^{(k)}\} \\
 &\quad + \frac{1}{4} \left( Re\{\mathbf{w}^{(k)H} \mathbf{R}_{y,r}^{(k)} \mathbf{w}^{(k)}\} + Re\{\mathbf{w}^{(k)H} \mathbf{R}_{y,i}^{(k)} \mathbf{w}^{(k)}\} \right. \\
 &\quad \left. + Re\{\mathbf{w}^{(k)H} \mathbf{R}_{y,r}^{(k)'} \mathbf{w}^{(k)*}\} - Re\{\mathbf{w}^{(k)H} \mathbf{R}_{y,i}^{(k)'} \mathbf{w}^{(k)*}\} \right)
 \end{aligned} \tag{B.4}$$

where

$$\begin{aligned}
 \mathbf{w}^{(k)} &= \mathbf{w}_{0,2Q-1}^{(k)} \\
 \sigma_y^2 &= E\{y^{(k)}(2m)y^{(k)*}(2m)\} \\
 &= E\{y^{(k)}(2m+1)y^{(k)*}(2m+1)\} \\
 \mathbf{p}_{y,r}^{(k)H} \mathbf{w}^{(k)} &= E\{y^{(k)}(2m)\hat{y}^{(k)*}(2m)\} \\
 \mathbf{p}_{y,i}^{(k)H} \mathbf{w}^{(k)} &= E\{y^{(k)}(2m+1)\hat{y}^{(k)*}(2m+1)\} \\
 \mathbf{w}^{(k)H} \mathbf{R}_{y,r}^{(k)} \mathbf{w}^{(k)} &= E\{\hat{y}^{(k)}(2m)\hat{y}^{(k)*}(2m)\} \\
 \mathbf{w}^{(k)H} \mathbf{R}_{y,i}^{(k)} \mathbf{w}^{(k)} &= E\{\hat{y}^{(k)}(2m+1)\hat{y}^{(k)*}(2m+1)\} \\
 \mathbf{w}^{(k)H} \mathbf{R}_{y,r}^{(k)'} \mathbf{w}^{(k)*} &= E\{\hat{y}^{(k)}(2m)\hat{y}^{(k)}(2m)\} \\
 \mathbf{w}^{(k)H} \mathbf{R}_{y,i}^{(k)'} \mathbf{w}^{(k)*} &= E\{\hat{y}^{(k)}(2m+1)\hat{y}^{(k)}(2m+1)\}
 \end{aligned}$$

To get the minimum cost function for subcarrier  $k$ ,  $J_{\min}^{(k)}$ , the optimal fractionally-spaced MMSE equalizer weights must be determined. To achieve that, the Wirtinger derivative is applied to Eq. (B.4), namely [263],

$$\frac{\partial}{\partial \mathbf{w}^{(k)*}} = \frac{1}{2} \begin{bmatrix} \frac{\partial}{\partial w_R^{(k)}(0)} + j \frac{\partial}{\partial w_I^{(k)}(0)} \\ \frac{\partial}{\partial w_R^{(k)}(1)} + j \frac{\partial}{\partial w_I^{(k)}(1)} \\ \vdots \\ \frac{\partial}{\partial w_R^{(k)}(2Q-1)} + j \frac{\partial}{\partial w_I^{(k)}(2Q-1)} \end{bmatrix}, \quad (\text{B.5})$$

where  $w_R^{(k)}(m)$  and  $w_I^{(k)}(m)$  are the real and imaginary components of  $w^{(k)}(m)$ . This yields

$$\begin{aligned} \frac{\partial J^{(k)}}{\partial \mathbf{w}^{(k)*}} &= -4(\mathbf{p}_{y,r}^{(k)} + \mathbf{p}_{y,i}^{(k)}) + 2(\mathbf{R}_{y,r}^{(k)} + \mathbf{R}_{y,i}^{(k)})\mathbf{w}^{(k)} \\ &\quad + 2(\mathbf{R}_{y,r}^{(k)'} - \mathbf{R}_{y,i}^{(k)'})\mathbf{w}^{(k)*} \\ &= 0 \end{aligned}$$

which can be equivalently written as

$$\begin{aligned} 2(\mathbf{p}_{y,r}^{(k)} + \mathbf{p}_{y,i}^{(k)}) &= (\mathbf{R}_{y,r}^{(k)} + \mathbf{R}_{y,i}^{(k)})\mathbf{w}^{(k)} \\ &\quad + (\mathbf{R}_{y,r}^{(k)'} - \mathbf{R}_{y,i}^{(k)'})\mathbf{w}^{(k)*}. \end{aligned} \quad (\text{B.6})$$

To solve for the optimal equalizer, Eq. (B.6) is arranged into a block matrix expression  $\mathbf{A}\mathbf{w} = 2\mathbf{p}$ , namely

$$\begin{bmatrix} \mathbf{A}_{11} & \mathbf{A}_{12} \\ \mathbf{A}_{21} & \mathbf{A}_{22} \end{bmatrix} \begin{bmatrix} \text{Re}(\mathbf{w}^{(k)}) \\ \text{Im}(\mathbf{w}^{(k)}) \end{bmatrix} = 2 \begin{bmatrix} \text{Re}(\mathbf{p}_{y,r}^{(k)} + \mathbf{p}_{y,i}^{(k)}) \\ \text{Im}(\mathbf{p}_{y,r}^{(k)} + \mathbf{p}_{y,i}^{(k)}) \end{bmatrix} \quad (\text{B.7})$$

where

$$\begin{aligned} \mathbf{A}_{11} &= \text{Re}(\mathbf{R}_{y,r}^{(k)} + \mathbf{R}_{y,i}^{(k)}) + \text{Re}(\mathbf{R}_{y,r}^{(k)'} - \mathbf{R}_{y,i}^{(k)'}) \\ \mathbf{A}_{12} &= -\text{Im}(\mathbf{R}_{y,r}^{(k)} + \mathbf{R}_{y,i}^{(k)}) + \text{Im}(\mathbf{R}_{y,r}^{(k)'} - \mathbf{R}_{y,i}^{(k)'}) \\ \mathbf{A}_{21} &= \text{Im}(\mathbf{R}_{y,r}^{(k)} + \mathbf{R}_{y,i}^{(k)}) + \text{Im}(\mathbf{R}_{y,r}^{(k)'} - \mathbf{R}_{y,i}^{(k)'}) \\ \mathbf{A}_{22} &= \text{Re}(\mathbf{R}_{y,r}^{(k)} + \mathbf{R}_{y,i}^{(k)}) - \text{Re}(\mathbf{R}_{y,r}^{(k)'} - \mathbf{R}_{y,i}^{(k)'}). \end{aligned}$$

The optimal equalizer weights are then determined by solving  $\mathbf{w} = 2\mathbf{A}^{-1}\mathbf{p}$ , where the inverse of the block matrix  $\mathbf{A}$  is [264]

$$\mathbf{A}^{-1} = \begin{bmatrix} \mathbf{A}_{11}^{-1} + \mathbf{A}_{11}^{-1}\mathbf{A}_{12}\mathbf{S}^{-1}\mathbf{A}_{21}\mathbf{A}_{11}^{-1} & -\mathbf{A}_{11}^{-1}\mathbf{A}_{12}\mathbf{S}^{-1} \\ -\mathbf{S}^{-1}\mathbf{A}_{21}\mathbf{A}_{11}^{-1} & \mathbf{S}^{-1} \end{bmatrix} \quad (\text{B.8})$$

and  $\mathbf{S} = \mathbf{A}_{22} - \mathbf{A}_{21}\mathbf{A}_{11}^{-1}\mathbf{A}_{12}$  is its *Schur complement*.

## Appendix C

# Subcarrier SNR Calculation for Multiple Antenna Systems

When conducting performance analysis of MIMO communication systems or any of its degenerate forms (i.e., MISO, SIMO, and SISO), it is important to determine the theoretical value for the SNR. Doing so allows for a fair comparison of performance metrics between different implementations. In the next four subsections, theoretical SNR expressions will be derived for MIMO systems and its degenerate cases when the communication system employs only transmit and/or receive diversity combining.

### C.1 SISO Scenario

The first scenario investigated is the *single-input single-output* or SISO communication system. Since the definition for the SNR is the ratio of the received power to the noise power [128, 257], the SNR of the SISO system shown in Fig. C.1 for subcarrier  $i$  is defined as

$$\gamma_i = \frac{\pi_i \cdot |H_i|^2}{\sigma_\nu^2} \quad (\text{C.1})$$

where  $\pi_i$  is the transmit signal power of  $x_i(n)$ ,  $\sigma_\nu^2$  is the power of the noise  $\nu(n)$ , and  $H_i$  is the frequency response of  $h(n)$  across subcarrier  $i$ .

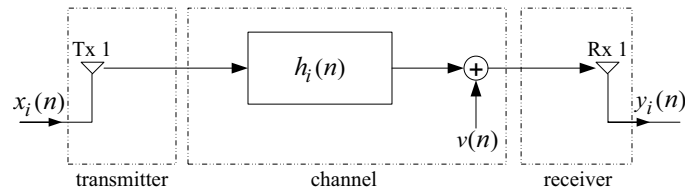


**Fig. C.1** Schematic of a SISO communication system ( $N_T = 1$ ,  $N_R = 1$ ).

## C.2 MISO Scenario

An example of a *multiple-input single-output* or MISO communication system is shown in Fig. C.2, where the ( $N_T = 3$ ,  $N_R = 1$ ) system is transmitting the same subcarrier signal,  $x_i(n)$ , across three different channel paths (i.e.,  $h_{i,11}(n)$ ,  $h_{i,21}(n)$ , and  $h_{i,31}(n)$ ). When compared with the SISO system, there are a number of significant differences. First, the transmit power is  $1/N_T$  relative to the SISO system. Assuming that the SISO system is transmitting at the maximum allowable power specified by a spectrum regulatory agency, if several transmitters emanate the same signal, their power levels must be reduced. This is done in order to avoid a violation of regulatory requirements when the signals combine constructively. Second, each transmitted signal passes through a different channel ( $N_T$  in total). Referring to Fig. 2.11, it is observed that each transmit antenna is at a different location. Thus, the multipath propagation is different between each transmit antenna and the receive antenna.

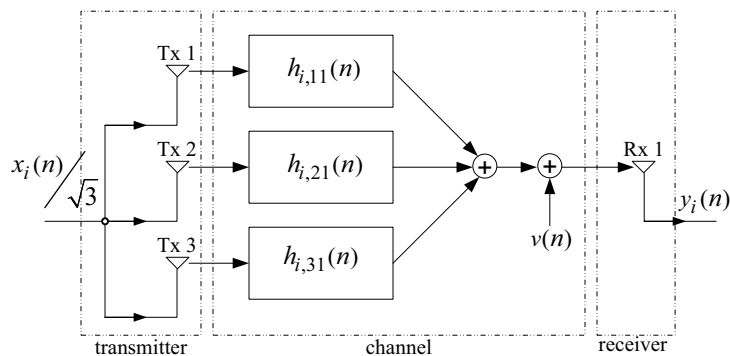


**Fig. C.2** Schematic of a MISO communication system ( $N_T = 3$ ,  $N_R = 1$ ).

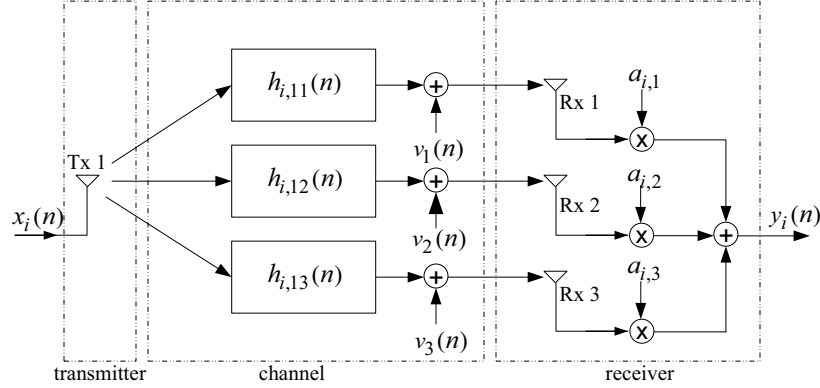


**Fig. C.3** Schematic of a SIMO communication system ( $N_T = 1$ ,  $N_R = 3$ ).

Using the definition for the SNR, the subcarrier SNR is given by

$$\gamma_i = \frac{\frac{\pi_i}{N_T} \cdot |H_{i,11}(\omega) + H_{i,21}(\omega) + \cdots + H_{i,N_T1}(\omega)|^2}{\sigma_\nu^2}. \quad (\text{C.2})$$

where  $H_{i,n_t1}(\omega) = \mathcal{F} \{h_{i,n_t1}(n)\}$ ,  $n_t = 1, \dots, N_T$ , are the channel frequency responses across subcarrier  $i$  due to multipath propagation between the receive antenna and transmit antennas  $1, \dots, N_T$ .

### C.3 SIMO Scenario

Unlike the MISO system, a *single-input multiple-output* or SIMO system, like the one shown in Fig. C.3, does not require a reduction in transmit power levels. On the other hand, it has a collection of  $N_R$  channel impulse responses (e.g.,  $h_{i,11}(n)$ ,  $\dots$ ,  $h_{i,1N_R}(n)$ ) that correspond to the paths between the transmit antenna and the  $N_R$  receive antennas.

When multiple receive antennas are employed, the inputs to the receive antennas of subcarrier  $i$  are combined using a set of weights  $\{a_{i,r}\}$ ,  $r = 1, \dots, N_R$ . These weights can be defined using any number of techniques, such as Antenna Selection, EGC, or MRC (refer to Section 2.6.2 for more information). Thus, for Fig. C.3 the post-combining SNR is given as

$$\gamma_i = \frac{\pi_i \cdot |a_{i,1} \cdot H_{i,11}(\omega) + a_{i,2} \cdot H_{i,12}(\omega) + \cdots + a_{i,N_R} \cdot H_{i,1N_R}(\omega)|^2}{(a_{i,1}^2 + a_{i,2}^2 + \cdots + a_{i,N_R}^2) \cdot \sigma_\nu^2}. \quad (\text{C.3})$$

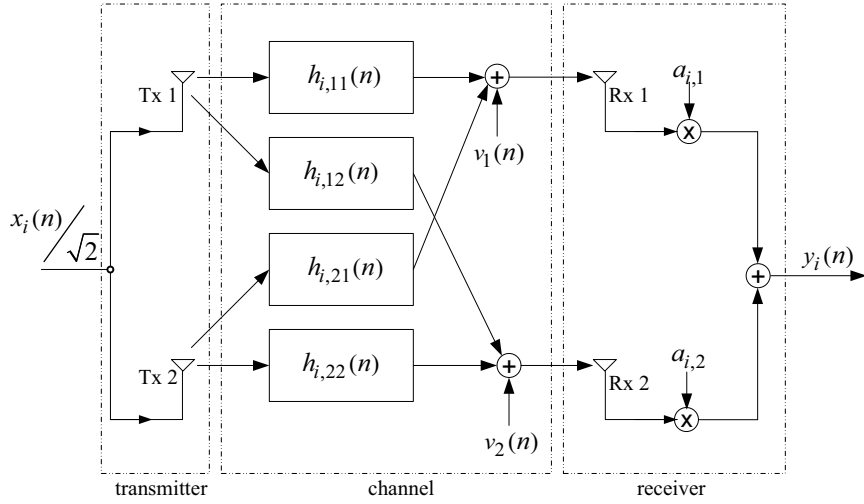


Fig. C.4 Schematic of a MIMO communication system ( $N_T = 2$ ,  $N_R = 2$ ).

## C.4 MIMO Scenario

Finally, the *multiple-input multiple output* or MIMO system is a combination of the MISO and SIMO systems, as shown in Fig. C.4 for the case of  $N_T = 2$  and  $N_R = 2$ . Thus, the post-combining SNR is equal to

$$\gamma_i = \frac{\frac{\pi_i}{N_T} \cdot |a_{i,1} \cdot (H_{i,11}(\omega) + \dots + H_{i,N_T1}(\omega)) + \dots + a_{i,N_R} \cdot (H_{i,1N_R}(\omega) + \dots + H_{i,N_TN_R}(\omega))|^2}{(a_{i,1}^2 + \dots + a_{i,N_R}^2) \cdot \sigma_\nu^2}. \quad (\text{C.4})$$

## Appendix D

# Normalization of MIMO Channel Model Correlation Matrix

In order to fairly compare the results of systems operating in a correlated MIMO channel with those operating in an uncorrelated MIMO channel, the correlation matrix  $\Sigma$  used by the channel model must be appropriately normalized to ensure that both channel models have the same average power. Extending Eq. (2.28) to the case where the transmitted signal is filtered by several channel impulse responses in parallel, the SNR for subcarrier  $i$  at the receiver output can be defined as

$$\gamma_i = \frac{\pi_i \left| \sum_{n_t=1}^{N_T} \sum_{n_r=1}^{N_R} H_{i,n_t n_r}(\omega) \right|^2}{\sigma_\nu^2}, \quad (\text{D.1})$$

which is similar to Eqs. (C.2), (C.3), and (C.4) with the exception of the gain terms.

The objective is to have the power of the sum of uncorrelated channel responses equal to the power of the sum of correlated channel responses. In other words,

$$E \left\{ \frac{1}{2\pi} \int_{-\pi}^{\pi} \left| \sum_{n_t=1}^{N_T} \sum_{n_r=1}^{N_R} H_{i,n_t n_r}(\omega) \right|^2 d\omega \right\} = E \left\{ \frac{1}{2\pi} \int_{-\pi}^{\pi} \left| \sum_{n_t=1}^{N_T} \sum_{n_r=1}^{N_R} H'_{i,n_t n_r}(\omega) \right|^2 d\omega \right\} \quad (\text{D.2})$$

where  $E\{\}$  is the expected value, and  $(.)'$  denotes the correlated version.

By Parseval's Relationship [91], Eq. (D.2) can be rewritten as

$$E \left\{ \sum_{n=-\infty}^{\infty} \left| \sum_{n_t=1}^{N_T} \sum_{n_r=1}^{N_R} h_{i,n_t n_r}(n) \right|^2 \right\} = E \left\{ \sum_{n=-\infty}^{\infty} \left| \sum_{n_t=1}^{N_T} \sum_{n_r=1}^{N_R} h'_{i,n_t n_r}(n) \right|^2 \right\}. \quad (\text{D.3})$$

The correlated channel impulse responses can be written in terms of the uncorrelated channel impulse response via the matrix equation

$$\underbrace{\begin{bmatrix} h'_{i,11}(n) \\ \vdots \\ h'_{i,N_T N_R}(n) \end{bmatrix}}_{\mathbf{H}'} = \underbrace{\begin{bmatrix} \rho_{i,11} & \cdots & \rho_{i,1(N_T \cdot N_R)} \\ \vdots & \ddots & \vdots \\ \rho_{i,(N_T \cdot N_R)1} & \cdots & \rho_{i,(N_T \cdot N_R)(N_T \cdot N_R)} \end{bmatrix}}_{\mathbf{P}} \cdot \underbrace{\begin{bmatrix} h_{i,11}(n) \\ \vdots \\ h_{i,N_T N_R}(n) \end{bmatrix}}_{\mathbf{H}} \quad (\text{D.4})$$

where the Cholesky Factorization is applied to the correlation matrix  $\mathbf{\Sigma}$  to yield the weight matrix  $\mathbf{P}$ . Therefore, expanding Eq. (D.3) yields

$$\begin{aligned} (N_T N_R) L \sigma_h^2 &= L \sigma_h^2 \sum_{k=1}^{N_T N_R} \left( \sum_{j=1}^{N_T N_R} \rho_{i,jk} \right)^2 \\ (N_T N_R) &= \sum_{k=1}^{N_T N_R} \left( \sum_{j=1}^{N_T N_R} \rho_{i,jk} \right)^2 \end{aligned} \quad (\text{D.5})$$

where  $L$  is the length of the channel impulse responses, the channel responses are i.i.d, and  $\sigma_h^2$  is the variance of the channel responses.

The simplest solution to achieve an equality in Eq. (D.3) is to multiply the weight matrix  $\mathbf{P}$  by a scaling factor  $\kappa$ . This means that the scaled correlation matrix is  $\kappa^2 \cdot \mathbf{\Sigma}$  and the right hand side of Eq. (D.5) is equal to

$$(N_T N_R) = \kappa^2 \sum_{k=1}^{N_T N_R} \left( \sum_{j=1}^{N_T N_R} \rho_{i,jk} \right)^2. \quad (\text{D.6})$$

Thus isolating for  $\kappa$  yields

$$\kappa = \sqrt{\frac{N_T N_R}{\sum_{k=1}^{N_T N_R} \left( \sum_{j=1}^{N_T N_R} \rho_{i,jk} \right)^2}}, \quad (\text{D.7})$$

which can then be applied to  $\Sigma$  to obtain an equivalence between the power of the sum of uncorrelated channel responses and the power of the sum of correlated channel responses.

# Appendix E

## Bit Error Rate Simulation Parameters

### E.1 Calculation of the Simulation Runtime Parameters

Some of the simulations performed were based on the Monte Carlo Method. Several parameters must be derived in order to ensure that these simulations have an adequate level of accuracy.

Consider the multicarrier system as a set of  $N$  series of  $n$  independent random variables occurring in parallel. Furthermore, all the random variables are defined to be Bernoulli with the probability of error for series  $i$  equal to  $p_i$ . Finally, the series are considered to be independent of each other.

Referring to [265] and [266], the error events for series  $i$  possess a binomial distribution, namely

$$B(n, p_i) = \binom{n}{k} p_i^k (1 - p_i)^{n-k} \quad (\text{E.1})$$

where  $k$  is the number of errors occurring within the series. Moreover, the mean and variance of the binomial distribution are  $\mu_i = p_i n$  and  $\sigma_i^2 = n p_i (1 - p_i)$ , respectively.

Using the statistics of the individual subcarriers defined above, the mean and variance of the overall transmission error can be derived. Noting the independence assumptions

made earlier, the mean can be written as

$$\mu = \sum_{i=1}^N \mu_i = n \cdot \sum_{i=1}^N p_i \quad (\text{E.2})$$

while the variance is defined as

$$\sigma^2 = \sum_{i=1}^N \sigma_i^2 = n \cdot \sum_{i=1}^N p_i (1 - p_i) \quad (\text{E.3})$$

Thus, using (E.2) and (E.3), the ratio of the standard deviation relative to the mean value is given by

$$\frac{\sigma}{\mu} = \frac{\sqrt{\sum_{i=1}^N p_i (1 - p_i)}}{\sqrt{n} \cdot \sum_{i=1}^N p_i} \quad (\text{E.4})$$

The use of (E.4) to determine the minimum value of  $n$  needed to achieve reliable simulation is essential in limiting the simulation run-time. Therefore, using the estimates for the error probabilities per subcarrier and the desired standard deviation as a percentage of the mean,  $\sigma/\mu$ , may one be able to determine  $n$ .

## References

- [1] American National Standards Institute, “Network to customer installation interfaces – asymmetric digital subscriber line (ADSL) metallic interface.” ANSI Standard T1.413-1998, Nov. 1998.
- [2] Institute of Electronics and Electrical Engineers, “Wireless LAN medium access control (MAC) and physical layer (PHY) specifications: High-speed physical layer in the 5 GHz band.” IEEE Standard 802.11a, Nov. 1999.
- [3] European Telecommunications Standards Institute, “Broadband radio access networks (BRAN): HIPERLAN type 2; physical (PHY) layer.” ETSI TS 101 475, Dec. 2001.
- [4] R. van Nee, G. Awater, M. Morikura, H. Takanashi, M. Webster, and K. W. Halford, “New high-rate wireless LAN standard,” *IEEE Commun. Mag.*, pp. 82–88, Dec. 1999.
- [5] R. Prasad, *Universal Wireless Personal Communications*. Artech House Mobile Communications, Norwood, MA, USA: Artech House, 1998.
- [6] T. Keller and L. Hanzo, “A convenient framework for time-frequency processing in wireless communications,” *Proc. IEEE*, vol. 88, pp. 611–640, May 2000.
- [7] B. Fox, “Discrete optimization via marginal analysis,” *Management Science*, vol. 13, pp. 210–216, Nov. 1966.
- [8] A. Segall, “Bit allocation and encoding for vector sources,” *IEEE Trans. Inform. Theory*, vol. 22, pp. 162–169, Mar. 1976.
- [9] A. Gersho and R. M. Gray, *Vector Quantization and Signal Compression*. Dordrecht, Netherlands: Kluwer Academic Publishers, 1991.
- [10] J. A. C. Bingham, *ADSL, VDSL, and Multicarrier Modulation*. New York, NY, USA: John Wiley and Sons, 2000.

- 
- [11] P. S. Chow, J. M. Cioffi, and J. A. C. Bingham, "A practical discrete multitone transceiver loading algorithm for data transmission over spectrally shaped channels," *IEEE Trans. Commun.*, vol. 43, pp. 773–775, Feb./Mar./Apr. 1995.
- [12] A. Leke and J. M. Cioffi, "A maximum rate loading algorithm for discrete multitone modulation systems," in *Proc. IEEE Global Telecommun. Conf.*, vol. 3, (Phoenix, AZ, USA), pp. 1514–1518, Nov. 1997.
- [13] L. M. C. Hoo, J. Tellado, and J. M. Cioffi, "Dual QoS loading algorithms for DMT systems offering CBR and VBR services," in *Proc. IEEE Global Telecommun. Conf.*, vol. 1, (Sydney, NSW, Australia), pp. 25–30, Nov. 1998.
- [14] B. S. Krongold, K. Ramchandran, and D. L. Jones, "Computationally efficient optimal power allocation algorithms for multicarrier communication systems," *IEEE Trans. Commun.*, vol. 48, pp. 23–27, Jan. 2000.
- [15] E. Baccarelli, A. Fasano, and A. Zucchi, "On the loading of peak-energy-limited multicarrier systems transmitting over spectrally-shaped crosstalk-impaired DSLs," in *Proc. IEEE Int. Conf. Commun.*, vol. 1, (Helsinki, Finland), pp. 310–314, June 2001.
- [16] E. Baccarelli, A. Fasano, and M. Biagi, "Novel efficient bit-loading algorithms for peak-energy-limited ADSL-type multicarrier systems," *IEEE Trans. Signal Process.*, vol. 50, pp. 1237–1247, May 2002.
- [17] A. Fasano, G. Di Blasio, E. Baccarelli, and M. Biagi, "Optimal discrete bit loading for DMT based constrained multicarrier systems," in *Proc. Int. Symp. Inform. Theory*, (Lausanne, Switzerland), p. 243, June 2002.
- [18] A. Fasano and G. Di Blasio, "Optimal discrete dynamic loading algorithms for multicarrier systems," in *IEEE Wkshp. Signal Process. Adv. Wireless Commun.*, (Rome, Italy), June 2003.
- [19] A. Fasano, "On the optimal discrete bit loading for multicarrier systems with constraints," in *Proc. 57th IEEE Veh. Technol. Conf. – Spring*, vol. 2, (Orlando, FL, USA), pp. 915–919, Sept. 2003.
- [20] K. Van Acker, G. Leus, M. Moonen, O. Van de Wiel, and T. Pollet, "Per tone equalization for DMT-based systems," *IEEE Trans. Commun.*, vol. 49, pp. 109–119, Jan. 2001.
- [21] K. Van Acker, *Equalization and Echo Cancellation for DMT-Based DSL Modems*. PhD thesis, Katholieke Universiteit Leuven, Leuven, Belgium, Jan. 2001.

- 
- [22] N. Benvenuto, S. Tomasin, and L. Tomba, "Equalization methods in OFDM and FMT systems for broadband wireless communications," *IEEE Trans. Commun.*, vol. 50, pp. 1413–1418, Sept. 2002.
- [23] R. S. Blum and J. H. Winters, "On optimum MIMO with antenna selection," in *Proc. IEEE Int. Conf. Commun.*, vol. 1, (New York, NY, USA), pp. 386–390, Apr. 2002.
- [24] R. S. Blum and J. H. Winters, "On optimum MIMO with antenna selection," *IEEE Commun. Lett.*, vol. 6, pp. 322–324, Aug. 2002.
- [25] R. S. Blum, "MIMO capacity with antenna selection and interference," in *Proc. IEEE Int. Conf. Acoust., Speech, Signal Process.*, vol. 4, (Hong Kong, China), pp. 824–827, Apr. 2003.
- [26] A. Gorokhov, "Antenna selection algorithms for MEA transmission systems," in *Proc. IEEE Int. Conf. Acoust., Speech, Signal Process.*, vol. 3, (Orlando, FL, USA), pp. 2857–2860, May 2002.
- [27] A. Gorokhov, "Performance bounds for antenna selection in MIMO systems," in *Proc. IEEE Int. Conf. Commun.*, vol. 5, (Anchorage, AK, USA), pp. 3021–3025, May 2003.
- [28] A. F. Molisch, M. Z. Win, and J. H. Winters, "Space-time-frequency (STF) coding for MIMO-OFDM systems," *IEEE Commun. Lett.*, vol. 6, pp. 370–372, Sept. 2002.
- [29] A. F. Molisch, M. Z. Win, and J. H. Winters, "Performance of reduced-complexity transmit/receive-diversity systems," in *Proc. Int. Symp. Wireless Personal Multimedia Commun.*, vol. 2, (Honolulu, HI, USA), pp. 738–742, Oct. 2002.
- [30] A. F. Molisch, "MIMO systems with antenna selection – An overview," in *Proc. Radio Wireless Conf.*, (Boston, MA, USA), pp. 167–170, Aug. 2003.
- [31] A. F. Molisch, M. Z. Win, and J. H. Winters, "Reduced-complexity transmit/receive-diversity systems," *IEEE Trans. Signal Process.*, vol. 51, pp. 2729–2738, Nov. 2003.
- [32] A. F. Molisch, "A generic model for MIMO wireless propagation channels in macro- and microcells," *IEEE Trans. Signal Process.*, vol. 52, pp. 61–71, Jan. 2004.
- [33] A. F. Molisch and M. Z. Win, "MIMO systems with antenna selection," *IEEE Microwave Mag.*, pp. 46–56, Mar. 2004.
- [34] R. P. Ramachandran, *Bandwidth Efficient Filter Banks for Transmultiplexers*. PhD thesis, McGill University, Montréal, QC, Canada, Sept. 1990.
- [35] P. P. Vaidyanathan, *Multirate Systems and Filter Banks*. Prentice Hall Signal Processing Series, Upper Saddle River, NJ, USA: Prentice Hall, 1993.

- 
- [36] N. J. Fliege, *Multirate Digital Signal Processing: Multirate Systems, Filter Banks, Wavelets*. New York, NY, USA: John Wiley and Sons, 1994.
- [37] S. D. Sandberg and M. A. Tzannes, "Overlapped discrete multitone modulation for high speed copper wire communications," *IEEE J. Select. Areas Commun.*, vol. 13, pp. 1571–1585, Dec. 1995.
- [38] S. Colieri, M. Ergen, A. Puri, and A. Bahai, "A study of channel estimation in OFDM systems," in *Proc. 56th IEEE Veh. Technol. Conf. – Fall*, vol. 2, (Vancouver, BC, Canada), pp. 894–898, Sept. 2002.
- [39] G. Cherubini, E. Eleftheriou, S. Olcer, and J. M. Cioffi, "Filter bank modulation techniques for very high-speed digital subscriber lines," *IEEE Commun. Mag.*, vol. 38, pp. 98–104, May 2000.
- [40] C. G. E. Eleftheriou, and S. Olcer, "Filtered multitone modulation for very high-speed digital subscriber lines," *IEEE J. Select. Areas Commun.*, vol. 20, pp. 1016–1028, June 2002.
- [41] J. A. C. Bingham, "Multicarrier modulation for data transmission: An idea whose time has come," *IEEE Commun. Mag.*, pp. 5–14, Apr. 1990.
- [42] B. R. Saltzberg, "Comparison of single-carrier and multitone digital modulation for ADSL applications," *IEEE Commun. Mag.*, pp. 114–121, Nov. 1998.
- [43] S. B. Weinstein and P. Ebert, "Data transmission by frequency division multiplexing using the discrete fourier transform," *IEEE Trans. Commun.*, vol. 19, pp. 628–634, Oct. 1971.
- [44] B. Hirosaki, "An analysis of automatic equalizers for orthogonally multiplexed QAM systems," *IEEE Trans. Commun.*, vol. 28, pp. 73–83, Jan. 1980.
- [45] B. Hirosaki, "An orthogonally multiplexed QAM system using the discrete fourier transform," *IEEE Trans. Commun.*, vol. 29, pp. 982–989, July 1981.
- [46] W. Y. Zou and Y. Wu, "COFDM: An overview," *IEEE Trans. Broadcast*, vol. 41, pp. 1–8, Mar. 1995.
- [47] J. Heiskala and J. Terry, *OFDM Wireless LANs: A Theoretical and Practical Guide*. Indianapolis, IN, USA: Sams Publishing, 2002.
- [48] A. Czylik, "Adaptive OFDM for wideband radio channels," in *Proc. IEEE Global Telecommun. Conf.*, vol. 1, (London, UK), pp. 713–718, Nov. 1996.

- 
- [49] H. Schmidt and K.-D. Kammeyer, "Reducing the peak to average power ratio of multicarrier signals by adaptive subcarrier selection," in *Proc. IEEE Int. Conf. Universal Personal Commun.*, vol. 2, (Florence, Italy), pp. 933–937, Oct. 1998.
- [50] A. N. Barreto and S. Furrer, "Adaptive bit loading for wireless OFDM systems," in *Proc. IEEE Int. Symp. Personal, Indoor, Mobile Radio Commun.*, vol. 2, (Florence, Italy), pp. 88–92, Oct. 2001.
- [51] M. Motegi and R. Kohno, "Optimum band allocation according to subband condition for BST-OFDM," in *Proc. IEEE Int. Symp. Personal, Indoor, Mobile Radio Commun.*, vol. 2, (London, UK), pp. 1236–1240, Sept. 2000.
- [52] M. Motegi and R. Kohno, "Optimum modulation assignment according to subband channel status for BST-OFDM," *IEICE Trans. Fundamentals*, vol. E84-A, pp. 1714–1722, July 2001.
- [53] J. Moon and S. Hong, "Adaptive code-rate and modulation for multi-user OFDM system in wireless communications," in *Proc. 56th IEEE Veh. Technol. Conf. – Fall*, vol. 4, (Vancouver, BC, Canada), pp. 1943–1947, Sept. 2002.
- [54] Z. Song, K. Zhang, and Y. L. Guan, "Joint bit-loading and power-allocation for OFDM systems based on statistical frequency-domain fading model," in *Proc. 56th IEEE Veh. Technol. Conf. – Fall*, vol. 2, (Vancouver, BC, Canada), pp. 724–728, Sept. 2002.
- [55] T. Keller and L. Hanzo, "Sub-band adaptive pre-equalized OFDM transmission," in *Proc. 50th IEEE Veh. Technol. Conf. – Fall*, vol. 1, (Amsterdam, Netherlands), pp. 334–338, Sept. 1999.
- [56] T. Yoshiki, S. Sampei, and N. Morinaga, "High bit rate transmission scheme with a multilevel transmit power control for the OFDM based adaptive modulation systems," in *Proc. 53rd IEEE Veh. Technol. Conf. – Spring*, vol. 1, (Rhodes, Greece), pp. 727–731, May 2001.
- [57] S. Y. Park and C. G. Kang, "Performance analysis of pilot symbol arrangement for OFDM system under time-varying multi-path Rayleigh fading channels," *IEICE Trans. Commun.*, vol. E84-B, pp. 36–45, Jan. 2001.
- [58] M.-X. Chang and Y. T. Su, "Model-based channel estimation for OFDM signals in rayleigh fading," *IEEE Trans. Commun.*, vol. 50, pp. 540–544, Apr. 2002.
- [59] R. Negi and J. M. Cioffi, "Blind OFDM symbol synchronization in ISI channels," *IEEE Trans. Commun.*, vol. 50, pp. 1525–1534, Sept. 2002.

- 
- [60] D. Landstrom, S. K. Wilson, J.-J. van de Beek, P. Odling, and P. O. Borjesson, "Symbol time offset estimation in coherent OFDM systems," *IEEE Trans. Commun.*, vol. 50, pp. 545–549, Apr. 2002.
- [61] M. Luise, M. Marselli, and R. Reggiannini, "Low-complexity blind carrier frequency recovery for OFDM signals over frequency-selective radio channels," *IEEE Trans. Commun.*, vol. 50, pp. 1182–1188, July 2002.
- [62] I. Koffman and V. Roman, "Broadband wireless access solutions based on OFDM access in IEEE 802.16," *IEEE Commun. Mag.*, vol. 40, pp. 96–103, Apr. 2002.
- [63] L. Goldfeld, V. Lyandres, and D. Wulich, "Minimum BER power loading for OFDM in fading channel," *IEEE Trans. Commun.*, vol. 50, pp. 1729–1733, Nov. 2002.
- [64] A. Garcia-Armada and J. M. Cioffi, "Multiuser constant-energy bit loading for M-PSK-modulated orthogonal frequency division multiplexing," in *Proc. IEEE Wireless Commun. Networking Conf.*, vol. 2, (Orlando, FL, USA), pp. 526–530, Mar. 2002.
- [65] M. R. Souryal and R. L. Pickholtz, "Adaptive modulation with imperfect channel information in OFDM," in *Proc. IEEE Int. Conf. Commun.*, vol. 6, (Helsinki, Finland), pp. 1861–1865, June 2001.
- [66] S. Ye, R. S. Blum, and L. J. Cimini, "Adaptive modulation for variable-rate OFDM systems with imperfect channel information," in *Proc. 55th IEEE Veh. Technol. Conf. – Spring*, vol. 2, (Birmingham, AL, USA), pp. 767–771, May 2002.
- [67] A. Scaglione and S. Barbarossa, "Optimal power loading for OFDM transmissions over underspread Rayleigh time-varying channels," in *Proc. IEEE Int. Conf. Acoust., Speech, Signal Process.*, vol. 5, (Istanbul, Turkey), pp. 2969–2972, June 2000.
- [68] D. L. Goeckel and G. Ananthaswamy, "On the design of multidimensional signal sets for OFDM systems," *IEEE Trans. Commun.*, vol. 50, pp. 442–452, Mar. 2002.
- [69] D. Bartolome and A. I. Perez-Neira, "Exploiting the cyclic prefix for beamforming in OFDM receivers," in *Proc. European Signal Processing Conf.*, vol. 3, (Toulouse, France), pp. 183–186, Sept. 2002.
- [70] M. Debbah, P. Loubaton, and M. de Courville, "Linear precoders for OFDM wireless communications with MMSE equalization: Facts and results," in *Proc. European Signal Processing Conf.*, vol. 3, (Toulouse, France), pp. 175–178, Sept. 2002.
- [71] G. Munz, S. Pfletschinger, and J. Spiedel, "An efficient waterfilling algorithm for multiple access OFDM," in *Proc. IEEE Global Telecommun. Conf.*, vol. 1, (Taipei, Taiwan), pp. 681–685, Nov. 2002.

- [72] T. Y. Al-Naffouri, A. Bahai, and A. Paulraj, "An EM-based OFDM receiver for time-variant channels," in *Proc. IEEE Global Telecommun. Conf.*, vol. 1, (Taipei, Taiwan), pp. 589–593, Nov. 2002.
- [73] W. Eberle, M. Badaroglu, V. Derudder, S. Thoen, P. Vandenameele, L. Van der Peree, M. Vergara, B. Gyselinckx, M. Engels, and I. Bolsens, "A digital 80 Mb/s OFDM transceiver IC for wireless LAN in the 5 GHz band," in *IEEE Int. Solid-State Circuits Conf.*, (San Francisco, CA, USA), pp. 74–75, 448, Feb. 2000.
- [74] W. Eberle, M. Badaroglu, V. Derudder, S. Thoen, P. Vandenameele, L. Van der Peree, M. Vergara, B. Gyselinckx, M. Engels, and I. Bolsens, "Flexible OFDM transceiver for a high-speed wireless LAN," in *Proc. 50th IEEE Veh. Technol. Conf. – Fall*, vol. 5, (Amsterdam, Netherlands), pp. 2677–2681, Sept. 1999.
- [75] L. Van der Perre, S. Thoen, P. Vandenameele, B. Gyselinckx, and M. Engels, "Adaptive loading strategy for a high speed OFDM-based WLAN," in *Proc. IEEE Global Telecommun. Conf.*, vol. 4, (Sydney, NSW, Australia), pp. 1936–1940, Nov. 1998.
- [76] A. A. Hutter, J. S. Hammerschmidt, E. de Carvalho, and J. M. Cioffi, "Receive diversity for mobile OFDM systems," in *Proc. IEEE Wireless Commun. Networking Conf.*, vol. 2, (Orlando, FL, USA), pp. 707–712, Mar. 2002.
- [77] Y. G. Li and L. J. Cimini, "Bounds on the interchannel interference of OFDM in time-varying impairments," *IEEE Trans. Commun.*, vol. 49, pp. 401–404, Mar. 2001.
- [78] L. Piazzo, "Optimum adaptive OFDM systems," *European Trans. Telecommun.*, vol. 14, pp. 205–212, May/June 2003.
- [79] T. Pollet, M. Peeters, M. Moonen, and L. Vandendorpe, "Equalization for DMT-based broadband modems," *IEEE Commun. Mag.*, vol. 38, pp. 106–113, May 2000.
- [80] I. Kalet, "The multitone channel," *IEEE Trans. Commun.*, vol. 37, pp. 119–124, Feb. 1989.
- [81] R. F. H. Fischer and J. B. Huber, "A new loading algorithm for discrete multi-tone transmission," in *Proc. IEEE Global Telecommun. Conf.*, vol. 1, (London, UK), pp. 724–728, Nov. 1996.
- [82] A. Leke and J. M. Cioffi, "Transmit optimization for time-invariant wireless channels utilizing a discrete multitone approach," in *Proc. IEEE Int. Conf. Commun.*, vol. 2, (Montreal, QC, Canada), pp. 954–958, June 1997.
- [83] J. Campello, "Practical bit loading for DMT," in *Proc. IEEE Int. Conf. Commun.*, vol. 2, (Vancouver, BC, Canada), pp. 801–805, June 1999.

- 
- [84] J. Campello, "Optimal discrete bit loading for multicarrier modulation systems," in *Proc. Int. Symp. Inform. Theory*, (Cambridge, MA, USA), p. 193, Aug. 1998.
- [85] T. Pollet and M. Peeters, "Synchronization with DMT modulation," *IEEE Commun. Mag.*, pp. 80–86, Apr. 1999.
- [86] J. Lee, R. V. Sonalkar, and J. M. Cioffi, "A multi-user rate and power control algorithm for VDSL," in *Proc. IEEE Global Telecommun. Conf.*, vol. 2, (Taipei, Taiwan), pp. 1264–1268, Nov. 2002.
- [87] J. Lee, R. V. Sonalkar, and J. M. Cioffi, "Multi-user discrete bit-loading for DMT-based DSL systems," in *Proc. IEEE Global Telecommun. Conf.*, vol. 2, (Taipei, Taiwan), pp. 1259–1263, Nov. 2002.
- [88] A. Maleki Tehrani, A. Hassibi, J. Cioffi, and S. Boyd, "An implementation of discrete multi-tone over slowly time-varying multiple-input/multiple-output channels," in *Proc. IEEE Global Telecommun. Conf.*, vol. 5, (Sydney, NSW, Australia), pp. 2806–2811, Nov. 1998.
- [89] W. Yu, G. Ginis, and J. M. Cioffi, "An adaptive multiuser power control algorithm for VDSL," in *Proc. IEEE Global Telecommun. Conf.*, vol. 1, (San Antonio, TX, USA), pp. 394–398, Nov. 2001.
- [90] B. R. Saltzberg, "Performance of an efficient parallel data transmission system," *IEEE Trans. Commun.*, vol. 15, pp. 805–811, Dec. 1967.
- [91] J. G. Proakis, *Digital Signal Processing: Principles, Algorithms, and Applications*. Upper Saddle River, NJ, USA: Prentice Hall, 3rd ed., 1996.
- [92] P. Siohan, C. Siclet, and N. Lacaille, "Analysis and design of OFDM/OQAM systems based on filterbank theory," *IEEE Trans. Signal Process.*, vol. 50, pp. 1170–1183, May 2002.
- [93] S. N. Diggavi, "Analysis of multicarrier transmission in time-varying channels," in *Proc. IEEE Int. Conf. Commun.*, vol. 3, (Montreal, QC, Canada), pp. 1191–1195, June 1997.
- [94] A. Doufexi, S. Armour, M. Butler, A. Nix, D. Bull, J. McGeehan, and P. Karlsson, "A comparison of the HIPERLAN/2 and IEEE 802.11a wireless LAN standards," *IEEE Commun. Mag.*, vol. 40, pp. 172–180, May 2002.
- [95] J. Khun-Jush, P. Schramm, G. Malmgren, and J. Torsner, "HiperLAN2: broadband wireless communications at 5 GHz," *IEEE Commun. Mag.*, vol. 40, pp. 130–136, June 2002.

- 
- [96] C. Heegard, J. T. Coffey, S. Gummadi, P. A. Murphy, R. Provencio, E. J. Rossin, S. Schrum, and M. B. Shoemake, "High performance wireless ethernet," *IEEE Commun. Mag.*, vol. 39, pp. 64–73, Nov. 2001.
- [97] C. Eklund, R. B. Marks, K. L. Stanwood, and S. Wang, "IEEE standard 802.16: a technical overview of the WirelessMAN air interface for broadband wireless access," *IEEE Commun. Mag.*, vol. 40, pp. 98–107, June 2002.
- [98] P. Mannion, "Smart antenna boosts IQ of WLANs, startup says," *EE Times*, 18 Aug. 2003.
- [99] J. Moon and Y. Kim, "Dual Rx boosts WLAN OFDM," *EE Times*, 29 Sep. 2003.
- [100] N. Wang and S. D. Blostein, "Adaptive zero-padding OFDM for wireless communications," in *Proc. 21st Queen's Biennial Symp. Commun.*, (Kingston, ON, Canada), pp. 111–115, May 2002.
- [101] Z. Wang, X. Ma, and G. B. Giannakis, "OFDM or single-carrier block transmissions?," *IEEE Trans. Commun.*, vol. 52, pp. 380–394, Mar. 2004.
- [102] A. D. Rizos, J. G. Proakis, and T. Q. Nguyen, "Comparison of DFT and cosine modulated filter banks in multicarrier modulation," in *Proc. IEEE Global Telecommun. Conf.*, vol. 2, (San Francisco, CA, USA), pp. 687–691, Nov. 1994.
- [103] J. Louveaux, *Filter Bank Based Multicarrier Modulation for xDSL Transmission*. PhD thesis, Université Catholique de Louvain, Louvain-la-Neuve, Belgium, May 2000.
- [104] A. Viholainen, *Transmultiplexer Design for VDSL Modems*. Master's thesis, Tampere University of Technology, Tampere, Finland, Aug. 1998.
- [105] A. Viholainen, J. Alhava, J. Helenius, J. Rinne, and M. Renfors, "Equalization in filter bank based multicarrier systems," in *Proc. Int. Conf. Electron., Circuits, Systems*, (Pafos, Cyprus), pp. 1467–1470, Sept. 1999.
- [106] A. Viholainen, J. Alhava, and M. Renfors, "Implementation of parallel cosine and sine modulated filter banks for equalized transmultiplexer systems," in *Proc. IEEE Int. Conf. Acoust., Speech, Signal Process.*, (Salt Lake City, UT, USA), pp. 3625–3628, May 2001.
- [107] A. Viholainen, T. H. Stitz, J. Alhava, T. Ihalainen, and M. Renfors, "Complex modulated critically sampled filter banks based on cosine and sine modulation," in *Proc. IEEE Int. Symp. Circuits, Systems*, vol. 1, (Scottsdale, AZ, USA), pp. 833–836, May 2002.

- 
- [108] R. P. Ramachandran and P. Kabal, "Bandwidth efficient transmultiplexers, part 1: Synthesis," *IEEE Trans. Signal Process.*, vol. 40, pp. 70–84, Jan. 1992.
- [109] R. P. Ramachandran and P. Kabal, "Bandwidth efficient transmultiplexers, part 2: Subband complements and performance aspects," *IEEE Trans. Signal Process.*, vol. 40, pp. 1108–1121, May 1992.
- [110] G. W. Wornell, "Emerging applications of multirate signal processing and wavelets in digital communications," *Proc. IEEE*, vol. 84, pp. 586–603, Apr. 1996.
- [111] A. Scaglione, G. Giannakis, and S. Barbarossa, "Redundant filterbank precoders and equalizers part 1: Unification and optimal design," *IEEE Trans. Signal Process.*, vol. 47, pp. 1988–2006, July 1999.
- [112] A. Scaglione, G. Giannakis, and S. Barbarossa, "Redundant filterbank precoders and equalizers part 2: Blind channel estimation, synchronization and direct equalization," *IEEE Trans. Signal Process.*, vol. 47, pp. 2007–2022, July 1999.
- [113] A. N. Akansu, M. V. Tazebay, and R. A. Haddad, "A new look at digital orthogonal transmultiplexers for CDMA communications," *IEEE Trans. Signal Process.*, vol. 45, pp. 263–267, Jan. 1997.
- [114] A. N. Akansu, P. Duhamel, X. Lin, and M. de Courville, "Orthogonal transmultiplexers in communications: A review," *IEEE Trans. Signal Process.*, vol. 46, pp. 979–995, Apr. 1998.
- [115] X. Lin and A. N. Akansu, "Nonmaximally decimated filterbank based precoder/post-equalizer for blind channel identification and optimal MMSE equalization," in *Proc. IEEE Int. Conf. Acoust., Speech, Signal Process.*, vol. 6, (Seattle, WA, USA), pp. 3505–3508, May 1998.
- [116] T. Karp and N. J. Fliege, "Modified DFT filter banks with perfect reconstruction," *IEEE Trans. Circuits, Systems – II*, vol. 46, pp. 1404–1414, Nov. 1999.
- [117] S. Mirabasi and K. Martin, "Design of prototype filter for near-perfect-reconstruction overlapped complex-modulated transmultiplexers," in *Proc. IEEE Int. Symp. Circuits, Systems*, vol. 1, (Scottsdale, AZ, USA), pp. 821–824, May 2002.
- [118] M. Sablatash and J. Lodge, "Spectrally efficient multiplexing of O-QPSK or VSB signals using wavelet packet-based filter banks," *Digital Signal Process.*, vol. 13, pp. 58–92, Jan. 2003.
- [119] S. Weiss, S. R. Dooley, R. W. Stewart, and A. K. Nandi, "Adaptive equalization in oversampled subbands," in *Proc. Asilomar Conf. Signals, Systems, Computers*, vol. 1, (Pacific Grove, CA, USA), pp. 389–393, Nov. 2002.

- 
- [120] T. Ihalainen, J. Alhava, A. Viholainen, H. Xing, J. Rinne, and M. Renfors, "On the performance of filter bank based multicarrier systems in xDSL and WLAN systems," in *Proc. IEEE Int. Conf. Commun.*, vol. 2, (New Orleans, LA, USA), pp. 1120–1124, June 2000.
- [121] A. Scaglione, G. Giannakis, and S. Barbarossa, "Filterbank transceivers optimizing information rate in block transmissions over dispersive channels," *IEEE Trans. Inform. Theory*, vol. 45, pp. 1019–1032, Apr. 1999.
- [122] B. Borna and T. N. Davidson, "Efficient filter bank design for filtered multitone modulation," in *Proc. IEEE Int. Conf. Commun.*, vol. 1, (Paris, France), pp. 38–42, June 2004.
- [123] Y.-P. Lin and S.-M. Phoong, "Minimum redundancy for ISI free FIR filterbank transceivers," *IEEE Trans. Signal Process.*, vol. 50, pp. 842–853, Apr. 2002.
- [124] J. Milanovic, T. N. Davidson, Z.-Q. Luo, and K. M. Wong, "Design of robust redundant precoding filter banks with zero-forcing equalizers for unknown frequency-selective channels," in *Proc. IEEE Int. Conf. Acoust., Speech, Signal Process.*, vol. 5, (Istanbul, Turkey), pp. 2761–2764, June 2000.
- [125] K. W. Martin, "Small side-lobe filter design for multitone data-communication applications," *IEEE Trans. Circuits, Systems – II*, vol. 45, pp. 1155–1161, Aug. 1998.
- [126] K.-W. Cheong and J. M. Cioffi, "Discrete wavelet transforms in multi-carrier modulation," in *Proc. IEEE Global Telecommun. Conf.*, vol. 5, (Sydney, NSW, Australia), pp. 2794–2799, Nov. 1998.
- [127] E. A. Lee and D. G. Messerschmitt, *Digital Communications*. Dordrecht, Netherlands: Kluwer Academic Publishers, 2nd ed., 1994.
- [128] R. W. Lucky, J. Salz, and E. J. Weldon, Jr, *Principles of Data Communication*. New York, NY, USA: McGraw-Hill, 1968.
- [129] R. Vaughan and J. B. Andersen, *Channels, Propagation and Antennas for Mobile Communications*. Electromagnetic Waves Series 50, Stevenage, UK: The Institution of Electrical Engineers, 2003.
- [130] A. A. M. Saleh and R. A. Valenzuela, "A statistical model for indoor multipath propagation," *IEEE J. Select. Areas Commun.*, vol. 5, pp. 128–137, Feb. 1987.
- [131] R. B. Ertel, P. Cardieri, K. W. Sowerby, T. S. Rappaport, and J. H. Reed, "Overview of spatial channel models for antenna array communication systems," *IEEE Personal Commun.*, vol. 5, pp. 10–22, Feb. 1998.

- 
- [132] Z. Ji, B.-H. Li, H.-X. Wang, H.-Y. Chen, and T. K. Sarkar, "Efficient ray tracing methods for propagation prediction for indoor wireless communications," *IEEE Antenna Propagat. Mag.*, vol. 43, pp. 41–49, Apr. 2001.
- [133] J. W. McKown and R. L. Hamilton, Jr., "Ray tracing as a design tool for radio networks," *IEEE Network Mag.*, pp. 27–30, Nov. 1991.
- [134] S. Thoen, L. Van der Perre, and M. Engels, "Modeling the channel time-variance for fixed wireless communications," *IEEE Commun. Lett.*, vol. 6, pp. 331–333, Aug. 2002.
- [135] W. C. Jakes, *Microwave Mobile Communications*. New York, NY, USA: IEEE Press, 1993.
- [136] J. Medbo and P. Schramm, "Channel models for HIPERLAN/2 in different indoor environments," Tech. Rep. ETSI EP BRAN 3ERI085B, European Telecommunications Standards Institute, Mar. 1998.
- [137] D. Chizhik, J. Ling, P. Wolniansky, R. Valenzuela, N. Costa, and K. Huber, "Multiple input multiple output measurements and modeling in Manhattan," in *Proc. 56th IEEE Veh. Technol. Conf. – Fall*, vol. 1, (Vancouver, BC, Canada), pp. 107–110, Sept. 2002.
- [138] R. Stridh, B. Ottersten, and P. Karlsson, "MIMO channel capacity on a measured indoor radio channel at 5.8 GHz," in *Proc. Asilomar Conf. Signals, Systems, Computers*, vol. 1, (Pacific Grove, CA, USA), pp. 733–737, Oct. 2000.
- [139] C. M. Tan, A. R. Nix, and M. A. Beach, "Dynamic spatial-temporal propagation measurement and super-resolution channel characterisation at 5.2 GHz in a corridor environment," in *Proc. 56th IEEE Veh. Technol. Conf. – Fall*, vol. 2, (Vancouver, BC, Canada), pp. 797–801, Sept. 2002.
- [140] A. Stamoulis, S. N. Diggavi, and N. Al-Dhahir, "Intercarrier interference in MIMO OFDM," *IEEE Trans. Signal Process.*, vol. 50, pp. 2451–2464, Oct. 2002.
- [141] A. M. Wyglinski, *Performance of CDMA Systems using Digital Beamforming with Mutual Coupling and Scattering Effects*. Master's thesis, Queen's University, Kingston, ON, Canada, Sept. 2000.
- [142] G. D. Durgin, *Space-Time Wireless Channels*. Prentice Hall Communications Engineering and Emerging Technologies Series, Upper Saddle River, NJ, USA: Prentice Hall, 2003.

- 
- [143] D.-S. Shiu, G. J. Foschini, M. J. Gans, and J. M. Kahn, "Fading correlation and its effect on the capacity of multielement antenna systems," *IEEE Trans. Commun.*, vol. 48, pp. 502–513, Mar. 2000.
- [144] R. H. Clarke, "A statistical theory of mobile radio reception," *Bell Sys. Tech. J.*, vol. 47, pp. 957–1000, Jul.-Aug. 1968.
- [145] J. P. Kermoal, L. Schumacher, P. E. Mogensen, and K. I. Pedersen, "Experimental investigation of correlation properties of MIMO radio channels for indoor picocell scenarios," in *Proc. 52nd IEEE Veh. Technol. Conf. – Fall*, vol. 1, (Boston, MA, USA), pp. 14–21, Sept. 2000.
- [146] K. Yu, M. Bergtsson, B. Ottersten, D. McNamara, P. Karlsson, and M. Beach, "Second order statistics of NLOS indoor MIMO channels based on 5.2 GHz measurements," in *Proc. IEEE Global Telecommun. Conf.*, vol. 1, (San Antonio, TX, USA), pp. 156–160, Nov. 2001.
- [147] A. van Zelst and J. S. Hammerschmidt, "A single coefficient spatial correlation model for multiple-input multiple-output (MIMO) radio channels," in *Proc. General Assembly Int. Union Radio Sci. (URSI)*, (Maastricht, Netherlands), pp. 1–4, Aug. 2002.
- [148] D. Gesbert, H. Bolcskei, D. A. Gore, and A. J. Paulraj, "Outdoor MIMO wireless channels: Models and performance prediction," *IEEE Trans. Commun.*, vol. 50, pp. 1926–1934, Dec. 2001.
- [149] D. Gesbert, H. Bolcskei, D. Gore, and A. Paulraj, "MIMO wireless channels: Capacity and performance prediction," in *Proc. IEEE Global Telecommun. Conf.*, vol. 2, (San Francisco, CA, USA), pp. 1083–1088, Nov. 2000.
- [150] P. Vandenameele, L. Van Der Perre, M. G. E. Engels, B. Gyselinckx, and H. J. De Man, "A combined OFDM/SDMA approach," *IEEE J. Select. Areas Commun.*, vol. 18, pp. 2312–2321, Nov. 2000.
- [151] W. Bai, C. He, L.-G. Jiang, and H.-W. Zhu, "Blind channel estimation in MIMO-OFDM systems," in *Proc. IEEE Global Telecommun. Conf.*, vol. 1, (Taipei, Taiwan), pp. 317–321, Nov. 2002.
- [152] Y. G. Li, J. H. Winters, and N. R. Sollenberger, "MIMO-OFDM for wireless communications: Signal detection with enhanced channel estimation," *IEEE Trans. Commun.*, vol. 50, pp. 1471–1477, Sept. 2002.
- [153] S. Catreux, V. Erceg, D. Gesbert, and R. W. Heath, Jr., "Adaptive modulation and MIMO coding for broadband wireless data networks," *IEEE Commun. Mag.*, vol. 40, pp. 108–115, June 2002.

- 
- [154] D. Hughes-Hartog, "Ensemble modem structure for imperfect transmission media." U.S. Patent Nos. 4,679,227 (Jul. 1987), 4,731,816 (Mar. 1988), and 4,833,706 (May 1989).
- [155] K. Balachandran, S. R. Kadaba, and S. Nanda, "Channel quality estimation and rate adaptation for cellular mobile radio," *IEEE J. Select. Areas Commun.*, vol. 17, pp. 1244–1256, July 1999.
- [156] I.-M. Kim and H.-M. Kim, "A new resource allocation scheme based on a PSNR criterion for wireless video transmission to stationary receivers over gaussian channels," *IEEE Trans. Wireless Commun.*, vol. 1, pp. 393–401, July 2002.
- [157] R. Kwan, P. Chong, and M. Rinne, "Analysis of the adaptive modulation and coding algorithm with the multicode transmission," in *Proc. 56th IEEE Veh. Technol. Conf. – Fall*, vol. 4, (Vancouver, BC, Canada), pp. 2007–2011, Sept. 2002.
- [158] K. Hamaguchi and E. Moriyama, "Performance of multicarrier/QAM-level-controlled adaptive modulation for land mobile communication systems," *IEICE Trans. Commun.*, vol. E81-B, pp. 770–776, Apr. 1998.
- [159] E. Uysal-Biykoglu, A. El Gamal, and B. Prabhakar, "Adaptive transmission of variable-rate data over a fading channel for energy-efficiency," in *Proc. IEEE Global Telecommun. Conf.*, vol. 1, (Taipei, Taiwan), pp. 97–101, Nov. 2002.
- [160] D. Qiao and S. Choi, "Goodput enhancement of IEEE 802.11a wireless LAN via link adaptation," in *Proc. IEEE Int. Conf. Commun.*, vol. 7, (Helsinki, Finland), pp. 1995–2000, June 2001.
- [161] S. Armour, A. Doufexi, A. Nix, and D. Bull, "A study of the impact of frequency selectivity on link adaptive wireless LAN systems," in *Proc. 56th IEEE Veh. Technol. Conf. – Fall*, vol. 2, (Vancouver, BC, Canada), pp. 738–742, Sept. 2002.
- [162] J. M. Torrance and L. Hanzo, "Optimisation of switching levels for adaptive modulation in slow Rayleigh fading," *Electron. Lett.*, vol. 32, pp. 1167–1169, 20th June 1996.
- [163] J. M. Torrance and L. Hanzo, "Upper bound performance of adaptive modulation in a slow Rayleigh fading channel," *Electron. Lett.*, vol. 32, pp. 718–719, 11th April 1996.
- [164] L. Hanzo, C. H. Wang, and M. S. Yee, *Adaptive Wireless Transceivers: Turbo-Coded, Turbo-Equalized and Space-Time Coded TDMA, CDMA, and OFDM Systems*. New York, NY, USA: John Wiley and Sons, 2002.

- 
- [165] S.-T. Chung and A. Goldsmith, "Adaptive multicarrier modulation for wireless systems," in *Proc. Asilomar Conf. Signals, Systems, Computers*, vol. 2, (Pacific Grove, CA, USA), pp. 1603–1607, Oct. 2000.
- [166] S.-T. Chung and A. J. Goldsmith, "Degrees of freedom in adaptive modulation: A unified view," *IEEE Trans. Commun.*, vol. 49, pp. 1561–1571, Sept. 2001.
- [167] S. Thoen, L. Van der Perre, B. Gyselinckx, M. Engels, and H. De Man, "Predictive adaptive loading for HIPERLAN II," in *Proc. 52nd IEEE Veh. Technol. Conf. – Fall*, vol. 5, (Boston, MA, USA), pp. 2166–2172, Sept. 2000.
- [168] S. Vishwanath, S. A. Jafar, and A. Goldsmith, "Optimum power and rate allocation strategies for multiple access fading channels," in *Proc. 53rd IEEE Veh. Technol. Conf. – Spring*, vol. 4, (Rhodes, Greece), pp. 2888–2892, May 2001.
- [169] S. Thoen, L. Van der Perre, M. Engels, and H. De Man, "Adaptive loading for OFDM/SDMA-based wireless networks," *IEEE Trans. Commun.*, vol. 50, pp. 1798–1810, Nov. 2002.
- [170] C. Y. Wong, R. S. Cheng, K. Ben Letaief, and R. D. Murch, "Multiuser OFDM with adaptive subcarrier, bit, and power allocation," *IEEE J. Select. Areas Commun.*, vol. 17, pp. 1747–1758, Oct. 1999.
- [171] J. C. Roh and B. D. Rao, "Adaptive modulation for multiple antenna channels," in *Proc. Asilomar Conf. Signals, Systems, Computers*, vol. 1, (Pacific Grove, CA, USA), pp. 526–530, Nov. 2002.
- [172] T. Haustein and H. Boche, "Optimal power allocation for MSE and bit-loading in MIMO systems and the impact of correlation," in *Proc. IEEE Int. Conf. Acoust., Speech, Signal Process.*, vol. 4, (Hong Kong, China), pp. 405–408, Apr. 2003.
- [173] X. Zhang and B. Ottersten, "Power allocation and bit loading for spatial multiplexing in MIMO systems," in *Proc. IEEE Int. Conf. Acoust., Speech, Signal Process.*, vol. 5, (Hong Kong, China), pp. 53–56, Apr. 2003.
- [174] J. H. Sung and J. R. Barry, "Bit-allocation strategies for MIMO fading channels with channel knowledge at transmitter," in *Proc. 57th IEEE Veh. Technol. Conf. – Spring*, vol. 2, (Jeju, South Korea), pp. 813–817, Apr. 2003.
- [175] J. H. Sung and J. R. Barry, "Rate-allocation strategies for closed-loop MIMO-OFDM," in *Proc. 58th IEEE Veh. Technol. Conf. – Fall*, (Orlando, FL, USA), Oct. 2003.
- [176] G. Ungerboeck, "Channel coding with multilevel/phase signals," *IEEE Trans. Inform. Theory*, vol. 28, pp. 55–67, Jan. 1982.

- 
- [177] W. Rhee and J. M. Cioffi, "Increase in capacity of multiuser OFDM system using dynamic subchannel allocation," in *Proc. 51st IEEE Veh. Technol. Conf. – Spring*, vol. 2, (Tokyo, Japan), pp. 1085–1089, May 2000.
- [178] L. M. C. Hoo, J. Tellado, and J. M. Cioffi, "Discrete dual QoS loading algorithms for multicarrier systems," in *Proc. IEEE Int. Conf. Commun.*, vol. 2, (Vancouver, BC, Canada), pp. 796–800, June 1999.
- [179] J. Kim, J.-T. Chen, and J. M. Cioffi, "Low complexity bit mapping algorithm for multi-carrier communication systems with fading channels," in *Proc. IEEE Int. Conf. Universal Personal Commun.*, vol. 2, (Florence, Italy), pp. 927–931, Oct. 1998.
- [180] C. H. Lim and J. M. Cioffi, "Performance of the adaptive rate MQAM with on/off power control," *IEEE Commun. Lett.*, vol. 5, pp. 16–18, Jan. 2001.
- [181] Y. Ding, T. N. Davidson, and K. M. Wong, "On improving the BER performance of rate-adaptive block-by-block transceivers, with applications to DMT," in *Proc. IEEE Global Telecommun. Conf.*, (San Francisco, CA, USA), pp. 1654–1658, Dec. 2003.
- [182] A. Leke and J. M. Cioffi, "Impact of imperfect channel knowledge on the performance of multicarrier systems," in *Proc. IEEE Global Telecommun. Conf.*, vol. 2, (Sydney, NSW, Australia), pp. 951–955, Nov. 1998.
- [183] Q. Su, L. J. Cimini, and R. S. Blum, "On the problem of channel mismatch in constant-bit-rate adaptive modulation," in *Proc. 55th IEEE Veh. Technol. Conf. – Spring*, vol. 2, (Birmingham, AL, USA), pp. 585–589, May 2002.
- [184] D. L. Goeckel, "Strongly robust adaptive signaling for time-varying channels," in *Proc. IEEE Int. Conf. Commun.*, vol. 1, (Atlanta, GA, USA), pp. 454–458, June 1998.
- [185] D. L. Goeckel, "Adaptive coding for fading channel using outdated channel estimates," in *Proc. 48th IEEE Veh. Technol. Conf.*, vol. 3, (Ottawa, ON, Canada), pp. 1925–1929, May 1998.
- [186] D. L. Goeckel, "Adaptive coding for time-varying channels using outdated fading estimates," *IEEE Trans. Commun.*, vol. 47, pp. 844–855, June 1999.
- [187] S. Falahati, A. Svensson, T. Ekman, and M. Sternad, "Adaptive modulation systems for predicted wireless channels," *IEEE Trans. Commun.*, vol. 52, pp. 307–316, Feb. 2004.
- [188] S. Sen, S. Pasupathy, and F. R. Kschischang, "Quantized feedback information for the SVD filtered MIMO based FEC coded DS-CDMA multiuser detection receiver," in *Proc. Int. Conf. Wireless Commun.*, (Calgary, AB, Canada), pp. 45–51, July 2003.

- 
- [189] R. D. Gitlin, J. F. Hayes, and S. B. Weinstein, *Data Communications Principles*. New York, NY, USA: Plenum Press, 1992.
- [190] L. W. Couch II, *Digital and Analog Communication Systems*. New York, NY, USA: Macmillan Publishing Company, 4th ed., 1993.
- [191] L. Goldfeld and V. Lyandres, "Capacity of the multicarrier channel with frequency-selective nakagami fading," *IEICE Trans. Commun.*, vol. E83-B, pp. 697–702, Mar. 2000.
- [192] Federal Communications Commission, "Part 15—radio frequency devices, subpart E—unlicensed national information infrastructure devices, section 403—definitions." Code of Federal Regulations – FCC 47CFR15.403, Oct. 2000.
- [193] W.-J. Choi, K.-W. Cheong, and J. M. Cioffi, "Adaptive modulation with limited peak power for fading channels," in *Proc. 51st IEEE Veh. Technol. Conf. – Spring*, vol. 3, (Tokyo, Japan), pp. 2568–2572, May 2000.
- [194] X.-G. Xia, "New precoding for intersymbol interference cancellation using non-maximally decimated multirate filterbanks with ideal FIR equalizers," *IEEE Trans. Signal Process.*, vol. 45, pp. 2431–2441, Oct. 1997.
- [195] D. Falconer, S. L. Ariyavisitakul, A. Benyamin-Seeyar, and B. Eidson, "Frequency domain equalization for single-carrier broadband wireless systems," *IEEE Commun. Mag.*, vol. 40, pp. 58–66, Apr. 2002.
- [196] X. Zhu and R. D. Murch, "Novel frequency-domain equalization architectures for a single-carrier wireless MIMO system," in *Proc. 56th IEEE Veh. Technol. Conf. – Fall*, vol. 2, (Vancouver, BC, Canada), pp. 874–878, Sept. 2002.
- [197] R. L.-U. Choi and R. D. Murch, "Frequency domain pre-equalization with transmit diversity for MISO broadband wireless communications," in *Proc. 56th IEEE Veh. Technol. Conf. – Fall*, vol. 3, (Vancouver, BC, Canada), pp. 1787–1791, Sept. 2002.
- [198] A. Czylik, "Degradation of multicarrier and single carrier transmission with frequency domain equalization due to pilot-aided channel estimation and frequency synchronization," in *Proc. IEEE Global Telecommun. Conf.*, vol. 1, (Phoenix, AZ, USA), pp. 27–31, Nov. 1997.
- [199] N. Al-Dhahir and J. M. Cioffi, "Optimum finite-length equalization for multicarrier transceivers," *IEEE Trans. Commun.*, vol. 44, pp. 56–64, Jan. 1996.
- [200] G. Leus and M. Moonen, "Per-tone equalization for MIMO OFDM systems," *IEEE Trans. Signal Process.*, vol. 51, pp. 2965–2975, Nov. 2003.

- 
- [201] T. Wiegand and N. J. Fliege, "Equalizers for transmultiplexers in orthogonal multiple carrier data transmission," in *Proc. European Signal Processing Conf.*, vol. 2, (Trieste, Italy), pp. 1211–1214, Sept. 1996.
- [202] G. L. Stuber, J. R. Barry, S. W. McLaughlin, Y. G. Li, M. A. Ingram, and T. G. Pratt, "Broadband MIMO-OFDM wireless communications," *Proc. IEEE*, vol. 92, pp. 271–294, Feb. 2004.
- [203] A. van Zelst and T. C. W. Schenk, "Implementation of a MIMO OFDM-based wireless LAN system," *IEEE Trans. Signal Process.*, vol. 52, pp. 483–494, Feb. 2004.
- [204] D. Gesbert, L. Haumonte, H. Bolcskei, R. Krishnamoorthy, and A. J. Paulraj, "Technologies and performance for non-line-of-sight broadband wireless access networks," *IEEE Commun. Mag.*, vol. 40, pp. 86–95, Apr. 2002.
- [205] H. Sampath, S. Talwar, J. Tellado, V. Erceg, and A. Paulraj, "A fourth-generation MIMO-OFDM broadband wireless system: design, performance, and field trial results," *IEEE Commun. Mag.*, vol. 40, pp. 143–149, Sept. 2002.
- [206] G. J. Foschini, "Layered space-time architecture for wireless communication in a fading environment when using multi-element antennas," *Bell Labs Tech. J.*, pp. 41–59, Autumn 1996.
- [207] G. J. Foschini and M. J. Gans, "On limits of wireless communications in a fading environment when using multiple antennas," *Wireless Personal Commun.*, vol. 6, pp. 311–335, 1998.
- [208] A. J. Paulraj, D. A. Gore, R. U. Nabar, and H. Bolcskei, "An overview of MIMO communications – a key to gigabit wireless," *Proc. IEEE*, vol. 92, pp. 198–218, Feb. 2004.
- [209] X. Zhu and R. D. Murch, "Performance analysis of maximum likelihood detection in a MIMO antenna system," *IEEE Trans. Commun.*, vol. 50, pp. 187–191, Feb. 2002.
- [210] S. Thoen, L. Van Der Perre, B. Gyselinckx, and M. Engels, "Adaptive loading for OFDM/SDMA-based wireless local networks," in *Proc. IEEE Global Telecommun. Conf.*, vol. 2, (San Francisco, CA, USA), pp. 767–771, Nov. 2000.
- [211] J. Kim and J. M. Cioffi, "Spatial multiuser access OFDM with antenna diversity with power control," in *Proc. 52nd IEEE Veh. Technol. Conf. – Fall*, vol. 1, (Boston, MA, USA), pp. 273–279, Sept. 2000.
- [212] Y. Xin and G. B. Giannakis, "Layered space-time OFDM with high-performance and high-rate," in *Proc. European Signal Processing Conf.*, vol. 3, (Toulouse, France), pp. 41–44, Sept. 2002.

- 
- [213] E. Visotsky and U. Madhow, "Space-time transmit precoding with imperfect feedback," *IEEE Trans. Inform. Theory*, vol. 47, pp. 2632–2639, Sept. 2001.
- [214] D. G. Manolakis, V. K. Ingle, and S. M. Kogon, *Statistical and Adaptive Signal Processing: Spectral Estimation, Signal Modeling, Adaptive Filtering and Array Processing*, ch. 11, pp. 683–686. New York, NY, USA: McGraw-Hill, 2000.
- [215] A. J. Paulraj and C. B. Papadias, "Space-time processing for wireless communications: Improving capacity, coverage, and quality in wireless networks by exploiting the spatial dimension," *IEEE Signal Process. Mag.*, pp. 49–83, Nov. 1997.
- [216] K. Sheikh, D. Gesbert, D. Gore, and A. Paulraj, "Smart antennas for broadband wireless access networks," *IEEE Commun. Mag.*, pp. 100–105, Nov. 1999.
- [217] A. P. Iserte, A. I. Perez-Neira, and M. A. Lagunas Hernandez, "Joint beamforming strategies in OFDM-MIMO systems," in *Proc. IEEE Int. Conf. Acoust., Speech, Signal Process.*, vol. 3, (Salt Lake City, UT, USA), pp. 2845–2848, May 2001.
- [218] A. P. Iserte, A. I. Perez-Neira, D. P. Palomar, and M. A. Lagunas Hernandez, "Power allocation techniques for joint beamforming in OFDM-MIMO channels," in *Proc. European Signal Processing Conf.*, vol. 1, (Toulouse, France), pp. 383–386, Sept. 2002.
- [219] A. P. Iserte, A. I. Perez-Neira, and M. A. Lagunas Hernandez, "Joint transceiver optimization in wireless multiuser MIMO-OFDM channels based on simulated annealing," in *Proc. European Signal Processing Conf.*, vol. 2, (Toulouse, France), pp. 421–424, Sept. 2002.
- [220] Y. G. Li and N. R. Sollenberger, "Adaptive antenna arrays for OFDM systems with cochannel interference," *IEEE Trans. Commun.*, vol. 47, pp. 217–229, Feb. 1999.
- [221] A. T. Alastalo and M. Kahola, "Smart-antenna operation for indoor wireless local-area networks using OFDM," *IEEE Trans. Wireless Commun.*, vol. 2, pp. 392–399, Mar. 2003.
- [222] C. K. Kim, "Pre-FFT adaptive beamforming algorithm for OFDM systems with array antenna," *IEICE Trans. Commun.*, vol. E86-B, pp. 1144–1148, Mar. 2003.
- [223] P. Xia, S. Zhou, and G. B. Giannakis, "Adaptive MIMO-OFDM based on partial channel state information," *IEEE Trans. Signal Process.*, vol. 52, pp. 202–213, Jan. 2004.
- [224] Y.-H. Pan, K. Ben Letaief, and Z. Cao, "Dynamic sub-channel allocation with adaptive beamforming for broadband OFDM wireless systems," in *Proc. IEEE Global Telecommun. Conf.*, vol. 1, (Taipei, Taiwan), pp. 711–715, Nov. 2002.

- 
- [225] R. T. Derryberry, S. D. Gray, D. M. Ionescu, G. Mandyam, and B. Raghothaman, "Transmit diversity in 3G CDMA systems," *IEEE Commun. Mag.*, vol. 40, pp. 68–75, Apr. 2002.
- [226] D. Gesbert, M. Shafi, D.-S. Shiu, P. J. Smith, and A. Naguib, "From theory to practice: An overview of MIMO space-time coded wireless systems," *IEEE J. Select. Areas Commun.*, vol. 21, pp. 281–302, Apr. 2003.
- [227] S. N. Diggavi, N. Al-Dhahir, A. Stamoulis, and A. R. Calderbank, "Great expectations: The value of spatial diversity in wireless networks," *Proc. IEEE*, vol. 92, pp. 219–270, Feb. 2004.
- [228] D. Agrawal, V. Tarokh, A. Naguib, and N. Seshadri, "Space-time coded OFDM for high data-rate wireless communication over wideband channels," in *Proc. 48th IEEE Veh. Technol. Conf.*, vol. 3, (Ottawa, ON, Canada), pp. 2232–2236, May 1998.
- [229] V. Tarokh, A. F. Naguib, N. Seshadri, and A. R. Calderbank, "Space-time codes for high data rate wireless communication: Performance criteria in the presence of channel estimation errors, mobility, and multiple paths," *IEEE Trans. Commun.*, vol. 47, pp. 199–207, Feb. 1999.
- [230] S. M. Alamouti, "A simple transmit diversity technique for wireless communications," *IEEE J. Select. Areas Commun.*, vol. 16, pp. 1451–1458, Oct. 1998.
- [231] N. Al-Dhahir, C. Fragouli, A. Stamoulis, W. Younis, and R. Calderbank, "Space-time processing for broadband wireless access," *IEEE Commun. Mag.*, vol. 40, pp. 136–142, Sept. 2002.
- [232] A. Dammann, R. Raulefs, and S. Kaiser, "Beamforming in combination with space-time diversity for broadband OFDM systems," in *Proc. IEEE Int. Conf. Commun.*, vol. 1, (New York, NY, USA), pp. 165–171, June 2002.
- [233] R. D. Murch and K. B. Letaief, "Antenna systems for broadband wireless access," *IEEE Commun. Mag.*, vol. 40, pp. 76–83, Apr. 2002.
- [234] A. Dammann and S. Kaiser, "Standard conformable antenna diversity techniques for OFDM and its application to the DVB-T system," in *Proc. IEEE Global Telecommun. Conf.*, vol. 5, (San Antonio, TX, USA), pp. 3100–3105, Nov. 2001.
- [235] D. A. Gore, R. W. Heath, and A. J. Paulraj, "Transmit selection in spatial multiplexing systems," *IEEE Commun. Lett.*, vol. 6, pp. 491–493, Nov. 2002.
- [236] A. Wittneben, "Analysis and comparison of optimal predictive transmitter selection and combining diversity for DECT," in *Proc. IEEE Global Telecommun. Conf.*, vol. 2, (Singapore), pp. 1527–1531, Nov. 1995.

- 
- [237] A. Gorokhov, "Transmit diversity versus SDMA: Analytic and numerical comparisons," in *Proc. IEEE Int. Conf. Commun.*, vol. 2, (New Orleans, LA, USA), pp. 1020–1024, June 2000.
- [238] Y. G. Li, J. C. Chuang, and N. R. Sollenberger, "Transmitter diversity for OFDM systems and its impact on high-rate data wireless networks," *IEEE J. Select. Areas Commun.*, vol. 17, pp. 1233–1243, July 1999.
- [239] N. R. Sollenberger, "Diversity and automatic link transfer for a TDMA wireless access link," in *Proc. IEEE Global Telecommun. Conf.*, vol. 1, (Houston, TX, USA), pp. 532–536, Nov. 1993.
- [240] S. Thoen, L. Van de Perre, B. Gyselinckx, and M. Engels, "Performance analysis of combined transmit-SC/receive-MRC," *IEEE Trans. Commun.*, vol. 49, pp. 5–8, Jan. 2001.
- [241] H. Shi, M. Katayama, T. Yamazato, H. Okada, and A. Ogawa, "An adaptive antenna selection scheme for transmit diversity in OFDM systems," in *Proc. 54th IEEE Veh. Technol. Conf. – Fall*, vol. 4, (Atlantic City, NJ, USA), pp. 2168–2172, Oct. 2001.
- [242] J. Rinne, "Subcarrier-based selection diversity reception of DVB-T in a mobile environment," in *Proc. 50th IEEE Veh. Technol. Conf. – Fall*, vol. 2, (Amsterdam, Netherlands), pp. 1043–1047, Sept. 1999.
- [243] S. Ben Slimane, "A low complexity antenna diversity receiver for OFDM based systems," in *Proc. IEEE Int. Conf. Commun.*, vol. 4, (Helsinki, Finland), pp. 1147–1151, June 2001.
- [244] X. Ouyang, M. Ghosh, and J. P. Meehan, "Optimal antenna diversity combining for IEEE 802.11a system," *IEEE Trans. Consumer Electron.*, vol. 48, pp. 738–742, Aug. 2002.
- [245] D. Lee, G. J. Saulnier, Z. Ye, and M. J. Medley, "Antenna diversity for an OFDM system in a fading channel," in *Proc. IEEE Military Commun. Conf.*, vol. 2, (Atlantic City, NJ, USA), pp. 1104–1109, Oct. 1999.
- [246] A. F. Molisch, M. Z. Win, and J. H. Winters, "Capacity of MIMO systems with antenna selection," in *Proc. IEEE Int. Conf. Commun.*, vol. 2, (Helsinki, Finland), pp. 570–574, June 2001.
- [247] A. Annamalai and C. Tellambura, "Analysis of hybrid selection/maximal-ratio diversity combiners with Gaussian errors," *IEEE Trans. Wireless Commun.*, vol. 1, pp. 498–512, July 2002.

- 
- [248] S. Sandhu, R. U. Nabar, D. A. Gore, and A. Paulraj, "Near-optimal selection of transmit antennas for a MIMO channel based on Shannon capacity," in *Proc. Asilomar Conf. Signals, Systems, Computers*, vol. 1, (Pacific Grove, CA, USA), pp. 567–571, Nov. 2000.
- [249] D. A. Gore, R. U. Nabar, and A. Paulraj, "Selecting an optimal set of transmit antennas for a low rank matrix channel," in *Proc. IEEE Int. Conf. Acoust., Speech, Signal Process.*, vol. 5, (Istanbul, Turkey), pp. 2785–2788, June 2000.
- [250] Y.-S. Choi, A. F. Molisch, M. Z. Win, and J. H. Winters, "Fast algorithms for antenna selection in MIMO systems," in *Proc. 58th IEEE Veh. Technol. Conf. – Fall*, (Orlando, FL, USA), Oct. 2003.
- [251] M. Gharavi-Alkhansari and A. B. Gershman, "Fast antenna subset selection in MIMO systems," *IEEE Trans. Signal Process.*, vol. 52, pp. 339–347, Feb. 2004.
- [252] A. F. Naguib, V. Tarokh, N. Seshadri, and A. R. Calderbank, "A space-time coding modem for high-data-rate wireless communications," *IEEE J. Select. Areas Commun.*, vol. 16, pp. 1459–1478, Oct. 1998.
- [253] Z. Liu, Y. Xin, and G. B. Giannakis, "Space-time-frequency coded OFDM over frequency-selective fading channels," *IEEE Trans. Signal Process.*, vol. 50, pp. 2465–2476, Oct. 2002.
- [254] A. M. Wyglinski, P. Kabal, and F. Labeau, "Adaptive filterbank multicarrier wireless systems for indoor environments," in *Proc. 56th IEEE Veh. Technol. Conf. – Fall*, vol. 1, (Vancouver, BC, Canada), pp. 336–340, Sept. 2002.
- [255] A. M. Wyglinski, P. Kabal, and F. Labeau, "Adaptive bit and power allocation for indoor wireless multicarrier systems," in *Proc. Int. Conf. Wireless Commun.*, (Calgary, AB, Canada), pp. 500–508, July 2003.
- [256] A. M. Wyglinski, F. Labeau, and P. Kabal, "Bit loading with BER-constraint for multicarrier systems," *IEEE Trans. Wireless Commun.*, 2004. To Appear.
- [257] J. G. Proakis, *Digital Communications*. New York, NY, USA: McGraw-Hill, 3rd ed., 1995.
- [258] A. M. Wyglinski, F. Labeau, and P. Kabal, "An efficient bit allocation algorithm for multicarrier modulation," in *Proc. IEEE Wireless Commun. Networking Conf.*, (Atlanta, GA, USA), pp. B–13, Mar. 2004.
- [259] A. M. Wyglinski, F. Labeau, and P. Kabal, "Effects of imperfect subcarrier SNR information on adaptive bit loading algorithms for multicarrier systems," in *Proc. IEEE Global Telecommun. Conf.*, (Dallas, TX, USA), Nov. 2004. To appear.

- 
- [260] A. M. Wyglinski, P. Kabal, and F. Labeau, "Variable-length subcarrier equalizers for multicarrier systems," in *Proc. 60th IEEE Veh. Technol. Conf. – Fall*, (Los Angeles, CA, USA), Sept. 2004. To appear.
- [261] A. M. Wyglinski, F. Labeau, and P. Kabal, "BER-constrained bit loading and antenna subset selection for MIMO wireless multicarrier systems." Submitted to *IEEE Int. Conf. Commun.*, 2004.
- [262] L. Zheng and D. N. C. Tse, "Diversity and multiplexing: A fundamental tradeoff in multiple-antenna channels," *IEEE Trans. Inform. Theory*, vol. 49, pp. 1073–1096, May 2003.
- [263] S. Haykin, *Adaptive Filter Theory*. Prentice Hall Information and System Sciences Series, Upper Saddle River, NJ, USA: Prentice Hall, 3rd ed., 1996.
- [264] T. K. Moon and W. C. Stirling, *Mathematical Methods and Algorithms in Signal Processing*. Upper Saddle River, NJ, USA: Prentice Hall, 2000.
- [265] M. C. Jeruchim, P. Balaban, and K. S. Shanmugan, *Simulation of Communication Systems: Modeling, Methodology, and Techniques*. Dordrecht, Netherlands: Kluwer Academic/Plenum Publishers, 2nd ed., 2000.
- [266] E. J. Dudewicz and S. N. Mishra, *Modern Mathematical Statistics*. Wiley Series in Probability and Mathematical Statistics, New York, NY, USA: John Wiley and Sons, 1988.